Signaling pathways regulating skeletal muscle metabolism and growth

Morgan Daughtry Zumbaugh

Dissertation submitted to the faculty of the Virginia Polytechnic Institute and State University in partial fulfillment of the requirements for the degree of

Doctor of Philosophy

In

Animal and Poultry Sciences

David E. Gerrard, Chair
Tim Hao Shi, Co-Chair
Sally E. Johnson
Robert P. Rhoads

November 20, 2020
Blacksburg, VA

Keywords: skeletal muscle metabolism, metabolic reprogramming, O-GlcNAcylation, interleukin-15, myogenesis

Signaling Pathways Regulating Skeletal Muscle Metabolism and Growth

Morgan Daughtry Zumbaugh

Abstract

Skeletal muscle can perceive cellular energy status and substrate availability and demonstrates remarkable plasticity in response to environmental changes. Nonetheless, how skeletal muscle and its resident stem cells (satellite cells; SCs) sense and respond to nutrient flux remains largely undefined. The dynamic post-translational modification O-GlcNAcylation has been shown to serve as a cellular nutrient sensor in a wide range of cells and tissues, yet its role in skeletal muscle and SCs remains unexplored. Here, we ablated skeletal muscle O-GlcNAc transferase (OGT), and thus O-GlcNAcylation, and found the knockout mice exhibited enhanced glucose uptake, insulin sensitivity, and resistance to high-fat diet induced obesity. Additionally, mKO mice had a 3-fold increase in circulating levels of interleukin-15 (IL-15), a potent anti-obesity cytokine, potentially through epigenetic regulation of *Il15* by OGT. To further investigate if there was a causal relationship between OGT ablation and the lean phenotype, we generated muscle specific OGT and interleukin-15 receptor alpha (IL-15rα) double knockout mice (mDKO). As a result, mDKO mice had blunted IL-15 secretion and minimal protection against HFD-induced obesity. Together, these data indicate the skeletal muscle OGT-IL15 axis plays an essential role in the maintenance of skeletal muscle and whole-body metabolic homeostasis.

As satellite cells (SCs) play an indispensable role in postnatal muscle growth and adult regenerative myogenesis, we investigated the role of O-GlcNAcylation in SC function. To this end, we conditionally ablated OGT in SCs (cKO) and found cKO mice had impaired SC proliferation, *in vivo* cycling properties, population stability, metabolic regulation, and adult

regenerative myogenesis. Together these findings show that SCs require O-GlcNAcylation, presumably to gauge nutritional signals, for proper function and metabolic homeostasis.

Another critical yet often neglected player in myogenesis are mitochondria. Traditionally depicted as a power plant in cells, mitochondria are critical for numerous nonconventional, energy-independent cellular process. To investigate the role of both mitochondrial energy production and alternative mitochondrial functions in myogenic regulation, we ablated *ATP synthase subunit beta* (ATP5β) and *ubiquinol-cytochrome c reductase* (UQCRFS1) in C2C12 myoblasts to disrupt mitochondrial ATP production and mitochondrial membrane potential, respectively. Ablation of UQCRFS1, but not ATP5β, impaired myoblast proliferation, although lack of either gene compromised myoblast fusion. Interestingly, addition of the potent myogenic stimulator IGF-1 rescued ATP5β fusion but could not override UQCRFS1 knockout effects on proliferation or differentiation. These data demonstrate mitochondrial ATP production is not the "metabolic switch" that governs myogenic progression but rather an alternative mitochondrial function.

In summary, skeletal muscle and their resident stem cell population (SCs) both use O-GlcNAcylation, feasibly to sense and respond to nutritional cues, for the maintenance of metabolic homeostasis and normal physiology. A deeper understand of both muscle and SC metabolic regulation may provide therapeutic targets to improve global metabolism and muscle growth.

Signaling Pathways Regulating Skeletal Muscle Metabolism and Growth

Morgan Daughtry Zumbaugh

General Audience Abstract

Skeletal muscle is responsible for approximately 20% of basal energy expenditure and 70-90% of insulin-mediated glucose disposal, and as such changes in skeletal muscle metabolism and insulin sensitivity have profound impacts on whole body metabolism. Skeletal muscle is a plastic tissue that can perceive nutrient availability, which permits metabolic adaptations to environmental changes. Deletion of the nutrient sensing pathway O-GlcNAcylation in skeletal muscle (mKO) protected mice from high-fat diet induced obesity and ameliorates whole-body insulin sensitivity. Skeletal muscle can secrete myokines to elicit endocrine effects on other tissues in the body, and as such, we proposed perturbation of this nutrient sensing pathway in skeletal muscle alters myokine secretion to elicit responses in other metabolically active tissues to support its energy requirements. Indeed, circulating levels of interleukin-15, a potent anti-obesity myokine, increased 3-fold in mKO mice. To determine the contribution of IL-15 to the mKO phenotype, we used a genetic approach to blunt IL-15 secretion from skeletal muscle (mDKO), which partially negated the lean mKO phenotype. Our findings show the ability of skeletal muscle to "sense" changes in nutrients through O-GlcNAcylation is necessary for proper muscle and whole-body metabolism. Moreover, this nutrient sensing mechanism is also important for proper muscle stem cell function, also known as satellite cells (SCs). Loss of O-GlcNAcylation in SCs impairs their ability to regenerate muscle after injury, which can be attributed to a reduced capacity to proliferate and an inability to maintain a healthy SC population. Interestingly, SCs lacking O-GlcNAcylation have a greater mitochondrial content. Using a myoblast cell line, we investigated the contribution of mitochondria to myogenesis, the formation of muscle, and found mitochondrial energy production

is dispensable in the myogenic process. Our studies show skeletal muscle and SCs rely on highly integrated signaling cascades that sense and respond to intrinsic metabolic changes and extrinsic nutritional cues to function properly.

Acknowledgments

Dr. David Gerrard: Thank you for your support and knowledge over the past 6 years. You have always pushed the limits of my capabilities to make me a better scientist. I will always be grateful for the opportunities and encouragement you have given me, not to mention your "gentle" guidance in my pursuit of this degree and beginning of an academic career. Although I hate to admit it, I suppose it is for the best that not all of my plans come to fruition. Thank you for being a great educator and mentor.

Dr. Tim Hao Shi: I don't know where to start with my thanks to you. I will always be grateful that you took me under your wing and taught me how to be a scientist. You recognized what I was capable of when I didn't even know how to use a pipette. I will miss our long conversations and will always cherish the friendship we have culminated over the past 6 years. Thank you for your continued support, guidance, and mentorship. There are not enough words.

Dr. Sally Johnson: Thank you for all of the support and encouragement you have provided during my time as a graduate student. Most important, thank you for always having an open door to helping me solve many of problems and for being a great source of information.

Dr. Robert Rhoads: Thank you for all of your help and great ideas during committee meetings. It has been an enormous pleasure working with you and thank you for being a part of my committee.

Dr. Kiho Lee: Thank you for taking the time to teach me about gene editing and model development using CRISPR-Cas9. Thank you for always having an open door and all of the support you have provided.

Dr. Samer El-Kadi: Thank you for always taking the time to help me. I appreciate the meetings we have had and knowledge you have given me during my time as a graduate student.

Con-Ning Yen, Jocelyn Bodmer, and Jordan Wicks: I think it is safe to say you all made graduate school easier (a relative term). Thank you all for your willingness to help at any given moment and for always saying yes when I ask for help (even when you wanted to say no). Thank you for always showing up in support and encouragement. You all have become like family to me over the years, and I will always cherish the time we have shared. Oh, and thank you for always being willing to blow off steam after work hours.

Meat Science and Muscle Biology lab members: Con-Ning Yen, Jocelyn Bodmer, Jordan Wicks, Madison Venhuizen, Rachel Daniels, Ashley Geiger, Jenny Elgin, Dr. Zhengxing Shen, Dr. Sulaiman Matarneh, Dr. Eric England, Richard Preisser, Samuel Gerrard, Enrica Berio, Giulia Baldi, Juan Morales Gomez, Mariane Beline, Kristine Ely, Laila Kirkpatrick: Thank you to each and every one of you for all of your help and guidance over the years. Thank you for help with developing and executing protocols, for the encouragement to keep going on the hard days, and most importantly for your friendship. I will always be grateful for the friendships I have formed with you all.

Undergraduate Students: Jennifer Cobb, Kelly Ramos, Krista Reynolds, Emily Oliver, Emma Helm, Catriona Gow, Eric Stewart, RJ Savino, Alexa Tracy, Kelsey O'Brien, Andrew Sparks,

Lauren Smith, and Han Bin Lee: Thank you for all of your help and contributions to the lab and projects. I greatly appreciate all of your help.

Dr. Amy Rizzo: Thank you for all of your help troubleshooting mice problems and for always being willing to assist with new project ideas. You have been a tremendous help, and I appreciate your help and knowledge over the past several years.

Melissa Makris: Thank you for all of your flow cytometry wisdom and knowledge. Thank you for your guidance and help for the past several years.

Family and Friends: Thank you all for all of your love, support, and encouragement. I cannot possibly thank you all but a special thanks to my parents: **Cheryl, Mark, and Wade.** You have supported me unconditionally throughout my education and life. Thank you for always being my number one fans. Also, thank you Chaquella for your support, humor, and love over the years. Another special thanks to the **Nash Family**: Thank you for always supporting and loving me as your own child. Another special thanks to the **Zumbaugh family**: Thank you for your support over the past four years and accepting me into your family. Much love to you all.

Chuck Zumbaugh: Thank you for all of your support. I will be eternally grateful for my graduate school experience because it gave me you. Thank you for always telling me I can do anything and always loving me. I cannot give you enough thanks. I love you.

Table of Contents

List of Figures

Chapter 1

Chapter 2

Chapter 3

Chapter 4

Chapter 5

Chapter 1. Review of Literature

Introduction

Beyond its fundamental function of locomotion and thermogenesis, skeletal muscle plays an essential role in whole body metabolic equilibrium. In healthy individuals, skeletal muscle represents about 40% of body mass, is responsible for roughly 20% of basal energy expenditure (Zurlo et al., 1990), and accounts for 70-90% of insulin mediated glucose disposal (DeFronzo et al., 1981; Shulman et al., 1990). As a result, modulation of skeletal muscle metabolism and insulin sensitivity has been proven to be an effective means of alleviating metabolic disorders (Izumiya et al., 2008; Meng et al., 2013; Song et al., 2013). Skeletal muscles are composed of a heterogeneous population of muscle cells with distinct metabolic characteristics (Holloszy, 1967) and demonstrate enormous plasticity to adapt to changing external stimuli including activity, load, nutritional factors, and external conditions. For example, endurance exercise or resistance training increases metabolic demand and subsequently increases skeletal muscle mitochondrial content and oxidative capacity (Donges et al., 2012; Di Donato et al., 2014). Contrarily, conditions associated with the onset of obesity such as excessive calorie intake in combination with a reduction in workload decrease oxidative capacity (Mootha et al., 2003) are hallmark initiators of metabolic syndrome and poor insulin sensitivity (Simoneau et al., 1995). However, diabetic and obese patients subjected to an exercise training regime have improved insulin sensitivity, albeit significantly blunted compared to healthy individuals (Rosholt et al., 1994; Han et al., 1997; Fueger et al., 2004). Overall, greater muscle oxidative capacity can provide protection against metabolic disorders, attenuate age-related muscle atrophy, and alleviate metabolic defects associated with some myopathies (Conley et al., 2000; Wang et al., 2004; Wenz et al., 2008; Wenz et al., 2009; Ljubicic et al., 2011). Therefore, the dynamic interplay between a set of highly

coordinated and integrated signaling cascades that respond to extrinsic and intrinsic stimuli are crucial for the regulation of skeletal muscle metabolism, and therefore whole-body metabolism.

Skeletal muscle metabolism

Skeletal muscle has the remarkable ability to adjust its energy expenditure according to energy demands. Within milliseconds, muscle can increase its energy expenditure 100-fold to transition between resting and active states (Sahlin et al., 1998). Despite these large fluctuations in energy demands, ATP concentrations remain relatively constant (Arnold et al., 1984; Heineman and Balaban, 1990), which depicts the striking precision of cellular energy production systems to equal demand. This metabolic control is governed by intricate signaling and feedback loops that relay cellular energy status to alter metabolic pathways within the cell.

Skeletal muscle metabolism is a series of complex biochemical processes that converts nutrients into chemical energy in the form of adenosine triphosphate (ATP). There are several metabolic pathways found in muscle cells that have different subcellular locations and substrate utilization with varying longevity. For brief, rapid mobilization of ATP, the phosphagen system is a reversible reaction that catalyzes the degradation of phosphocreatine by creatine kinase to produce brief supplies of ATP (PCr + ADP ↔ Cr + ATP). Additionally, the enzyme adenylate kinase collaborates with the phosphagen system to contribute to short-term energy buffering (2 ADP ↔ 1 ATP + 1 AMP). Adenylate kinase is also an important contributor to reporting cellular energy status by translating relatively small changes in the ATP:ADP ratio into large changes in AMP concentrations. The concentration of cellular AMP is a sensitive indicator of cellular energy status, and small increases are potent allosteric activators of several key enzymes in glycolysis to increase ATP production. These temporary energy buffering systems maintain ATP levels until other energy production systems are fully active.

Glycolysis converts glucose into pyruvate through a series of enzymatic reactions and can upregulate 100 times faster than oxidative phosphorylation (Pfeiffer et al., 2001). Large glycogen stores in muscle allow for rapid mobilization of glucose-1-phosphate by glycogen phosphorylase to fuel glycolysis, which is the predominate energy source during high-intensity exercise (Katz et al., 1986; Hargreaves and Richter, 1988). Alternatively, glucose transporter type 4 (GLUT4) permits plasma glucose uptake, although rate of uptake is limited by the transport of GLUT4 to the cell surface (Zisman et al., 2000). Translocation of GLUT4 vesicles can be stimulated by insulin in response to high blood glucose levels after feeding, however, its translocation is impaired with insulin resistance and/or diabetes (Zorzano et al., 1996; Zierath et al., 1998; Tremblay et al., 2001). Alternatively, contractile activity from acute exercise can stimulate GLUT4 translocation in an insulin-independent manner (Hayashi et al., 1997; Kennedy et al., 1999; Jessen and Goodyear, 2005). Once within the cells, glucose is rapidly phosphorylated by hexokinase to produce glucose-6-phosphate (G6P) to prevent its outward diffusion and maintain the concentration gradient for continued glucose influx. In either case of glycogen breakdown or glucose uptake, G6P can then stem into anabolic (pentose phosphate pathway), metabolic signaling (hexosamine biosynthetic pathway), or catabolic (glycolysis) pathways depending on cellular demands.

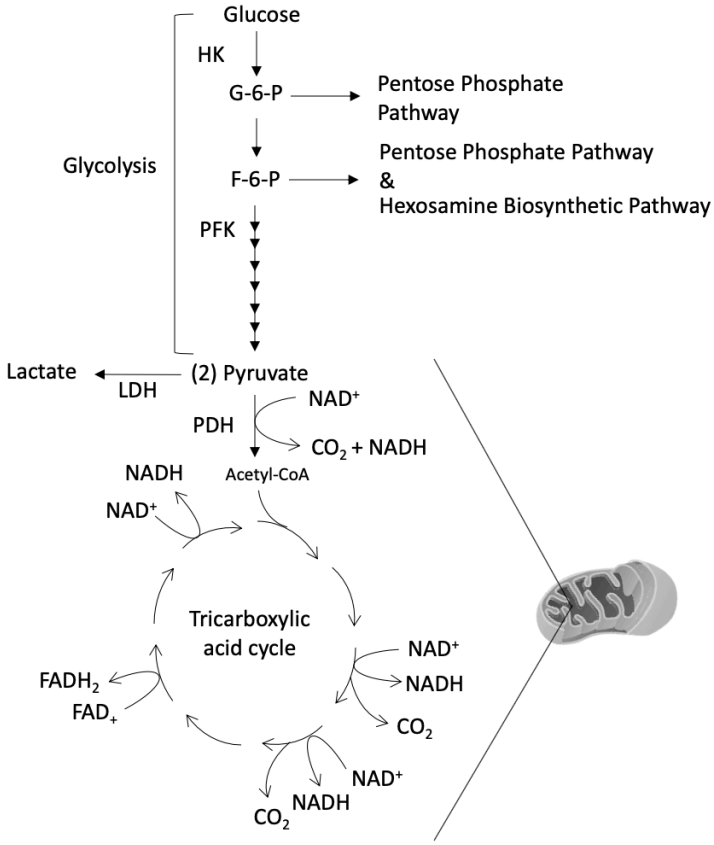

Figure 1-1. Major metabolic pathways in skeletal muscle. Glucose or glycogen can be metabolized through glycolysis to yield pyruvate, which can be converted to acetyl-CoA by pyruvate dehydrogenase (PDH) or converted to lactate by lactate dehydrogenase (LDH). Alternatively, the glycolytic intermediates glucose-6-phosphae (G-6-P) or fructose-6-phosphate (F-6-P) can be redirected to the pentose phosphate pathway, for biosynthetic processes, or to the hexosamine biosynthetic pathway, for metabolic signaling. If pyruvate is converted to acetyl-CoA, it can feed into the tricarboxylic acid cycle (TCA) to be fully oxidized, providing the reducing equivalents NADH and $FADH_2$, or exit the cycle to contribute to biosynthetic processes. Fatty acids or amino acids can also feed into various points of the TCA cycle for oxidation or anaplerosis. Abbreviations: HK = hexokinase; PFK = phosphofructokinase.

The pentose phosphate pathway (PPP) emanates from the glycolytic intermediates G6P and fructose-6-phosphate (F6P) for synthesis of metabolites that are imperative for skeletal muscle anabolism including ribulose-5-phosphate for nucleic acid synthesis, erythrose-4-phosphate for aromatic amino acid synthesis, and NADPH for reductive biosynthesis reactions such as lipogenesis. The two enzymes glucose-6-phosphate dehydrogenase (G6PDH) and 6-

phosphogluconate dehydrogenase (6PGDH) are often used to assess PPP activity because they catalyze the first committed step in the PPP and the final step that produces ribulose 5-phosphate, respectively. Activity of the PPP is quite low in skeletal muscle compared to other tissue types (Battistuzzi et al., 1985), which is not surprising considering skeletal muscle is a terminally differentiated tissue. However, regenerating muscle, 24 hrs after damage, increases G6PD and 6PGDH activity 9-fold compared to the undamaged controls (Wagner et al., 1978). Further, the skeletal muscle-specific overexpression of AKT1 induces muscle hypertrophy (Izumiya et al., 2008), which is accompanied by a 3.5- and 2.3-fold increase in G6PD and 6PGDH transcripts, respectively (Wu et al., 2017). These results collectively suggest greater PPP flux augments skeletal muscle growth.

The hexosamine biosynthetic pathway (HBP) is a metabolic signaling pathway that diverts about 2-3% of cellular glucose from glycolysis (Marshall et al., 1991). It originates from the glycolytic intermediate F6P and is catalyzed by the rate-limiting enzyme glutamine: fructose 6-phosphate amidotransferase (GFAT), which converts F6P and glutamine to glucosamine-6-phosphate and glutamate. The subsequent steps of the HBP generate uridine diphosphate N-acetylglucosamine (UDP-GlcNAc). Collectively, UDP-GlcNAc is indicative of the cellular nutrient flux by integrating carbohydrate, lipid, nucleotide, and protein metabolism (Slawson et al., 2010; Hanover et al., 2012; Ruan et al., 2013). As such, levels of UDP-GlcNAc correspond to cellular nutrient status, and conditions of nutrient excess or scarcity are respective stimulants or inhibitors of UDP-GlcNAc synthesis. Ultimately, UDP-GlcNAc is the donor substrate for the post-translational modification, O-GlcNAcylation, which modifies cell behavior according to fluctuating nutrient conditions (Harwood and Hanover, 2014).

On the other hand, once F6P is converted to fructose-1,6-bisphosphate by phosphofructokinase (PFK), it is committed to glycolysis and then undergoes a sequential, multi-step conversion to pyruvate. Pyruvate can then be converted to lactate by lactate dehydrogenase (LDH) or acetyl CoA by pyruvate dehydrogenase (PDH). During periods of rapid glycolytic flux, or in anaerobic conditions, pyruvate is converted to lactate which can then be shuttled to the liver for hepatic gluconeogenesis to replenish glycogen stores (Brooks, 1986). Alternatively, pyruvate can be transported into the mitochondrial matrix for oxidation but must first traverse the outer mitochondrial membrane, presumably though the porin channel (Huizing et al., 1996), and the inner mitochondrial membrane, through the mitochondrial pyruvate carrier (Bricker et al., 2012; Herzig et al., 2012). Once inside the matrix, PDH converts pyruvate into acetyl-CoA to power the TCA cycle, or less frequently pyruvate carboxylase converts pyruvate into oxaloacetate to support anaplerosis. As PDH is the major link between glycolysis and the TCA cycle, it is an important molecular switch that controls the transition between the two metabolic pathways and is tightly regulated via phosphorylation. A balance between pyruvate dehydrogenase kinases (PDKs) and pyruvate dehydrogenase phosphatases (PDPs) regulate the pyruvate dehydrogenase complex (PDC) in response to nutritional status. Pyruvate dehydrogenase kinase-4 (PDK4) is largely found in skeletal muscle (Bowker-Kinley et al., 1998) and has an increased activity during periods of starvation or high fat feeding (Wu et al., 1998; Holness et al., 2000; Jeoung et al., 2006; Jeoung and Harris, 2008), which suggests PDK4 plays an important role in dietary regulation of carbohydrate oxidation.

Once converted to acetyl-CoA, it can be fully oxidized in the TCA cycle to produce the reducing equivalents NADH and $FADH_2$ for ATP synthesis, or its intermediates can exit the cycle through biosynthetic processes. Although the TCA cycle is often referred to as a “cycle”, implying

a unidirectional and defined series of reactions, there are many entry and exit points that allow for both catabolic and anabolic processes in response to different energy demands. During anabolic conditions, TCA intermediates can be shuttled from the mitochondrial matrix into the cytosol for fatty acid, amino acid, and nucleotide synthesis (Ahn and Metallo, 2015). Contrarily, high energy demands provoke catabolic processes, and intermediates undergo multiple oxidation steps to supply the electron transport chain (ETC) with reducing equivalents (NADH and $FADH_2$) to replenish ATP stores through oxidative phosphorylation.

Not surprisingly, the TCA cycle is tightly coupled to energy demand through complex feedback loops. Accumulation of NADH is a potent inhibitor of all TCA cycle regulatory enzymes, and as such, malfunctions in the ETC inhibit the TCA cycle (Martinez-Reyes and Chandel, 2020). Similarly, high ATP concentrations or accumulation of TCA cycle intermediates inhibit several TCA enzymes. Conversely, high energy demands increase AMP levels, which is an allosteric activator of the regulatory TCA cycle enzymes. While allosteric regulation provides dynamic feedback to keep the TCA cycle in-check, it is also governed by other signaling pathways that provide another layer of regulation. In skeletal muscle, mitochondria are largely found anchored to the sarcoplasmic reticulum (SR) (Boncompagni et al., 2009), which allows for bidirectional signaling between the two organellar systems. More specifically, the calcium released from the SR during muscle contraction can be sequestered by mitochondria, which subsequently stimulates the TCA cycle and mitochondrial ATP production by activating pyruvate dehydrogenase, α-ketoglutarate dehydrogenase, isocitrate dehydrogenase, and the F_1F_0-ATPase (McCormack and Denton, 1979; McCormack et al., 1990; McCormack and Denton, 1993; Hansford, 1994). The parallel activation of muscle contraction and mitochondrial metabolism simultaneously initiates muscle contraction and ATP production to match energy demand with energy supply effectively

(Korzeniewski, 2007). In summary, skeletal muscle metabolism is tightly regulated through a series of complex biochemical processes orchestrated by a hierarchy of catabolic and anabolic events.

Mitochondria bioenergetics and dynamics

Although mitochondria are frequently denoted as the powerhouse of the cell, they also play a central role in metabolic signaling (Hansford and Zorov, 1998; Bohovych and Khalimonchuk, 2016; Martinez-Reyes and Chandel, 2020), reactive oxygen species production/signaling and scavenging (Skulachev, 1996; Aon et al., 2010; Brand, 2010), cell death (Goldstein et al., 2000), ion and metabolite transport (Palmieri and Pierri, 2010), iron-sulfur protein biogenesis (Nuth et al., 2002; Bulteau et al., 2004; Yoon and Cowan, 2004), and calcium homeostasis (Deluca and Engstrom, 1961; Vasington and Murphy, 1962; Rottenberg and Scarpa, 1974). Mitochondria have two membranes, the porous outer mitochondrial membrane (OMM) and selective inner mitochondrial membrane (IMM), which give rise to the inner membrane space (IMS) and mitochondrial matrix. Residing in the IMM, electron transport chain complexes transfer electrons from reducing equivalents to electron acceptors through several redox reactions that are coupled with the transfer of protons from the matrix to the IMS, generating an electrochemical gradient (Figure 1-2). The mitochondrial membrane potential, or electrochemical gradient, is harnessed for ATP production but is also the driving force for its other central metabolic roles.

Four transmembrane protein complexes and two electron carriers are the basis for generating the mitochondrial membrane potential (Figure 1-2). Through a series of redox reactions, electrons are transported from complex to complex while pumping protons from the matrix to the IMS. Complex I (CI) and Complex (II) oxidize the electron carriers NADH or $FADH_2$, respectively, to reduce the electron carrier ubiquinol. In the process, CI pumps protons

across the IMM whereas CI does not. Complex III (CIII) and Complex IV (CIV) then catalyze the electron transfer from ubiquinol to cytochrome c and from cytochrome c to oxygen, respectively, to produce water and pump protons. Protons in the IMS can then re-enter the matrix through the F_1F_0 ATPase, also known as Complex V (CV), where the energy generated from protons flowing down a concentration gradient is harnessed to phosphorylate ADP to produce ATP, termed oxidative phosphorylation. The majority of proton re-entry is coupled to ATP production, however, alternative routes of re-entry exist that bypass CV, such as uncoupling proteins to produce heat or the nicotinamide nucleotide transhydrogenase to replenish the NADPH pool for biosynthetic processes (Figure 1-2).

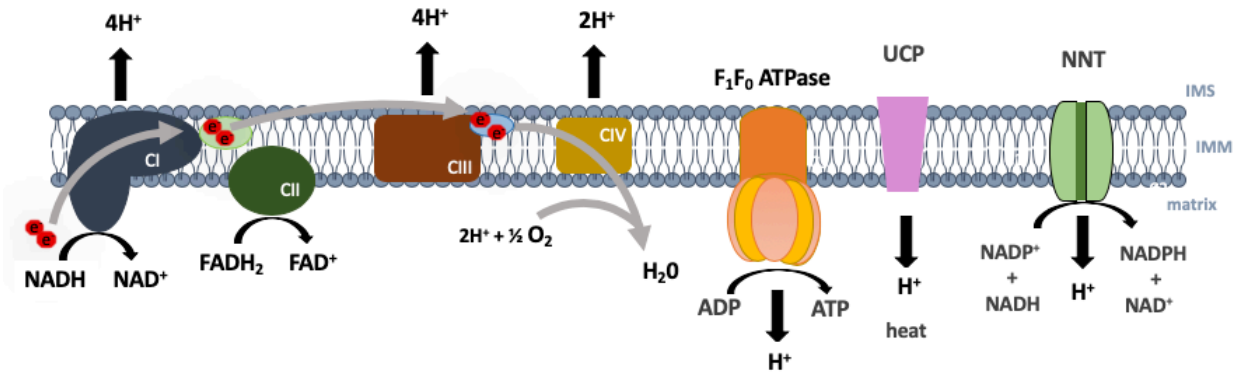

Figure 1-2. The electron transport chain and generation of the electrochemical gradient. The electron transport chain (ETC) consists of four transmembrane protein complexes (CI-CIV) and two electron transfer carriers, ubiquinone and cytochrome c. The electron donors, NADH and $FADH_2$, are oxidized by Complex I (CI) or Complex II (CII), respectively, to reduce the first electron carrier ubiquinone to ubiquinol. Although both CI and CII transport electrons, CI also pumps four protons into the IMS while CII does not pump protons. Complex III (CIII) catalyzes the transfer of electrons from the first electron carrier to the second (ubiquinol to cytochrome c) and pumps four protons into the IMS. Complex IV (CIV) catalyzes the transfer of electrons from cytochrome c to the terminal electron carrier oxygen to produce water and pumps protons. In normal physiological conditions, proton re-entry into the matrix largely occurs through the F_1F_0 ATPase, coupling the electrochemical gradient to ATP production. However, there are alternative re-entry points that are uncoupled from ATP production, such as uncoupling proteins (UCPs) to produce heat and the nicotinamide nucleotide transhydrogenase (NNT) to replenish NAPDH pools for biosynthetic processes and reactive oxygen species scavenging.

Although ETC complexes are routinely simplified as linear complexes in numerical order with a 1:1 ratio of complexes, their stoichiometry varies considerably (Schagger and Pfeiffer, 2001). Within the IMM folds, or cristae, complexes can be found as freely floating or in super-assembled structures known as supercomplexes. In mammalian cells, supercomplexes are largely composed of a combination of CI, CIII, and CIV, whereas the contribution of CII and CV to the formation of supercomplexes remains poorly understood (Acin-Perez et al., 2008). Their formation, although not comprehensively understood, have been suggested to play a role in complex stability (Acin-Perez et al., 2004; Diaz et al., 2006), electron transport efficiency (Bianchi et al., 2004), and control of ROS production (Ghelli et al., 2013; Maranzana et al., 2013). Interestingly, supercomplex formation varies with exercise (Greggio et al., 2017), indicating supercomplexes may be an adaptive mechanism to meet increased energy demands.

In skeletal muscle, mitochondria are quite responsive to a range of intermittent and continuous stimuli including exercise (Menshikova et al., 2006), nutritional factors (Mishra et al., 2015), aging (Coggan et al., 1992; Cooper et al., 1992; Short et al., 2005), and disease (Simoneau et al., 1995; Mootha et al., 2003; Patti et al., 2003) to name a few. Mitochondrial adaptations include the ability to alter their abundance, ETC activity (oxidative capacity), coupling, and structure. Of those, the most rapid and fluid response is the alteration of structure (Eisner et al., 2014), which allows for dynamic mitochondrial remodeling to adapt to the cellular environment (Glancy et al., 2015). Mitochondrial dynamics are a coalition of fusion and fission events that are important for mitochondrial biogenesis, stress mitigation, and quality control by enabling the removal of damaged mitochondria (mitophagy; Figure 1-3). Fusion is mediated by mitofusion proteins (Mfn1 and Mfn2) and optic atrophy protein 1 (Opa1) to fuse the inner and outer mitochondrial membranes, respectively (Koshiba et al., 2004; Meeusen et al., 2004; Meeusen et

al., 2006; Song et al., 2009). Deletion of Mfn1 and Mfn2 in skeletal muscle decreases oxidative capacity, reduces mitochondrial DNA abundance (mtDNA), reduces muscle mass, and eventually leads to lethality (Chen et al., 2010). On the other hand, fission events require the translocation of dynamin-related protein 1 (Drp1) from the cytosol to wrap around the outer membrane and cleave it (Ji et al., 2015; Kalia et al., 2018; Fonseca et al., 2019). Although there are other proteins involved in fission, loss of Drp1 inhibits fission and results in hyperfusion of mitochondria (Fonseca et al., 2019). Skeletal muscle specific ablation of Drp1 results in muscle atrophy, altered mitochondrial morphology, and impaired mitochondrial respiration (Favaro et al., 2019). Together, the maintenance of proper mitochondrial fusion and fission is essential for skeletal muscle homeostasis.

Mitochondrial dynamics also permit a fluid response to changing nutritional factors. Muscle cells isolated from the extensor digitorum longus (EDL) incubated in media containing acetoacetate for 24 hours, an oxidative substrate, have greater connectivity than those treated with glucose for the same amount of time. As a result, elongated mitochondrial networks are predominant in oxidative fibers and have high rates of fusion, whereas a greater proportion of punctate mitochondria are found in glycolytic fibers (Mishra et al., 2015). Moreover, in conditions of nutrient deprivation, mitochondria elongate by downregulating fission events to protect against mitophagy and maximize energy production (Gomes et al., 2011). Collectively, the rate of fusion and fission events determine mitochondrial interconnectivity and permit dynamic metabolic adaptations.

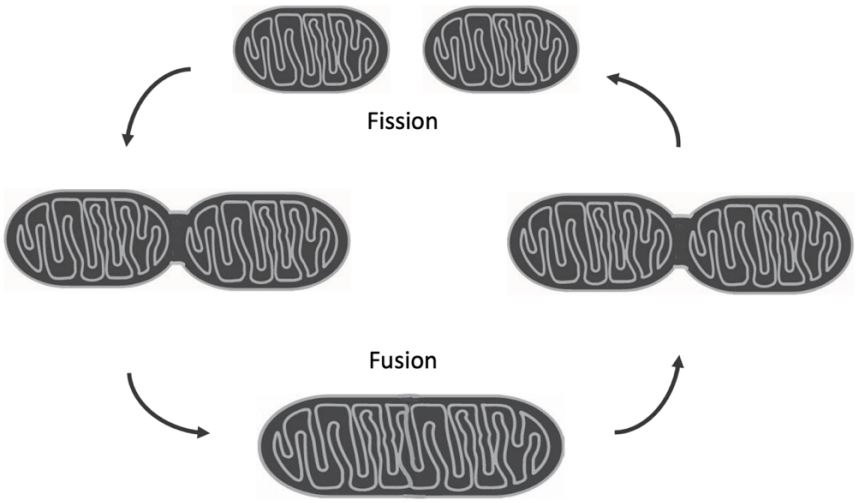

Figure 1-3. An overview of mitochondrial dynamics. Skeletal muscle mitochondria form a dynamic network that is constantly adapting to changing external and internal stimuli. Punctate mitochondria can fuse together to form an interconnected network permitting an increase in oxidative capacity, dispersal of mitochondrial damage to promote survival, or an exchange of mitochondrial content (mtDNA and metabolites). Contrarily, mitochondria can undergo fission to remove damaged mitochondria through mitophagy, facilitate mitochondrial trafficking, or adapt to metabolic changes.

Mitochondria are also a key regulator of cytosolic free Ca^{2+}concentrations and Ca^{2+}-mediated signaling (Nicholls, 1978; Nicholls and Scott, 1980). Calcium enters the matrix through the mitochondrial calcium uniporter (MCU) (Baughman et al., 2011; De Stefani et al., 2011) and Ca^{2+} efflux is mediated by the $Na^{+}/Ca2^{+}$ exchanger (NCLX). The ability of mitochondria to sequester Ca^{2+} is pivotal in skeletal muscle glucose oxidation (Gherardi et al., 2019), substrate utilization (Kwong et al., 2018), and activation of several TCA enzymes (McCormack and Denton, 1979; McCormack et al., 1990; McCormack and Denton, 1993). Deletion of the MCU, and therefore the majority of mitochondrial Ca^{2+} uptake, in skeletal muscle induces atrophy, impairs glucose oxidation, and alters substrate preference (Mammucari et al., 2015; Kwong et al., 2018; Gherardi et al., 2019). Contrarily, MCU overexpression results in profound skeletal muscle hypertrophy through the activation of PGC-1α and PI 3-kinase/Akt pathway (Mammucari et al.,

2015) highlighting the importance of mitochondrial Ca^{2+} signaling in the regulation of skeletal muscle mass.

Regulators of skeletal muscle growth and metabolism

Skeletal muscle growth is orchestrated by a hierarchy of complex anabolic and catabolic biological processes that dictate the rate of protein accretion. Skeletal muscle is composed of a heterogenous population of muscle cells (myofibers) with varying metabolic characteristics and rates of myofibrillar, mitochondrial, and sarcoplasmic protein turnover. Myofibers can be classified according to predominate type of energy metabolism (glycolytic or oxidative metabolism) and speed of contraction (fast or slow). Slow-twitch muscle fibers have a greater rate of protein synthesis than fast-twitch fibers which can be attributed to duration of contraction and mitochondrial abundance, as mitochondrial proteins have higher fractional synthesis rates than myofibrillar proteins (Jaleel et al., 2008). However, slow fibers also have high rates of protein degradation, presumably due to a high mitochondrial content prone to damage from reactive oxygen species, that has a net result of low rates of protein accretion (Lewis et al., 1984) and relatively small fiber size. Therefore, metabolism is a contributing factor to muscle accretion rate and can be exploited to manipulate growth rate and efficiency of substrate utilization.

The two major regulatory pathways of protein accretion are the insulin-like growth factor 1 (IGF-1) / phosphoinositide-3-kinase-Akt (PI 3-kinase-Akt) / protein kinase B (PKB) / mammalian target of rapamycin (mTOR) pathway and the myostatin pathway, which are respective positive and negative regulators of protein synthesis. Binding of IGF-1 to its receptor activates PI 3-kinase, which phosphorylates phosphoinositide-4,5-biphosphate (PIP2) generating phosphoinositide-3,4,5-triphosphate (PIP3) to act as a docking site for phosphoinositide-dependent kinase 1 (PDK1) to activate Akt. Activation of Akt inhibits protein degradation through

the repression of the forkhead box protein (FOXO) family of transcription factors and stimulates protein synthesis through the activation of mTOR and glycogen synthase kinase 3β (GSK3β). In skeletal muscle, loss of the IGF-1 receptor induces muscle atrophy (Mavalli et al., 2010), whereas IGF-1 overexpression stimulates hypertrophy (Coleman et al., 1995; Musaro et al., 2001; Fiorotto et al., 2003). Similarly, the activation of its downstream target Akt in skeletal muscle induces profound hypertrophy (Lai et al., 2004; Blaauw et al., 2009), whereas deletion of the downstream target mTOR results in impaired postnatal growth and development of severe myopathy (Risson et al., 2009). Activation of the IGF-1 pathway and its downstream targets are required for efficient myogenesis and muscle hypertrophy.

On the other hand, myostatin is a negative regulator of muscle growth. Natural mutations of the myostatin gene have been discovered in in sheep (Clop et al., 2006), cattle (Grobet et al., 1997; McPherron and Lee, 1997), dogs (Mosher et al., 2007), and humans (Schuelke et al., 2004) that result in gene disruption and a subsequent increase in muscle mass. In mice, myostatin deletion results in a 2-fold increase in muscle mass and decreased adipose tissue deposition (McPherron and Lee, 2002; Hamrick et al., 2006), whereas overexpression of myostatin in skeletal muscle results in a reduction of muscle mass (Reisz-Porszasz et al., 2003). Myostatin and IGF-1 have a dynamic interplay that modulates muscle accretion through “tips and balances” between the two pathways. The PI3K/Akt axis is common to both pathways and permits cross-talk, which is essential to normal muscle growth and physiology. Overexpression of myostatin downregulates Akt/mTOR signaling and subsequently decreases protein synthesis (Amirouche et al., 2009). Contrarily, myostatin deletion increases PKB and mTOR activity (Lipina et al., 2010), although presence of the IGF-1 receptor is necessary for efficient hypertrophy (Kalista et al., 2012).

While proper myostatin and IGF-1 cross-talk is essential for muscle growth and maintenance, just as important is the maintenance of metabolic homeostasis. Highly integrated signaling pathways that are tightly coupled to nutrient availability and cellular energy status are responsible for regulating muscle metabolism and protein turnover. The intracellular energy sensor 5'-adenosine monophosphate-activated protein kinase (AMPK) dynamically regulates muscle metabolism by relaying signals of energetic stress. As ATP is hydrolyzed, AMP levels rise and decrease the ATP:AMP ratio to activate AMPK, which promotes catabolic processes and suppresses anabolic processes to replenish ATP stores. As such, activation of AMPK decreases protein synthesis, an anabolic process, demonstrated by a 45% decrease in skeletal muscle fractional rate of protein synthesis one hour after injection of the AMPK activating drug AICAR (Bolster et al., 2002). AMPK activation decreases protein accretion rates by suppressing mTOR activity and activating FOXO and uncoordinated 51-like kinase 1 (ULK1), regulators of the autophagy pathway (Lee et al., 2010; Kim et al., 2011). Mutation of the AMPKγ3 subunit in mice (Garcia-Roves et al., 2008) and pigs (Scheffler et al., 2014) results in constitutive activation of AMPK, which increases mitochondrial biogenesis and enhances oxidative capacity of glycolytic muscle. Surprisingly, its chronic activation does not impact muscle growth (Carr et al., 2006), which may be attributed to a compensatory or adaptive mechanism that can override the negative regulation of AMPK on protein synthesis. In fact, Scheffler et al. (2014) found the AMPKγ3^{R200Q} mutant pigs had an increase in Akt expression, a positive regulator of muscle growth that may account for the normal growth of these pigs. Nonetheless, skeletal muscle-specific double knockout of AMPKα1 and AMPKα2 increased soleus muscle mass (Lander et al., 2010), which implicates AMPK as a regulator of muscle mass. As a result, the AMPK pathway has become a target to counteract metabolic disorders without negatively impacting muscle mass, as an increase

in oxidative capacity enhances the ability of muscle to combat energetic stress providing protection against muscle wasting and metabolic diseases (Conley et al., 2000; Wang et al., 2004; Wenz et al., 2008; Wenz et al., 2009; Ljubicic et al., 2011).

Nutrient Sensing in Skeletal Muscle

Muscle cells can perceive cellular energy status and substrate availability, and as such, muscle is a plastic tissue that permits metabolic adaptations to environmental changes. During times of nutrient surplus, such as those after feeding, muscle can "sense" the availability of substrates and increase protein accretion. Conversely, periods of scarcity results in repartition of nutrients away from anabolic processes. The dynamic post-translational modification O-linked-β-D-N-acetylglucosamine (O-GlcNAc) serves as a widespread nutrient gauge by cycling on and off O-linked N-acetylglucosamine (O-GlcNAc) moieties to serine and threonine residues of nuclear, cytosolic, and mitochondrial proteins (Hanover et al., 2012). The donor substrate, uridine diphosphate N-acetylglucosamine (UDP-GlcNAc), is a product of the hexosamine biosynthetic pathway (HBP) and its levels reflect the collective cellular nutrient flux by incorporating nucleotide, carbohydrate, lipid, and protein metabolism. A pair of enzymes, O-GlcNAc transferase (OGT) and O-GlcNAcase (OGA), are responsible for the respective addition and removal of O-GlcNAc from target proteins to modify their function to adapt to cellular nutrient abundance. Collectively, this post-translational modification acts as a nutrient sensing pathway because levels of UDP-GlcNAc, and thus O-GlcNAcylation, correspond to cellular nutrient status (Walgren et al., 2003; Housley et al., 2008; Kang et al., 2008).

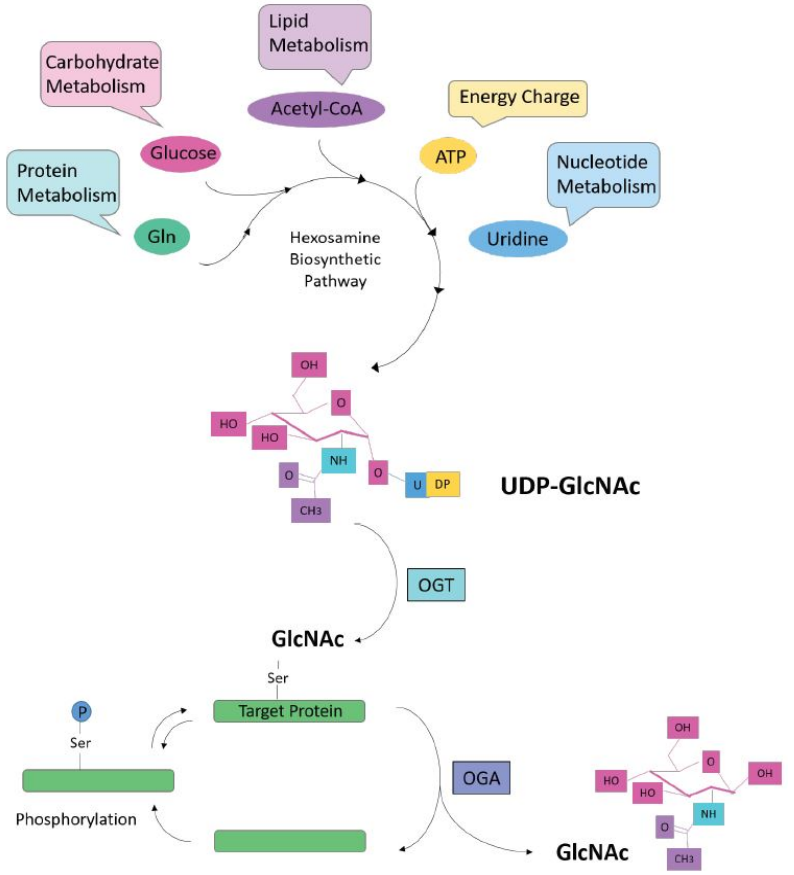

Figure 1-4. O-GlcNAc signaling pathway. Figure modified from Hanover et al. (2012). The hexosamine biosynthetic pathway incorporates metabolites from protein, carbohydrate, lipid, energy, and nucleotide metabolism to synthesize UDP-GlcNAc, which fluctuates with cellular nutrient status. O-GlcNAc transferase (OGT) transfers UDP-GlcNAc to any of its thousands of target proteins and O-GlcNAcase (OGA) removes the O-GlcNAc moiety, known as O-GlcNAcylation, to modulate protein function. O-GlcNAcylation occurs in a similar manner to phosphorylation and may be as widespread, but O-GlcNAcylation patterns correlate to cellular nutrient status and is only mediated through the enzymes OGT and OGA.

A single gene encodes OGT, however, three isoforms originate from alternative splicing. The two predominant isoforms are nucleocytoplasmic OGT (ncOGT) and mitochondrial OGT (mOGT), which contains an N-terminal mitochondrion targeting sequence. A short isoform of OGT exists, but its functionality remains largely unclear. Until recently, global cellular O-GlcNAcylation has been largely accredited to ncOGT; however, Banerjee et al. (2015) showed the pyrimidine nucleotide carrier transports UDP-GlcNAc into the matrix and blocking this transporter

lowers mitochondrial O-GlcNAcylation, which suggests robust O-GlcNAc cycling occurs within mitochondria. Sacoman and colleagues (2017) were able to knockdown cellular OGT and mOGT in HeLa cells by targeting unique sequences of the splice variants. Knockdown of mOGT altered mitochondrial content, function, and membrane potential, however, knockdown of both mOGT and ncOGT increased mitochondrial content and restored membrane potential. These data suggest cross-talk between the two isoforms of OGT exist to mediate mitochondrial integrity and function, yet its relation to nutrient status remains elusive.

Several metabolic enzymes are targets of O-GlcNAcylation. Phosphofructokinase-1 (PFK), a rate-limiting glycolytic enzyme, is inhibited by O-GlcNAcylation resulting in the redirection of glucose to the pentose phosphate pathway (PPP) in cancer cells (Yi et al., 2012). O-GlcNAcylation of glucose-6-phosphate dehydrogenase (G6PD), the rate limiting enzyme of the PPP, increases its activity and glucose flux through the PPP in lung cancer cells (Rao et al., 2015). Prolonged exposure of cells to glucose enhances cellular O-GlcNAcylation and subsequently increases glycolytic flux (Marshall et al., 1991; Hanover et al., 1999; Bond and Hanover, 2015). In cardiomyocytes, Hu and colleagues (Hu et al., 2008) reported several subunits of the electron transport chain are O-GlcNAcylated in high glucose conditions, which decrease complex activity and mitochondrial respiration (Hu et al., 2009). Interestingly, removal of O-GlcNAcylation in high glucose conditions restores mitochondrial function to that of cells exposed to normal glucose. These data show that elevated glucose availability signals an increase in O-GlcNAcylation of key regulatory protens to modulate metabolism.

Glucose and glutamine are both considered rate limiting in the hexosamine biosynthetic pathway, and as such are potent stimulators of UDP-GlcNAc synthesis and thus O-GlcNAcylation (Walgren et al., 2003; Swamy et al., 2016). Excess free fatty acids also increase UDP-GlcNAc

levels in rat skeletal muscle, although the subsequent glucose uptake and handling are markedly different than that stimulated by excess glucose (Hawkins et al., 1997b). Hawkins and colleagues (1997) suggested a mechanism in which an increase in acetyl-CoA decreases the rate of pyruvate oxidation and inhibits PFK by an accumulation of tricarboxylic acid intermediates. Unfortunately, further investigation into these findings have been neglected, and the fundamentals of fatty acids in O-GlcNAcylation remain poorly defined. However, these data show UDP-GlcNAc levels increase in response to several nutrients and their downstream metabolic adaptations vary uniquely.

O-GlcNAcylation has been well documented in skeletal muscle and has emerged to have an important role in maintaining proper skeletal muscle glucose handling and insulin sensitivity. As skeletal muscle is the largest metabolically active tissue in the body and is responsible for the majority of insulin-mediated glucose disposal, skeletal muscle O-GlcNAcylation has become a key player in global metabolism. Early investigations in muscle suggested a correlation between nutrient abundance and insulin resistance in rodents. Indeed, overexpression of GLUT4 in skeletal muscle results in chronic exposure of muscle to glucose, which is accompanied by greater UDP-GlcNAc levels and the development of insulin resistance in mice (Buse et al., 1996). Further, prolonged fatty acids and uridine exposure increase UDP-GlcNAc levels and reduce skeletal muscle insulin sensitivity (Hawkins et al., 1997a; Hawkins et al., 1997b). Contrarily, ablation of OGT, and thus O-GlcNAcylation, in skeletal muscle protects mice from high fat diet induced obesity and insulin resistance (Shi et al., 2018). Collectively, these data document the existence of intact hexamine biosynthesis signaling and O-GlcNAcylation in muscle and strongly argue that O-GlcNAcylation is part of the complex nutrient sensing machinery that is critical for skeletal muscle metabolism and global health.

Skeletal Muscle as an Endocrine Organ

Skeletal muscle is one of the largest tissues in the body responsible for 70-90% of insulin-mediated glucose disposal making it a major contributor to global metabolism (DeFronzo et al., 1981; Shulman et al., 1990; Watt et al., 2006; Bostrom et al., 2012; Funai et al., 2013; Song et al., 2013). As such, modulation of skeletal muscle metabolism (Izumiya et al., 2008; Meng et al., 2013) and insulin sensitivity (Song et al., 2013) has been proven to be an effective means of alleviating metabolic disorders. Further, muscle is also able to secrete cytokines, known as myokines, to elicit endocrine and paracrine effects on other tissues in the body. Following the discovery of interleukin-6 as a myokine, research uncovering other myokines surged in attempt to find new therapeutic approaches to metabolic diseases. The myokine interleukin-15 (IL-15) was discovered in 1994 due to its structural similarities to interleukin-2 (IL-2) (Grabstein et al., 1994) and has since emerged as a potent anti-obesity myokine.

Signaling and secretion of IL-15 occurs in a unique manner relying on the formation of complexes with its high-affinity receptor, interluekin-15 receptor alpha (IL-15rα). Co-expression of IL-15 and IL15rα results in high levels of IL-15 protein within the cell and culture media; however, expression of IL-15 alone resulted in low levels of IL-15 expression and an impaired ability to translocate to the cell membrane (Bergamaschi et al., 2008). Therefore, complexing of IL-15 and IL-15rα increases stabilty, secretion, and bioavaliabilty of IL-15 (Rubinstein et al., 2006; Stoklasek et al., 2006; Bergamaschi et al., 2008). Global knockout of IL-15rα increased muscle oxidative enzymes and reduced adipose tissue mass, initially suggesting IL-15rα is not necessary for effective IL-15 secretion and modulation of global metabolism (Pistilli et al., 2011). However, muscle-specific ablation of IL-15rα did not decrease body weight or fat mass and had minimal impact on muscle oxidative enzymes (O'Connell et al., 2015). The reported differences

in muscle and whole-body metabolism between the global and muscle specific knockout may be attributed to the global knockout lacking IL-15rα in the central nervous system. IL-15 can cross the blood-brain barrier (Wu et al., 2010b) and modulation of IL-15/IL-15rα impacts behavior including sleep patterns (Kubota et al., 2001), anxiety behavior pathways (Wu et al., 2010a), and antidepression pathways (Wu et al., 2011), which highlights the profound impacts of central nervous system IL-15 on the body. The muscle-specific deletion of IL-15rα therefore defined its importance in modulating muscle and global metabolism (O'Connell et al., 2015), presumably through the stabilization and secretion of muscle IL-15.

The IL-15 gene encodes for two isoforms that produce identical proteins but have different signal sequences. The long signal peptide isoform (LSP-IL15) harbours an ineffecient secretory signal peptide and the short signal peptide isoform (SSP-IL15) is stored intracellularly in the nucleus and cytoplasm (Tagaya et al., 1997). Replacement of the natural LSP with the efficient secratory signal peptide of IL-2, driven by human skeletal actin promoter, greatly increased IL-15 expression in skeletal muscle and circulation, which resulted in a profound reduction in fat mass with minimal impact on muscle mass (Quinn et al., 2009).

Prolonged stimulation of muscle by IL-15 evokes profound changes in muscle metabolism and reduces adipositiy. Conversely, mice lacking a functional *Il15* gene are obese (Barra et al., 2010). Treatment of muscle with IL-15 increased skeletal muscle glucose uptake and GLUT4 expression (Busquets et al., 2006), suggesting skeletal muscle IL-15 amelorates insulin sensitivity. Further, admininstration of IL-15 to rat muscle for 7 days decreased white fat 33% and circulating trigylcerides 20% (Carbo et al., 2001), indicating muscle IL-15 may augment insulin sensitivity through an increase in fatty acid metabolism and oxidative capacity. Indeed, overexpression of skeletal muscle IL-15 increases PGC1α, SIRT1, and UCP2 expression (Quinn et al., 2013), all

highly indicative of a shift to a more oxidative phenotype. Additionally, respiratory control ratio decreased in mice overexpressing skeletal muscle IL-15 (Quinn et al., 2013), which is consistent with a shift to preferentially utilize fatty acids as a lipid source rather than glucose. While IL-15 has little effect on skeletal muscle accretion (Quinn et al., 2009; Pistilli and Quinn, 2013), it mobilizes energy substrates from other tissue repositiories to support its needs and subsequently improve whole body metabolism.

Metabolic and Nutritional Regulation of Satellite Cells

Adult skeletal muscle contains a heterogeneous population of stem cells, known as satellite cells (SCs), that contribute to postnatal muscle growth, maintenance, and repair (Mauro, 1961; Moss and Leblond, 1971; Kuang et al., 2007; Lepper et al., 2011). Adult SCs are predominately in a quiescent state and can activate to support several rounds of proliferation before undergoing self-renewal or terminal differentiation (Schultz et al., 1978; Snow, 1978). Orchestration of these behaviors are tightly synchronized by integrated signaling cascades that relay unfolding intrinsic and extrinsic stimuli.

Intrinsically, metabolic reprogramming is a strong regulator of SC behavior, during which metabolic shifts occur to accommodate demands of different growth stages. Quiescent SCs have a relatively low metabolic rate but can be separated into two distinct metabolic populations. The population with a lower metabolic rate has a delayed cell cycle entry, a slower mitotic rate, and are less transcriptionally primed for myogenic commitment. Contrarily, the population with higher metabolic activity are more responsive to activation (Rocheteau et al., 2012). Once activated, SCs begin to proliferate, accompanied by an increase in glycolysis and glutaminolysis to meet energy demands and support macromolecule biosynthesis, which is essential for proliferating cells (Lunt and Vander Heiden, 2011). Within 48 hrs of differentiation, mitochondrial content and oxidative

capacity increase to shift to a more oxidative metabolism (Moyes et al., 1997; Remels et al., 2010). Disruption of this shift through inhibition of mitochondrial protein synthesis (Korohoda et al., 1993; Hamai et al., 1997; Rochard et al., 2000), mitochondrial fission (Bloemberg and Quadrilatero, 2016), mitochondrial DNA replication (Brunk and Yaffe, 1976; Herzberg et al., 1993), or inhibition of OxPhos confines myoblast to a proliferative, single cell state and obstructs myoblast differentiation.

Glucose oxidation is also required for efficient myogenic differentiation and preventing glucose entry into the TCA cycle through deletion of pyruvate dehydrogenase inhibits differentiation (Hori et al., 2019). Glucose restriction in myoblasts activates AMPK-activated protein kinase (AMPK) (Fulco et al., 2008), a cellular sensor of metabolic stress regulated by changes in AMP and ATP levels. Activation of AMPK with the drug AICAR reduces G1/S cell cycle progression and inhibits myotube formation (Williamson et al., 2007). On the other hand, deletion of AMPKα1 in SCs impairs adult regenerative myogenesis, and SCs lacking AMPKα1 transplanted into WT muscles have a diminished myogenic capacity (Fu et al., 2016). In addition to impaired regeneration, these cells proliferate more slowly in culture (Fu et al., 2015), which was attributed to the loss of AMPK obstructing Warburg-like glycolysis. In proliferating cells, an increase in Warburg-like glycolysis is stimulated by AMPK through a decrease in ATP to ADP ratios to support proliferation, whereas non-proliferating cells have a higher ratio of ATP to ADP accompanied by greater mitochondrial function (Maldonado and Lemasters, 2014). Collectively, these findings highlight the importance of AMPK translating cellular energy status to modulate myoblast metabolism for efficient myogenic progression.

Extrinsically, conditions of nutrient excess or scarcity are also perceived by SCs and alter their behavior accordingly. High circulating levels of amino acids promote SC lineage progression

through the mTOR pathway (Dai et al., 2015), a cellular nutrient sensor that regulates protein synthesis rates. For example, supplementation of lysine, the first limiting amino acid in high carbohydrate diets (Li et al., 2012; Zeng et al., 2013), increases mTOR activity, which suppress proteolysis through the autophagic-lysosomal system (Sato et al., 2014) and increases SC proliferation (Jin et al., 2019). Further, leucine supplementation promotes proliferation, differentiation, and skeletal muscle regeneration through the mTORC1 pathway (Pereira et al., 2014; Dai et al., 2015), and leucine restriction inhibitions differentiation (Averous et al., 2012). Inhibition of mTOR in myoblasts cultured in high leucine concentrations decreases proliferative capacity and protein synthesis (Han et al., 2008). Further, disruption of this nutrient sensing through the conditional deletion of mTOR in adult satellite cells impairs SC proliferation, differentiation, and muscle regeneration (Zhang et al., 2015). Collectively, these findings show the mTOR pathway is essential to translate fluctuations in nutrient abundance to modulate myoblast behavior. In addition to promoting protein synthesis to support myogenesis, mTOR also regulates myogenesis through the expression of several myogenic regulatory factors including Myf5 and MyoD (Averous et al., 2012; Hatfield et al., 2015; Zhang et al., 2015), which play a role in SC activation and transient proliferation (Braun et al., 1992; Rudnicki et al., 1992; Ustanina et al., 2007), and myogenin, which is required for terminal myoblast differentiation (Hasty et al., 1993; Nabeshima et al., 1993). Collectively, these findings demonstrate the necessity of adequate nutrients and mTOR activation for proper SC function.

On the other hand, overfeeding or excessive substrate availability negatively impacts SC function (Peterson et al., 2008; D'Souza et al., 2015; Fausnacht et al., 2020). For example, high levels of glucose inhibits myogenic differentiation (Grzelkowska-Kowalczyk et al., 2013) and induces insulin resistance in C2C12 myotubes, which is accompanied by a decrease in Akt

phosphorylation (Luo et al., 2019). Activation of the PI3K/Akt pathway is essential for efficient glucose uptake, and pharmacological activation of Akt rescues myogenic differentiation in cells exposed to high glucose (Luo et al., 2019), whereas inhibition of PI3K (Tureckova et al., 2001) or Akt (Luo et al., 2019) recapitulates the high glucose phenotype and inhibits differentiation. These findings demonstrate the PI3K/Akt pathway can "sense" changes in nutrient concentrations to alter SC behavior. Alternatively, short-term calorie restriction improves SC function and increases oxidative metabolism (Cerletti et al., 2012). However, discrepancies in the effectiveness and response to caloric restriction have been reported in regards to sex, age, and length of restriction (Boldrin et al., 2017; Abreu et al., 2020).

Summary

Improvements in skeletal muscle metabolism and insulin sensitivity enhances whole-body metabolism and can ameliorate metabolic diseases. Skeletal muscle plasticity is contingent upon highly integrated signaling cascades that sense and respond to intrinsic changes in energy status and extrinsic nutritional cues. Elucidation of these signaling cascades will provide novel therapeutic targets to regulate skeletal muscle metabolism and alleviate a multitude of metabolic disorders. Specifically, greater oxidative capacity increases glucose clearance rates, fatty acid oxidation, and resting metabolic rate (Zampino et al., 2020), which provides substantial protection against metabolic disorders. However, it is important to consider the consequences on muscle mass, as oxidative muscles have lower rates of protein accretion and therefore a smaller size. In contrast, glycolytic metabolism permits greater hypertrophy as glycolytic substrates can "branch off" as anabolic intermediates for biosynthetic processes, whereas oxidative substrates are metabolized in the tricarboxylic acid cycle which expels carbon, a counterproductive exchange. Although glycolytic metabolism permits greater hypertrophy, diminished muscle oxidative

capacity is detrimental to whole-body metabolism. Nonetheless, enhanced muscle oxidative capacity can be accompanied by hypertrophy (Scheffler et al., 2014). Therefore, a deeper understanding of the nutrient responsive pathways, such as O-GlcNAcylation and the PI 3-kinase/Akt/mTOR pathway, that dictate skeletal muscle metabolism and growth will empower scientist to improve quality of life and ameliorate metabolic disorders.

References

Abreu, P., J. D. C. Serna, A. C. Munhoz, and A. J. Kowaltowski. 2020. Calorie restriction changes muscle satellite cell proliferation in a manner independent of metabolic modulation. Mech Ageing Dev 192:111362. doi: 10.1016/j.mad.2020.111362

Acin-Perez, R., M. P. Bayona-Bafaluy, P. Fernandez-Silva, R. Moreno-Loshuertos, A. Perez-Martos, C. Bruno, C. T. Moraes, and J. A. Enriquez. 2004. Respiratory complex III is required to maintain complex I in mammalian mitochondria. Mol Cell 13(6):805-815. doi: 10.1016/s1097-2765(04)00124-8

Acin-Perez, R., P. Fernandez-Silva, M. L. Peleato, A. Perez-Martos, and J. A. Enriquez. 2008. Respiratory active mitochondrial supercomplexes. Mol Cell 32(4):529-539. doi: 10.1016/j.molcel.2008.10.021

Ahn, C. S., and C. M. Metallo. 2015. Mitochondria as biosynthetic factories for cancer proliferation. Cancer Metab 3(1):1. doi: 10.1186/s40170-015-0128-2

Amirouche, A., A. C. Durieux, S. Banzet, N. Koulmann, R. Bonnefoy, C. Mouret, X. Bigard, A. Peinnequin, and D. Freyssenet. 2009. Down-regulation of Akt/mammalian target of rapamycin signaling pathway in response to myostatin overexpression in skeletal muscle. Endocrinology 150(1):286-294. doi: 10.1210/en.2008-0959

Aon, M. A., S. Cortassa, and B. O'Rourke. 2010. Redox-optimized ROS balance: a unifying hypothesis. Biochim Biophys Acta 1797(6-7):865-877. doi: 10.1016/j.bbabio.2010.02.016

Arnold, D. L., P. M. Matthews, and G. K. Radda. 1984. Metabolic recovery after exercise and the assessment of mitochondrial function in vivo in human skeletal muscle by means of 31P NMR. Magn Reson Med 1(3):307-315. doi: 10.1002/mrm.1910010303

Averous, J., J. C. Gabillard, I. Seiliez, and D. Dardevet. 2012. Leucine limitation regulates myf5 and myoD expression and inhibits myoblast differentiation. Exp Cell Res 318(3):217-227. doi: 10.1016/j.yexcr.2011.10.015

Banerjee, P. S., J. Ma, and G. W. Hart. 2015. Diabetes-associated dysregulation of O-GlcNAcylation in rat cardiac mitochondria. Proc Natl Acad Sci U S A 112(19):6050-6055. doi: 10.1073/pnas.1424017112

Barra, N. G., S. Reid, R. MacKenzie, G. Werstuck, B. L. Trigatti, C. Richards, A. C. Holloway, and A. A. Ashkar. 2010. Interleukin-15 contributes to the regulation of murine adipose tissue and human adipocytes. Obesity (Silver Spring) 18(8):1601-1607. doi: 10.1038/oby.2009.445

Battistuzzi, G., M. D'Urso, D. Toniolo, G. M. Persico, and L. Luzzatto. 1985. Tissue-specific levels of human glucose-6-phosphate dehydrogenase correlate with methylation of specific sites at the 3' end of the gene. Proc Natl Acad Sci U S A 82(5):1465-1469. doi: 10.1073/pnas.82.5.1465

Baughman, J. M., F. Perocchi, H. S. Girgis, M. Plovanich, C. A. Belcher-Timme, Y. Sancak, X. R. Bao, L. Strittmatter, O. Goldberger, R. L. Bogorad, V. Koteliansky, and V. K. Mootha. 2011. Integrative genomics identifies MCU as an essential component of the mitochondrial calcium uniporter. Nature 476(7360):341-345. doi: 10.1038/nature10234

Bergamaschi, C., M. Rosati, R. Jalah, A. Valentin, V. Kulkarni, C. Alicea, G. M. Zhang, V. Patel, B. K. Felber, and G. N. Pavlakis. 2008. Intracellular interaction of interleukin-15 with its receptor alpha during production leads to mutual stabilization and increased bioactivity. J Biol Chem 283(7):4189-4199. doi: 10.1074/jbc.M705725200

Bianchi, C., M. L. Genova, G. Parenti Castelli, and G. Lenaz. 2004. The mitochondrial respiratory chain is partially organized in a supercomplex assembly: kinetic evidence using flux control analysis. J Biol Chem 279(35):36562-36569. doi: 10.1074/jbc.M405135200

Blaauw, B., M. Canato, L. Agatea, L. Toniolo, C. Mammucari, E. Masiero, R. Abraham, M. Sandri, S. Schiaffino, and C. Reggiani. 2009. Inducible activation of Akt increases skeletal muscle mass and force without satellite cell activation. FASEB J 23(11):3896-3905. doi: 10.1096/fj.09-131870

Bloemberg, D., and J. Quadrilatero. 2016. Effect of mitochondrial fission inhibition on C2C12 differentiation. Data Brief 7:634-640. doi: 10.1016/j.dib.2016.02.070

Bohovych, I., and O. Khalimonchuk. 2016. Sending Out an SOS: Mitochondria as a Signaling Hub. Front Cell Dev Biol 4:109. doi: 10.3389/fcell.2016.00109

Boldrin, L., J. A. Ross, C. Whitmore, B. Doreste, C. Beaver, A. Eddaoudi, D. J. Pearce, and J. E. Morgan. 2017. The effect of calorie restriction on mouse skeletal muscle is sex, strain and time-dependent. Sci Rep 7(1):5160. doi: 10.1038/s41598-017-04896-y

Bolster, D. R., S. J. Crozier, S. R. Kimball, and L. S. Jefferson. 2002. AMP-activated protein kinase suppresses protein synthesis in rat skeletal muscle through down-regulated mammalian target of rapamycin (mTOR) signaling. J Biol Chem 277(27):23977-23980. doi: 10.1074/jbc.C200171200

Boncompagni, S., A. E. Rossi, M. Micaroni, G. V. Beznoussenko, R. S. Polishchuk, R. T. Dirksen, and F. Protasi. 2009. Mitochondria are linked to calcium stores in striated muscle by developmentally regulated tethering structures. Mol Biol Cell 20(3):1058-1067. doi: 10.1091/mbc.E08-07-0783

Bond, M. R., and J. A. Hanover. 2015. A little sugar goes a long way: the cell biology of O-GlcNAc. J Cell Biol 208(7):869-880. doi: 10.1083/jcb.201501101

Bostrom, P., J. Wu, M. P. Jedrychowski, A. Korde, L. Ye, J. C. Lo, K. A. Rasbach, E. A. Bostrom, J. H. Choi, J. Z. Long, S. Kajimura, M. C. Zingaretti, B. F. Vind, H. Tu, S. Cinti, K. Hojlund, S. P. Gygi, and B. M. Spiegelman. 2012. A PGC1-alpha-dependent myokine that drives brown-fat-like development of white fat and thermogenesis. Nature 481(7382):463-468. doi: 10.1038/nature10777

Bowker-Kinley, M. M., W. I. Davis, P. Wu, R. A. Harris, and K. M. Popov. 1998. Evidence for existence of tissue-specific regulation of the mammalian pyruvate dehydrogenase complex. Biochem J 329 (Pt 1):191-196. doi: 10.1042/bj3290191

Brand, M. D. 2010. The sites and topology of mitochondrial superoxide production. Exp Gerontol 45(7-8):466-472. doi: 10.1016/j.exger.2010.01.003

Braun, T., M. A. Rudnicki, H. H. Arnold, and R. Jaenisch. 1992. Targeted inactivation of the muscle regulatory gene Myf-5 results in abnormal rib development and perinatal death. Cell 71(3):369-382. doi: 10.1016/0092-8674(92)90507-9

Bricker, D. K., E. B. Taylor, J. C. Schell, T. Orsak, A. Boutron, Y. C. Chen, J. E. Cox, C. M. Cardon, J. G. Van Vranken, N. Dephoure, C. Redin, S. Boudina, S. P. Gygi, M. Brivet, C. S. Thummel, and J. Rutter. 2012. A mitochondrial pyruvate carrier required for pyruvate uptake in yeast, Drosophila, and humans. Science 337(6090):96-100. doi: 10.1126/science.1218099

Brooks, G. A. 1986. The lactate shuttle during exercise and recovery. Med Sci Sports Exerc 18(3):360-368. doi: 10.1249/00005768-198606000-00019

Brunk, C. F., and D. Yaffe. 1976. The reversible inhibition of myoblast fusion by ethidium bromide (EB). Exp Cell Res 99(2):310-318. doi: 10.1016/0014-4827(76)90588-7

Bulteau, A. L., H. A. O'Neill, M. C. Kennedy, M. Ikeda-Saito, G. Isaya, and L. I. Szweda. 2004. Frataxin acts as an iron chaperone protein to modulate mitochondrial aconitase activity. Science 305(5681):242-245. doi: 10.1126/science.1098991

Buse, M. G., K. A. Robinson, B. A. Marshall, and M. Mueckler. 1996. Differential effects of GLUT1 or GLUT4 overexpression on hexosamine biosynthesis by muscles of transgenic mice. J Biol Chem 271(38):23197-23202. doi: 10.1074/jbc.271.38.23197

Busquets, S., M. Figueras, V. Almendro, F. J. Lopez-Soriano, and J. M. Argiles. 2006. Interleukin-15 increases glucose uptake in skeletal muscle. An antidiabetogenic effect of the cytokine. Biochim Biophys Acta 1760(11):1613-1617. doi: 10.1016/j.bbagen.2006.09.001

Carbo, N., J. Lopez-Soriano, P. Costelli, B. Alvarez, S. Busquets, F. M. Baccino, L. S. Quinn, F. J. Lopez-Soriano, and J. M. Argiles. 2001. Interleukin-15 mediates reciprocal regulation of adipose and muscle mass: a potential role in body weight control. Biochim Biophys Acta 1526(1):17-24. doi: 10.1016/s0304-4165(00)00188-4

Carr, C. C., J. B. Morgan, E. P. Berg, S. D. Carter, and F. K. Ray. 2006. Growth performance, carcass composition, quality, and enhancement treatment of fresh pork identified through deoxyribonucleic acid marker-assisted selection for the Rendement Napole gene. J Anim Sci 84(4):910-917. doi: 10.2527/2006.844910x

Cerletti, M., Y. C. Jang, L. W. Finley, M. C. Haigis, and A. J. Wagers. 2012. Short-term calorie restriction enhances skeletal muscle stem cell function. Cell Stem Cell 10(5):515-519. doi: 10.1016/j.stem.2012.04.002

Chen, H., M. Vermulst, Y. E. Wang, A. Chomyn, T. A. Prolla, J. M. McCaffery, and D. C. Chan. 2010. Mitochondrial fusion is required for mtDNA stability in skeletal muscle and tolerance of mtDNA mutations. Cell 141(2):280-289. doi: 10.1016/j.cell.2010.02.026

Clop, A., F. Marcq, H. Takeda, D. Pirottin, X. Tordoir, B. Bibe, J. Bouix, F. Caiment, J. M. Elsen, F. Eychenne, C. Larzul, E. Laville, F. Meish, D. Milenkovic, J. Tobin, C. Charlier, and M. Georges. 2006. A mutation creating a potential illegitimate microRNA target site in the myostatin gene affects muscularity in sheep. Nat Genet 38(7):813-818. doi: 10.1038/ng1810

Coggan, A. R., R. J. Spina, D. S. King, M. A. Rogers, M. Brown, P. M. Nemeth, and J. O. Holloszy. 1992. Histochemical and enzymatic comparison of the gastrocnemius muscle of young and elderly men and women. J Gerontol 47(3):B71-76. doi: 10.1093/geronj/47.3.b71

Coleman, M. E., F. DeMayo, K. C. Yin, H. M. Lee, R. Geske, C. Montgomery, and R. J. Schwartz. 1995. Myogenic vector expression of insulin-like growth factor I stimulates muscle cell differentiation and myofiber hypertrophy in transgenic mice. J Biol Chem 270(20):12109-12116. doi: 10.1074/jbc.270.20.12109

Conley, K. E., S. A. Jubrias, and P. C. Esselman. 2000. Oxidative capacity and ageing in human muscle. J Physiol 526 Pt 1:203-210. doi: 10.1111/j.1469-7793.2000.t01-1-00203.x

Cooper, J. M., V. M. Mann, and A. H. Schapira. 1992. Analyses of mitochondrial respiratory chain function and mitochondrial DNA deletion in human skeletal muscle: effect of ageing. J Neurol Sci 113(1):91-98. doi: 10.1016/0022-510x(92)90270-u

D'Souza, D. M., K. E. Trajcevski, D. Al-Sajee, D. C. Wang, M. Thomas, J. E. Anderson, and T. J. Hawke. 2015. Diet-induced obesity impairs muscle satellite cell activation and muscle repair through alterations in hepatocyte growth factor signaling. Physiol Rep 3(8)doi: 10.14814/phy2.12506

Dai, J. M., M. X. Yu, Z. Y. Shen, C. Y. Guo, S. Q. Zhuang, and X. S. Qiu. 2015. Leucine Promotes Proliferation and Differentiation of Primary Preterm Rat Satellite Cells in Part through mTORC1 Signaling Pathway. Nutrients 7(5):3387-3400. doi: 10.3390/nu7053387

De Stefani, D., A. Raffaello, E. Teardo, I. Szabo, and R. Rizzuto. 2011. A forty-kilodalton protein of the inner membrane is the mitochondrial calcium uniporter. Nature 476(7360):336-340. doi: 10.1038/nature10230

DeFronzo, R. A., E. Jacot, E. Jequier, E. Maeder, J. Wahren, and J. P. Felber. 1981. The effect of insulin on the disposal of intravenous glucose. Results from indirect calorimetry and hepatic and femoral venous catheterization. Diabetes 30(12):1000-1007. doi: 10.2337/diab.30.12.1000

Deluca, H. F., and G. W. Engstrom. 1961. Calcium uptake by rat kidney mitochondria. Proc Natl Acad Sci U S A 47:1744-1750. doi: 10.1073/pnas.47.11.1744

Di Donato, D. M., D. W. West, T. A. Churchward-Venne, L. Breen, S. K. Baker, and S. M. Phillips. 2014. Influence of aerobic exercise intensity on myofibrillar and mitochondrial protein synthesis in young men during early and late postexercise recovery. Am J Physiol Endocrinol Metab 306(9):E1025-1032. doi: 10.1152/ajpendo.00487.2013

Diaz, F., H. Fukui, S. Garcia, and C. T. Moraes. 2006. Cytochrome c oxidase is required for the assembly/stability of respiratory complex I in mouse fibroblasts. Mol Cell Biol 26(13):4872-4881. doi: 10.1128/MCB.01767-05

Donges, C. E., N. A. Burd, R. Duffield, G. C. Smith, D. W. West, M. J. Short, R. Mackenzie, L. D. Plank, P. R. Shepherd, S. M. Phillips, and J. A. Edge. 2012. Concurrent resistance and aerobic exercise stimulates both myofibrillar and mitochondrial protein synthesis in sedentary middle-aged men. J Appl Physiol (1985) 112(12):1992-2001. doi: 10.1152/japplphysiol.00166.2012

Eisner, V., G. Lenaers, and G. Hajnoczky. 2014. Mitochondrial fusion is frequent in skeletal muscle and supports excitation-contraction coupling. J Cell Biol 205(2):179-195. doi: 10.1083/jcb.201312066

Fausnacht, D. W., R. P. McMillan, N. E. Boutagy, R. A. Lupi, M. M. Harvey, B. M. Davy, K. P. Davy, R. P. Rhoads, and M. W. Hulver. 2020. Overfeeding and Substrate Availability, But Not Age or BMI, Alter Human Satellite Cell Function. Nutrients 12(8)doi: 10.3390/nu12082215

Favaro, G., V. Romanello, T. Varanita, M. Andrea Desbats, V. Morbidoni, C. Tezze, M. Albiero, M. Canato, G. Gherardi, D. De Stefani, C. Mammucari, B. Blaauw, S. Boncompagni, F. Protasi, C. Reggiani, L. Scorrano, L. Salviati, and M. Sandri. 2019. DRP1-mediated mitochondrial shape controls calcium homeostasis and muscle mass. Nat Commun 10(1):2576. doi: 10.1038/s41467-019-10226-9

Fiorotto, M. L., R. J. Schwartz, and M. C. Delaughter. 2003. Persistent IGF-I overexpression in skeletal muscle transiently enhances DNA accretion and growth. FASEB J 17(1):59-60. doi: 10.1096/fj.02-0289fje

Fonseca, T. B., A. Sanchez-Guerrero, I. Milosevic, and N. Raimundo. 2019. Mitochondrial fission requires DRP1 but not dynamins. Nature 570(7761):E34-E42. doi: 10.1038/s41586-019-1296-y

Fu, X., M. Zhu, S. Zhang, M. Foretz, B. Viollet, and M. Du. 2016. Obesity Impairs Skeletal Muscle Regeneration Through Inhibition of AMPK. Diabetes 65(1):188-200. doi: 10.2337/db15-0647

Fu, X., M. J. Zhu, M. V. Dodson, and M. Du. 2015. AMP-activated protein kinase stimulates Warburg-like glycolysis and activation of satellite cells during muscle regeneration. J Biol Chem 290(44):26445-26456. doi: 10.1074/jbc.M115.665232

Fueger, P. T., D. P. Bracy, C. M. Malabanan, R. R. Pencek, D. K. Granner, and D. H. Wasserman. 2004. Hexokinase II overexpression improves exercise-stimulated but not insulin-stimulated muscle glucose uptake in high-fat-fed C57BL/6J mice. Diabetes 53(2):306-314. doi: 10.2337/diabetes.53.2.306

Fulco, M., Y. Cen, P. Zhao, E. P. Hoffman, M. W. McBurney, A. A. Sauve, and V. Sartorelli. 2008. Glucose restriction inhibits skeletal myoblast differentiation by activating SIRT1 through AMPK-mediated regulation of Nampt. Dev Cell 14(5):661-673. doi: 10.1016/j.devcel.2008.02.004

Funai, K., H. Song, L. Yin, I. J. Lodhi, X. Wei, J. Yoshino, T. Coleman, and C. F. Semenkovich. 2013. Muscle lipogenesis balances insulin sensitivity and strength through calcium signaling. J Clin Invest 123(3):1229-1240. doi: 10.1172/JCI65726

Garcia-Roves, P. M., M. E. Osler, M. H. Holmstrom, and J. R. Zierath. 2008. Gain-of-function R225Q mutation in AMP-activated protein kinase gamma3 subunit increases mitochondrial biogenesis in glycolytic skeletal muscle. J Biol Chem 283(51):35724-35734. doi: 10.1074/jbc.M805078200

Ghelli, A., C. V. Tropeano, M. A. Calvaruso, A. Marchesini, L. Iommarini, A. M. Porcelli, C. Zanna, V. De Nardo, A. Martinuzzi, F. Wibrand, J. Vissing, I. Kurelac, G. Gasparre, N. Selamoglu, F. Daldal, and M. Rugolo. 2013. The cytochrome b p.278Y>C mutation causative of a multisystem disorder enhances superoxide production and alters supramolecular interactions of respiratory chain complexes. Hum Mol Genet 22(11):2141-2151. doi: 10.1093/hmg/ddt067

Gherardi, G., L. Nogara, S. Ciciliot, G. P. Fadini, B. Blaauw, P. Braghetta, P. Bonaldo, D. De Stefani, R. Rizzuto, and C. Mammucari. 2019. Loss of mitochondrial calcium uniporter rewires skeletal muscle metabolism and substrate preference. Cell Death Differ 26(2):362-381. doi: 10.1038/s41418-018-0191-7

Glancy, B., L. M. Hartnell, D. Malide, Z. X. Yu, C. A. Combs, P. S. Connelly, S. Subramaniam, and R. S. Balaban. 2015. Mitochondrial reticulum for cellular energy distribution in muscle. Nature 523(7562):617-620. doi: 10.1038/nature14614

Goldstein, J. C., N. J. Waterhouse, P. Juin, G. I. Evan, and D. R. Green. 2000. The coordinate release of cytochrome c during apoptosis is rapid, complete and kinetically invariant. Nat Cell Biol 2(3):156-162. doi: 10.1038/35004029

Gomes, L. C., G. Di Benedetto, and L. Scorrano. 2011. During autophagy mitochondria elongate, are spared from degradation and sustain cell viability. Nat Cell Biol 13(5):589-598. doi: 10.1038/ncb2220

Grabstein, K. H., J. Eisenman, K. Shanebeck, C. Rauch, S. Srinivasan, V. Fung, C. Beers, J. Richardson, M. A. Schoenborn, M. Ahdieh, and et al. 1994. Cloning of a T cell growth factor that interacts with the beta chain of the interleukin-2 receptor. Science 264(5161):965-968. doi: 10.1126/science.8178155

Greggio, C., P. Jha, S. S. Kulkarni, S. Lagarrigue, N. T. Broskey, M. Boutant, X. Wang, S. Conde Alonso, E. Ofori, J. Auwerx, C. Canto, and F. Amati. 2017. Enhanced Respiratory Chain Supercomplex Formation in Response to Exercise in Human Skeletal Muscle. Cell Metab 25(2):301-311. doi: 10.1016/j.cmet.2016.11.004

Grobet, L., L. J. Martin, D. Poncelet, D. Pirottin, B. Brouwers, J. Riquet, A. Schoeberlein, S. Dunner, F. Menissier, J. Massabanda, R. Fries, R. Hanset, and M. Georges. 1997. A deletion in the bovine myostatin gene causes the double-muscled phenotype in cattle. Nat Genet 17(1):71-74. doi: 10.1038/ng0997-71

Grzelkowska-Kowalczyk, K., W. Wieteska-Skrzeczynska, K. Grabiec, and J. Tokarska. 2013. High glucose-mediated alterations of mechanisms important in myogenesis of mouse C2C12 myoblasts. Cell Biol Int 37(1):29-35. doi: 10.1002/cbin.10004

Hamai, N., M. Nakamura, and A. Asano. 1997. Inhibition of mitochondrial protein synthesis impaired C2C12 myoblast differentiation. Cell Struct Funct 22(4):421-431. doi: 10.1247/csf.22.421

Hamrick, M. W., C. Pennington, C. N. Webb, and C. M. Isales. 2006. Resistance to body fat gain in 'double-muscled' mice fed a high-fat diet. Int J Obes (Lond) 30(5):868-870. doi: 10.1038/sj.ijo.0803200

Han, B., J. Tong, M. J. Zhu, C. Ma, and M. Du. 2008. Insulin-like growth factor-1 (IGF-1) and leucine activate pig myogenic satellite cells through mammalian target of rapamycin (mTOR) pathway. Mol Reprod Dev 75(5):810-817. doi: 10.1002/mrd.20832

Han, D. H., P. A. Hansen, H. H. Host, and J. O. Holloszy. 1997. Insulin resistance of muscle glucose transport in rats fed a high-fat diet: a reevaluation. Diabetes 46(11):1761-1767. doi: 10.2337/diab.46.11.1761

Hanover, J. A., M. W. Krause, and D. C. Love. 2012. Bittersweet memories: linking metabolism to epigenetics through O-GlcNAcylation. Nat Rev Mol Cell Biol 13(5):312-321. doi: 10.1038/nrm3334

Hanover, J. A., Z. Lai, G. Lee, W. A. Lubas, and S. M. Sato. 1999. Elevated O-linked N-acetylglucosamine metabolism in pancreatic beta-cells. Arch Biochem Biophys 362(1):38-45. doi: 10.1006/abbi.1998.1016

Hansford, R. G. 1994. Physiological role of mitochondrial Ca2+ transport. J Bioenerg Biomembr 26(5):495-508. doi: 10.1007/BF00762734

Hansford, R. G., and D. Zorov. 1998. Role of mitochondrial calcium transport in the control of substrate oxidation. Mol Cell Biochem 184(1-2):359-369.

Hargreaves, M., and E. A. Richter. 1988. Regulation of skeletal muscle glycogenolysis during exercise. Can J Sport Sci 13(4):197-203.

Harwood, K. R., and J. A. Hanover. 2014. Nutrient-driven O-GlcNAc cycling - think globally but act locally. J Cell Sci 127(Pt 9):1857-1867. doi: 10.1242/jcs.113233

Hasty, P., A. Bradley, J. H. Morris, D. G. Edmondson, J. M. Venuti, E. N. Olson, and W. H. Klein. 1993. Muscle deficiency and neonatal death in mice with a targeted mutation in the myogenin gene. Nature 364(6437):501-506. doi: 10.1038/364501a0

Hatfield, I., I. Harvey, E. R. Yates, J. R. Redd, L. T. Reiter, and D. Bridges. 2015. The role of TORC1 in muscle development in Drosophila. Sci Rep 5:9676. doi: 10.1038/srep09676

Hawkins, M., I. Angelov, R. Liu, N. Barzilai, and L. Rossetti. 1997a. The tissue concentration of UDP-N-acetylglucosamine modulates the stimulatory effect of insulin on skeletal muscle glucose uptake. J Biol Chem 272(8):4889-4895. doi: 10.1074/jbc.272.8.4889

Hawkins, M., N. Barzilai, R. Liu, M. Hu, W. Chen, and L. Rossetti. 1997b. Role of the glucosamine pathway in fat-induced insulin resistance. J Clin Invest 99(9):2173-2182. doi: 10.1172/JCI119390

Hayashi, T., J. F. Wojtaszewski, and L. J. Goodyear. 1997. Exercise regulation of glucose transport in skeletal muscle. Am J Physiol 273(6):E1039-1051. doi: 10.1152/ajpendo.1997.273.6.E1039

Heineman, F. W., and R. S. Balaban. 1990. Phosphorus-31 nuclear magnetic resonance analysis of transient changes of canine myocardial metabolism in vivo. J Clin Invest 85(3):843-852. doi: 10.1172/JCI114511

Herzberg, N. H., R. Zwart, R. A. Wolterman, J. P. Ruiter, R. J. Wanders, P. A. Bolhuis, and C. van den Bogert. 1993. Differentiation and proliferation of respiration-deficient human myoblasts. Biochim Biophys Acta 1181(1):63-67. doi: 10.1016/0925-4439(93)90091-e

Herzig, S., E. Raemy, S. Montessuit, J. L. Veuthey, N. Zamboni, B. Westermann, E. R. Kunji, and J. C. Martinou. 2012. Identification and functional expression of the mitochondrial pyruvate carrier. Science 337(6090):93-96. doi: 10.1126/science.1218530

Holloszy, J. O. 1967. Biochemical adaptations in muscle. Effects of exercise on mitochondrial oxygen uptake and respiratory enzyme activity in skeletal muscle. J Biol Chem 242(9):2278-2282.

Holness, M. J., A. Kraus, R. A. Harris, and M. C. Sugden. 2000. Targeted upregulation of pyruvate dehydrogenase kinase (PDK)-4 in slow-twitch skeletal muscle underlies the stable modification of the regulatory characteristics of PDK induced by high-fat feeding. Diabetes 49(5):775-781. doi: 10.2337/diabetes.49.5.775

Hori, S., Y. Hiramuki, D. Nishimura, F. Sato, and A. Sehara-Fujisawa. 2019. PDH-mediated metabolic flow is critical for skeletal muscle stem cell differentiation and myotube formation during regeneration in mice. FASEB J 33(7):8094-8109. doi: 10.1096/fj.201802479R

Housley, M. P., J. T. Rodgers, N. D. Udeshi, T. J. Kelly, J. Shabanowitz, D. F. Hunt, P. Puigserver, and G. W. Hart. 2008. O-GlcNAc regulates FoxO activation in response to glucose. J Biol Chem 283(24):16283-16292. doi: 10.1074/jbc.M802240200

Hu, Y., J. Suarez, E. Fricovsky, H. Wang, B. T. Scott, S. A. Trauger, W. Han, Y. Hu, M. O. Oyeleye, and W. H. Dillmann. 2009. Increased enzymatic O-GlcNAcylation of mitochondrial proteins impairs mitochondrial function in cardiac myocytes exposed to high glucose. J Biol Chem 284(1):547-555. doi: 10.1074/jbc.M808518200

Huizing, M., W. Ruitenbeek, F. P. Thinnes, V. DePinto, U. Wendel, F. J. Trijbels, L. M. Smit, H. J. ter Laak, and L. P. van den Heuvel. 1996. Deficiency of the voltage-dependent anion channel: a novel cause of mitochondriopathy. Pediatr Res 39(5):760-765. doi: 10.1203/00006450-199605000-00003

Izumiya, Y., T. Hopkins, C. Morris, K. Sato, L. Zeng, J. Viereck, J. A. Hamilton, N. Ouchi, N. K. LeBrasseur, and K. Walsh. 2008. Fast/Glycolytic muscle fiber growth reduces fat mass and improves metabolic parameters in obese mice. Cell Metab 7(2):159-172. doi: 10.1016/j.cmet.2007.11.003

Jaleel, A., K. R. Short, Y. W. Asmann, K. A. Klaus, D. M. Morse, G. C. Ford, and K. S. Nair. 2008. In vivo measurement of synthesis rate of individual skeletal muscle mitochondrial proteins. Am J Physiol Endocrinol Metab 295(5):E1255-1268. doi: 10.1152/ajpendo.90586.2008

Jeoung, N. H., and R. A. Harris. 2008. Pyruvate dehydrogenase kinase-4 deficiency lowers blood glucose and improves glucose tolerance in diet-induced obese mice. Am J Physiol Endocrinol Metab 295(1):E46-54. doi: 10.1152/ajpendo.00536.2007

Jeoung, N. H., P. Wu, M. A. Joshi, J. Jaskiewicz, C. B. Bock, A. A. Depaoli-Roach, and R. A. Harris. 2006. Role of pyruvate dehydrogenase kinase isoenzyme 4 (PDHK4) in glucose homoeostasis during starvation. Biochem J 397(3):417-425. doi: 10.1042/BJ20060125

Jessen, N., and L. J. Goodyear. 2005. Contraction signaling to glucose transport in skeletal muscle. J Appl Physiol (1985) 99(1):330-337. doi: 10.1152/japplphysiol.00175.2005

Ji, W. K., A. L. Hatch, R. A. Merrill, S. Strack, and H. N. Higgs. 2015. Actin filaments target the oligomeric maturation of the dynamin GTPase Drp1 to mitochondrial fission sites. Elife 4:e11553. doi: 10.7554/eLife.11553

Jin, C. L., J. L. Ye, J. Yang, C. Q. Gao, H. C. Yan, H. C. Li, and X. Q. Wang. 2019. mTORC1 Mediates Lysine-Induced Satellite Cell Activation to Promote Skeletal Muscle Growth. Cells 8(12)doi: 10.3390/cells8121549

Kalia, R., R. Y. Wang, A. Yusuf, P. V. Thomas, D. A. Agard, J. M. Shaw, and A. Frost. 2018. Structural basis of mitochondrial receptor binding and constriction by DRP1. Nature 558(7710):401-405. doi: 10.1038/s41586-018-0211-2

Kalista, S., O. Schakman, H. Gilson, P. Lause, B. Demeulder, L. Bertrand, M. Pende, and J. P. Thissen. 2012. The type 1 insulin-like growth factor receptor (IGF-IR) pathway is mandatory for the follistatin-induced skeletal muscle hypertrophy. Endocrinology 153(1):241-253. doi: 10.1210/en.2011-1687

Kang, E. S., D. Han, J. Park, T. K. Kwak, M. A. Oh, S. A. Lee, S. Choi, Z. Y. Park, Y. Kim, and J. W. Lee. 2008. O-GlcNAc modulation at Akt1 Ser473 correlates with apoptosis of murine pancreatic beta cells. Exp Cell Res 314(11-12):2238-2248. doi: 10.1016/j.yexcr.2008.04.014

Katz, A., S. Broberg, K. Sahlin, and J. Wahren. 1986. Leg glucose uptake during maximal dynamic exercise in humans. Am J Physiol 251(1 Pt 1):E65-70. doi: 10.1152/ajpendo.1986.251.1.E65

Kennedy, J. W., M. F. Hirshman, E. V. Gervino, J. V. Ocel, R. A. Forse, S. J. Hoenig, D. Aronson, L. J. Goodyear, and E. S. Horton. 1999. Acute exercise induces GLUT4 translocation in skeletal muscle of normal human subjects and subjects with type 2 diabetes. Diabetes 48(5):1192-1197. doi: 10.2337/diabetes.48.5.1192

Kim, J., M. Kundu, B. Viollet, and K. L. Guan. 2011. AMPK and mTOR regulate autophagy through direct phosphorylation of Ulk1. Nature cell biology 13(2):132-141. doi: 10.1038/ncb2152

Korohoda, W., Z. Pietrzkowski, and K. Reiss. 1993. Chloramphenicol, an inhibitor of mitochondrial protein synthesis, inhibits myoblast fusion and myotube differentiation. Folia Histochem Cytobiol 31(1):9-13.

Korzeniewski, B. 2007. Regulation of oxidative phosphorylation through parallel activation. Biophys Chem 129(2-3):93-110. doi: 10.1016/j.bpc.2007.05.013

Koshiba, T., S. A. Detmer, J. T. Kaiser, H. Chen, J. M. McCaffery, and D. C. Chan. 2004. Structural basis of mitochondrial tethering by mitofusin complexes. Science 305(5685):858-862. doi: 10.1126/science.1099793

Kuang, S., K. Kuroda, F. Le Grand, and M. A. Rudnicki. 2007. Asymmetric self-renewal and commitment of satellite stem cells in muscle. Cell 129(5):999-1010. doi: 10.1016/j.cell.2007.03.044

Kubota, T., R. A. Brown, J. Fang, and J. M. Krueger. 2001. Interleukin-15 and interleukin-2 enhance non-REM sleep in rabbits. Am J Physiol Regul Integr Comp Physiol 281(3):R1004-1012. doi: 10.1152/ajpregu.2001.281.3.R1004

Kwong, J. Q., J. Huo, M. J. Bround, J. G. Boyer, J. A. Schwanekamp, N. Ghazal, J. T. Maxwell, Y. C. Jang, Z. Khuchua, K. Shi, D. M. Bers, J. Davis, and J. D. Molkentin. 2018. The mitochondrial calcium uniporter underlies metabolic fuel preference in skeletal muscle. JCI Insight 3(22)doi: 10.1172/jci.insight.121689

Lai, K. M., M. Gonzalez, W. T. Poueymirou, W. O. Kline, E. Na, E. Zlotchenko, T. N. Stitt, A. N. Economides, G. D. Yancopoulos, and D. J. Glass. 2004. Conditional activation of akt in adult skeletal muscle induces rapid hypertrophy. Mol Cell Biol 24(21):9295-9304. doi: 10.1128/MCB.24.21.9295-9304.2004

Lander, L., R. m. Mourner, J. Leclerc, M. Pende, M. Foretz, and B. Viollet. 2010. Coordinated maintenance of muscle cell size control by AMP-activated protein kinase. The FASEB Journal 24(9):3555-3561. doi: 10.1096/fj.10-155994

Lee, J. W., S. Park, Y. Takahashi, and H. G. Wang. 2010. The association of AMPK with ULK1 regulates autophagy. PloS one 5(11):e15394. doi: 10.1371/journal.pone.0015394

Lepper, C., T. A. Partridge, and C. M. Fan. 2011. An absolute requirement for Pax7-positive satellite cells in acute injury-induced skeletal muscle regeneration. Development 138(17):3639-3646. doi: 10.1242/dev.067595

Lewis, S. E., F. J. Kelly, and D. F. Goldspink. 1984. Pre- and post-natal growth and protein turnover in smooth muscle, heart and slow- and fast-twitch skeletal muscles of the rat. Biochem J 217(2):517-526. doi: 10.1042/bj2170517

Li, P., Z. Zeng, D. Wang, L. Xue, R. Zhang, and X. Piao. 2012. Effects of the standardized ileal digestible lysine to metabolizable energy ratio on performance and carcass characteristics of growing-finishing pigs. J Anim Sci Biotechnol 3(1):9. doi: 10.1186/2049-1891-3-9

Lipina, C., H. Kendall, A. C. McPherron, P. M. Taylor, and H. S. Hundal. 2010. Mechanisms involved in the enhancement of mammalian target of rapamycin signalling and hypertrophy in skeletal muscle of myostatin-deficient mice. FEBS Lett 584(11):2403-2408. doi: 10.1016/j.febslet.2010.04.039

Ljubicic, V., P. Miura, M. Burt, L. Boudreault, S. Khogali, J. A. Lunde, J. M. Renaud, and B. J. Jasmin. 2011. Chronic AMPK activation evokes the slow, oxidative myogenic program and triggers beneficial adaptations in mdx mouse skeletal muscle. Hum Mol Genet 20(17):3478-3493. doi: 10.1093/hmg/ddr265

Lunt, S. Y., and M. G. Vander Heiden. 2011. Aerobic glycolysis: meeting the metabolic requirements of cell proliferation. Annu Rev Cell Dev Biol 27:441-464. doi: 10.1146/annurev-cellbio-092910-154237

Luo, W., L. Ai, B. F. Wang, and Y. Zhou. 2019. High glucose inhibits myogenesis and induces insulin resistance by down-regulating AKT signaling. Biomed Pharmacother 120:109498. doi: 10.1016/j.biopha.2019.109498

Maldonado, E. N., and J. J. Lemasters. 2014. ATP/ADP ratio, the missed connection between mitochondria and the Warburg effect. Mitochondrion 19 Pt A:78-84. doi: 10.1016/j.mito.2014.09.002

Mammucari, C., G. Gherardi, I. Zamparo, A. Raffaello, S. Boncompagni, F. Chemello, S. Cagnin, A. Braga, S. Zanin, G. Pallafacchina, L. Zentilin, M. Sandri, D. De Stefani, F. Protasi, G. Lanfranchi, and R. Rizzuto. 2015. The mitochondrial calcium uniporter controls skeletal muscle trophism in vivo. Cell Rep 10(8):1269-1279. doi: 10.1016/j.celrep.2015.01.056

Maranzana, E., G. Barbero, A. I. Falasca, G. Lenaz, and M. L. Genova. 2013. Mitochondrial respiratory supercomplex association limits production of reactive oxygen species from complex I. Antioxid Redox Signal 19(13):1469-1480. doi: 10.1089/ars.2012.4845

Marshall, S., V. Bacote, and R. R. Traxinger. 1991. Discovery of a metabolic pathway mediating glucose-induced desensitization of the glucose transport system. Role of hexosamine biosynthesis in the induction of insulin resistance. J Biol Chem 266(8):4706-4712.

Martinez-Reyes, I., and N. S. Chandel. 2020. Mitochondrial TCA cycle metabolites control physiology and disease. Nat Commun 11(1):102. doi: 10.1038/s41467-019-13668-3

Mauro, A. 1961. Satellite cell of skeletal muscle fibers. J Biophys Biochem Cytol 9:493-495. doi: 10.1083/jcb.9.2.493

Mavalli, M. D., D. J. DiGirolamo, Y. Fan, R. C. Riddle, K. S. Campbell, T. van Groen, S. J. Frank, M. A. Sperling, K. A. Esser, M. M. Bamman, and T. L. Clemens. 2010. Distinct growth hormone receptor signaling modes regulate skeletal muscle development and insulin sensitivity in mice. J Clin Invest 120(11):4007-4020. doi: 10.1172/JCI42447

McCormack, J. G., and R. M. Denton. 1979. The effects of calcium ions and adenine nucleotides on the activity of pig heart 2-oxoglutarate dehydrogenase complex. Biochem J 180(3):533-544. doi: 10.1042/bj1800533

McCormack, J. G., and R. M. Denton. 1993. Mitochondrial Ca2+ transport and the role of intramitochondrial Ca2+ in the regulation of energy metabolism. Dev Neurosci 15(3-5):165-173. doi: 10.1159/000111332

McCormack, J. G., A. P. Halestrap, and R. M. Denton. 1990. Role of calcium ions in regulation of mammalian intramitochondrial metabolism. Physiol Rev 70(2):391-425. doi: 10.1152/physrev.1990.70.2.391

McPherron, A. C., and S. J. Lee. 1997. Double muscling in cattle due to mutations in the myostatin gene. Proc Natl Acad Sci U S A 94(23):12457-12461. doi: 10.1073/pnas.94.23.12457

McPherron, A. C., and S. J. Lee. 2002. Suppression of body fat accumulation in myostatin-deficient mice. J Clin Invest 109(5):595-601. doi: 10.1172/JCI13562

Meeusen, S., R. DeVay, J. Block, A. Cassidy-Stone, S. Wayson, J. M. McCaffery, and J. Nunnari. 2006. Mitochondrial inner-membrane fusion and crista maintenance requires the dynamin-related GTPase Mgm1. Cell 127(2):383-395. doi: 10.1016/j.cell.2006.09.021

Meeusen, S., J. M. McCaffery, and J. Nunnari. 2004. Mitochondrial fusion intermediates revealed in vitro. Science 305(5691):1747-1752. doi: 10.1126/science.1100612

Meng, Z. X., S. Li, L. Wang, H. J. Ko, Y. Lee, D. Y. Jung, M. Okutsu, Z. Yan, J. K. Kim, and J. D. Lin. 2013. Baf60c drives glycolytic metabolism in the muscle and improves systemic glucose homeostasis through Deptor-mediated Akt activation. Nat Med 19(5):640-645. doi: 10.1038/nm.3144

Menshikova, E. V., V. B. Ritov, L. Fairfull, R. E. Ferrell, D. E. Kelley, and B. H. Goodpaster. 2006. Effects of exercise on mitochondrial content and function in aging human skeletal muscle. J Gerontol A Biol Sci Med Sci 61(6):534-540. doi: 10.1093/gerona/61.6.534

Mishra, P., G. Varuzhanyan, A. H. Pham, and D. C. Chan. 2015. Mitochondrial Dynamics is a Distinguishing Feature of Skeletal Muscle Fiber Types and Regulates Organellar Compartmentalization. Cell Metab 22(6):1033-1044. doi: 10.1016/j.cmet.2015.09.027

Mootha, V. K., C. M. Lindgren, K. F. Eriksson, A. Subramanian, S. Sihag, J. Lehar, P. Puigserver, E. Carlsson, M. Ridderstrale, E. Laurila, N. Houstis, M. J. Daly, N. Patterson, J. P. Mesirov, T. R. Golub, P. Tamayo, B. Spiegelman, E. S. Lander, J. N. Hirschhorn, D. Altshuler, and L. C. Groop. 2003. PGC-1alpha-responsive genes involved in oxidative phosphorylation are coordinately downregulated in human diabetes. Nat Genet 34(3):267-273. doi: 10.1038/ng1180

Mosher, D. S., P. Quignon, C. D. Bustamante, N. B. Sutter, C. S. Mellersh, H. G. Parker, and E. A. Ostrander. 2007. A mutation in the myostatin gene increases muscle mass and enhances racing performance in heterozygote dogs. PLoS Genet 3(5):e79. doi: 10.1371/journal.pgen.0030079

Moss, F. P., and C. P. Leblond. 1971. Satellite cells as the source of nuclei in muscles of growing rats. Anat Rec 170(4):421-435. doi: 10.1002/ar.1091700405

Moyes, C. D., O. A. Mathieu-Costello, N. Tsuchiya, C. Filburn, and R. G. Hansford. 1997. Mitochondrial biogenesis during cellular differentiation. Am J Physiol 272(4 Pt 1):C1345-1351. doi: 10.1152/ajpcell.1997.272.4.C1345

Musaro, A., K. McCullagh, A. Paul, L. Houghton, G. Dobrowolny, M. Molinaro, E. R. Barton, H. L. Sweeney, and N. Rosenthal. 2001. Localized Igf-1 transgene expression sustains hypertrophy and regeneration in senescent skeletal muscle. Nat Genet 27(2):195-200. doi: 10.1038/84839

Nabeshima, Y., K. Hanaoka, M. Hayasaka, E. Esumi, S. Li, I. Nonaka, and Y. Nabeshima. 1993. Myogenin gene disruption results in perinatal lethality because of severe muscle defect. Nature 364(6437):532-535. doi: 10.1038/364532a0

Nicholls, D. G. 1978. The regulation of extramitochondrial free calcium ion concentration by rat liver mitochondria. Biochem J 176(2):463-474. doi: 10.1042/bj1760463

Nicholls, D. G., and I. D. Scott. 1980. The regulation of brain mitochondrial calcium-ion transport. The role of ATP in the discrimination between kinetic and membrane-potential-dependent calcium-ion efflux mechanisms. Biochem J 186(3):833-839. doi: 10.1042/bj1860833

Nuth, M., T. Yoon, and J. A. Cowan. 2002. Iron-sulfur cluster biosynthesis: characterization of iron nucleation sites for assembly of the [2Fe-2S]2+ cluster core in IscU proteins. J Am Chem Soc 124(30):8774-8775. doi: 10.1021/ja0264596

O'Connell, G., G. Guo, J. Stricker, L. S. Quinn, A. Ma, and E. E. Pistilli. 2015. Muscle-specific deletion of exons 2 and 3 of the IL15RA gene in mice: effects on contractile properties of fast and slow muscles. J Appl Physiol (1985) 118(4):437-448. doi: 10.1152/japplphysiol.00704.2014

Palmieri, F., and C. L. Pierri. 2010. Mitochondrial metabolite transport. Essays Biochem 47:37-52. doi: 10.1042/bse0470037

Patti, M. E., A. J. Butte, S. Crunkhorn, K. Cusi, R. Berria, S. Kashyap, Y. Miyazaki, I. Kohane, M. Costello, R. Saccone, E. J. Landaker, A. B. Goldfine, E. Mun, R. DeFronzo, J. Finlayson, C. R. Kahn, and L. J. Mandarino. 2003. Coordinated reduction of genes of oxidative metabolism in humans with insulin resistance and diabetes: Potential role of PGC1 and NRF1. Proc Natl Acad Sci U S A 100(14):8466-8471. doi: 10.1073/pnas.1032913100

Pereira, M. G., I. L. Baptista, E. O. Carlassara, A. S. Moriscot, M. S. Aoki, and E. H. Miyabara. 2014. Leucine supplementation improves skeletal muscle regeneration after cryolesion in rats. PLoS One 9(1):e85283. doi: 10.1371/journal.pone.0085283

Peterson, J. M., R. W. Bryner, and S. E. Alway. 2008. Satellite cell proliferation is reduced in muscles of obese Zucker rats but restored with loading. Am J Physiol Cell Physiol 295(2):C521-528. doi: 10.1152/ajpcell.00073.2008

Pfeiffer, T., S. Schuster, and S. Bonhoeffer. 2001. Cooperation and competition in the evolution of ATP-producing pathways. Science 292(5516):504-507. doi: 10.1126/science.1058079

Pistilli, E. E., S. Bogdanovich, F. Garton, N. Yang, J. P. Gulbin, J. D. Conner, B. G. Anderson, L. S. Quinn, K. North, R. S. Ahima, and T. S. Khurana. 2011. Loss of IL-15 receptor alpha

alters the endurance, fatigability, and metabolic characteristics of mouse fast skeletal muscles. J Clin Invest 121(8):3120-3132. doi: 10.1172/JCI44945

Pistilli, E. E., and L. S. Quinn. 2013. From anabolic to oxidative: reconsidering the roles of IL-15 and IL-15Ralpha in skeletal muscle. Exerc Sport Sci Rev 41(2):100-106. doi: 10.1097/JES.0b013e318275d230

Quinn, L. S., B. G. Anderson, J. D. Conner, and T. Wolden-Hanson. 2013. IL-15 overexpression promotes endurance, oxidative energy metabolism, and muscle PPARdelta, SIRT1, PGC-1alpha, and PGC-1beta expression in male mice. Endocrinology 154(1):232-245. doi: 10.1210/en.2012-1773

Quinn, L. S., B. G. Anderson, L. Strait-Bodey, A. M. Stroud, and J. M. Argiles. 2009. Oversecretion of interleukin-15 from skeletal muscle reduces adiposity. Am J Physiol Endocrinol Metab 296(1):E191-202. doi: 10.1152/ajpendo.90506.2008

Rao, X., X. Duan, W. Mao, X. Li, Z. Li, Q. Li, Z. Zheng, H. Xu, M. Chen, P. G. Wang, Y. Wang, B. Shen, and W. Yi. 2015. O-GlcNAcylation of G6PD promotes the pentose phosphate pathway and tumor growth. Nat Commun 6:8468. doi: 10.1038/ncomms9468

Reisz-Porszasz, S., S. Bhasin, J. N. Artaza, R. Shen, I. Sinha-Hikim, A. Hogue, T. J. Fielder, and N. F. Gonzalez-Cadavid. 2003. Lower skeletal muscle mass in male transgenic mice with muscle-specific overexpression of myostatin. Am J Physiol Endocrinol Metab 285(4):E876-888. doi: 10.1152/ajpendo.00107.2003

Remels, A. H., R. C. Langen, P. Schrauwen, G. Schaart, A. M. Schols, and H. R. Gosker. 2010. Regulation of mitochondrial biogenesis during myogenesis. Mol Cell Endocrinol 315(1-2):113-120. doi: 10.1016/j.mce.2009.09.029

Risson, V., L. Mazelin, M. Roceri, H. Sanchez, V. Moncollin, C. Corneloup, H. Richard-Bulteau, A. Vignaud, D. Baas, A. Defour, D. Freyssenet, J. F. Tanti, Y. Le-Marchand-Brustel, B. Ferrier, A. Conjard-Duplany, K. Romanino, S. Bauche, D. Hantai, M. Mueller, S. C. Kozma, G. Thomas, M. A. Ruegg, A. Ferry, M. Pende, X. Bigard, N. Koulmann, L. Schaeffer, and Y. G. Gangloff. 2009. Muscle inactivation of mTOR causes metabolic and dystrophin defects leading to severe myopathy. J Cell Biol 187(6):859-874. doi: 10.1083/jcb.200903131

Rochard, P., A. Rodier, F. Casas, I. Cassar-Malek, S. Marchal-Victorion, L. Daury, C. Wrutniak, and G. Cabello. 2000. Mitochondrial activity is involved in the regulation of myoblast differentiation through myogenin expression and activity of myogenic factors. J Biol Chem 275(4):2733-2744. doi: 10.1074/jbc.275.4.2733

Rocheteau, P., B. Gayraud-Morel, I. Siegl-Cachedenier, M. A. Blasco, and S. Tajbakhsh. 2012. A subpopulation of adult skeletal muscle stem cells retains all template DNA strands after cell division. Cell 148(1-2):112-125. doi: 10.1016/j.cell.2011.11.049

Rosholt, M. N., P. A. King, and E. S. Horton. 1994. High-fat diet reduces glucose transporter responses to both insulin and exercise. Am J Physiol 266(1 Pt 2):R95-101. doi: 10.1152/ajpregu.1994.266.1.R95

Rottenberg, H., and A. Scarpa. 1974. Calcium uptake and membrane potential in mitochondria. Biochemistry 13(23):4811-4817. doi: 10.1021/bi00720a020

Ruan, H. B., J. P. Singh, M. D. Li, J. Wu, and X. Yang. 2013. Cracking the O-GlcNAc code in metabolism. Trends Endocrinol Metab 24(6):301-309. doi: 10.1016/j.tem.2013.02.002

Rubinstein, M. P., M. Kovar, J. F. Purton, J. H. Cho, O. Boyman, C. D. Surh, and J. Sprent. 2006. Converting IL-15 to a superagonist by binding to soluble IL-15R{alpha}. Proc Natl Acad Sci U S A 103(24):9166-9171. doi: 10.1073/pnas.0600240103

Rudnicki, M. A., T. Braun, S. Hinuma, and R. Jaenisch. 1992. Inactivation of MyoD in mice leads to up-regulation of the myogenic HLH gene Myf-5 and results in apparently normal muscle development. Cell 71(3):383-390. doi: 10.1016/0092-8674(92)90508-a

Sacoman, J. L., R. Y. Dagda, A. R. Burnham-Marusich, R. K. Dagda, and P. M. Berninsone. 2017. Mitochondrial O-GlcNAc Transferase (mOGT) Regulates Mitochondrial Structure, Function, and Survival in HeLa Cells. J Biol Chem 292(11):4499-4518. doi: 10.1074/jbc.M116.726752

Sahlin, K., M. Tonkonogi, and K. Soderlund. 1998. Energy supply and muscle fatigue in humans. Acta Physiol Scand 162(3):261-266. doi: 10.1046/j.1365-201X.1998.0298f.x

Sato, T., Y. Ito, T. Nedachi, and T. Nagasawa. 2014. Lysine suppresses protein degradation through autophagic-lysosomal system in C2C12 myotubes. Mol Cell Biochem 391(1-2):37-46. doi: 10.1007/s11010-014-1984-8

Schagger, H., and K. Pfeiffer. 2001. The ratio of oxidative phosphorylation complexes I-V in bovine heart mitochondria and the composition of respiratory chain supercomplexes. J Biol Chem 276(41):37861-37867. doi: 10.1074/jbc.M106474200

Scheffler, T. L., J. M. Scheffler, S. Park, S. C. Kasten, Y. Wu, R. P. McMillan, M. W. Hulver, M. I. Frisard, and D. E. Gerrard. 2014. Fiber hypertrophy and increased oxidative capacity can occur simultaneously in pig glycolytic skeletal muscle. Am J Physiol Cell Physiol 306(4):C354-363. doi: 10.1152/ajpcell.00002.2013

Schuelke, M., K. R. Wagner, L. E. Stolz, C. Hubner, T. Riebel, W. Komen, T. Braun, J. F. Tobin, and S. J. Lee. 2004. Myostatin mutation associated with gross muscle hypertrophy in a child. N Engl J Med 350(26):2682-2688. doi: 10.1056/NEJMoa040933

Schultz, E., M. C. Gibson, and T. Champion. 1978. Satellite cells are mitotically quiescent in mature mouse muscle: an EM and radioautographic study. J Exp Zool 206(3):451-456. doi: 10.1002/jez.1402060314

Shi, H., A. Munk, T. S. Nielsen, M. R. Daughtry, L. Larsson, S. Li, K. F. Hoyer, H. W. Geisler, K. Sulek, R. Kjobsted, T. Fisher, M. M. Andersen, Z. Shen, U. K. Hansen, E. M. England, Z. Cheng, K. Hojlund, J. F. P. Wojtaszewski, X. Yang, M. W. Hulver, R. F. Helm, J. T. Treebak, and D. E. Gerrard. 2018. Skeletal muscle O-GlcNAc transferase is important for muscle energy homeostasis and whole-body insulin sensitivity. Mol Metab 11:160-177. doi: 10.1016/j.molmet.2018.02.010

Short, K. R., M. L. Bigelow, J. Kahl, R. Singh, J. Coenen-Schimke, S. Raghavakaimal, and K. S. Nair. 2005. Decline in skeletal muscle mitochondrial function with aging in humans. Proc Natl Acad Sci U S A 102(15):5618-5623. doi: 10.1073/pnas.0501559102

Shulman, G. I., D. L. Rothman, T. Jue, P. Stein, R. A. DeFronzo, and R. G. Shulman. 1990. Quantitation of muscle glycogen synthesis in normal subjects and subjects with non-insulin-dependent diabetes by 13C nuclear magnetic resonance spectroscopy. N Engl J Med 322(4):223-228. doi: 10.1056/NEJM199001253220403

Simoneau, J. A., S. R. Colberg, F. L. Thaete, and D. E. Kelley. 1995. Skeletal muscle glycolytic and oxidative enzyme capacities are determinants of insulin sensitivity and muscle composition in obese women. FASEB J 9(2):273-278.

Skulachev, V. P. 1996. Role of uncoupled and non-coupled oxidations in maintenance of safely low levels of oxygen and its one-electron reductants. Q Rev Biophys 29(2):169-202. doi: 10.1017/s0033583500005795

Slawson, C., R. J. Copeland, and G. W. Hart. 2010. O-GlcNAc signaling: a metabolic link between diabetes and cancer? Trends Biochem Sci 35(10):547-555. doi: 10.1016/j.tibs.2010.04.005

Snow, M. H. 1978. An autoradiographic study of satellite cell differentiation into regenerating myotubes following transplantation of muscles in young rats. Cell Tissue Res 186(3):535-540. doi: 10.1007/BF00224941

Song, R., W. Peng, Y. Zhang, F. Lv, H. K. Wu, J. Guo, Y. Cao, Y. Pi, X. Zhang, L. Jin, M. Zhang, P. Jiang, F. Liu, S. Meng, X. Zhang, P. Jiang, C. M. Cao, and R. P. Xiao. 2013. Central role of E3 ubiquitin ligase MG53 in insulin resistance and metabolic disorders. Nature 494(7437):375-379. doi: 10.1038/nature11834

Song, Z., M. Ghochani, J. M. McCaffery, T. G. Frey, and D. C. Chan. 2009. Mitofusins and OPA1 mediate sequential steps in mitochondrial membrane fusion. Mol Biol Cell 20(15):3525-3532. doi: 10.1091/mbc.E09-03-0252

Stoklasek, T. A., K. S. Schluns, and L. Lefrancois. 2006. Combined IL-15/IL-15Ralpha immunotherapy maximizes IL-15 activity in vivo. J Immunol 177(9):6072-6080. doi: 10.4049/jimmunol.177.9.6072

Swamy, M., S. Pathak, K. M. Grzes, S. Damerow, L. V. Sinclair, D. M. van Aalten, and D. A. Cantrell. 2016. Glucose and glutamine fuel protein O-GlcNAcylation to control T cell self-renewal and malignancy. Nat Immunol 17(6):712-720. doi: 10.1038/ni.3439

Tagaya, Y., G. Kurys, T. A. Thies, J. M. Losi, N. Azimi, J. A. Hanover, R. N. Bamford, and T. A. Waldmann. 1997. Generation of secretable and nonsecretable interleukin 15 isoforms through alternate usage of signal peptides. Proc Natl Acad Sci U S A 94(26):14444-14449. doi: 10.1073/pnas.94.26.14444

Tremblay, F., C. Lavigne, H. Jacques, and A. Marette. 2001. Defective insulin-induced GLUT4 translocation in skeletal muscle of high fat-fed rats is associated with alterations in both Akt/protein kinase B and atypical protein kinase C (zeta/lambda) activities. Diabetes 50(8):1901-1910. doi: 10.2337/diabetes.50.8.1901

Tureckova, J., E. M. Wilson, J. L. Cappalonga, and P. Rotwein. 2001. Insulin-like growth factor-mediated muscle differentiation: collaboration between phosphatidylinositol 3-kinase-Akt-signaling pathways and myogenin. J Biol Chem 276(42):39264-39270. doi: 10.1074/jbc.M104991200

Ustanina, S., J. Carvajal, P. Rigby, and T. Braun. 2007. The myogenic factor Myf5 supports efficient skeletal muscle regeneration by enabling transient myoblast amplification. Stem Cells 25(8):2006-2016. doi: 10.1634/stemcells.2006-0736

Vasington, F. D., and J. V. Murphy. 1962. Ca ion uptake by rat kidney mitochondria and its dependence on respiration and phosphorylation. J Biol Chem 237:2670-2677.

Wagner, K. R., F. C. Kauffman, and S. R. Max. 1978. The pentose phosphate pathway in regenerating skeletal muscle. Biochem J 170(1):17-22. doi: 10.1042/bj1700017

Walgren, J. L., T. S. Vincent, K. L. Schey, and M. G. Buse. 2003. High glucose and insulin promote O-GlcNAc modification of proteins, including alpha-tubulin. Am J Physiol Endocrinol Metab 284(2):E424-434. doi: 10.1152/ajpendo.00382.2002

Wang, Y. X., C. L. Zhang, R. T. Yu, H. K. Cho, M. C. Nelson, C. R. Bayuga-Ocampo, J. Ham, H. Kang, and R. M. Evans. 2004. Regulation of muscle fiber type and running endurance by PPARdelta. PLoS Biol 2(10):e294. doi: 10.1371/journal.pbio.0020294

Watt, M. J., N. Dzamko, W. G. Thomas, S. Rose-John, M. Ernst, D. Carling, B. E. Kemp, M. A. Febbraio, and G. R. Steinberg. 2006. CNTF reverses obesity-induced insulin resistance by activating skeletal muscle AMPK. Nat Med 12(5):541-548. doi: 10.1038/nm1383

Wenz, T., F. Diaz, B. M. Spiegelman, and C. T. Moraes. 2008. Activation of the PPAR/PGC-1alpha pathway prevents a bioenergetic deficit and effectively improves a mitochondrial myopathy phenotype. Cell Metab 8(3):249-256. doi: 10.1016/j.cmet.2008.07.006

Wenz, T., S. G. Rossi, R. L. Rotundo, B. M. Spiegelman, and C. T. Moraes. 2009. Increased muscle PGC-1alpha expression protects from sarcopenia and metabolic disease during aging. Proc Natl Acad Sci U S A 106(48):20405-20410. doi: 10.1073/pnas.0911570106

Williamson, D. L., D. C. Butler, and S. E. Alway. 2007. AMPK regulation of proliferation and differentiation in C2C12 culture models. The FASEB Journal 21(6):A1205-A1206. doi: 10.1096/fasebj.21.6.A1205-d

Wu, C. L., Y. Satomi, and K. Walsh. 2017. RNA-seq and metabolomic analyses of Akt1-mediated muscle growth reveals regulation of regenerative pathways and changes in the muscle secretome. BMC Genomics 18(1):181. doi: 10.1186/s12864-017-3548-2

Wu, P., J. Sato, Y. Zhao, J. Jaskiewicz, K. M. Popov, and R. A. Harris. 1998. Starvation and diabetes increase the amount of pyruvate dehydrogenase kinase isoenzyme 4 in rat heart. Biochem J 329 (Pt 1):197-201. doi: 10.1042/bj3290197

Wu, X., Y. He, H. Hsuchou, A. J. Kastin, J. C. Rood, and W. Pan. 2010a. Essential role of interleukin-15 receptor in normal anxiety behavior. Brain Behav Immun 24(8):1340-1346. doi: 10.1016/j.bbi.2010.06.012

Wu, X., H. Hsuchou, A. J. Kastin, Y. He, R. S. Khan, K. P. Stone, M. S. Cash, and W. Pan. 2011. Interleukin-15 affects serotonin system and exerts antidepressive effects through IL15Ralpha receptor. Psychoneuroendocrinology 36(2):266-278. doi: 10.1016/j.psyneuen.2010.07.017

Wu, X., W. Pan, K. P. Stone, Y. Zhang, H. Hsuchou, and A. J. Kastin. 2010b. Expression and signaling of novel IL15Ralpha splicing variants in cerebral endothelial cells of the blood-brain barrier. J Neurochem 114(1):122-129. doi: 10.1111/j.1471-4159.2010.06729.x

Yi, W., P. M. Clark, D. E. Mason, M. C. Keenan, C. Hill, W. A. Goddard, 3rd, E. C. Peters, E. M. Driggers, and L. C. Hsieh-Wilson. 2012. Phosphofructokinase 1 glycosylation regulates cell growth and metabolism. Science 337(6097):975-980. doi: 10.1126/science.1222278

Yoon, T., and J. A. Cowan. 2004. Frataxin-mediated iron delivery to ferrochelatase in the final step of heme biosynthesis. J Biol Chem 279(25):25943-25946. doi: 10.1074/jbc.C400107200

Zampino, M., R. D. Semba, F. Adelnia, R. G. Spencer, K. W. Fishbein, J. A. Schrack, E. M. Simonsick, and L. Ferrucci. 2020. Greater skeletal muscle oxidative capacity is associated with higher resting metabolic rate: results from the Baltimore Longitudinal Study of Aging. J Gerontol A Biol Sci Med Sci doi: 10.1093/gerona/glaa071

Zeng, P. L., H. C. Yan, X. Q. Wang, C. M. Zhang, C. Zhu, G. Shu, and Q. Y. Jiang. 2013. Effects of dietary lysine levels on apparent nutrient digestibility and serum amino Acid absorption mode in growing pigs. Asian-Australas J Anim Sci 26(7):1003-1011. doi: 10.5713/ajas.2012.12555

Zhang, P., X. Liang, T. Shan, Q. Jiang, C. Deng, R. Zheng, and S. Kuang. 2015. mTOR is necessary for proper satellite cell activity and skeletal muscle regeneration. Biochem Biophys Res Commun 463(1-2):102-108. doi: 10.1016/j.bbrc.2015.05.032

Zierath, J. R., A. Krook, and H. Wallberg-Henriksson. 1998. Insulin action in skeletal muscle from patients with NIDDM. Mol Cell Biochem 182(1-2):153-160.

Zisman, A., O. D. Peroni, E. D. Abel, M. D. Michael, F. Mauvais-Jarvis, B. B. Lowell, J. F. Wojtaszewski, M. F. Hirshman, A. Virkamaki, L. J. Goodyear, C. R. Kahn, and B. B. Kahn.

2000. Targeted disruption of the glucose transporter 4 selectively in muscle causes insulin resistance and glucose intolerance. Nat Med 6(8):924-928. doi: 10.1038/78693

Zorzano, A., P. Munoz, M. Camps, C. Mora, X. Testar, and M. Palacin. 1996. Insulin-induced redistribution of GLUT4 glucose carriers in the muscle fiber. In search of GLUT4 trafficking pathways. Diabetes 45 Suppl 1:S70-81. doi: 10.2337/diab.45.1.s70

Zurlo, F., K. Larson, C. Bogardus, and E. Ravussin. 1990. Skeletal muscle metabolism is a major determinant of resting energy expenditure. J Clin Invest 86(5):1423-1427. doi: 10.1172/JCI114857

Chapter 2. Skeletal muscle O-GlcNAc transferase is important for muscle energy homeostasis and whole-body insulin sensitivity

Reprinted from Molecular Metabolism. Hao Shi, Alexander Munk, Thomas T. Nielsen, Morgan R. Daughtry, Louise Larsson, Kasper F. Høyer, Hannah Geisler, Karolina Sulek, Rasmus Kjøbsted, Taylor Fisher, Marianne M. Andersen, Zhengxing Shen, Ulrik K. Hansen, Eric M. England, Zhiyong Cheng, Kurt Højlund, Jørgen F.P. Wojtaszewski, Xiaoyong Yang, Matthew W. Hulver, Richard F. Helm, David E. Gerrard. 2018. Skeletal muscle O-GlcNAc transferase is important for muscle energy homeostasis and whole-body insulin sensitivity. Molecular metabolism. 11: 160–177.

Author Contributions

HS, AM, JTT, and DEG designed the experiments. HS, AM, TSN, MRD, LL, SL, KF, HWG, KS, RK, TF, MMA, ZS, and UKH conducted experiments and analyzed the data. EME, ZC, MWH, and RFH provided expertise for data interpretation. JFPW and KH performed the human experiments. XY provided founder OGT KO mice. HS, AM, JTT, and DEG wrote the manuscript. All authors read and approved the final version of the paper. JTT and DEG secured funding and provided supervision.

Abstract

Objective

Given that cellular O-GlcNAcylation levels are thought to be real-time measures of cellular nutrient status and dysregulated O-GlcNAc signaling is associated with insulin resistance, we evaluated the role of O-GlcNAc transferase (OGT), the enzyme that mediates O-GlcNAcylation, in skeletal muscle.

Methods

We assessed O-GlcNAcylation levels in skeletal muscle from obese, type 2 diabetic people, and we characterized muscle-specific OGT knockout (mKO) mice in metabolic cages and measured energy expenditure and substrate utilization pattern using indirect calorimetry. Whole

body insulin sensitivity was assessed using the hyperinsulinemic euglycemic clamp technique and tissue-specific glucose uptake was subsequently evaluated. Tissues were used for histology, qPCR, Western blot, co-immunoprecipitation, and chromatin immunoprecipitation analyses.

Results

We found elevated levels of O-GlcNAc-modified proteins in obese, type 2 diabetic people compared with well-matched obese and lean controls. Muscle-specific OGT knockout mice were lean, and whole body energy expenditure and insulin sensitivity were increased in these mice, consistent with enhanced glucose uptake and elevated glycolytic enzyme activities in skeletal muscle. Moreover, enhanced glucose uptake was also observed in white adipose tissue that was browner than that of WT mice. Interestingly, mKO mice had elevated mRNA levels of *Il15* in skeletal muscle and increased circulating IL-15 levels. We found that OGT in muscle mediates transcriptional repression of *Il15* by O-GlcNAcylating Enhancer of Zeste Homolog 2 (EZH2).

Conclusions

Elevated muscle O-GlcNAc levels paralleled insulin resistance and type 2 diabetes in humans. Moreover, OGT-mediated signaling is necessary for proper skeletal muscle metabolism and whole-body energy homeostasis, and our data highlight O-GlcNAcylation as a potential target for ameliorating metabolic disorders.

Keywords: O-GlcNAc signaling, Type 2 diabetes, N-acetyl-d-glucosamine, Tissue cross talk, Epigenetic regulation of *Il15* transcription, Insulin sensitivity

Introduction

Protein modification by O-linked β-D-N-acetylglucosamine (O-GlcNAc) is a post-translational event that results in the transfer of a sugar derivative emanating from the hexosamine biosynthetic pathway to a variety of cellular proteins (Bond and Hanover, 2013). Several lines of evidence support the notion that the addition and removal of an O-GlcNAc moiety from serine and threonine hydroxyls by O-GlcNAc transferase (OGT) and O-GlcNAcase (OGA), respectively, serve as an integrated cellular nutrient sensor. First, the amount of O-GlcNAc-modified cellular proteins increases in response to elevated nutrient and energy availabilities (Slawson et al., 2010). Second, the activity of key signaling molecules in the canonical insulin signaling pathway, such as the β subunit of the insulin receptor, IRS1, IRS2, p85 and p110 subunits of PI3K, PDK1, and Akt is generally inhibited by OGT-dependent O-GlcNAcylation (Issad et al., 2010; Lefebvre et al., 2010; Xu et al., 2012; Ruan et al., 2013; Bullen et al., 2014). Third, transcription co-factors such as FOXO1 and PGC-1α, which are master regulators of gluconeogenesis and lipid metabolism, respectively, are targeted by OGT which results in the stabilization of the proteins (Ruan et al., 2012). Fourth, OGT and the energy sensor AMP-activated protein kinase (AMPK) physically interact and mutually modify each other's function and/or localization (Bullen et al., 2014; Xu et al., 2014). Accordingly, dysregulation of cellular O-GlcNAcylation may be involved in the pathogenesis of a number of metabolic diseases, including obesity and type 2 diabetes (Hanover et al., 2012; Harwood and Hanover, 2014). This is evidenced by findings showing critical roles of O-GlcNAcylation status in AgRP and α-CaMKII positive neurons for maintaining whole body energy balance in mice (Ruan et al., 2014; Lagerlof et al., 2016).

Skeletal muscle is an important metabolic tissue and plays essential roles in locomotion and thermogenesis, both having significant impacts on global glucose metabolism and insulin

sensitivity (Watt et al., 2006; Bostrom et al., 2012; Funai et al., 2013; Song et al., 2013). Skeletal muscle utilizes a highly complex set of intercalated and coordinated signaling mechanisms to respond to altered environmental nutritional cues (Baskin et al., 2015; Hardie et al., 2016; Ross et al., 2016). Previous studies have suggested that dysregulated O-GlcNAc signaling in skeletal muscle is associated with the development of several metabolic diseases. For example, over-expression of OGT in muscle and adipose tissue causes insulin resistance and impairs glucose transport, respectively (McClain et al., 2002; Love and Hanover, 2005). In addition, overexpression of OGA, which eliminates O-GlcNAcylation, impairs myogenesis and induces muscle atrophy (Huang et al., 2011; Ogawa et al., 2012). These findings suggest that O-GlcNAcylation may be part of a complex signaling mechanism within skeletal muscle that is responsible for monitoring cellular nutrient availability and conveying this information to downstream targets to induce metabolic adaptation. Apart from the studies mentioned above, however, the precise role of O-GlcNAcylation in skeletal muscle remains largely unexplored. Herein, we show that skeletal muscle from type 2 diabetic humans has elevated O-GlcNAcylation levels compared with matched controls. Moreover, we show that knockout of OGT in skeletal muscle in mice causes alterations of muscle metabolism that improves whole-body insulin sensitivity and increases energy expenditure. We propose a mechanism whereby lack of OGT results in perturbed regulation of *Il15* expression, which subsequently drives the observed phenotype.

Materials and methods

Human Samples

Human skeletal muscle samples were obtained from a previous study (Hojlund et al., 2009). In short, muscle samples were obtained from the vastus lateralis muscle (Bergström needle

biopsy) before and after a 4-hour euglycemic hyperinsulinemic clamp (40 mU * m^{-2} * min^{-1}) under local anesthesia. Muscle biopsy samples were quickly blotted free of blood and frozen in liquid nitrogen. Muscle lysates were prepared from freeze-dried muscle dissected free of visible blood, fat, and connective tissue and homogenized as previously described (Birk and Wojtaszewski, 2006). Lysates were collected from the supernatant of homogenates centrifuged for 20 min at 16,000 *g* and 4 °C. Total protein content in lysates was analyzed by the bicinchoninic acid method (ThermoFisher Scientific). Muscle lysates were prepared in Laemmli buffer and heated for 10 min at 96 °C after which equal amounts of protein were separated by SDS-PAGE. Proteins were transferred to PVDF membranes and incubated with the indicated antibodies.

Animals

Mice were generated and experiments performed at either the Novo Nordisk Foundation Center for Basic Metabolic Research, University of Copenhagen, or Virginia Polytechnic Institute and State University. Muscle specific *Ogt* deletion was achieved by breeding $HSA^{Cre/+}$; $Ogt^{LoxP/Y}$ (JaxMice, strain: B6.Cg-Tg(ACTA1-cre)79Jme/J) males with $Ogt^{LoxP/LoxP}$ females to generate $HSA^{+/+}$; $Ogt^{LoxP/Y}$ (WT) and $HSA^{Cre/+}$; $Ogt^{LoxP/Y}$ (mKO) mice. Inducible muscle-specific OGT knockout mice were generated by breeding HSA-rtTA / TRE-Cre (JaxMice, strain B6; C3-Tg(ACTA1-rtTA,tetO-Cre)102Monk/J) male mice with $Ogt^{LoxP/LoxP}$ females. All procedures were approved by the Danish Animal Experiments Inspectorate and complied with the European convention for protection of vertebrate animals used for scientific purposes (EU Directive 2010/63/EU for animal experiments), or they were approved by Institutional Animal Care and Use Committee of the Virginia Polytechnic Institute and State University and complied with the National Institutes of Health guidelines (NIH Publications No. 8023). Mice were group-housed in an enriched environment with a 12 h light:12 h dark cycle with *ad libitum* feed (#1310, Altromin

for mice at University of Copenhagen, and #2918, Envigo for mice at Virginia Polytechnic Institute and State University) and water in a temperature-controlled (22 °C ± 1 °C) room. Mice used for HFD study were fed Teklad rodent diets (#TD.06414, Envigo) with 60% calories coming from fat. The fatty acid profile (% of total fat) is as follows: 37% saturated, 47% monounsaturated, 16% polyunsaturated. The control diet was the standard chow (#2918, Envigo). Mice were fed HFD or normal chow from 4 weeks of age for the indicated weeks.

Whole body metabolic assessment

Whole body metabolic phenotyping was performed at Virginia Tech Metabolic Phenotyping Core using the TSE LabMaster Indirect Calorimetry System. For acclimation purpose, mice were housed in a mock LabMaster cage for one week before they were transferred to recording cages to measure locomotor activity and indirect calorimetry. Mice were fed *ad libitum* during the indicated experimental period. Cage activity, energy expenditure normalized to lean body mass, and respiratory exchange rates were recorded for a 48-h period at the interval of 20 min. Whole body composition was measured by MRI (Minispec Whole Body Composition Analyzer, Bruker). Rectal temperature was recorded at 4PM using an ETI Microtherma 2 Type T thermometer (ThermoWorks). The probe was inserted into the anal ducts of the mice (around 2 cm) when animal was awake in the absence of anesthesia.

Histology and immunohistochemistry

Muscle, WAT, liver, and pancreas were collected from WT and mKO mice and fixed in 10% neutral buffered formalin (0.4% sodium phosphate monobasic, 0.65% sodium phosphate dibasic, 10% formalin, pH 6.8) overnight. The tissues were then washed twice in 70% ethanol, and paraffin-embedded. For H&E staining, tissue sections were de-paraffinized with two exchanges of xylene, rehydrated in 100%, 95%, and 70% ethanol respectively. After a brief wash in water,

sections were stained in Harris hematoxylin for 8 min, washed in running water for 1 min, soaked in 0.2% ammonia water for 1 min. After washing in running water for 5 min, the tissue sections were rinsed in 95% ethanol for 10 s. Sections were then counterstained with eosin solution for 30 s, dehydrated in 95% ethanol, 100% ethanol, and xylene, and mounted for microscopy. For immunohistochemical staining, paraffin-embedded sections were de-paraffinized and re-hydrated, and antigen was retrieved by heating the sections in boiling sodium citrate buffer (10 mM sodium citrate, 0.05% Tween 20, pH 6.0) for 30 min. After cooling down at room temperature for 20 min, tissue sections were blocked in 5% goat serum for 1 h at room temperature before applying primary antibodies anti-UCP1 (#10983 Abcam) or anti-succinate dehydrogenase (#14715 Abcam), 1:200 diluted in 5% goat serum. After incubation in the primary antibody overnight at 4 °C, sections were washed in 1 x PBS three times with 5 min each. The sections were then incubated in Alexa Fluor 488 conjugated goat anti rabbit IgG (#A-11078 ThermoFisher Scientific) or Alexa Fluor 555 goat anti mouse IgG (#A-21424 ThermoFisher Scientific) highly cross-absorbed antibodies, respectively, for 1 h at room temperature, washed in PBS, and mounted in fluorescent mounting medium for microscopy. Images were taken using a Nikon ECLIPSE Ti-E fluorescent microscope (Nikon Instruments).

Ex vivo EDL and soleus muscle contractility assay

Isolated soleus and extensor digitorum longus (EDL) muscles from male mice (12–16 weeks of age) were used for muscle contractility assays. Muscles were incubated at 30 °C in oxygenated (95% O2 and 5% CO2) physiological salt solution as previously described in (Wolff et al., 2006) for Figure 1M–P and in (Treebak et al., 2009) for Figure 1Q–T. The buffer was continuously oxygenated with 95% O2 and 5% CO2 during the incubation period and maintained at 30 °C. For results shown in Figure 1M–P, muscles were set to an initial resting tension of 10 mN

(optimal length, L0; 300B, Aurora Scientific) and maintained by a stepper motor. Dynamic Muscle Control software (DMC Version 4.1.6, Aurora Scientific) was used to control the force and position inputs of the servomotor arm and the stepper motor. For results shown in Figure 1M–O, the stimulated muscle was subjected to 3 isometric twitches and two tetani (150 Hz) each separated by 1 min. For Figure 1P, the muscle was subjected to a force frequency protocol consisting of 6 stimulations of increasing frequency (1, 30, 50, 80, 100, and 150 Hz), one min apart. For results shown in Figure 1Q–T, muscles were incubated in a muscle strip myograph system (820MS, DMT, Denmark) at a 5–6 mN tension. Muscles were stimulated to contract using the following protocol: stimulus frequency 100 Hz; stimulus width 0.2 ms; stimulus train duration 1 sec train every 15 sec. The total stimulation protocol was 9 min.

Hyperinsulinemic euglycemic clamp experiments

The hyperinsulinemic euglycemic clamp was performed in conscious, unrestrained male mice at 17–19 weeks of age as previously described (Jensen et al., 2016). For the surgical catheterization, mice were anesthetized with isoflurane (2.5% for induction, 1.5% for maintenance). Lidocain (7 mg/kg; Xylocain, AstraZeneca, Sweden) and Carprofen (10 mg/kg; Rimadyl, Pfizer, USA) were administered preoperatively for analgesia. All surgical procedures were conducted using strictly aseptic techniques. The carotid artery and jugular vein were cannulated and the catheters were externalized on the back (caudal to the scapulae) with a dual channel vascular access button (Instech, PA, USA). After surgery, the catheters were locked with heparinized saline (200 U/mL) and the animals recovered for 6–7 days. Body weight was recorded before and 24 h after the operation and on the day of the clamp. The inclusion criteria following surgery were a weight loss of less than 10% and a hematocrit above 35% by day 6–7. All mice fulfilled these criteria. On the day of the clamp experiment, mice were fasted for 5 h starting at

7:30 AM (t = −300 min) by placing them in a clean cage with bedding and nesting material, and free access to water. At t = −120 min the mice were placed in a new cage of ~20 × 20 cm, the catheters were flushed with heparinized saline (10 U/mL) and the mice were connected to the infusion lines. A tracer equilibration period was started at t = −90 min by infusion of a 1.2 μCi priming dose of [3-3H]glucose (Product no. NET331C005 MC; Perkin Elmer, USA) followed by a constant 0.04 μCi/min infusion of [3-3H]glucose for 90 min. Blood samples were collected for the assessment of baseline hematocrit level (40 μL) as well as basal glucose levels and turnover rates at t = −15 min (50 μL) and −5 min (100 μL), respectively. The clamp was initiated at t = 0 min with continuous infusions of human insulin (4 mU/kg/min; Actrapid, Novo Nordisk, Denmark) and washed red blood cells obtained from a donor mouse to compensate for the blood loss due to repeated sampling (5 μL/min of 50% RBC in 10 U/ml heparinized saline). Blood glucose was measured every 10 min (Contour XT; Bayer, USA) and euglycemia was maintained by adjusting a variable infusion of 50% glucose containing 0.06 μCi/μL of [3-3H]glucose tracer. Between t = 80 and t = 120 min blood samples (50–100 μL) were collected in 10 min intervals and processed for determination of [3-3H]glucose specific activity. At t = 110 min hematocrit was measured again to ensure that hematocrit levels were stable. At t = 120 min a 12 μCi bolus of 2-[1–14C]-deoxy-d-glucose (Product no. NEC495250UC; Perkin Elmer, USA) was injected and blood samples were collected at t = 122, 125, 135, 145, and 155 min, respectively. These samples were processed for determination of 2-[1–14C]-deoxy-d-glucose specific activity. After the final blood sample, mice were euthanized with a lethal dose of pentobarbital and tissues were collected and snap-frozen in liquid nitrogen. The tissues were processed for determination of 2-[1–14C]-deoxy-d-glucose specific activity in order to calculate tissue-specific glucose uptake.

Clamp sample processing and calculations

Plasma samples were deproteinized with $Ba(OH)_2$ and $ZnSO_4$, and aliquots of each supernatant were transferred to 2 scintillation vials. To determine plasma [3-3H]glucose, one of the aliquots was dried and resuspended in MilliQ water to remove $3H_2O$ and the other was counted directly (Hidex 300 SL). Supernatants for 2-[1–14C]-deoxy-d-glucose determinations were counted directly. Total plasma glucose concentration was determined by adding a reaction mix (200 mM Tris–HCl, 500 mM MgCl2, 5.2 mM ATP, 2.8 mM NADP, and 148 μg of a hexokinase and G6PDH mixture (Roche, Germany) pH 7.4) to each sample and measuring absorbance at 340 nm. Parameters related to glucose turnover rates (Ra, Rd, endoRa, glycolysis) were calculated as previously described (Ayala et al., 2006). Tissues were homogenized in ice-cold lysis buffer (pH 7.4, 10% glycerol, 1% IGEPAL, 50 mM Hepes, 150 mM NaCl, 10 mM NaF, 1 mM EDTA, 1 mM EGTA, 20 mM sodium pyrophosphate, 2 mM sodium orthovanadate, 1 mM sodium-pyrophosphate, 5 mM nicotinamide, 4 μM Thiamet G, and protease inhibitors (SigmaFast)). Aliquots of each crude homogenate were transferred to two 1.5 mL tubes and deproteinized with 4.5% perchloric acid or $Ba(OH)_2$ + $ZnSO_4$. Supernatants were transferred to scintillation vials and counted to determine 2-[1–14C]-deoxy-d-glucose content. Tissue-specific glucose uptake rates were calculated as described previously (Ferre et al., 1985).

Insulin and glucose tolerance test

Mice were fasted for four hours before insulin tolerance test (ITT). Bovine insulin (Sigma) was prepared in sterile saline and intraperitoneally injected at the dosage of 1 U/kg body weight. Blood glucose level was measured at 0, 15, 30, 60, 90, and 120 min after insulin injection using OneTouch Ultra2 test strip and glucometer. For glucose tolerance test (GTT), mice were fasted overnight (16 h) before the experiment, glucose was intraperitoneally injected at the dosage of 2 g/kg body weight, and blood collection and measurement were the same as ITT.

Skeletal muscle mitochondrial isolation

Isolation of mitochondria from skeletal muscle was performed as previously described (Frezza et al., 2007). Briefly, quadriceps femoris and gastrocnemius muscles were collected in buffer containing 67 mM sucrose, 50 mM Tris/HCl, 50 mM KCl, 10 mM EDTA/Tris, and 10% BSA (Sigma). Before homogenization, muscle samples were minced with scissors, and digested in PBS containing 0.05% trypsin (Invitrogen) and 10 mM EDTA (Sigma) for 30 min. Muscles were homogenized with a Teflon pestle at the speed of 1,600 rpm and mitochondria were isolated by differential centrifugation.

Respirometry of isolated mitochondria

Mitochondrial respiration was measured using an XF24 extracellular flux analyzer (Seahorse bioscience) as previously described (Gerencser et al., 2009). Freshly isolated mitochondria were seeded at 5 μg per well in a Seahorse XF Cell Culture Microplate. Mitochondria were suspended in a sucrose/mannitol solution containing pyruvate (10 mM) and malate (5 mM). Mitochondria were mixed for 25 sec before the measurement cycles. Oxygen consumption rates (OCRs) at basal conditions (state 2), ADP (5 mM) stimulation (state 3), ADP exhaustion (state 4), oligomycin (2 μM) induction (state 4°), and FCCP (0.3 μM) induction were measured to assess mitochondrial oxidative capacity. All experiments were performed at 37 °C.

Fatty acid oxidation and PDH activity assay

Fatty acid oxidation was assessed in muscle homogenates as previously described (Frisard et al., 2010). Briefly, [1–^{14}C]-palmitic acid (Perkin Elmer) was used as the substrate, $^{14}CO_2$ production and ^{14}C-labeled acid-soluble metabolites were measured by liquid scintillation counting. Pyruvate dehydrogenase (PDH) activity was assayed using [1–^{14}C]-

pyruvate as substrate, enzyme catalyzed release of $^{14}CO_2$ was counted to reflect PDH enzyme activity.

Citrate synthase (CS) and malate dehydrogenase (MDH) activity assay

CS and MDH activities were determined as previously described (Frisard et al., 2010). CS activity was determined by the rate of DNTB reduction upon exposure to acetyl CoA, the product (TNB) is measured spectrophotometrically at 412 nm. Malate dehydrogenase (MDH) activity was determined by the rate of NADH oxidation in the presence of oxaloacetate and measured at 340 nm.

Western blot analysis

Skeletal muscle samples used in Figure 7, Figure 8 were lysed in RIPA buffer (in mM: 200 NaCl, 20 Tris-Cl at pH 8.0, 1 EDTA, 1 EGTA, 1% Nonidet P-40, 0.5% sodium deoxycholate, 0.1% SDS, 2.5 sodium pyrophosphate, 1 β-glycerol phosphate, 1 Na_3VO_4, and protease inhibitor cocktail (Sigma) and protein concentration was determined using a Bicinchoninic Acid (BCA) Protein Assay kit (Pierce). All other tissue samples were processed using steel bead homogenization (Tissue Lyser II, Qiagen) in ice-cold lysis buffer (pH 7.4; 10% glycerol; 1% IGEPAL; Hepes, 50 mM; NaCl, 150 mM; NaF, 10 mM; EDTA, 1 mM; EGTA, 1 mM; sodium pyrophosphate, 20 mM; sodium orthovanadate, 2 mM; sodium-pyrophosphate 1 mM; nicotinamide 5 mM; Thiamet G 4 μM and protease inhibitors (SigmaFast, Sigma Aldrich) according to manufacturer's instructions). Equal amounts of protein were separated using SDS-PAGE and transferred to PVDF membranes. Antibodies used for Western blot analyses were: anti-OGT (#SAB2101676 Sigma), anti-O-GlcNAc (#2739 Abcam), anti-ATP synthase β subunit (#A-21351 ThermoFisher Scientific), anti-succinate dehydrogenase A subunit (SDHA) (#14715 Abcam), OGT (#5368 CST), O-GlcNAc (CTD110.6 #9875 CST), OGA (#124807 Abcam),

Hexokinase II (#2867 CST), PFK1 (#166722 Santa Cruz Biotechnology (SCBT)), PDH (#C54G1 CST), PDH pS293 (#ABS204 Millipore), PDH pS300 (#ABS194 Millipore), ACC pS79/257 (#07–300 Millipore), Insulin receptor β (#3025 CST), IRS1 (#23822 CST), AKT 1/2/3 (#9272 CST), AKT pT308 (#9275 CST), AKT pS473 (#9271 CST), AKT1 (#5298 SCBT), TBC1D4 (#07–741 Millipore), TBC1D4 pS711 (Custom), TBC1D4 pS324 (Custom), ATGL (#2138 CST), HSL (#4107 CST), HSL pS563 (#4139 CST), GFAT1 (#125069 Abcam), GLUT4 (#PA1-1065 Thermo Fisher).

Metabolomics analysis

OGT mKO (n = 10) and WT (n = 8) mice underwent a hyperinsulinemic euglycemic clamp. Following this procedure muscle samples were collected, frozen in liquid nitrogen, and stored at −80 °C. Whole muscle sample was pulverized under liquid nitrogen and 30 ± 3 mg (exact mass was noted) underwent metabolomics analysis. Methanol at concentrations 50%, 80%, and 100% with water was used for the metabolites extraction from the muscles. Metabolites were profiled using liquid chromatography combined with mass spectrometry. Following data bucketing and normalization, student t-test with false discovery rate analysis was performed. Detailed metabolomics analysis is available in the Supplementary Materials.

Quantitative RT-PCR

Directzol RNA Miniprep Kit (Zymo Research) was used to extract total RNA from skeletal muscle or adipose tissue. High-Capacity cDNA Reverse Transcription Kit (Thermo Fisher Scientific) was used to perform reverse transcription. Fast SYBR Green Master Mix (Thermo Fisher Scientific) and 7500 Fast Real Time PCR System (Thermo Fisher Scientific) were used to carry out qPC reaction. Primers used in this paper were published elsewhere (Kim et al., 2013). Quantification was performed using ΔΔCT method.

Muscle extract collection and SVF cell isolation

Muscle extracts were collected by isolating both WT and mKO gastrocnemius muscles and placing them in DMEM for 2 h at 37 °C with 80rpm agitation. The conditioned media were collected, and protein concentration determined. The conditioned media were mixed with SVF cell differentiation media to assess the effect of muscle extracts on SVF cell differentiation. For SVF cell isolation, inguinal WATs were collected from adult C57BL/6J mice, minced, and transferred to digestion medium (Ham's F10 medium containing 500 units per mL collagenase II 10% horse serum, 1% penicillin/streptomycin, and 0.1% gentamycin) for 1 h at 37 °C with 80 rpm agitation. To stop the digestion, complete medium (DMEM containing 10% FBS and 1% penicillin/streptomycin) was added followed by triturating 20 times to generate a homogenous mixture. The cells were centrifuged at 450 *g* for 5 min, and the supernatant was discarded. The pellet containing the SVF cells was re-suspended in complete medium, filtered through a 40 μM cell strainer, and the throughput was centrifuged. The pellet was re-suspended in complete medium and plated onto a 15 cm collagen-coated dish. Two hours later the cells were washed with PBS to remove alternate cell types. After reaching confluence, the cells were re-plated on 12-well collagen-coated dishes at 1,000 cells per mm^2. Twenty-four hours after plating, cells were changed to induction medium (complete medium containing 5 μg/μl insulin, 1 nM 3,3′,5-triiodo-l-thyronine, 125 μM indomethacin, 2 μg/mL dexamethasone, and 0.5 mM 3-isobutyl-1-methylxanthine), mixed with WT and mKO muscle extracts in the presence or absence of IL15 antibody. After 72 h the cells were changed to maintenance medium (complete medium containing 5 μg/μL insulin and 1 nM 3,3′,5-triiodo-l-thyronine) with muscle extracts with or without IL15 antibody. After 96 h, the cells were fixed with 10% formalin, stained with Oil Red O, and imaged.

Immunoprecipitation (IP)

For IP, gastrocnemius muscles were isolated from mice, minced and homogenized in NP40 lysis buffer (50 mM Tris–HCl, 1% NP40, 150 mM NaCl, 1 mM EDTA) in the presence of 1 mM PMSF, 1 μg/mL leupeptin, 1 μg/mL aprotinin, 1 μg/mL pepstatin, 1 mM Na_3VO_4, 1 mM NaF, and 40 μM PUGNAc. Antibodies against O-GlcNAc (Abcam, RL2) and EZH2 (Abcam) were incubated with 500 μg of total protein overnight at 4 °C with agitation, respectively. The immune complexes were incubated with protein A beads, washed, and eluted using sample buffer for further immunoblotting analysis.

Chromatin immunoprecipitation (ChIP)

ChIP was performed as previously described (Nelson et al., 2006). The precipitated chromatin was purified and DNA was quantified using quantitative RT-PCR. The ChIP-grade antibodies against O-GlcNAc, EZH2, and H3K27me3 were bought from Abcam. Primers for the *Il15* promoter were as follows: forward GCC TGT TTG GGA ACA GTA AAC; reverse CAA CTT AAA GAT GCT GCC TTA CC.

Statistical analyses

Results are presented as means ± SEM. Levene's test for homogeneity of variances was performed prior to statistical comparisons between groups. Data were log10 transformed if Levene's test was significant. In all cases, this was sufficient to obtain equal variance. Comparison between two groups was performed using Student's *t* test with two-tailed distribution. For multiple-group comparisons, one-way and two-way ANOVAs were used to test for no differences among the group means. In case of significant interactions, Tukey's multiple comparison test was performed post hoc. $p < 0.05$ was considered statistical significant.

Results

Type 2 diabetes is associated with elevated O-GlcNAcylation levels in skeletal muscle

We hypothesized that increased blood glucose concentrations observed in type 2 diabetic people would result in elevated O-GlcNAcylation of proteins in skeletal muscle. Vastus lateralis muscle biopsies were obtained before and after a 4-hour hyperinsulinemic euglycemic clamp from well-matched lean, obese, and obese, insulin resistant type 2 diabetic patients (Hojlund et al., 2009). We found that 'global' O-GlcNAcylation levels were significantly increased in type 2 diabetic people independent of insulin compared with controls (Figure 2-1A). Moreover, we quantified protein abundance of key O-GlcNAc-related enzymes OGT, OGA, and glutamine:fructose-6-phosphate amidotransferase (GFAT), all of which showed no difference in total protein abundance (Supplementary Figure 2-1 A-C). These data show that O-GlcNAcylation increases in muscle tissue with blood glucose levels and suggest that skeletal muscle OGT may be involved in the development of insulin resistance and type 2 diabetes in humans. These data prompted us to investigate further the role of OGT in skeletal muscle.

Mice lacking muscle OGT have a lean phenotype

To assess the role of OGT in skeletal muscle, we bred male mice harboring Cre recombinase the expression of which was driven by the human skeletal α-actin promoter (HSA-Cre mice) with *Ogt* floxed homozygous female mice to generate muscle-specific hemizygous OGT knockout (mKO) and wild type (WT) mice. OGT was ablated in skeletal muscle as evidenced by the lack of OGT protein in tibialis anterior (TA), soleus, and extensor digitorum longus (EDL) muscle of mKO mice, (Figure 2-1B). Consequently, O-GlcNAcylation levels in these muscles were greatly reduced (Figure 2-1C). Moreover, levels of O-GlcNAcase (OGA) were significantly reduced in all three muscles (Figure 2-1D), suggesting a corresponding compensatory mechanism of the reciprocal cellular O-GlcNAcylation. Additionally, and as expected, we found no difference in OGT protein levels in the heart (Supplementary Figure 2-2A). By 12 weeks of age, mKO mice

had similar body weights compared with WT controls (Figure 2-1E). However, after 12 weeks of age, mice lacking muscle OGT were significantly smaller than WT mice (Figure 2-1E), yet no differences in muscle cross sectional area or muscle fiber number were noted in the soleus or EDL muscles (Supplementary Figure 2-2 B-D). This reduction in body mass was associated with a reduction in whole-body fat accumulation (Figure 1F), but not lean mass (Figure 2-1G) at 16 weeks of age in mKO compared to their WT littermates. Consistently, muscle weights of TA, soleus, and EDL did not differ among genotypes at 16 weeks of age (Figure 2-1H). Fat depots, including the anterior subcutaneous white adipose tissue (AsW), inguinal white adipose tissue (IngW), and epididymal white adipose tissue (EpiW), but not the brown adipose tissue (BAT), were greatly reduced in mKO compared to those of WT mice (Figure 2-1I,J). This reduction in fat mass was partly due to smaller adipocytes (Figure 2-1K) and a corresponding browning of white adipose tissue as assessed by immunohistochemistry analysis for UCP1 (Figure 2-1L). No differences in *Ucp1* gene expression in BAT were observed (Supplementary Figure 2-2E). To assess whether muscle function was impacted by OGT ablation, we assessed muscle contractile properties. No differences in single-twitch force (Figure 2-1M), half-relaxation time of the single twitch (Figure 2-1N), or time to peak tension (Figure 2-1O) were observed between WT and mKO EDL muscles. Muscle force of EDL during tetanic contractions increased gradually with stimulation frequency, but no differences were noted between genotypes (Figure 2-1P). Moreover, we did not observe any differences between WT and mKO soleus and EDL muscles in terms of force production during a single tetanic contraction or fatigue-ability during repeated tetanic contractions (Figure 2-1 Q–T). Collectively, these data show that mKO mice have a lean phenotype due to a reduction in whole-body fat mass, yet no functional alterations in muscle growth, development, or function were identified.

Muscle-specific ablation of OGT enhances energy expenditure

To investigate the mechanism of the lean phenotype in mice lacking OGT in skeletal muscle, we assessed whole body energy metabolism by indirect calorimetry over a period of 48 h. Interestingly, we found that mKO mice were less active than WT mice in both light and dark phases of the day (Figure 2-2A,B). While mKO mice had less cage activity, their energy expenditure normalized to lean body mass was greater than WT mice (Figure 2-2C,D). Additionally, mKO mice had a higher respiratory exchange ratio (RER) compared to WT mice (Figure 2-2E,F), indicating that these mice have greater reliance on carbohydrates than fat for energy production. Food intake did not differ between genotypes (Figure 2-2G), but water consumption was greater in the mKO mice (Figure 2-2H). Given mKO mice weigh less than WT mice from 3 months of age (Figure 2-2E) and have less cage activity (Figure 2-2A,B), we hypothesized that ablation of muscle OGT caused an increase in energy expenditure in the form of heat production. Higher rectal temperatures were indeed noted for mKO mice compared to that of WT mice (Figure 2-2I). Taken together, these findings suggest that skeletal muscle OGT and O-GlcNAcylation may regulate muscle energy metabolism, which may affect activity and whole-body energy balance.

Lack of OGT in skeletal muscle affects glucose homeostasis, insulin signaling, and whole-body insulin sensitivity

To determine how ablation of OGT in skeletal muscle affects the ability of muscle to handle energy substrates, we performed a hyperinsulinemic euglycemic clamp to assess whole-body insulin sensitivity. Mice were clamped at 6 mM of blood glucose (Figure 2-3A,B), and mKO mice displayed a profound increase in glucose infusion rate (GIR) (Figure 2-3C,D). Interestingly, insulin levels at basal and during the clamp were significantly reduced in the mKO compared to WT mice

(Figure 2-3E). We found glucose uptake was markedly increased in TA, gastrocnemius, and triceps from mKO mice compared to WT mice, yet the differences were not consistent among muscles as there was no difference in glucose uptake in the EDL, quadriceps, and soleus muscles between genotypes (Figure 2-3F). In white adipose tissues, there were noticeable increases in glucose uptake in EpiW and IngW (Figure 2-3G). In contrast, brown adipose tissue (BAT) displayed a 50% decrease in glucose uptake, and there was no change of glucose uptake in heart or brain (Figure 2-3H). Glycogen levels in the liver after the clamp was increased in mKO mice, but skeletal muscle glycogen levels were not different between genotypes (Figure 2-3I). However, liver glycogen of the non-insulin-stimulated mKO cohort, used as blood donors for the clamped mice, was also increased (Figure 2-3J). While our data suggest that skeletal muscle and white adipose tissue are mainly responsible for the enhanced GIR in the mKO mice, the liver may play an important role in whole-body glucose utilization in these mice. In clamped gastrocnemius muscle, in which glucose uptake was increased, both total Akt protein abundance and Akt phosphorylation at T308 and S473 were increased in mKO mice compared to WT littermates (Figure 2-3K). Total Akt1 protein levels did not differ between genotypes (Figure 2-3L), suggesting that the enhanced level of Akt in the mKO mice is due to increased Akt2 abundance. Interestingly, the difference in Akt signaling between genotypes was not associated with differences in TBC1D4 phosphorylation status (Figure 2-3M); however, GLUT4 levels were significantly increased in the gastrocnemius muscle of the mKO mice compared to WT mice (Figure 2-3N). These data suggest that differences observed in whole body insulin sensitivity may not be due to classical insulin signaling events in skeletal muscle but may still be mediated by a larger increase in GLUT4 at the plasma membrane at a given insulin concentration.

Loss of OGT alters global muscle metabolism

Because loss of OGT in skeletal muscle resulted in increased energy expenditure and whole-body insulin sensitivity, we explored metabolic changes in skeletal muscle that could explain the lean phenotype of mKO mice. To this end, we investigated muscle metabolite levels in the gastrocnemius of clamped mice. Using an LC/MS-based metabolomics analysis, we identified 41 metabolites that differed between genotypes (Figure 2-4A). Of these, fructose 1,6 biphosphate (Fru-1,6P) and phosphoenolpyruvate (PEP) were reduced by 52% and 72%, respectively, in mKO muscle compared to WT muscle (Figure 2-4B). Western blot analyses revealed that hexokinase II (HKII) and phosphofructokinase 1 (PFK1) protein levels were unchanged (Supplementary Figure 2-2F,G). However, basal activity of pyruvate dehydrogenase (PDH) in non-insulin-stimulated gastrocnemius muscle was enhanced in mKO mice compared to WT mice (Figure 2-4C), and phosphorylation of PDH at S293 and S300 was decreased in clamped gastrocnemius muscle from mKO mice compared to WT mice (Figure 2-4D). These results indicate that, in response to insulin, glycolytic flux downstream of PEP is increased or that glucose is shunted into other pathways upstream of Fru-1,6P. The level of UDP-GlcNAc was upregulated by more than 300% in mKO (Figure 2-4E,F) compared to WT mice, and this increase was accompanied by a 3-fold upregulation of GFAT, which is the rate-limiting enzyme in the hexosamine biosynthesis pathway (HBP) (Figure 2-4G). Together, our data suggest that mKO muscle upregulates activities of both glycolysis and the HBP at least in clamped mice. However, the importance of the two pathways for glucose disposal in basal or clamp settings cannot be quantitatively evaluated using the available data.

Apart from changes in intracellular glucose metabolism, the metabolomics analysis indicated changes in fatty acid oxidation. Acetyl carnitine level (Figure 2-4H) was upregulated several fold in mKO mice compared to WT mice, so was the CoA precursor pantothenic acid

(Figure 2-4I), indicating that mKO mice exhibited increased capacity to shuttle fatty acids from the cytosol into the mitochondria. This was supported by the finding of increased *Cpt1α* and *Cpt1β* mRNA expression (Supplementary Figure 2-2H), although only *Cpt1α* levels were significantly changed. In addition, we found the total level of hormone sensitive lipase (HSL) to be unaltered, but HSL phosphorylation at S563, a surrogate measure of HSL activity, was significantly increased in mKO mice compared to WT mice (Figure 2-4J). Furthermore, adipose triglyceride lipase (ATGL) protein level was upregulated by 1.75 fold in mKO mice (Figure 2-4K). To assess whether beta-oxidation was altered, we measured fatty acid oxidation (FAO) in unstimulated gastrocnemius muscle. Interestingly, while there was no difference in complete fatty acid oxidation between WT and mKO muscles (Figure 2-4L), mKO muscles contained a significantly higher level of acid-soluble metabolites (ASM) (Figure 2-4M), a hallmark of incomplete FAO. However, mRNA levels of genes involved in FAO (i.e., *Acadl* and *Acadm*) were not significantly changed (Supplementary Figure 2-2H). Together, these data indicate that mKO muscle attempts to increase fatty acid oxidation, but increased ASMs suggest that complete oxidation of fatty acids may be impaired in skeletal muscle of these mice.

OGT ablation alters muscle oxidative capacity

In general, slow-twitch myofibers are enriched with mitochondria, capillaries and myoglobin, and they predominately use oxidative phosphorylation for ATP production. Fast-twitch myofibers, on the other hand, are more glycolytic and deposit greater amounts of glycogen as an energy reserve (Gunning and Hardeman, 1991; Bassel-Duby and Olson, 2006; Richard et al., 2011). To test whether OGT ablation causes changes in muscle fiber type composition, and thus oxidative capacity, we measured the expression of myosin heavy chain (MyHC) I (*Myh7*), IIa (*Myh2*), IIx (*Myh1*), and IIb (*Myh4*) genes in the gastrocnemius muscle. Type I MyHC gene

expression was significantly upregulated and type IIb MyHC gene expression was downregulated in OGT ablated muscle (Figure 2-5A). Consistent with increases in *Myh7* expression, the corresponding protein levels were also elevated in OGT mKO muscles (Figure 2-5A, inset). Moreover, three-dimensional confocal microscopy revealed that mKO muscle contains more mitochondria compared to WT muscle (Figure 2-5B), and increased mitochondrial content was confirmed by an increased mitochondrial DNA to nuclear DNA ratio in the gastrocnemius muscle (Figure 2-5B). Citrate synthase and malate dehydrogenase activity were also higher in white part of the gastrocnemius muscle from mKO mice (Figure 2-5C,D). However, when we measured the abundance of specific proteins in the OXPHOS complexes, we found complex V to be increased (although not significantly), whereas complex I and IV were reduced significantly in mKO compared to WT muscle (Figure 2-5E). To test the function of the mitochondria, we isolated mitochondria from gastrocnemius muscle and measured oxygen consumption rates. We found that mitochondria from mKO muscle have compromised respiration control ratio of state 3/state 4, indicating dysfunctional mitochondria (Figure 2-5F). Taken together, we show that dysregulation of O-GlcNAcylation in skeletal muscle drives muscle to a slower contracting, oxidative phenotype but perhaps at the expense of properly functional mitochondria.

High-fat diet fails to induce insulin resistance in mice lacking muscle OGT

Because mice lacking OGT in skeletal muscle are leaner, have higher energy expenditure, and are more insulin sensitive than WT mice, we challenged these mice with a high-fat diet (HFD) and monitored glucose metabolism and insulin action. WT mice fed a HFD for 24 weeks gained significantly more weight than the HFD-fed mKO mice (Figure 2-6A). At the end of HFD feeding, no differences in skeletal muscle fiber size were found, whereas the IngW of mKO mice exhibited significant browning compared with that of WT mice (Figure 2-6B). In IngW, mRNA expression

of genes involved in browning was also significantly upregulated (Supplementary Figure 2-2I). In the liver of WT mice lipid accumulation was wide-spread, whereas very little was detected in the mKO mice (Figure 2-6C). Moreover, hypertrophy of pancreatic islets was evident in the WT mice but no such obesity-induced pathology was noted in mKO mice (Figure 2-6C). Consistently, blood glucose levels after a 4-h fast in mKO mice fed 12 (Figure 2-6D) or 22 (Figure 2-6E) weeks of HFD were significantly lower than in WT controls. In addition, after 22 weeks on the HFD, blood glucose levels of WT mice did not respond to 16 h of fasting but decreased even further in the mKO mice compared with the 4 h fast (Figure 2-6E). Results from glucose and insulin tolerance tests (Figure 2-6 F–I) showing improved glycemic control in the mKO mice, further support the notion that dysregulation of skeletal muscle OGT may modulate obesity-related phenotypes in other tissues to regulate whole body insulin sensitivity.

Inducible ablation of OGT in skeletal muscle recapitulates the mKO mouse

To exclude the possibility that the aforementioned observations were simply a consequence of OGT-mediated defects early in development, we generated inducible muscle-specific OGT KO (imKO) mice by crossing floxed OGT mice with tetracycline/doxycycline inducible HSA-cre mouse. Five-month-old adult mice were fed chow containing doxycycline for two weeks to induce knockout of OGT in skeletal muscle. Approximately six months after OGT ablation, we evaluated mice with regard to muscle and fat masses, energy expenditure, and insulin tolerance. Western blot analyses using anti-OGT and O-GlcNAc antibodies confirmed OGT ablation in skeletal muscle (Figure 2-7A). imKO mice had reduced body weights after OGT ablation (Figure 2-7B). Similar to mKO mice, imKO mice had normal muscle mass (Figure 2-7C), reduced fat mass (Figure 2-7D,E) and enhanced energy expenditure (Figure 2-7F). Furthermore, imKO mice were more insulin responsive than their WT counterparts, as evidenced by glucose (Figure 2-7G) and insulin

(Figure 2-7H) tolerance tests, respectively. These data show ablation of OGT in adult skeletal muscle recapitulates the OGT mKO phenotype suggesting that suppression of O-GlcNAc signaling in skeletal muscle of adult mice promotes an increase in whole body energy metabolism and reduces adiposity.

OGT ablation results in augmented skeletal muscle Interleukin-15 production

To determine how muscle-specific knockout of OGT affects adipose tissue, we analyzed a panel of myokines that are known to exert local and systemic effects on adipose tissue function. Of the six myokines selected, only *Il15* and *Adipoq* was significantly up-regulated in mKO muscle (Figure 2-8A,B). Because circulating IL-15 has well-documented anti-obesity effects (Ye, 2015), we analyzed serum IL-15 levels and found that circulating IL-15 concentrations in mKO mice were consistently 2.5-fold higher than WT mice (Figure 2-8C). To investigate a potential connection between elevated IL-15 and reduced fat mass, we used an *in vitro* cell culture system in which stromal vascular fraction (SVF) cells were cultured with muscle extracts from either WT or mKO mice to evaluate the effect on lipid accumulation. Extracts from mKO muscle inhibited SVF cell differentiation as evidenced by less lipid droplet formation (Oil-Red-O staining) compared with muscle extracts from WT mice (Figure 2-8D). However, this inhibition was released when an IL-15-neutralizing antibody was introduced into the media (Figure 2-8D). Furthermore, quantitative RT-PCR of the lipogenic genes revealed that *Acaca, Fasn, and Srebf1c* were significantly reduced in mKO muscle extract-treated SVF cells (Figure 2-8E). These results show that muscle from mice lacking a functional OGT in muscle produce greater levels of circulating IL-15 that may affect adipose tissue development and function. Our data also suggest that OGT may be directly involved in regulating *Il15*gene expression in skeletal muscle.

At the molecular level, OGT has been shown to repress gene expression epigenetically. It was shown that O-GlcNAcylation stabilizes histone methyltransferase enhancer of zeste homolog 2 (EZH2), which facilitates the formation of the trimethylation of histone 3 at lysine 27 (H3K27me3) thereby repressing gene expression in human MCF-7 cells (Chu et al., 2014). To explore the possible existence of a similar mechanism in skeletal muscle, we used co-immunoprecipitation (Co-IP) to study the interaction of OGT and EZH2. Co-IP results revealed that OGT can O-GlcNAcylate EZH2 in skeletal muscle (Figure 2-8F). To assess whether the OGT and EZH2 interaction has any relevance to *Il15* gene regulation, we conducted a chromatin immunoprecipitation (ChIP) assay. O-GlcNAc, EZH2, and H3K27me3 were all enriched at the *Il15*promoter region (Figure 2-8 G–I). These findings suggest the existence of the OGT-EZH2-H3K27me3 axis in skeletal muscle, similar to the mechanism responsible for controlling gene repression in a human adenocarcinoma cell line. These results indicate that the increases in circulating IL-15 we observed in mKO mice are likely mediated by epigenetic regulation of the *Il15* gene locus.

Discussion

Despite its discovery three decades ago, the physiological significance of O-GlcNAcylation as a nutrient sensor has only recently been recognized (Hart, 2014). O-GlcNAc is a dynamic posttranslational modification that is targeted to Ser/Thr residues by O-GlcNAc transferase (OGT) and removed by O-GlcNAcase (OGA). The substrate for OGT is UDP-GlcNAc, a product of the hexosamine biosynthetic pathway (HBP). UDP-GlcNAc is an ideal gauge of metabolic status because levels reflect fluxes through a number of metabolic pathways, especially carbohydrate metabolism. Based on our finding that O-GlcNAcylation levels were elevated in skeletal muscle from T2D people, we hypothesized that OGT may be important for nutrient sensing in this tissue

and for whole body insulin sensitivity. Data presented herein clearly demonstrate that skeletal muscle OGT is centrally important for maintaining muscle energy homeostasis, mitochondrial function, and insulin sentivity. Moreover, we show that *Il15* gene transcription is epigenetically controlled by OGT. Thus, given the role of IL-15 in exogenous lipid partitioning (Duan et al., 2017), OGT in skeletal muscle is important not only for the ability to survey cellular nutrient status but also for regulation of substrate availability.

OGT mKO mice were markedly more insulin sensitive compared with WT controls. *In vivo* studies involving manipulation of the HBP support this finding. Mice that transgenically overexpress GFAT in GLUT4 expressing tissues show an opposite phenotype with decreased whole body insulin sensitivity measured using the hyperinsulinimic euglycemic clamp technique (Cooksey et al., 1999). Likewise, if OGT is overexpressed using a similar approach, whole body insulin sensitivity is also decreased, and mice display hyperinsulinemia (McClain et al., 2002). Thus, manipulation of flux through the HBP appears to affect insulin action, and the HBP could serve as a potential pharmacological target. Interestingly, not all muscle types from the OGT mKO mice showed enhanced glucose uptake in response to insulin compared with WT littermates. We have only analyzed the gastrocnemius muscle from the clamp experiment; therefore, we are not currently able to explain these muscle type differences. However, it was recently shown that IL-15 activates the JAK3/STAT3 pathway in skeletal muscle cells, and this induces glucose uptake (Krolopp et al., 2016). Therefore, we speculate that the responsiveness to IL-15 may be different between muscle types in OGT mKO mice. Further studies are necessary to address this intriguing observation.

Based on PDH activity and the level of glycolytic intermediates in the gastrocnemius muscle in response to insulin, knockout of OGT appears to alter glycolytic flux. Overexpression of OGT

in SY5Y cells decreases glycolysis (Tan et al., 2014), and several proteins within the glycolytic pathway are known to be O-GlcNAcylated in rat skeletal muscle (Cieniewski-Bernard et al., 2004) and in HEK293 cells (Hahne et al., 2013). Thus, our data are in line with the idea that OGT may act as a mediator of this pathway. Moreover, since manipulation of O-GlcNAc signaling affects mitochondrial function and dynamics in cardiac myocytes (Gawlowski et al., 2012), in muscle cells *in vitro* (Wang et al., 2016), and in skeletal muscle (the present study), it is conceivable that changes in glycolytic flux can be explained in part by changes in the capacity or efficiency for ATP generation by oxidative phosphorylation.

Lack of discernable histological and functional anomalies in skeletal muscle of OGT mKO mice argues that OGT may not be requisite for normal muscle function. This is somewhat surprising given the widely abundant nature of O-GlcNAcylation on structural muscle proteins (Bond and Hanover, 2013). However, the idea that O-GlcNAcylation is a part of a complex nutrient-sensing pathway, whereby protein O-GlcNAcylation serves as a niche-based nutrient sentinel for cells, remains intriguing especially from a whole organismal vantage point. Indeed, surveying nutrient availability is important in times of both nutrient plenty and scarcity. Nutrient availability is one of the most effective means of controlling epigenetic events (Hanover et al., 2012). We show that *Il15* expression is a consequence of OGT ablation in skeletal muscle. Specifically, we observed nearly a 5-fold increase in skeletal muscle *Il15* mRNA expression, which resulted in a corresponding increase in circulating levels of IL-15 in mKO mice. Given that O-GlcNAcylation parallels nutrient availability in cells (Arias et al., 2004; Yang et al., 2008) and that chromatin is a major site of O-GlcNAcylation (Ozcan et al., 2010; Sakabe and Hart, 2010; Fujiki et al., 2011; Zhang et al., 2011), we hypothesized that OGT plays a role in the epigenetic regulation of *Il15* gene expression (Hanover et al., 2012; Lewis and Hanover, 2014). Indeed, OGT

O-GlcNAcylates EZH2, a key part of the polycomb repressive complex 2 (PRC2), which may repress *Il15* expression through H3K27me3 modifications (Hanover et al., 2012). Using co-immunoprecipitation and chromatin immunoprecipitation assays, we found that OGT, EZH2, and H3K27me3 localize to *Il15* promoter sequences and that the increase in muscle-specific IL-15 production is, in part, due to epigenetic modification of the promoter. Moreover, our data are clearly in line with the repressive effect of OGT on *Il15* expression in muscle. We cannot exclude the possibility that OGT ablation results in other yet unknown skeletal muscle permutation(s) that may directly or indirectly disrupt other cellular pathways that increase muscle energy expenditure and lead to a leaner phenotype. Nor can we rule out other molecular 'insults' that may drive increases in cytokine production (Rinnov et al., 2014) in our KO mice. Even so, muscle-derived IL-15 production increases in response to a whole-body energy imbalance (Gleeson, 2000) and may in part explain a number of the characteristics displayed in mice lacking effective O-GlcNAc signaling events in skeletal muscle.

IL15 is highly expressed in human skeletal muscle tissue compared to most other tissues of the body (Grabstein et al., 1994) suggesting a critical role for the growth and maintenance of skeletal muscle. Recent studies show that IL-15 have little effect on skeletal muscle accretion (Quinn et al., 2009; Pistilli and Quinn, 2013) and raise the possibility that IL-15 acts as a means to elicit responses in distal whole body repositories as a means of mobilizing energy substrates to support its needs. Indeed, IL-15 is now known as a myokine that targets remote tissues to liberate energy resources (Pedersen et al., 2007). Furthermore, prolonged stimulation of muscle by IL-15 increases *Ppargc1a*, *Sirt1*, and *Ucp2* expression, all highly indicative of the conversion of skeletal muscle to a more oxidative phenotype (Quinn et al., 2013). Congruent with this, OGT mKO mice were indeed more oxidative than WT mice as evidenced by greater mitochondrial DNA

and enzyme contents and greater amounts of type I myosin heavy chain isoform. These data argue that OGT mKO mice have greater capacity to oxidize energy substrates, which is in line with calorimetry estimates showing that these mice exhibit greater energy expenditure regardless of the time-of-day studied.

Despite many similarities between the *Il15* transgenic model (Quinn et al., 2013) and the OGT mKO model, they differ on key aspects. OGT mKO mice were more sedentary than controls, which differs from mice over-expressing *Il15* (Quinn et al., 2013). Whether the increase in body temperature affects the desire to move or whether loss of OGT in tissues somehow keeps animals from moving requires additional attention. Even so, both models show increases in markers indicative of enhanced oxidative capacity. Despite this, OGT mKO mice have higher utilization of glucose relative to fatty acids as evidenced by the higher RER. Increased energy expenditure in combination with impaired mitochondrial function may account for this phenotype, and our current thinking is that lack of OGT may increase oxidative capacity but may also result in mitochondrial insults rendering the mitochondrial machinery impaired.

Mice lacking functional OGT were smaller than their WT littermates. However, this reduction in weight was not due to decreased muscle mass but rather a 50% reduction in adipose tissue weight. Curiously, mice receiving exogenous IL-15 experience similar reductions in whole-body adiposity without reductions in food intake (Carbo et al., 2000; Carbo et al., 2001; Alvarez et al., 2002). This is also observed in rats administered recombinant IL-15 and mice overexpressing an *Il15* transgene (Almendro et al., 2006; Quinn et al., 2009; Quinn et al., 2013). Conversely, those mice lacking a functional *Il15* gene are obese (Barra et al., 2010). Fat cells of OGT mKO mice were also smaller suggesting OGT ablation in skeletal muscle altered lipogenesis and lipolysis in adipose tissue, two well-known IL-15 functions (Carbo et al., 2001; Ajuwon and Spurlock, 2004).

Additionally, inguinal white adipose tissue contained greater levels of UCP1 protein and many browning marker genes were also upregulated. These data suggest up-regulation of muscle IL-15 in response to OGT ablation in skeletal muscle may be responsible for a leaner phenotype, perhaps by partitioning substrates away from adipose tissue and/or increasing energy expenditure in skeletal muscle. To address this thesis further, we subjected mKO mice to a high-fat diet to induce obesity (Surwit et al., 1988). As expected, over-fed mKO mice were leaner and had improved blood glucose levels compared to WT controls suggesting ablation of OGT in skeletal muscle altered whole body glucose tolerance. These findings supported our thesis, as those mice over-expressing IL-15 are also protected from this type of induced obesity (Quinn et al., 2009). Even so, however, discrepancies between *Il15* overexpressing mice and OGT mKO mice are not surprising given the magnitude of increases observed in overexpressing models and the fact that OGT ablation likely impacts the function of many cytosolic, nuclear, and mitochondrial proteins (Hahne et al., 2013).

In preparation of this manuscript, two studies were published on the role of OGT in skeletal muscle using skeletal muscle-specific OGT KO mice. In one study, no differences in glucose metabolism were observed between OGT KO and WT (Ida et al., 2017). However, animals used were 10–12 weeks of age, and, as our data show that the phenotype of muscle-specific OGT KO mice develops from 12 weeks of age, we believe that the authors simply missed the phenotype of the mice in that study. This was confirmed in a follow-up study performed by the same authors in which muscle-specific OGT KO mice were studied at older age (Murata et al., 2018). In that study, the observed phenotype of the OGT KO mice corroborated our findings of enhanced energy expenditure, improved whole body insulin sensitivity, and the resistance to obesity in response to HFD feeding.

In summary, results of the present study demonstrate a role of OGT in the maintenance of skeletal muscle energy metabolism and whole-body metabolic homeostasis. Lack of OGT results in increased whole body energy expenditure, altered muscle substrate utilization, and loss in the ability of muscle cells to regulate *Il15* expression. Consequences of increased plasma IL-15 levels likely include changes in the ability to store and metabolize energy substrates, which improves whole-body insulin sensitivity and enhances resistance to obesity. From an evolutionary viewpoint, it makes sense for animals to have a mechanism in place that regulates partitioning of substrates from energy stores. For instance, during fasting, flux through the HBP would be reduced. Consequently, UDP-GlcNAc levels would be lowered, which would result in diminished OGT activity. In turn, the inhibitory effects on *Il15* expression would be released, allowing an elevation in circulating levels of IL-15, which would promote mobilization of lipids from adipose depots. Further studies are needed to fully understand how other whole body and tissue-specific functions are impacted by OGT ablation in muscle. Moreover, additional work is required to dissect more precisely the differences observed between mKO mice and models in which circulating IL-15 levels are elevated.

Aknowledgements

The authors would like to thank Prof. Thomas Mandrup-Poulsen, University of Copenhagen, and Dr. LeBris S. Quinn for constructive comments during the manuscript preparation. Support for this study was provided by the Novo Nordisk Foundation Center for Basic Metabolic Research. The Novo Nordisk Foundation Center for Basic Metabolic Research is an independent Research Center at the University of Copenhagen that is partially funded by an unrestricted donation from the Novo Nordisk Foundation, http://metabol.ku.dk). JTT was supported by the Novo Nordisk Foundation (Excellence Project Award; NNF14OC0009315), by

the Danish Council for Independent Research (Research Project Grant; DFF-4004-00235), and by the European Foundation for the Study of Diabetes (EFSD/Lilly Research Fellowship). JFPW was supported by the Novo Nordisk Foundation (NNF 160C0023046) and The Danish Medical Research Council (DFF-6110-00498B).

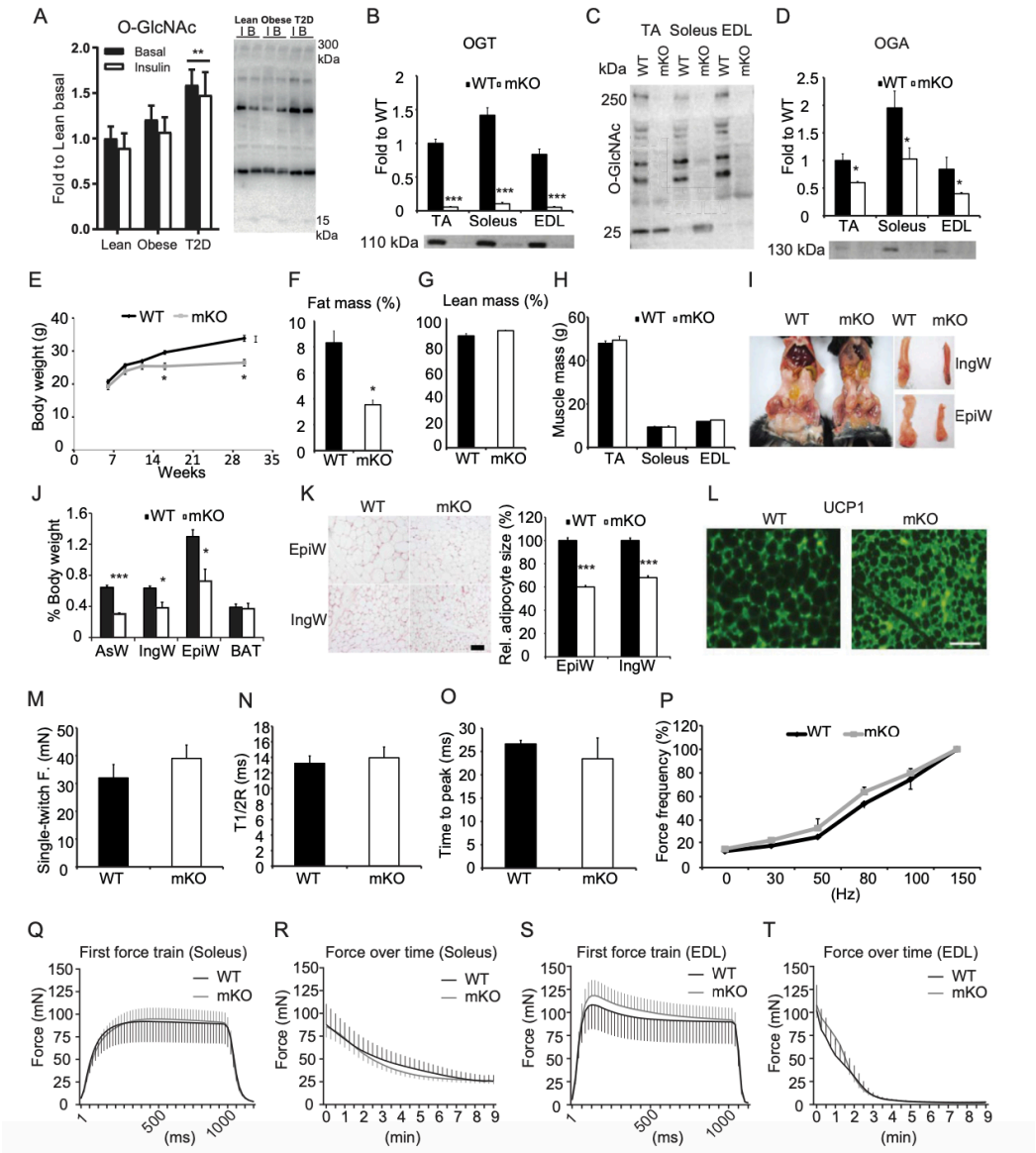

Figure 2-1. Mice lacking OGT in skeletal muscle exhibit reduced fat mass but normal skeletal muscle morphology and contractility. (A) O-GlcNAc levels in human skeletal muscles of lean, obese, and type 2 diabetic individuals at basal **(B)** and after a hyperinsulinemic euglycemic clamp (Insulin (I)). Lane intensities were quantified between 15 and 300 kDa. Sample size of 8e10 people per group. Data are mean SEM and analyzed by two-way repeated measures ANOVA; ** indicates $p < 0.01$. **(B)** OGT, **(C)** O-GlcNAc, and **(D)** OGA immunoblotted in tibialis anterior (TA), soleus, and extensor digitorum longus (EDL) muscles from WT and mKO mice (n 1⁄4 4). **(E)** Body weights of WT and mKO mice measured at 6, 9, 12, 16, and 30 weeks of age (n 1⁄4 6e10). (FeH) Body composition: fat percentage **(F)**, lean percentage **(G)**, and muscle weights **(H)** of TA, soleus, and EDL in 16-week-old WT and mKO mice (n 1⁄4 10). **(I)** Images comparing abdominal, inguinal (IngW) and epididymal (EpiW) white adipose tissue (WAT) depots from WT and mKO mice. **(J)** Quantification of adipose tissue weights expressed as percentage (%) body weight (n 1⁄4 10). **(K)** Representative micrographs of H&E stained sections from epididymal (EpiW) and inguinal (IngW) white adipose tissues (WAT) of WT and mKO mice. Scale bar, 100

mm. The relative size of adipocytes in the EpiW and IngW of mKO mice was expressed as a percentage of WT (n 1⁄4 10). **(L)** Immunoreactive uncoupling protein 1 (UCP1) in IngW of WT (left) and mKO (right) mice. Scale bar, 100 mm. (MeO) EDL muscle single-twitch contraction force **(M)**, time-to-half relaxation tension (T1/2R; n 1⁄4 10) (N), and time to peak of tension (n 1⁄4 10) **(O)**. **(P)** EDL muscle contractile force in response to increased stimulation frequency (n 1⁄4 10). Data normalized to force at 150 Hz. **(Q,R)** First force train at 100Hz, 1 sec duration in soleus (Q; n 1⁄4 5), and fatigue-ability measured as force produced over consecutive force trains at 100 Hz, 1 sec duration in soleus (R; n 1⁄4 5). **(S,T)** First force train at 100 Hz, 1 sec duration in EDL (S; n 1⁄4 5), and fatigue-ability measured as force produced over consecutive force trains at 100 Hz, 1 sec duration in EDL (T; n 1⁄4 5). Data in B-T are means SEM from 16-week-old male mice. *p < 0.05; **p < 0.01; ***p < 0.001 compared with WT mice.

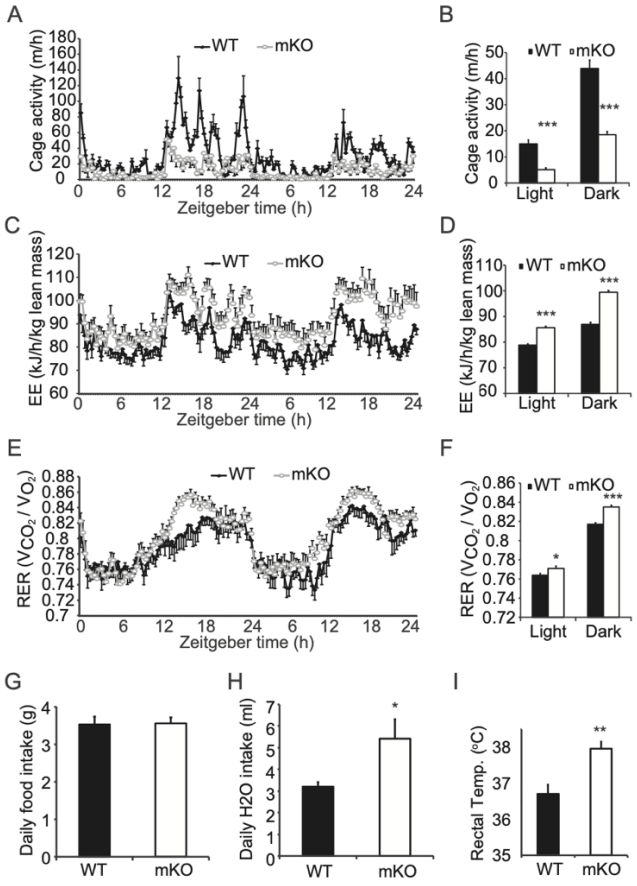

Figure 2-2. OGT mKO mice are less active and have higher whole-body energy expenditure. **(A-F)** Cage activity (real-time, A, and tabular, B), energy expenditure per lean body mass (EE) (real-time, C, and tabular, D) and respiratory exchange ratio (RER) (real-time, E, and tabular, F) for WT and mKO mice (n 1⁄4 10). Measurements were recorded every 20 min using TSE Lab-Master System. A, C, and E: X-axis represents zeitgeber time, with 0 at lights on. (GeI) Daily food intake **(G)** and water consumption **(H)**, and rectal temperatures **(I)** for WT and mKO mice (n 1⁄4 10). Data represent means SEM from 16-week-old male mice. *p < 0.05; **p < 0.01; ***p < 0.001 compared with WT mice.

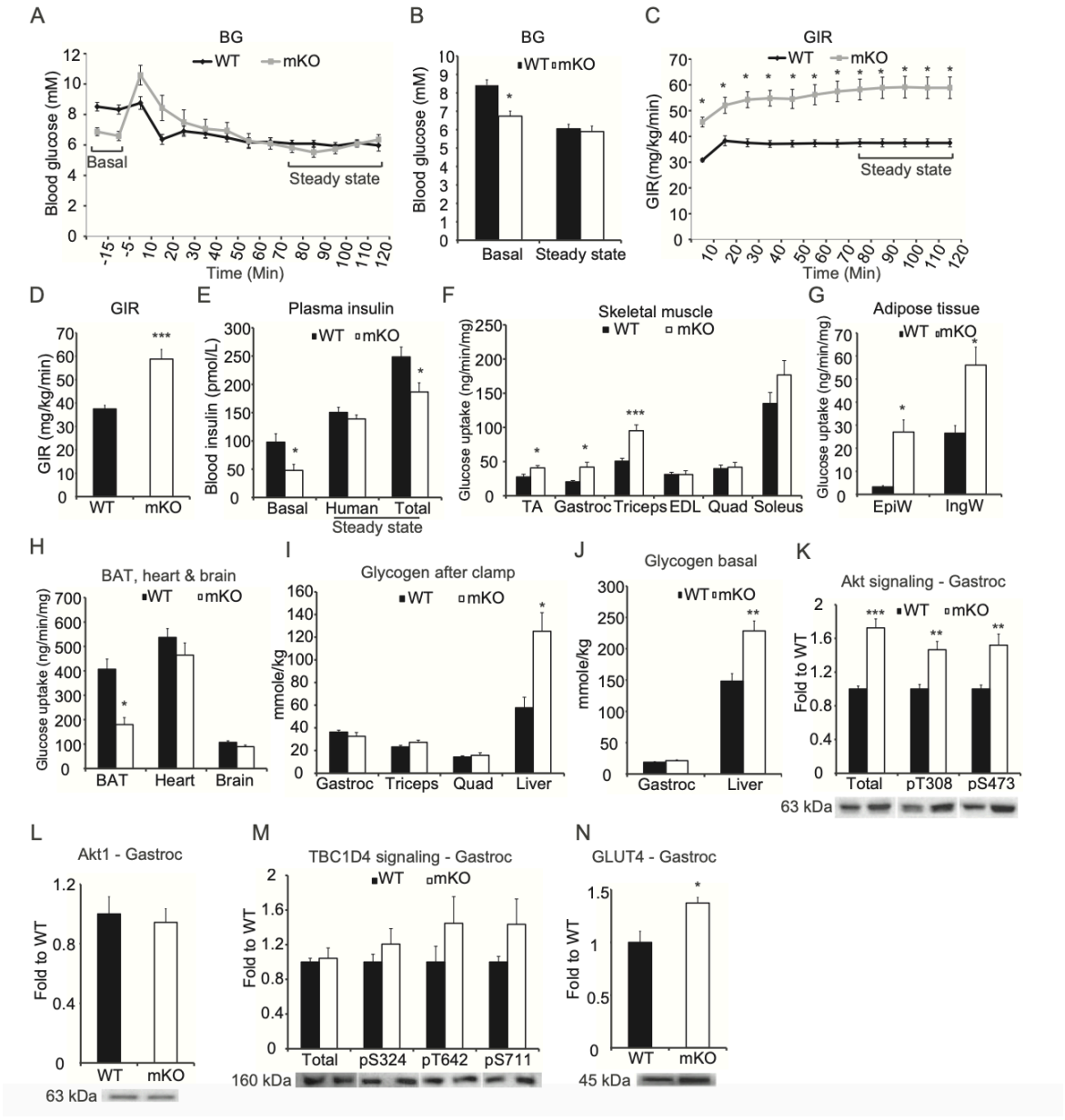

Figure 2-3. Lack of OGT in skeletal muscle affects glucose homeostasis and insulin signaling. **(A-B)** Blood glucose levels before and during a hyperinsulinemic euglycemic clamp performed using 4 mU/kg/min of insulin. **(C-D)** Glucose infusion rates (GIR) during clamp. **(E)** Plasma insulin levels before and during steady state of the clamp. **(F)** Glucose uptake in skeletal muscles after steady state. **(G)** Glucose uptake in adipose tissues after steady state. **(H)** Glucose uptake in BAT, heart, and brain after steady state. **(I)** Glycogen in gastrocnemius, triceps, quadriceps and liver from clamped mice. **(J)** Glycogen in gastrocnemius and liver from 5-hour fasted mice. **(K)** Immunoblot of Akt and Akt phosphorylation of pS473 and pT308 in gastrocnemius. **(L)** Immunoblot of Akt1 in gastrocnemius from clamped mice. **(M)** Immunoblot of TBC1D4 and TBC1D4 phosphorylation of, pS324, pT642, and pS711 in gastrocnemius. **(N)** Immunoblot of GLUT4 in gastrocnemius. Data represent means SEM from n 1⁄4 8e10 mice in each genotype. Mice were 18-week-old males. *p < 0.05; **p < 0.01; ***p < 0.001 compared with WT mice.

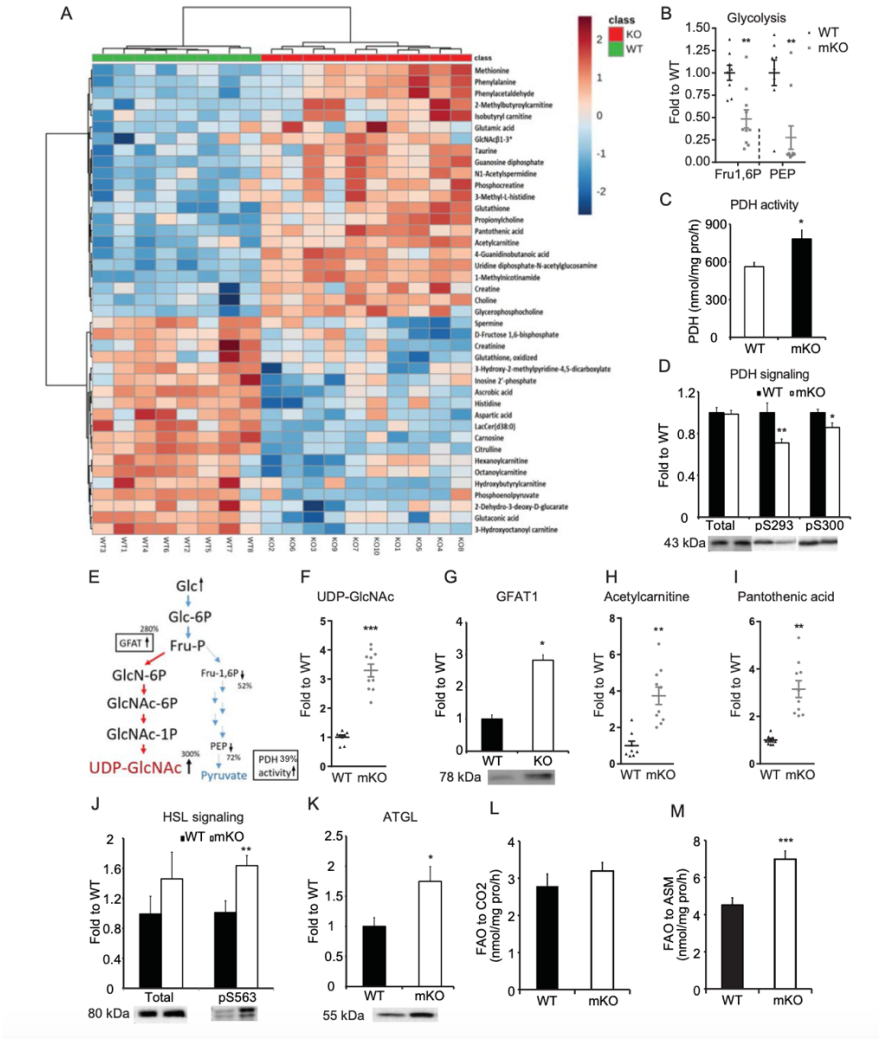

Figure 2-4. Loss of skeletal muscle OGT alters global muscle metabolism. (A) Metabolome heat map of gastrocnemius muscle from clamped mice. Metabolites were measured using LC-MS. **(B)** Glycolytic metabolites from metabolome. Fructose 1 6-bisphosphate (Fru1,6P) and phosphoenolpyruvate (PEP). **(C)** Pyruvate dehydrogenase (PDH) activity in the gastrocnemius muscle was assayed with the substrate [1e14C] pyruvate by measuring enzyme-catalyzed release of 14CO2. **(D)** Immunoblot of PDH phosphorylation at pS293 and pS300 in gastrocnemius from clamped mice. **(E)** Illustration of metabolites and regulation of glycolysis and hexosamine biosynthetic pathway. **(F)** UDP-GlcNAc levels from the metabolomics analysis. **(G)** Immunoblot of GFAT1 in gastrocnemius from clamped mice. **(H)** Acetylcarnitine levels from the metabolomics analysis. **(I)** Pantothenic acid levels from the metabolomics analysis. **(J)** Immunoblot of HSL and HSL pS563 in gastrocnemius from clamped mice. **(K)** Immunoblot of ATGL in gastrocnemius from clamped mice. **(L)** Complete oxidation of [1e14C]-palmitic acid to CO2 in gastrocnemius muscle of WT and mKO mice. **(M)** Incomplete oxidation of [1e14C]-palmitic acid to acid-soluble metabolites (ASM) in gastrocnemius muscle. Data represent means SEM from n 1⁄4 8e10, 18-week-old (Panel A, B, C, F, G, H, I, J, and K) and n 1⁄4 10, 16-week-old (Panel D, L, and M) male mice in each genotype. *p < 0.05; **p < 0.01; ***p < 0.001 compared with WT mice.

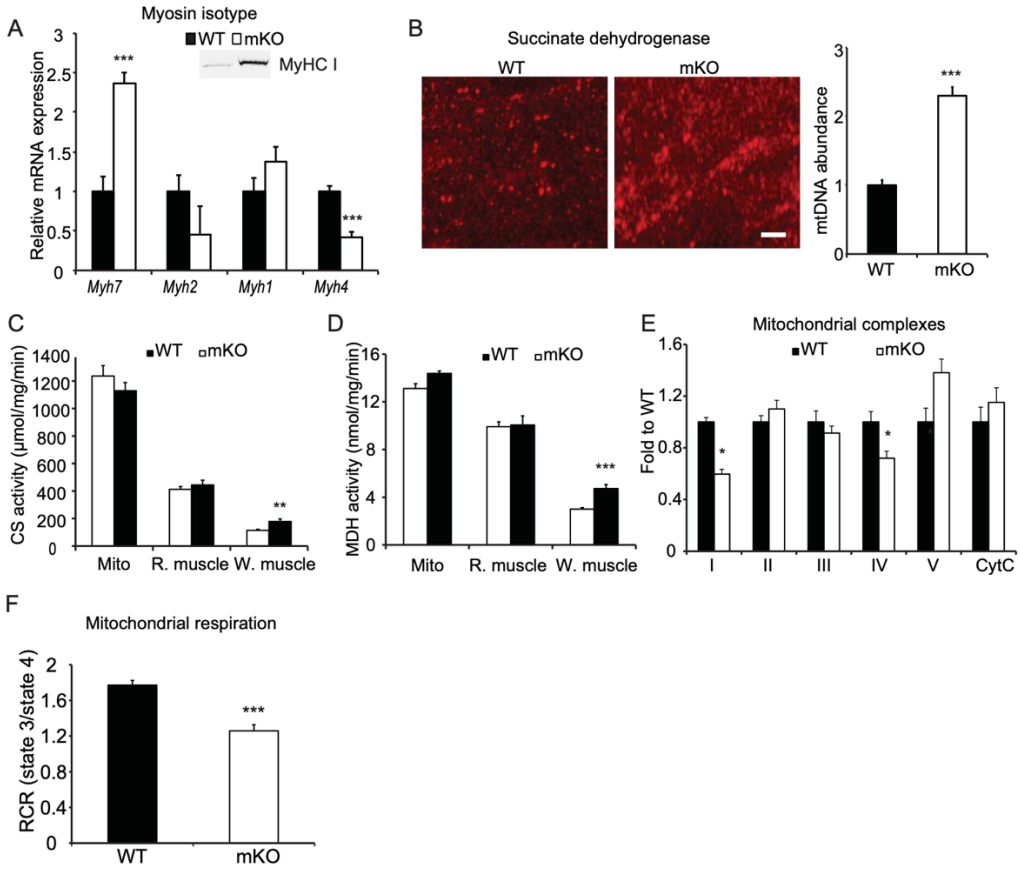

Figure 2-5. Loss of skeletal muscle OGT increases type I myosin heavy chain-containing fibers but impairs maximal oxidative capacity. (A) Relative mRNA expression of myosin heavy chain (MyHC) I (Myh7), MyHC IIa (Myh2), MyHC IIx (Myh1), and MyHC IIb (Myh4) in the gastrocnemius muscle. Inset, immunoreactivity of MyHC I in the gastrocnemius muscles of WT and mKO muscle. **(B)** Mitochondrial abundance. Left: three-dimensional confocal images showing the difference in mitochondria in gastrocnemius muscle cross- sections of WT and mKO stained with succinate dehydrogenase antibody (left panel). Bar, 5 mm. Right: mitochondrial DNA (mtDNA) abundance in the gastrocnemius muscles of WT and mKO mice. MteCo1 DNA was measured using qPCR and normalized to genomic Nrip1 DNA. **(C-D)** Citrate synthase (CS, C) and malate dehydrogenase (MDH, D) activities in isolated mitochondria (Mito), and red (R.) and white (W.) portions of the gastrocnemius muscles of WT and mKO mice. **(E)** Abundance of mitochondrial complexes in gastrocnemius from clamped mice. **(F)** Mitochondria were isolated from WT and mKO gastrocnemius muscle, and oxygen consumption was measured using Seahorse. Respiration control ratio of state 3/state 4 was calculated based on oxygen consumption rate (OCR) in each state. Data represent means SEM from n 1⁄4 10, 16-week-old male mice in each genotype. *p < 0.05; **p < 0.01; ***p < 0.001 compared with WT mice.

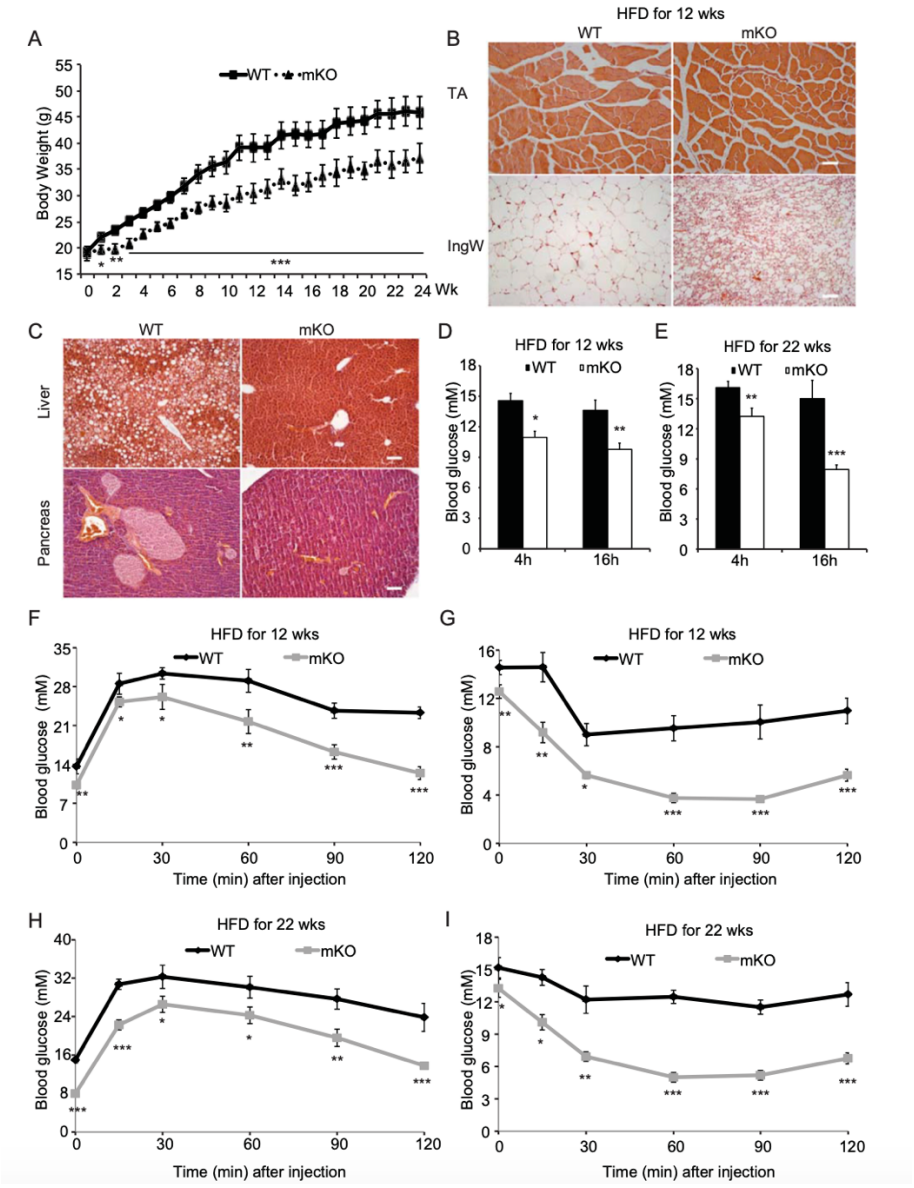

Figure 2-6. A high fat diet fails to induce glucose and insulin intolerance in mice lacking muscle OGT. (A) Weekly (Wk) body weights of WT and mKO mice during 24 wks of HFD. HFD feeding started at 4 weeks of age. **(B)** Cross-sections of the tibialis anterior (TA, top row) muscle and inguinal WAT (IngW, bottom row) of WT (left column) and mKO (right column) mice fed HFD for 24 wks. **(C)** Photo micrographs of H&E stained liver (top row) and pancreas (bottom row) sections of WT (left column) and mKO (right column) mice fed HFD for 24 wks. **(D)** Blood glucose levels of WT and mKO mice fed a HFD for 12 wks and fasted for 4 and 16 h, respectively. **(E)** Blood glucose levels in WT and mKO mice fed a HFD for 22 wks and fasted for 4 and 16 h, respectively. (FeG) Glucose **(F)** and insulin **(G)** tolerance tests of WT and mKO male mice fed a HFD for 12 wks (HeI) Glucose **(H)** and insulin **(I)** tolerance tests of WT and mKO male mice fed a HFD for 22 wks. Data represent means SEM from n 1⁄4 12 male mice in each genotype. *p < 0.05; **p < 0.01; ***p < 0.001 compared with WT control mice.

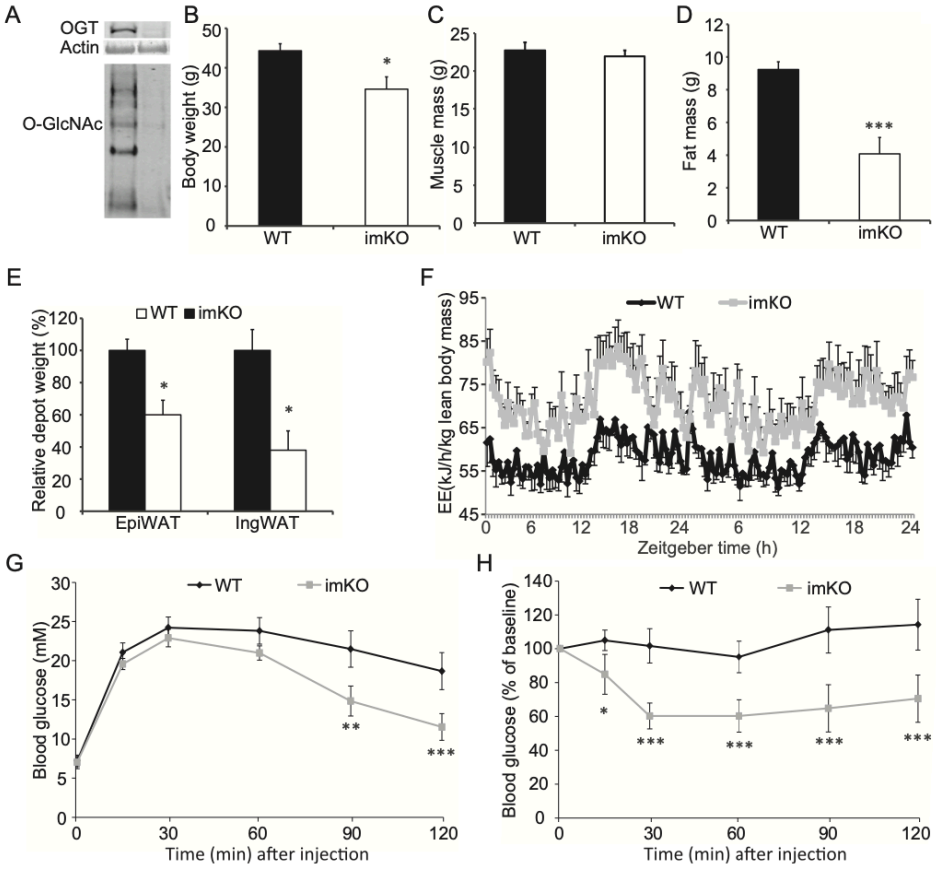

Figure 2-7. Inducible knockout of OGT in skeletal muscle recapitulates the mKO mouse. OGT knockout was induced when mice were 5 months old by feeding doxycycline food for two weeks. Subsequently, mice were fed normal chow for 6 months before analysis. (A) Muscle from WT and imKO mice were immunoblotted with anti-OGT and -O-GlcNAc antibodies respectively. Equal amount of total protein was loaded across all the lanes. **(B-F)** Body weight (B), muscle mass (C), fat mass (D), fat depots (E), and energy expenditure (EE) (F) were assessed. **(G-H)** Glucose tolerance test (GTT) (G) and insulin tolerance test (ITT) (H). Data represent means SEM from n 1⁄4 10 male mice in each genotype. *p < 0.05; **p < 0.01; ***p < 0.001 compared with WT control mice.

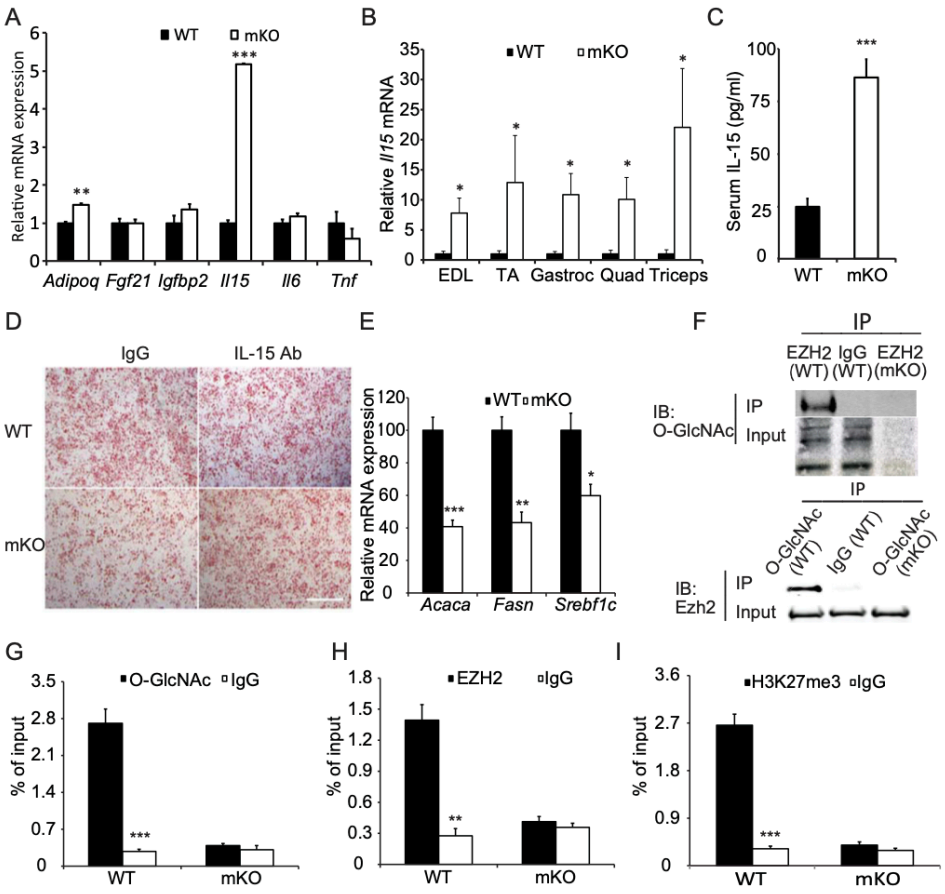

Figure 2-8: OGT knockout results in augmented Interleukin-15 production in skeletal muscle. (A) Expression of myokines in the gastrocnemius muscles of WT and mKO mice fed HFD for 22 wks **(B)** IL-15 mRNA expression in skeletal muscles from clamped mice (n ¼ 8e10, 18-week-old male mice). **(C)** Serum IL-15 levels in WT and mKO mice fed HFD for 22 wks (n ¼ 10). **(D)** Oil red-O staining of cultured stromal vascular fraction cells isolated from mouse IngW and induced to differentiate in the presence or absence of gastrocnemius muscle extracts from WT (top row) and mKO (bottom row) mice with (right) or without (left) IL15 neutralizing antibodies. Scale bar, 1 mm. **(E)** Expression of lipogenic genes in IngW (n ¼ 10). **(F)** Immunoprecipitation was performed using anti-EZH2 and anti-O-GlcNAc antibodies respectively, and immunoblotted with O-GlcNAc and EZH2 antibodies respectively. (GeI) Chromatin immunoprecipitation using antibodies against O-GlcNAc **(G)**, EZH2 **(H)**, and H3K27me3 **(I)**, respectively. Quantitative RT-PCR was used to quantify IL-15 promoter sequence as detailed in Methods. *$p < 0.05$, **$p < 0.01$, ***$p < 0.001$ compared to WT or corresponding antibody-treated samples.

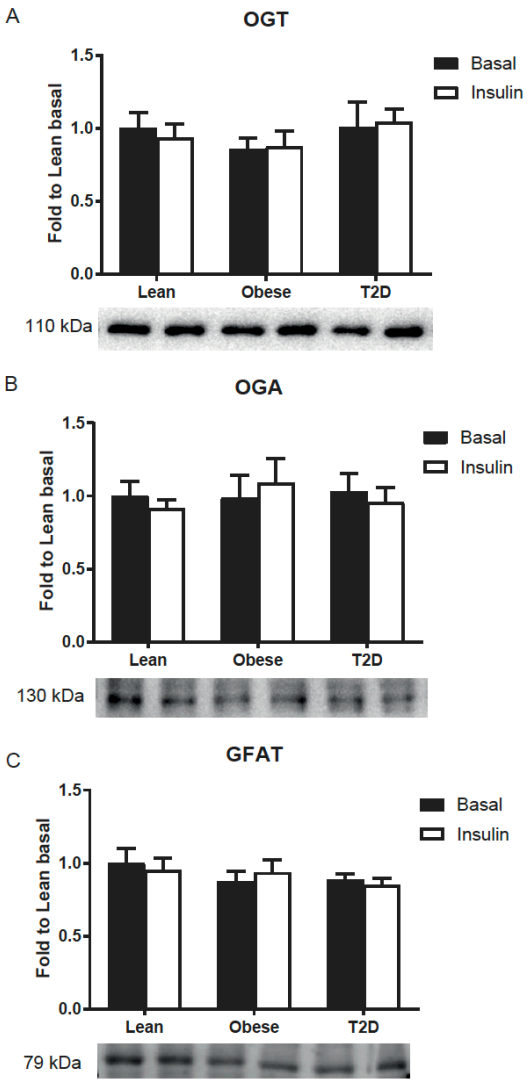

Supplementary Figure 2-1. Relative protein abundance measured by Western blot analyses of O-GlcNAc pathway-related proteins in human skeletal muscles of lean, obese, and type 2 diabetic individuals at basal and at the end of a hyperinsulinemic euglycemic clamp (i.e., Insulin). **(A)** OGT abundance, **(B)** OGA abundance, **(C)** GFAT abundance. Sample size of 8-10 people per group with mean +/- SEM. Statistical analysis was performed by two-way repeated measures ANOVA. No statistical differences were detected.

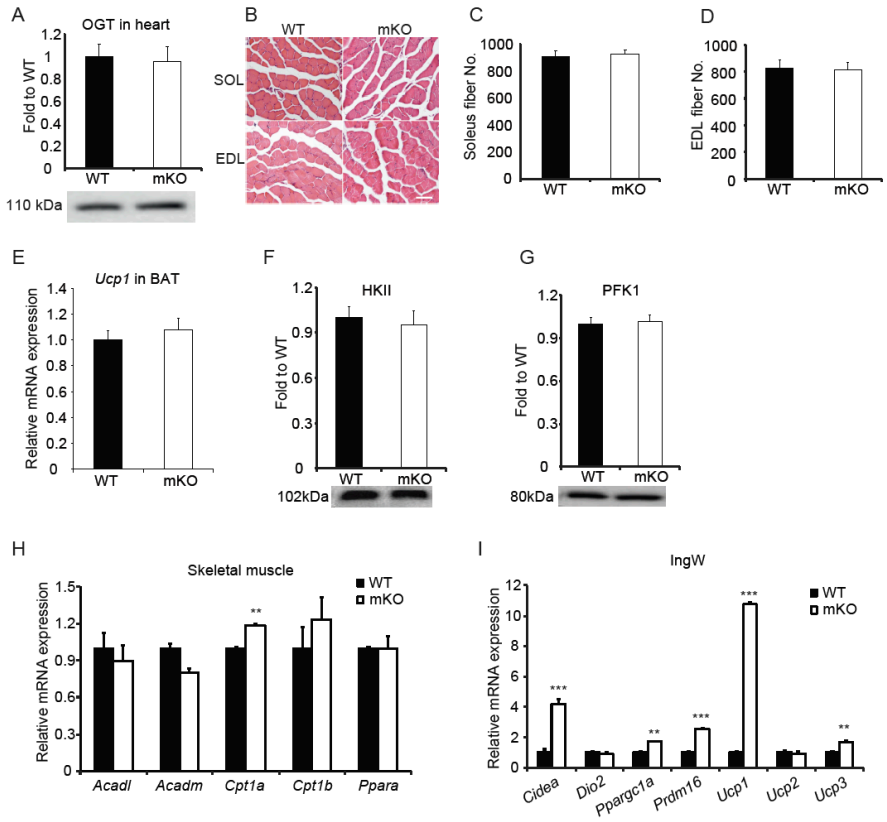

Supplementary Figure 2-2. (A) Immunoblot with anti-OGT in WT and mKO heart (n=5). **(B)** H&E staining of mouse soleus and EDL muscle cross sections. Scale bars, 100 μm. **(C,D)** Total myofiber numbers in soleus (C) and EDL (D) muscles from WT and mKO mice (n=5). **(E)** Ucp1 mRNA abundance in WT and mKO brown adipose tissue (BAT) (n=10). **(F)** Immunoblot of HKII in gastrocnemius from clamped mice (n=8-10). **(G)** Immunoblot of PFK1 in gastrocnemius from clamped mice (n=8-10). **(H)** Relative transcript abundances of genes related to beta-oxidation in skeletal muscle of WT and mKO mice (n=10). **(I)** Relative transcript abundances of thermogenic and brown adipocyte-like genes in IngW of WT and mKO mice (n=10). Data represent means ± SEM from 18-week-old (Panel B, F, and G) and 16-week-old (Panel C, D, E, H and I) male mice in each genotype. * $p<0.05$; ** $p<0.01$; *** $p<0.001$ compared with WT mice.

References

Ajuwon, K. M., and M. E. Spurlock. 2004. Direct regulation of lipolysis by interleukin-15 in primary pig adipocytes. Am J Physiol Regul Integr Comp Physiol 287(3):R608-611. doi: 10.1152/ajpregu.00192.2004

Almendro, V., S. Busquets, E. Ametller, N. Carbo, M. Figueras, G. Fuster, J. M. Argiles, and F. J. Lopez-Soriano. 2006. Effects of interleukin-15 on lipid oxidation: disposal of an oral [(14)C]-triolein load. Biochim Biophys Acta 1761(1):37-42. doi: 10.1016/j.bbalip.2005.12.006

Alvarez, B., N. Carbo, J. Lopez-Soriano, R. H. Drivdahl, S. Busquets, F. J. Lopez-Soriano, J. M. Argiles, and L. S. Quinn. 2002. Effects of interleukin-15 (IL-15) on adipose tissue mass in rodent obesity models: evidence for direct IL-15 action on adipose tissue. Biochim Biophys Acta 1570(1):33-37. doi: 10.1016/s0304-4165(02)00148-4

Arias, E. B., J. Kim, and G. D. Cartee. 2004. Prolonged incubation in PUGNAc results in increased protein O-Linked glycosylation and insulin resistance in rat skeletal muscle. Diabetes 53(4):921-930. doi: 10.2337/diabetes.53.4.921

Ayala, J. E., D. P. Bracy, O. P. McGuinness, and D. H. Wasserman. 2006. Considerations in the design of hyperinsulinemic-euglycemic clamps in the conscious mouse. Diabetes 55(2):390-397. doi: 10.2337/diabetes.55.02.06.db05-0686

Barra, N. G., S. Reid, R. MacKenzie, G. Werstuck, B. L. Trigatti, C. Richards, A. C. Holloway, and A. A. Ashkar. 2010. Interleukin-15 contributes to the regulation of murine adipose tissue and human adipocytes. Obesity (Silver Spring) 18(8):1601-1607. doi: 10.1038/oby.2009.445

Baskin, K. K., B. R. Winders, and E. N. Olson. 2015. Muscle as a "mediator" of systemic metabolism. Cell Metab 21(2):237-248. doi: 10.1016/j.cmet.2014.12.021

Bassel-Duby, R., and E. N. Olson. 2006. Signaling pathways in skeletal muscle remodeling. Annu Rev Biochem 75:19-37. doi: 10.1146/annurev.biochem.75.103004.142622

Birk, J. B., and J. F. Wojtaszewski. 2006. Predominant alpha2/beta2/gamma3 AMPK activation during exercise in human skeletal muscle. J Physiol 577(Pt 3):1021-1032. doi: 10.1113/jphysiol.2006.120972

Bond, M. R., and J. A. Hanover. 2013. O-GlcNAc cycling: a link between metabolism and chronic disease. Annu Rev Nutr 33:205-229. doi: 10.1146/annurev-nutr-071812-161240

Bostrom, P., J. Wu, M. P. Jedrychowski, A. Korde, L. Ye, J. C. Lo, K. A. Rasbach, E. A. Bostrom, J. H. Choi, J. Z. Long, S. Kajimura, M. C. Zingaretti, B. F. Vind, H. Tu, S. Cinti, K. Hojlund, S. P. Gygi, and B. M. Spiegelman. 2012. A PGC1-alpha-dependent myokine that drives brown-fat-like development of white fat and thermogenesis. Nature 481(7382):463-468. doi: 10.1038/nature10777

Bullen, J. W., J. L. Balsbaugh, D. Chanda, J. Shabanowitz, D. F. Hunt, D. Neumann, and G. W. Hart. 2014. Cross-talk between two essential nutrient-sensitive enzymes: O-GlcNAc transferase (OGT) and AMP-activated protein kinase (AMPK). J Biol Chem 289(15):10592-10606. doi: 10.1074/jbc.M113.523068

Carbo, N., J. Lopez-Soriano, P. Costelli, B. Alvarez, S. Busquets, F. M. Baccino, L. S. Quinn, F. J. Lopez-Soriano, and J. M. Argiles. 2001. Interleukin-15 mediates reciprocal regulation of adipose and muscle mass: a potential role in body weight control. Biochim Biophys Acta 1526(1):17-24. doi: 10.1016/s0304-4165(00)00188-4

Carbo, N., J. Lopez-Soriano, P. Costelli, S. Busquets, B. Alvarez, F. M. Baccino, L. S. Quinn, F. J. Lopez-Soriano, and J. M. Argiles. 2000. Interleukin-15 antagonizes muscle protein waste in tumour-bearing rats. Br J Cancer 83(4):526-531. doi: 10.1054/bjoc.2000.1299

Chu, C. S., P. W. Lo, Y. H. Yeh, P. H. Hsu, S. H. Peng, Y. C. Teng, M. L. Kang, C. H. Wong, and L. J. Juan. 2014. O-GlcNAcylation regulates EZH2 protein stability and function. Proc Natl Acad Sci U S A 111(4):1355-1360. doi: 10.1073/pnas.1323226111

Cieniewski-Bernard, C., B. Bastide, T. Lefebvre, J. Lemoine, Y. Mounier, and J. C. Michalski. 2004. Identification of O-linked N-acetylglucosamine proteins in rat skeletal muscle using two-dimensional gel electrophoresis and mass spectrometry. Mol Cell Proteomics 3(6):577-585. doi: 10.1074/mcp.M400024-MCP200

Cooksey, R. C., L. F. Hebert, Jr., J. H. Zhu, P. Wofford, W. T. Garvey, and D. A. McClain. 1999. Mechanism of hexosamine-induced insulin resistance in transgenic mice overexpressing glutamine:fructose-6-phosphate amidotransferase: decreased glucose transporter GLUT4 translocation and reversal by treatment with thiazolidinedione. Endocrinology 140(3):1151-1157. doi: 10.1210/endo.140.3.6563

Duan, Y., F. Li, W. Wang, Q. Guo, C. Wen, Y. Li, and Y. Yin. 2017. Interleukin-15 in obesity and metabolic dysfunction: current understanding and future perspectives. Obes Rev 18(10):1147-1158. doi: 10.1111/obr.12567

Ferre, P., A. Leturque, A. F. Burnol, L. Penicaud, and J. Girard. 1985. A method to quantify glucose utilization in vivo in skeletal muscle and white adipose tissue of the anaesthetized rat. Biochem J 228(1):103-110. doi: 10.1042/bj2280103

Frezza, C., S. Cipolat, and L. Scorrano. 2007. Organelle isolation: functional mitochondria from mouse liver, muscle and cultured fibroblasts. Nat Protoc 2(2):287-295. doi: 10.1038/nprot.2006.478

Frisard, M. I., R. P. McMillan, J. Marchand, K. A. Wahlberg, Y. Wu, K. A. Voelker, L. Heilbronn, K. Haynie, B. Muoio, L. Li, and M. W. Hulver. 2010. Toll-like receptor 4 modulates skeletal muscle substrate metabolism. Am J Physiol Endocrinol Metab 298(5):E988-998. doi: 10.1152/ajpendo.00307.2009

Fujiki, R., W. Hashiba, H. Sekine, A. Yokoyama, T. Chikanishi, S. Ito, Y. Imai, J. Kim, H. H. He, K. Igarashi, J. Kanno, F. Ohtake, H. Kitagawa, R. G. Roeder, M. Brown, and S. Kato. 2011. GlcNAcylation of histone H2B facilitates its monoubiquitination. Nature 480(7378):557-560. doi: 10.1038/nature10656

Funai, K., H. Song, L. Yin, I. J. Lodhi, X. Wei, J. Yoshino, T. Coleman, and C. F. Semenkovich. 2013. Muscle lipogenesis balances insulin sensitivity and strength through calcium signaling. J Clin Invest 123(3):1229-1240. doi: 10.1172/JCI65726

Gawlowski, T., J. Suarez, B. Scott, M. Torres-Gonzalez, H. Wang, R. Schwappacher, X. Han, J. R. Yates, 3rd, M. Hoshijima, and W. Dillmann. 2012. Modulation of dynamin-related protein 1 (DRP1) function by increased O-linked-beta-N-acetylglucosamine modification (O-GlcNAc) in cardiac myocytes. J Biol Chem 287(35):30024-30034. doi: 10.1074/jbc.M112.390682

Gerencser, A. A., A. Neilson, S. W. Choi, U. Edman, N. Yadava, R. J. Oh, D. A. Ferrick, D. G. Nicholls, and M. D. Brand. 2009. Quantitative microplate-based respirometry with correction for oxygen diffusion. Anal Chem 81(16):6868-6878. doi: 10.1021/ac900881z

Gleeson, M. 2000. Interleukins and exercise. J Physiol 529 Pt 1:1. doi: 10.1111/j.1469-7793.2000.00001.x

Grabstein, K. H., J. Eisenman, K. Shanebeck, C. Rauch, S. Srinivasan, V. Fung, C. Beers, J. Richardson, M. A. Schoenborn, M. Ahdieh, and et al. 1994. Cloning of a T cell growth factor that interacts with the beta chain of the interleukin-2 receptor. Science 264(5161):965-968. doi: 10.1126/science.8178155

Gunning, P., and E. Hardeman. 1991. Multiple mechanisms regulate muscle fiber diversity. FASEB J 5(15):3064-3070. doi: 10.1096/fasebj.5.15.1835946

Hahne, H., N. Sobotzki, T. Nyberg, D. Helm, V. S. Borodkin, D. M. van Aalten, B. Agnew, and B. Kuster. 2013. Proteome wide purification and identification of O-GlcNAc-modified proteins using click chemistry and mass spectrometry. J Proteome Res 12(2):927-936. doi: 10.1021/pr300967y

Hanover, J. A., M. W. Krause, and D. C. Love. 2012. Bittersweet memories: linking metabolism to epigenetics through O-GlcNAcylation. Nat Rev Mol Cell Biol 13(5):312-321. doi: 10.1038/nrm3334

Hardie, D. G., B. E. Schaffer, and A. Brunet. 2016. AMPK: An Energy-Sensing Pathway with Multiple Inputs and Outputs. Trends Cell Biol 26(3):190-201. doi: 10.1016/j.tcb.2015.10.013

Hart, G. W. 2014. Three Decades of Research on O-GlcNAcylation - A Major Nutrient Sensor That Regulates Signaling, Transcription and Cellular Metabolism. Front Endocrinol (Lausanne) 5:183. doi: 10.3389/fendo.2014.00183

Harwood, K. R., and J. A. Hanover. 2014. Nutrient-driven O-GlcNAc cycling - think globally but act locally. J Cell Sci 127(Pt 9):1857-1867. doi: 10.1242/jcs.113233

Hojlund, K., J. B. Birk, D. K. Klein, K. Levin, A. J. Rose, B. F. Hansen, J. N. Nielsen, H. Beck-Nielsen, and J. F. Wojtaszewski. 2009. Dysregulation of glycogen synthase COOH- and NH2-terminal phosphorylation by insulin in obesity and type 2 diabetes mellitus. J Clin Endocrinol Metab 94(11):4547-4556. doi: 10.1210/jc.2009-0897

Huang, P., S. R. Ho, K. Wang, B. C. Roessler, F. Zhang, Y. Hu, D. B. Bowe, J. E. Kudlow, and A. J. Paterson. 2011. Muscle-specific overexpression of NCOATGK, splice variant of O-GlcNAcase, induces skeletal muscle atrophy. Am J Physiol Cell Physiol 300(3):C456-465. doi: 10.1152/ajpcell.00124.2010

Ida, S., K. Morino, O. Sekine, N. Ohashi, S. Kume, T. Chano, K. Iwasaki, N. Harada, N. Inagaki, S. Ugi, and H. Maegawa. 2017. Diverse metabolic effects of O-GlcNAcylation in the pancreas but limited effects in insulin-sensitive organs in mice. Diabetologia 60(9):1761-1769. doi: 10.1007/s00125-017-4327-y

Issad, T., E. Masson, and P. Pagesy. 2010. O-GlcNAc modification, insulin signaling and diabetic complications. Diabetes Metab 36(6 Pt 1):423-435. doi: 10.1016/j.diabet.2010.09.001

Jensen, B. A., T. S. Nielsen, A. M. Fritzen, J. B. Holm, E. Fjaere, A. K. Serup, K. Borkowski, S. Risis, S. I. Paerregaard, I. Sogaard, A. Poupeau, M. Poulsen, T. Ma, C. Sina, B. Kiens, L. Madsen, K. Kristiansen, and J. T. Treebak. 2016. Dietary fat drives whole-body insulin resistance and promotes intestinal inflammation independent of body weight gain. Metabolism 65(12):1706-1719. doi: 10.1016/j.metabol.2016.09.002

Kim, K. H., Y. T. Jeong, H. Oh, S. H. Kim, J. M. Cho, Y. N. Kim, S. S. Kim, D. H. Kim, K. Y. Hur, H. K. Kim, T. Ko, J. Han, H. L. Kim, J. Kim, S. H. Back, M. Komatsu, H. Chen, D. C. Chan, M. Konishi, N. Itoh, C. S. Choi, and M. S. Lee. 2013. Autophagy deficiency leads to protection from obesity and insulin resistance by inducing Fgf21 as a mitokine. Nat Med 19(1):83-92. doi: 10.1038/nm.3014

Krolopp, J. E., S. M. Thornton, and M. J. Abbott. 2016. IL-15 Activates the Jak3/STAT3 Signaling Pathway to Mediate Glucose Uptake in Skeletal Muscle Cells. Front Physiol 7:626. doi: 10.3389/fphys.2016.00626

Lagerlof, O., J. E. Slocomb, I. Hong, Y. Aponte, S. Blackshaw, G. W. Hart, and R. L. Huganir. 2016. The nutrient sensor OGT in PVN neurons regulates feeding. Science 351(6279):1293-1296. doi: 10.1126/science.aad5494

Lefebvre, T., V. Dehennaut, C. Guinez, S. Olivier, L. Drougat, A. M. Mir, M. Mortuaire, A. S. Vercoutter-Edouart, and J. C. Michalski. 2010. Dysregulation of the nutrient/stress sensor O-GlcNAcylation is involved in the etiology of cardiovascular disorders, type-2 diabetes and Alzheimer's disease. Biochim Biophys Acta 1800(2):67-79. doi: 10.1016/j.bbagen.2009.08.008

Lewis, B. A., and J. A. Hanover. 2014. O-GlcNAc and the epigenetic regulation of gene expression. J Biol Chem 289(50):34440-34448. doi: 10.1074/jbc.R114.595439

Love, D. C., and J. A. Hanover. 2005. The hexosamine signaling pathway: deciphering the "O-GlcNAc code". Sci STKE 2005(312):re13. doi: 10.1126/stke.3122005re13

McClain, D. A., W. A. Lubas, R. C. Cooksey, M. Hazel, G. J. Parker, D. C. Love, and J. A. Hanover. 2002. Altered glycan-dependent signaling induces insulin resistance and hyperleptinemia. Proc Natl Acad Sci U S A 99(16):10695-10699. doi: 10.1073/pnas.152346899

Murata, K., K. Morino, S. Ida, N. Ohashi, M. Lemecha, S. Y. Park, A. Ishikado, S. Kume, C. S. Choi, O. Sekine, S. Ugi, and H. Maegawa. 2018. Lack of O-GlcNAcylation enhances exercise-dependent glucose utilization potentially through AMP-activated protein kinase activation in skeletal muscle. Biochem Biophys Res Commun 495(2):2098-2104. doi: 10.1016/j.bbrc.2017.12.081

Nelson, J. D., O. Denisenko, and K. Bomsztyk. 2006. Protocol for the fast chromatin immunoprecipitation (ChIP) method. Nat Protoc 1(1):179-185. doi: 10.1038/nprot.2006.27

Ogawa, M., H. Mizofuchi, Y. Kobayashi, G. Tsuzuki, M. Yamamoto, S. Wada, and K. Kamemura. 2012. Terminal differentiation program of skeletal myogenesis is negatively regulated by O-GlcNAc glycosylation. Biochim Biophys Acta 1820(1):24-32. doi: 10.1016/j.bbagen.2011.10.011

Ozcan, S., S. S. Andrali, and J. E. Cantrell. 2010. Modulation of transcription factor function by O-GlcNAc modification. Biochim Biophys Acta 1799(5-6):353-364. doi: 10.1016/j.bbagrm.2010.02.005

Pedersen, B. K., T. C. Akerstrom, A. R. Nielsen, and C. P. Fischer. 2007. Role of myokines in exercise and metabolism. J Appl Physiol (1985) 103(3):1093-1098. doi: 10.1152/japplphysiol.00080.2007

Pistilli, E. E., and L. S. Quinn. 2013. From anabolic to oxidative: reconsidering the roles of IL-15 and IL-15Ralpha in skeletal muscle. Exerc Sport Sci Rev 41(2):100-106. doi: 10.1097/JES.0b013e318275d230

Quinn, L. S., B. G. Anderson, J. D. Conner, and T. Wolden-Hanson. 2013. IL-15 overexpression promotes endurance, oxidative energy metabolism, and muscle PPARdelta, SIRT1, PGC-1alpha, and PGC-1beta expression in male mice. Endocrinology 154(1):232-245. doi: 10.1210/en.2012-1773

Quinn, L. S., B. G. Anderson, L. Strait-Bodey, A. M. Stroud, and J. M. Argiles. 2009. Oversecretion of interleukin-15 from skeletal muscle reduces adiposity. Am J Physiol Endocrinol Metab 296(1):E191-202. doi: 10.1152/ajpendo.90506.2008

Richard, A. F., J. Demignon, I. Sakakibara, J. Pujol, M. Favier, L. Strochlic, F. Le Grand, N. Sgarioto, A. Guernec, A. Schmitt, N. Cagnard, R. Huang, C. Legay, I. Guillet-Deniau, and P. Maire. 2011. Genesis of muscle fiber-type diversity during mouse embryogenesis relies on Six1 and Six4 gene expression. Dev Biol 359(2):303-320. doi: 10.1016/j.ydbio.2011.08.010

Rinnov, A., C. Yfanti, S. Nielsen, T. C. Akerstrom, L. Peijs, A. Zankari, C. P. Fischer, and B. K. Pedersen. 2014. Endurance training enhances skeletal muscle interleukin-15 in human male subjects. Endocrine 45(2):271-278. doi: 10.1007/s12020-013-9969-z

Ross, F. A., C. MacKintosh, and D. G. Hardie. 2016. AMP-activated protein kinase: a cellular energy sensor that comes in 12 flavours. FEBS J 283(16):2987-3001. doi: 10.1111/febs.13698

Ruan, H. B., M. O. Dietrich, Z. W. Liu, M. R. Zimmer, M. D. Li, J. P. Singh, K. Zhang, R. Yin, J. Wu, T. L. Horvath, and X. Yang. 2014. O-GlcNAc transferase enables AgRP neurons to suppress browning of white fat. Cell 159(2):306-317. doi: 10.1016/j.cell.2014.09.010

Ruan, H. B., X. Han, M. D. Li, J. P. Singh, K. Qian, S. Azarhoush, L. Zhao, A. M. Bennett, V. T. Samuel, J. Wu, J. R. Yates, 3rd, and X. Yang. 2012. O-GlcNAc transferase/host cell factor C1 complex regulates gluconeogenesis by modulating PGC-1alpha stability. Cell Metab 16(2):226-237. doi: 10.1016/j.cmet.2012.07.006

Ruan, H. B., J. P. Singh, M. D. Li, J. Wu, and X. Yang. 2013. Cracking the O-GlcNAc code in metabolism. Trends Endocrinol Metab 24(6):301-309. doi: 10.1016/j.tem.2013.02.002

Sakabe, K., and G. W. Hart. 2010. O-GlcNAc transferase regulates mitotic chromatin dynamics. J Biol Chem 285(45):34460-34468. doi: 10.1074/jbc.M110.158170

Slawson, C., R. J. Copeland, and G. W. Hart. 2010. O-GlcNAc signaling: a metabolic link between diabetes and cancer? Trends Biochem Sci 35(10):547-555. doi: 10.1016/j.tibs.2010.04.005

Song, R., W. Peng, Y. Zhang, F. Lv, H. K. Wu, J. Guo, Y. Cao, Y. Pi, X. Zhang, L. Jin, M. Zhang, P. Jiang, F. Liu, S. Meng, X. Zhang, P. Jiang, C. M. Cao, and R. P. Xiao. 2013. Central role of E3 ubiquitin ligase MG53 in insulin resistance and metabolic disorders. Nature 494(7437):375-379. doi: 10.1038/nature11834

Surwit, R. S., C. M. Kuhn, C. Cochrane, J. A. McCubbin, and M. N. Feinglos. 1988. Diet-induced type II diabetes in C57BL/6J mice. Diabetes 37(9):1163-1167. doi: 10.2337/diab.37.9.1163

Tan, E. P., M. T. Villar, L. E, J. Lu, J. E. Selfridge, A. Artigues, R. H. Swerdlow, and C. Slawson. 2014. Altering O-linked beta-N-acetylglucosamine cycling disrupts mitochondrial function. J Biol Chem 289(21):14719-14730. doi: 10.1074/jbc.M113.525790

Treebak, J. T., J. B. Birk, B. F. Hansen, G. S. Olsen, and J. F. Wojtaszewski. 2009. A-769662 activates AMPK beta1-containing complexes but induces glucose uptake through a PI3-kinase-dependent pathway in mouse skeletal muscle. Am J Physiol Cell Physiol 297(4):C1041-1052. doi: 10.1152/ajpcell.00051.2009

Wang, X., Z. Feng, X. Wang, L. Yang, S. Han, K. Cao, J. Xu, L. Zhao, Y. Zhang, and J. Liu. 2016. O-GlcNAcase deficiency suppresses skeletal myogenesis and insulin sensitivity in mice through the modulation of mitochondrial homeostasis. Diabetologia 59(6):1287-1296. doi: 10.1007/s00125-016-3919-2

Watt, M. J., N. Dzamko, W. G. Thomas, S. Rose-John, M. Ernst, D. Carling, B. E. Kemp, M. A. Febbraio, and G. R. Steinberg. 2006. CNTF reverses obesity-induced insulin resistance by activating skeletal muscle AMPK. Nat Med 12(5):541-548. doi: 10.1038/nm1383

Wolff, A. V., A. K. Niday, K. A. Voelker, J. A. Call, N. P. Evans, K. P. Granata, and R. W. Grange. 2006. Passive mechanical properties of maturing extensor digitorum longus are not affected by lack of dystrophin. Muscle Nerve 34(3):304-312. doi: 10.1002/mus.20588

Xu, J., S. Wang, B. Viollet, and M. H. Zou. 2012. Regulation of the proteasome by AMPK in endothelial cells: the role of O-GlcNAc transferase (OGT). PLoS One 7(5):e36717. doi: 10.1371/journal.pone.0036717

Xu, X. J., R. J. Valentine, and N. B. Ruderman. 2014. AMP-activated Protein Kinase (AMPK): Does This Master Regulator of Cellular Energy State Distinguish Insulin Sensitive from Insulin Resistant Obesity? Curr Obes Rep 3(2):248-255. doi: 10.1007/s13679-014-0095-x

Yang, W. H., S. Y. Park, H. W. Nam, D. H. Kim, J. G. Kang, E. S. Kang, Y. S. Kim, H. C. Lee, K. S. Kim, and J. W. Cho. 2008. NFkappaB activation is associated with its O-GlcNAcylation state under hyperglycemic conditions. Proc Natl Acad Sci U S A 105(45):17345-17350. doi: 10.1073/pnas.0806198105

Ye, J. 2015. Beneficial metabolic activities of inflammatory cytokine interleukin 15 in obesity and type 2 diabetes. Front Med 9(2):139-145. doi: 10.1007/s11684-015-0377-z

Zhang, S., K. Roche, H. P. Nasheuer, and N. F. Lowndes. 2011. Modification of histones by sugar beta-N-acetylglucosamine (GlcNAc) occurs on multiple residues, including histone H3 serine 10, and is cell cycle-regulated. J Biol Chem 286(43):37483-37495. doi: 10.1074/jbc.M111.284885

Chapter 3. Skeletal muscle O-GlcNAc transferase regulates global metabolism partially through interleukin-15

Abstract

Besides its roles in locomotion and thermogenesis, skeletal muscle plays a significant role in global glucose metabolism and insulin sensitivity through complex nutrient sensing networks. Our previous work showed that muscle-specific ablation of O-GlcNAc transferase (OGT) led to a lean phenotype through enhanced interleukin-15 (IL-15) expression. We also showed OGT epigenetically modified and repressed the *Il15* promoter. However, whether there is a causal relationship between OGT ablation-induced IL-15 secretion and the lean phenotype remains unknown. To address this question, we generated muscle specific OGT and interleukin-15 receptor alpha subunit (IL-15rα) double knockout mice (mDKO). Deletion of IL-15rα in skeletal muscle impaired IL-15 secretion. When fed a high-fat diet, mDKO mice were no longer protected against HFD-induced obesity compared to wild-type mice. After 22-wks of HFD feeding, mDKO mice had an intermediate body weight and glucose sensitivity compared to wild-type and OGT knockout mice. Taken together, these data suggest OGT action is partially mediated by IL-15. Our work suggests that interfering the OGT-IL15 nutrient sensing axis may provide a new avenue to combating obesity and its related metabolic disorders and provide some clarity into how the O-GlcNAc nutrient signaling pathway leads to a lean phenotype.

Key words: O-GlcNAc signaling, interleukin-15, tissue cross-talk, insulin sensitivity, myokines

Introduction

Skeletal muscle is a major contributor to whole body metabolism and accounts for 70-90% of insulin mediated glucose disposal (DeFronzo et al., 1981; Shulman et al., 1990; Watt et al., 2006; Bostrom et al., 2012; Funai et al., 2013; Song et al., 2013). Skeletal muscle maintains its mass, functionality, and metabolism through highly integrated signaling cascades to sense and respond to nutritional cues (Winder et al., 2000; Ebert et al., 2010; Ljubicic et al., 2011; Shi et al., 2018). The dynamic post-translational modification O-linked-β-D-N-acetylglucosamine (O-GlcNAc) serves as a widespread nutrient gauge by cycling on and off UDP-GlcNAc, an end product of the hexosamine biosynthetic pathway (HBP) that integrates carbohydrate, lipid, protein, energy, and nucleotide metabolism (Slawson et al., 2010; Hanover et al., 2012; Ruan et al., 2013). Specifically, O-GlcNAc transferase (OGT) and O-GlcNAcase (OGA) are responsible for the respective addition and removal of UDP-GlcNAc to modify target protein function according to fluctuating nutrient conditions (Issad et al., 2010; Ruan et al., 2012; Harwood and Hanover, 2014; Ruan et al., 2014). For example, hyper-O-GlcNAcylation from prolonged exposure to PUGNAc, an OGA inhibitor, reduces skeletal muscle glucose disposal and attenuates insulin sensitivity (Arias et al., 2004). Additionally, chronic exposure of skeletal muscle to glucose, through GLUT4 overexpression, increases muscle UDP-GlcNAc levels and leads to the development of insulin resistance (Buse et al., 1996). Prolonged fatty acid or uridine exposure also increase muscle UDP-GlcNAc concentrations and attenuate muscle insulin sensitivity (Hawkins et al., 1997a; Hawkins et al., 1997b).

As dysregulation of O-GlcNAcylation has been implicated in numerous metabolic disorders (Hanover et al., 2012; Ruan et al., 2013; Harwood and Hanover, 2014) and modulation of skeletal muscle metabolism can alter global metabolism (Izumiya et al., 2008; Meng et al.,

2013), we previously investigated the role of skeletal muscle O-GlcNAcylation in whole body metabolic regulation. We found skeletal muscle O-GlcNAcylation plays an essential role in systemic energy homeostasis, and deletion of skeletal muscle OGT (mKO) protects mice from high-fat diet induced obesity and ameliorates whole-body insulin sensitivity (Shi et al., 2018).

The mKO phenotype bears a striking resemblance to mice overexpressing skeletal muscle specific interleukin-15 (IL-15). Overexpression of IL-15 in skeletal muscle also increased energy expenditure, increased expression of muscle oxidative enzymes, and protected mice from HFD induced obesity and insulin resistance; however, activity level and substrate utilization of these mice did not resemble mKO mice (Quinn et al., 2009; Quinn et al., 2011; Quinn et al., 2013). Indeed, mKO mice had a 5-fold increase in *Il15* expression in skeletal muscle and a 3-fold increase in IL-15 serum protein concentrations, therefore we hypothesized OGT participates in the epigenetic regulation of *Il15* gene expression (Shi et al., 2018). In fact, EZH2, a key catalytic component of the polycomb repressive complex (PRC2), is a site of O-GlcNAcylation that may repress *Il15* expression through H3K27me3 methylation (Hanover et al., 2012; Chu et al., 2014; Lewis and Hanover, 2014). We found that OGT, EZH2, and H3K27me3 localized to the *Il15* promotor providing strong evidence OGT transcriptionally regulates *Il15* expression in skeletal muscle. However, we were unable to exclude OGT deletion did not perturb other cellular pathways that may contribute to the lean mKO phenotype. As a result, we aimed to determine if OGT action on global metabolism is attributed to IL-15 secretion using a genetic approach.

Secretion of IL-15 occurs in a unique manner that relies on the complexing of IL-15 and its high-affinity receptor, interleukin-15 receptor alpha (IL-15rα) to increase the stability, secretion, and bioavailability of IL-15 (Rubinstein et al., 2006a; Stoklasek et al., 2006). Co-expression of IL-15 and IL-15rα in human 293 cells increases secretion and stability of both

molecules *in vitro* and *in vivo* (Bergamaschi et al., 2008). In skeletal muscle, deletion of Il-15rα reduced IL-15 serum concentrations (O'Connell et al., 2015). Therefore, we generated skeletal muscle specific OGT and IL-15rα double knockout mice (mDKO) to determine the contribution of IL-15 secretion to OGT action. After feeding a high fat diet (HFD) for 22-wks, mDKO mice exhibited an intermediate phenotype between mKO and WT mice corroborating our previous hypothesis that loss of OGT perturbs *Il15* expression and, at least partially, drives the mKO phenotype and suggests IL-15 may be partially responsible for the lean phenotype observed in those mice lacking a functional *Ogt* gene.

Materials and Methods

Animals

Mice were generated and maintained at Virginia Polytechnic Institute and State University and all experiments were approved by the Institution for Animal Use and Care Committee. Muscle specific *Ogt* and *Il15ra* deletion was accomplished by breeding $HSA^{Cre/+}$; $Ogt^{LoxP/Y}$; $Il15ra^{LoxP/LoxP}$ males (Jax Mice strains: B6.Cg-Tg(ACTA1-cre)79Jme/J; B6.129-Ogt^{tm1Gwh}/J; C57BL/6-$Il15ra^{tm2.1Ama}$/J) with $Ogt^{loxP/loxP}$; $Il15ra^{LoxP/LoxP}$ females to generate $HSA^{Cre/+}$; $Ogt^{LoxP/Y}$; $Il15ra^{LoxP/LoxP}$ (mDKO) and $HSA^{+/+}$; $Ogt^{LoxP/Y}$; $Il15ra^{LoxP/LoxP}$ (WT) males. Mice were group housed with a 12 hr light: 12 hr dark cycle with *ad libitum* feed. At 4-wks of age, mice were fed Teklad rodent diets (#TD.06414, Envigo) with 60% of calories coming from fat. The fatty acid profile (% of total fat) is as follows: 37% saturated, 47% monounsaturated, 16% polyunsaturated.

Body Composition

Body composition was determined after 22-wks of HFD using a Bruker minispec LF90 TD-NMR analyzer (Bruker, Billerica, MA).

Tissue sample collection

Mice were euthanized by carbon dioxide followed by cervical dislocation. *Tibialis anterior* (TA) and *Gastrocnemius* (GA) muscles and inguinal and epididymal white adipose tissue depots were collected and weighed.

Quantitative RT-PCR

Directzol RNA Miniprep Kit (Zymo Research) was used to extract total RNA from the gastrocnemius muscle. High-Capacity cDNA Reverse Transcription Kit (Thermo Fisher Scientific) was used to perform reverse transcription. Fast SYBR Green Master Mix (Thermo Fisher Scientific) and 7500 Fast Real Time PCR System (Thermo Fisher Scientific) were used to carry out qPCR reaction. Quantification was performed using ΔΔCT method. Primers for OGT, IL-15rα, and IL-15 were as follows: OGT forward AAG AGG CAC GCA TTT TTG AC; OGT reverse ATG GGG TTG CAG TTC GAT AG; IL-15rα forward TGT CCA CCT CCC GTA TCT ATT; IL-15rα reverse AAA GCC AGA GTT ACA GAC ATA CC; IL-15 forward TCT TCA AAG CAC TGC CTC TTC; IL-15 reverse CCT CCT GTA GGC TGG TTA TCT.

Serum IL-15 quantification

Serum was collected from mice after 22-wks of HFD feeding. Serum levels of IL-15/IL15rα complex was determined using IL-15/IL-15R Complex Mouse ELISA kit (Invitrogen, Carlsbad, CA) according to the manufacturer's instructions.

Glucose and Insulin Tolerance Testing

Mice were fasted for 4 hrs before insulin tolerance testing (ITT). Bovine insulin (Sigma) was prepared in sterile saline and intraperitoneally injected at the dosage of 1 U/kg body weight.

Blood glucose level was measured at 0, 15, 60, 90, and 120 min after insulin injection using OneTouch Ultra2 test strip and glucometer. For glucose tolerance testing (GTT), mice were fasted for 16 hrs before experiments were conducted. Glucose was intraperitoneally injected at 2 g/kg body weight, and blood collection and measurement were the same as ITT.

Statistical Analysis

Results are presented as means ± SEM. Data was analyzed using a student *t*-test. A p-value of less than or equal to 0.05 was considered significant. Comparisons were between WT and mDKO. Red dotted lines represent means from 5 mKO mice for reference and were not included in statistical analysis.

Results

Deletion of OGT and IL-15rα in skeletal muscle increased muscle Il15 gene expression but diminished serum IL-15 protein concentrations

To generate OGT and IL-15rα double knockout mice, we bred male mice harboring Cre-recombinase driven by the expression of the human skeletal α-actin promotor (HSA-Cre mice) with *Ogt* and *Il15rα* floxed female mice to generate OGT and IL-15rα muscle-specific double knockout mice (mDKO). Gene expression of *Il15ra* ($P = 0.011$) and *Ogt* ($P < 0.0001$) were significantly reduced in mDKO muscle compared to WT (Fig. 3-1A,B), confirming deletion of OGT and IL-15rα in skeletal muscle. We also measured *Il15* gene expression in mDKO muscle to determine if the simultaneous loss of OGT and IL-15rα recapitulated the dysregulated *Il15* expression observed in mKO mice. Indeed, *Il15* expression increased 2-fold in mDKO muscle ($P = 0.004$; Fig. 3-1C) confirming OGT regulates *Il15* expression in mDKO skeletal muscle, albeit concurrent deletion of IL-15rα abated the magnitude of increase observed in mKO mice. In contrast, circulating IL-15 protein concentration tended to decrease in mDKO mice ($P = 0.086$;

Fig. 3-1D). These data indicate the loss of IL-15rα impeded IL-15 secretion into circulation even though its gene expression was upregulated in skeletal muscle.

Congruent loss of OGT and IL-15rα diminished the protection against HFD-induced obesity observed in mKO mice

To test whether OGT action mediated through IL-15 in the context of obesity, we subjected mDKO mice to 22-wks of a high-fat diet (HFD). Body weights of mDKO mice were reduced compared to WT mice after 4-wks of HFD feeding; however, mDKO body weights appear to be greater than muscle-specific OGT single knockout (mKO) mice (Fig. 3-2A). It appeared that mDKO mice had similar fat depots to WT mice (Fig. 3-2B). Indeed, there were no significant differences in total fat mass (Fig. 3-2C), inguinal white adipose tissue mass (IngW; Fig. 3-2D), or epididymal white adipose tissue mass (EpiW; Fig. 3-2D) between WT and mDKO mice after 22-wks of HFD feeding, although both WT and mDKO mice appeared to have greater fat accumulation than mKO mice (indicated by the dotted red line; Fig. 3-2C). Surprisingly, mDKO gastrocnemius (GA; $P = 0.017$) and tibialis anterior (TA; $P = 0.003$) weights increased compared to WT mice (Fig. 3-2F), although total lean mass did not differ (Fig. 3-2E). Previously, we reported mKO mice had a higher body temperature that corresponded to an increase in energy expenditure in mKO mice. Body temperatures of mDKO mice were lower than WT mice ($P = 0.012$; Fig. 3-2G) suggesting decreased circulating levels of IL-15 may reverse the enhanced energy expenditure observed in mKO mice. Collectively, these data indicate the higher energy expenditure and leaner phenotype in mKO mice may be partially mediated through IL-15, as the decreased circulating IL-15 levels in mDKO mice negated this phenotype.

Mice lacking OGT and IL-15 exhibited glucose intolerance after HFD feeding

To investigate whether deletion of OGT and IL-15rα could negate the mKO protection against metabolic perturbations associated with obesity, we fed the mice a HFD. After 12-wks of HFD feeding, blood glucose levels were lower in mDKO mice after 4 hrs of fasting compared to WT ($P = 0.054$; Fig. 3-3A), but there was no difference after 16 hrs of fasting (Fig. 3-3C). Although WT and mDKO mice had similar blood glucose levels throughout the glucose tolerance testing (Fig. 3-3B), their blood glucose levels appeared to be higher than mKO suggesting impaired glucose uptake. Insulin tolerance testing revealed lower blood glucose levels 60 min after insulin injection in mDKO mice compared to WT (Fig. 3-3D).

After 22-wks of HFD feeding, there were no differences between WT and mDKO blood glucose levels after 4 (Fig. 3-4A) or 16 hrs (Fig. 3-4C) of fasting. Blood glucose levels of WT and mDKO mice remained the same throughout glucose tolerance testing, although mDKO mice had higher blood glucose levels than WT mice 60 min after the glucose injection (Fig. 3-4B). Insulin tolerance testing at 22-wks mirrored those from 12-wks of HFD feeding. These data indicate mDKO mice are susceptible to HFD-induced metabolic disorders but still retain some level of protection from the loss of OGT.

Discussion

Previously, we showed the importance of skeletal muscle O-GlcNAcylation in the maintenance of whole-body metabolic homeostasis. Ablation of OGT, and thus O-GlcNAcylation, in skeletal muscle (mKO) resulted in increased energy expenditure, improved insulin sensitivity, protection against HFD-induced obesity, and dysregulation of muscle interleukin-15 (*Il15)* expression. We also showed the OGT-EZH2-H3K27me3 axis plays a critical role in the epigenetic regulation of *Il15* expression. However, it remains unknown if the increased IL-15 secretion alone caused the OGT phenotype.

It is reported that the complexing of Il-15 and IL-15rα increase the stability, secretion, and bioavailability of IL-15 (Rubinstein et al., 2006b; Stoklasek et al., 2006; Bergamaschi et al., 2008). Global knockout of IL-15rα resulted in an increase in muscle oxidative enzymes and reduced adipose tissue mass, initially suggesting IL-15rα is not needed for effective IL-15 secretion and modulation of global metabolism (Pistilli et al., 2011). However, muscle-specific ablation of IL-15rα did not decrease body weight or fat mass and had minimal impact on muscle oxidative enzymes (O'Connell et al., 2015). The reported differences in muscle and whole-body metabolism between the global and muscle specific knockout may be attributed to the global knockout lacking IL-15rα in the central nervous system. IL-15 crosses the blood-brain barrier (Wu et al., 2010b) and modulation of IL-15/IL-15rα impacts sleep patterns (Kubota et al., 2001), anxiety behavior pathways (Wu et al., 2010a), and antidepression pathways (Wu et al., 2011), which collectively depict the profound impacts of central nervous system IL-15rα on the body. The muscle-specific deletion of IL-15rα therefore defined its importance in modulating muscle and global metabolism (O'Connell et al., 2015), presumably through the stabilization and secretion of IL-15. We targeted both OGT and IL-15rα in skeletal muscle to generate a model that obstructs IL-15 over-secretion from skeletal muscle lacking OGT. Mice harboring loxP sites flanking exons 2 and 3 of *Il15rα* (O'Connell et al., 2015), that respectively encode the sushi domain and linker region that play a role in the high affinity binding of IL-15 to IL-15rα (Dubois et al., 1999; Bouchaud et al., 2008), were used to generate OGT and IL-15rα double knockout mice. We showed that deleting IL-15rα in skeletal muscle had minimal impact on *Il15* gene expression within muscle, whereas it impaired the secretion of IL-15 into circulation. Using this strategy, we found obstruction of IL-15 secretion partially negated the *OGT* single knockout phenotype.

To determine whether the obstruction of IL-15 secretion in mDKO mice could reverse the lean mKO phenotype, we fed a HFD for 22-wks and found mDKO mice exhibited an intermediate phenotype between WT and mKO mice. These findings suggest that enhanced IL-15 circulation contributes, at least in part, to the lean phenotype observed in mKO mice. Although mDKO mice had greater similarities to WT mice than mKO mice, mDKO mice did not fully recapitulate the WT phenotype. Although there was no difference in fat mass and minimal differences in glucose disposal between WT and mKO mice, mDKO mice were markedly different in insulin-stimulated glucose uptake 60 min after insulin administration. Although circulating levels of IL-15 decreased in mDKO mice, IL-15 expression in muscle remained elevated which may explain the discrepancies between mDKO GTT and ITT data given IL-15 is an established activator of the PI-3-kinase/Akt (Zhao and Huang, 2012; Lai et al., 2013) and Jak/STAT pathways (Johnston et al., 1995; Krolopp et al., 2016). As perturbations of both pathways have been implicated in the pathogenesis of metabolic diseases including insulin resistance (Dodington et al., 2018; Huang et al., 2018), it is possible the increased expression of IL-15 in mDKO muscle may improve glucose uptake upon insulin administration. These findings suggest IL-15 participates in, but is not the sole contributor, to OGT global action. However, this is not surprising given OGT has thousands of known target proteins that regulate a wide range of cellular processes including protein localization, the cell cycle, signal transduction, mitochondrial bioenergetics, protein degradation, gene expression, and epigenetic regulation (Love and Hanover, 2005; Zachara et al., 2015). Even so, it is apparent that IL-15 is a major contributor to skeletal muscle OGT-mediated effects on local and global metabolism.

Acknowledgements

The authors wish to thank Con-Ning Yen, Jennifer Cobb, RJ Savino, and Jocelyn Bodmer for their contributions to the study.

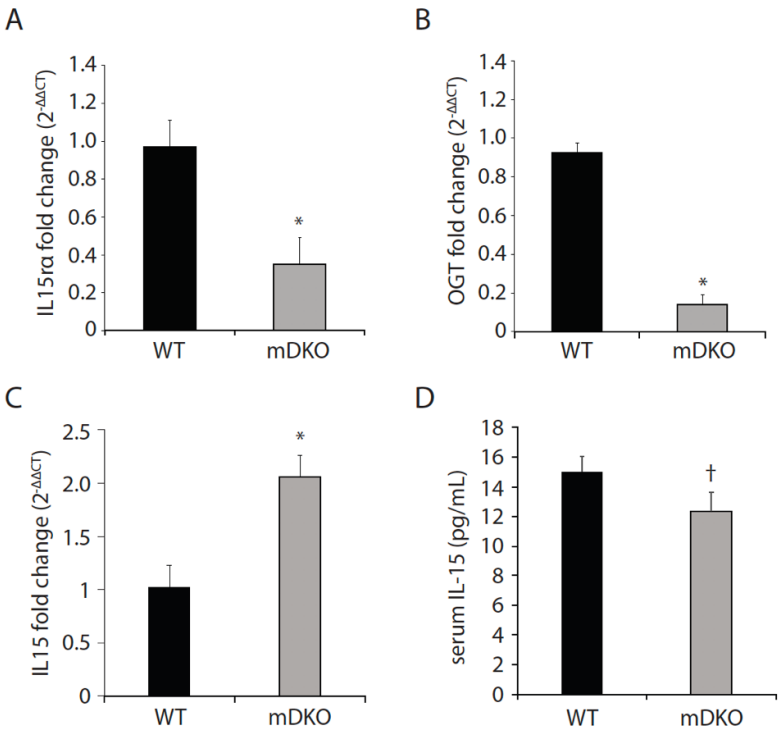

Figure 3-1. OGT and IL-15rα double knockout in skeletal muscle perturbed elevated IL-15 secretion. (A-D) Relative gene expression of **(A)** IL-15rα, **(B)** OGT, and **(C)** IL-15 in the gastrocnemius muscles of WT and mDKO mice fed a HFD for 22-wks. n = 7 **(D)** Serum IL-15 levels in WT and mDKO mice fed a HFD for 22-wks. n = 8. Values are means ± SEM. * $p < 0.05$, † $p < 0.08$ when compared to WT.

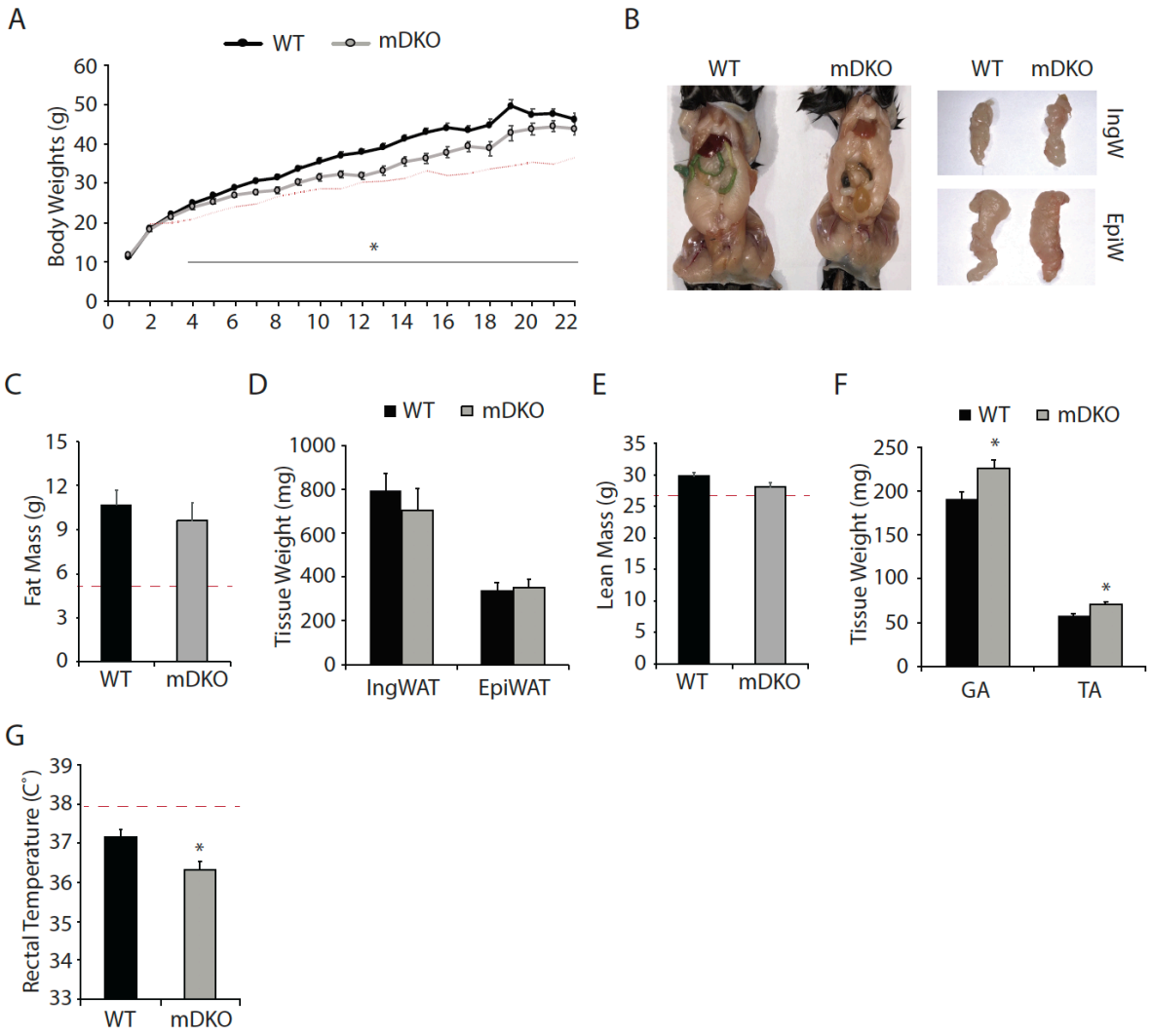

Figure 3-2. Loss of OGT and IL-15rα in skeletal muscle diminished the lean phenotype observed in OGT single knockout mice. (A) Weekly body weights of WT and mDKO mice during 22-wks of HFD feeding. HFD feeding started at 4-wks of age. n = 11-14. **(B)** Representative images comparing abdominal, inguinal (IngW), and epididymal (EpiW) white adipose tissue depots from WT and mDKO mice. **(C)** Rectal temperature of WT and mDKO mice. n =8-11. **(D-E)** (D) Lean composition and (E) muscle weights of tibialis anterior (TA) and gastrocnemius (GA) muscles of WT and mDKO mice after 22-wks of HFD feeding. n = 8-11. **(F-G)** (F) Fat composition and (G) weights of inguinal (IngW), and epididymal (EpiW) white adipose tissue depots of WT and mDKO mice after 22-wks of HFD feeding. n = 8-11. Values are means ± SEM. * $p < 0.05$ when compared to WT. Red dotted lines are values from 5 muscle specific OGT knockout mice (mKO) for reference.

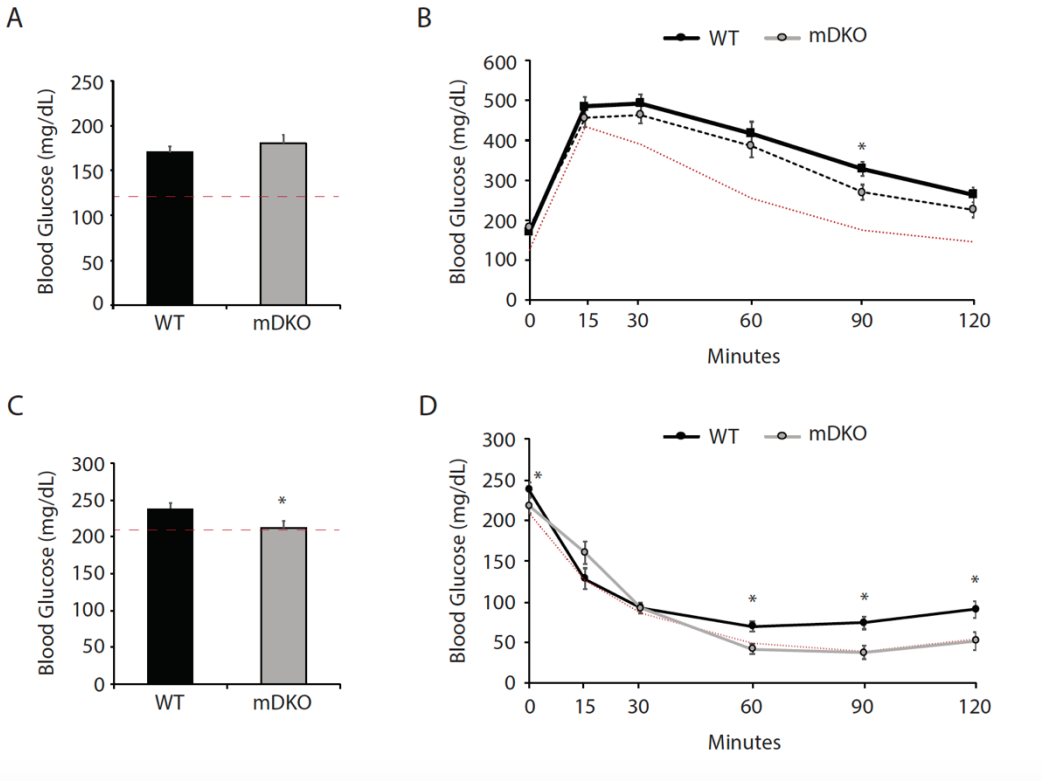

Figure 3-3. Glucose and insulin tolerance testing after 12-wks of HFD feeding. **(A)** Resting blood glucose levels after 16 hrs of fasting in WT and mDKO mice. **(B)** Glucose tolerance test of WT and mDKO mice. **(C)** Resting blood glucose levels after 4 hrs of fasting in WT and mDKO mice. **(D)** Insulin tolerance test of WT and mDKO mice. Values are means ± SEM. n = 12-13. * $p < 0.05$ when compared to WT. Red dotted lines are values from 5 muscle specific OGT knockout mice (mKO) for reference.

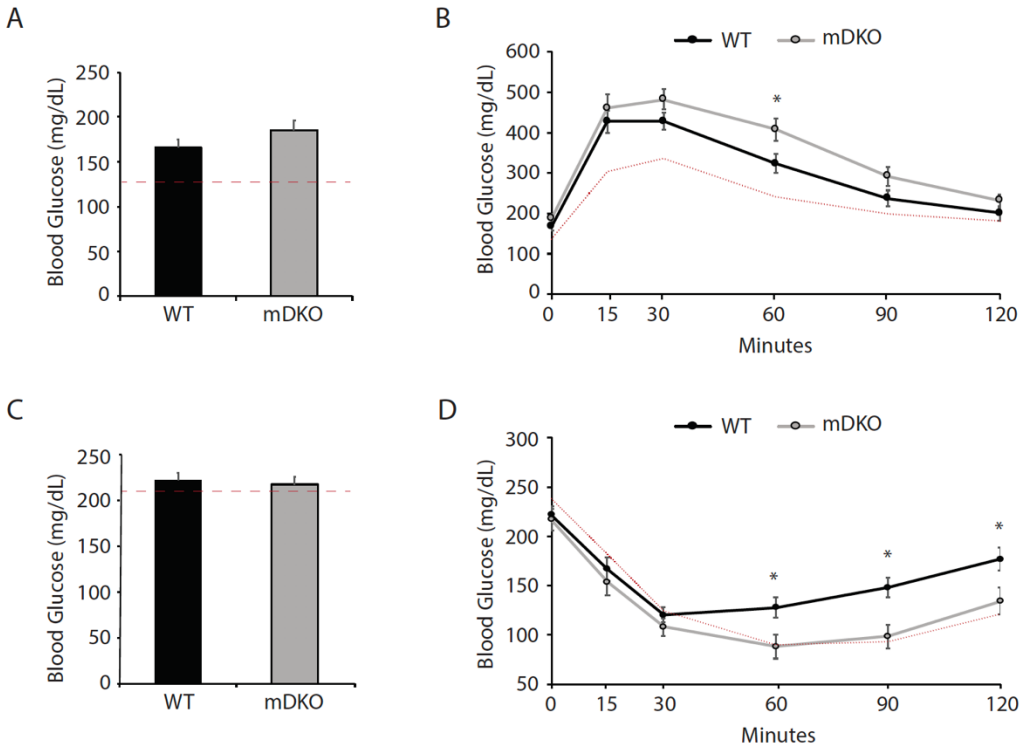

Figure 3-4. Glucose and insulin tolerance testing after 22-wks of HFD feeding. **(A)** Resting blood glucose levels after 16 hrs of fasting in WT and mDKO mice. **(B)** Glucose tolerance test of WT and mDKO mice. **(C)** Resting blood glucose levels after 4 hrs of fasting in WT and mDKO mice. **(D)** Insulin tolerance test of WT and mDKO mice. Values are means ± SEM. n = 7-10. * $p < 0.05$ when compared to WT. Red dotted lines are values from 5 muscle specific OGT knockout mice (mKO) for reference.

References

Arias, E. B., J. Kim, and G. D. Cartee. 2004. Prolonged incubation in PUGNAc results in increased protein O-Linked glycosylation and insulin resistance in rat skeletal muscle. Diabetes 53(4):921-930. doi: 10.2337/diabetes.53.4.921

Bergamaschi, C., M. Rosati, R. Jalah, A. Valentin, V. Kulkarni, C. Alicea, G. M. Zhang, V. Patel, B. K. Felber, and G. N. Pavlakis. 2008. Intracellular interaction of interleukin-15 with its receptor alpha during production leads to mutual stabilization and increased bioactivity. J Biol Chem 283(7):4189-4199. doi: 10.1074/jbc.M705725200

Bostrom, P., J. Wu, M. P. Jedrychowski, A. Korde, L. Ye, J. C. Lo, K. A. Rasbach, E. A. Bostrom, J. H. Choi, J. Z. Long, S. Kajimura, M. C. Zingaretti, B. F. Vind, H. Tu, S. Cinti, K. Hojlund, S. P. Gygi, and B. M. Spiegelman. 2012. A PGC1-alpha-dependent myokine that drives brown-fat-like development of white fat and thermogenesis. Nature 481(7382):463-468. doi: 10.1038/nature10777

Bouchaud, G., L. Garrigue-Antar, V. Sole, A. Quemener, Y. Boublik, E. Mortier, H. Perdreau, Y. Jacques, and A. Plet. 2008. The exon-3-encoded domain of IL-15ralpha contributes to IL-15 high-affinity binding and is crucial for the IL-15 antagonistic effect of soluble IL-15Ralpha. J Mol Biol 382(1):1-12. doi: 10.1016/j.jmb.2008.07.019

Buse, M. G., K. A. Robinson, B. A. Marshall, and M. Mueckler. 1996. Differential effects of GLUT1 or GLUT4 overexpression on hexosamine biosynthesis by muscles of transgenic mice. J Biol Chem 271(38):23197-23202. doi: 10.1074/jbc.271.38.23197

Chu, C. S., P. W. Lo, Y. H. Yeh, P. H. Hsu, S. H. Peng, Y. C. Teng, M. L. Kang, C. H. Wong, and L. J. Juan. 2014. O-GlcNAcylation regulates EZH2 protein stability and function. Proc Natl Acad Sci U S A 111(4):1355-1360. doi: 10.1073/pnas.1323226111

DeFronzo, R. A., E. Jacot, E. Jequier, E. Maeder, J. Wahren, and J. P. Felber. 1981. The effect of insulin on the disposal of intravenous glucose. Results from indirect calorimetry and hepatic and femoral venous catheterization. Diabetes 30(12):1000-1007. doi: 10.2337/diab.30.12.1000

Dodington, D. W., H. R. Desai, and M. Woo. 2018. JAK/STAT - Emerging Players in Metabolism. Trends Endocrinol Metab 29(1):55-65. doi: 10.1016/j.tem.2017.11.001

Dubois, S., F. Magrangeas, P. Lehours, S. Raher, J. Bernard, O. Boisteau, S. Leroy, S. Minvielle, A. Godard, and Y. Jacques. 1999. Natural splicing of exon 2 of human interleukin-15 receptor alpha-chain mRNA results in a shortened form with a distinct pattern of expression. J Biol Chem 274(38):26978-26984. doi: 10.1074/jbc.274.38.26978

Ebert, S. M., A. M. Monteys, D. K. Fox, K. S. Bongers, B. E. Shields, S. E. Malmberg, B. L. Davidson, M. Suneja, and C. M. Adams. 2010. The transcription factor ATF4 promotes skeletal myofiber atrophy during fasting. Mol Endocrinol 24(4):790-799. doi: 10.1210/me.2009-0345

Funai, K., H. Song, L. Yin, I. J. Lodhi, X. Wei, J. Yoshino, T. Coleman, and C. F. Semenkovich. 2013. Muscle lipogenesis balances insulin sensitivity and strength through calcium signaling. J Clin Invest 123(3):1229-1240. doi: 10.1172/JCI65726

Hanover, J. A., M. W. Krause, and D. C. Love. 2012. Bittersweet memories: linking metabolism to epigenetics through O-GlcNAcylation. Nat Rev Mol Cell Biol 13(5):312-321. doi: 10.1038/nrm3334

Harwood, K. R., and J. A. Hanover. 2014. Nutrient-driven O-GlcNAc cycling - think globally but act locally. J Cell Sci 127(Pt 9):1857-1867. doi: 10.1242/jcs.113233

Hawkins, M., I. Angelov, R. Liu, N. Barzilai, and L. Rossetti. 1997a. The tissue concentration of UDP-N-acetylglucosamine modulates the stimulatory effect of insulin on skeletal muscle glucose uptake. J Biol Chem 272(8):4889-4895. doi: 10.1074/jbc.272.8.4889

Hawkins, M., N. Barzilai, R. Liu, M. Hu, W. Chen, and L. Rossetti. 1997b. Role of the glucosamine pathway in fat-induced insulin resistance. J Clin Invest 99(9):2173-2182. doi: 10.1172/JCI119390

Huang, X., G. Liu, J. Guo, and Z. Su. 2018. The PI3K/AKT pathway in obesity and type 2 diabetes. Int J Biol Sci 14(11):1483-1496. doi: 10.7150/ijbs.27173

Issad, T., E. Masson, and P. Pagesy. 2010. O-GlcNAc modification, insulin signaling and diabetic complications. Diabetes Metab 36(6 Pt 1):423-435. doi: 10.1016/j.diabet.2010.09.001

Izumiya, Y., T. Hopkins, C. Morris, K. Sato, L. Zeng, J. Viereck, J. A. Hamilton, N. Ouchi, N. K. LeBrasseur, and K. Walsh. 2008. Fast/Glycolytic muscle fiber growth reduces fat mass and improves metabolic parameters in obese mice. Cell Metab 7(2):159-172. doi: 10.1016/j.cmet.2007.11.003

Johnston, J. A., C. M. Bacon, D. S. Finbloom, R. C. Rees, D. Kaplan, K. Shibuya, J. R. Ortaldo, S. Gupta, Y. Q. Chen, J. D. Giri, and et al. 1995. Tyrosine phosphorylation and activation of STAT5, STAT3, and Janus kinases by interleukins 2 and 15. Proc Natl Acad Sci U S A 92(19):8705-8709. doi: 10.1073/pnas.92.19.8705

Krolopp, J. E., S. M. Thornton, and M. J. Abbott. 2016. IL-15 Activates the Jak3/STAT3 Signaling Pathway to Mediate Glucose Uptake in Skeletal Muscle Cells. Front Physiol 7:626. doi: 10.3389/fphys.2016.00626

Kubota, T., R. A. Brown, J. Fang, and J. M. Krueger. 2001. Interleukin-15 and interleukin-2 enhance non-REM sleep in rabbits. Am J Physiol Regul Integr Comp Physiol 281(3):R1004-1012. doi: 10.1152/ajpregu.2001.281.3.R1004

Lai, Y. G., M. S. Hou, A. Lo, S. T. Huang, Y. W. Huang, H. F. Yang-Yen, and N. S. Liao. 2013. IL-15 modulates the balance between Bcl-2 and Bim via a Jak3/1-PI3K-Akt-ERK pathway to promote CD8alphaalpha+ intestinal intraepithelial lymphocyte survival. Eur J Immunol 43(9):2305-2316. doi: 10.1002/eji.201243026

Lewis, B. A., and J. A. Hanover. 2014. O-GlcNAc and the epigenetic regulation of gene expression. J Biol Chem 289(50):34440-34448. doi: 10.1074/jbc.R114.595439

Ljubicic, V., P. Miura, M. Burt, L. Boudreault, S. Khogali, J. A. Lunde, J. M. Renaud, and B. J. Jasmin. 2011. Chronic AMPK activation evokes the slow, oxidative myogenic program and triggers beneficial adaptations in mdx mouse skeletal muscle. Hum Mol Genet 20(17):3478-3493. doi: 10.1093/hmg/ddr265

Love, D. C., and J. A. Hanover. 2005. The hexosamine signaling pathway: deciphering the "O-GlcNAc code". Sci STKE 2005(312):re13. doi: 10.1126/stke.3122005re13

Meng, Z. X., S. Li, L. Wang, H. J. Ko, Y. Lee, D. Y. Jung, M. Okutsu, Z. Yan, J. K. Kim, and J. D. Lin. 2013. Baf60c drives glycolytic metabolism in the muscle and improves systemic glucose homeostasis through Deptor-mediated Akt activation. Nat Med 19(5):640-645. doi: 10.1038/nm.3144

O'Connell, G., G. Guo, J. Stricker, L. S. Quinn, A. Ma, and E. E. Pistilli. 2015. Muscle-specific deletion of exons 2 and 3 of the IL15RA gene in mice: effects on contractile properties of fast and slow muscles. J Appl Physiol (1985) 118(4):437-448. doi: 10.1152/japplphysiol.00704.2014

Pistilli, E. E., S. Bogdanovich, F. Garton, N. Yang, J. P. Gulbin, J. D. Conner, B. G. Anderson, L. S. Quinn, K. North, R. S. Ahima, and T. S. Khurana. 2011. Loss of IL-15 receptor alpha

alters the endurance, fatigability, and metabolic characteristics of mouse fast skeletal muscles. J Clin Invest 121(8):3120-3132. doi: 10.1172/JCI44945

Quinn, L. S., B. G. Anderson, J. D. Conner, E. E. Pistilli, and T. Wolden-Hanson. 2011. Overexpression of interleukin-15 in mice promotes resistance to diet-induced obesity, increased insulin sensitivity, and markers of oxidative skeletal muscle metabolism. Int J Interferon Cytokine Mediat Res 3:29-42. doi: 10.2147/IJICMR.S19007

Quinn, L. S., B. G. Anderson, J. D. Conner, and T. Wolden-Hanson. 2013. IL-15 overexpression promotes endurance, oxidative energy metabolism, and muscle PPARdelta, SIRT1, PGC-1alpha, and PGC-1beta expression in male mice. Endocrinology 154(1):232-245. doi: 10.1210/en.2012-1773

Quinn, L. S., B. G. Anderson, L. Strait-Bodey, A. M. Stroud, and J. M. Argiles. 2009. Oversecretion of interleukin-15 from skeletal muscle reduces adiposity. Am J Physiol Endocrinol Metab 296(1):E191-202. doi: 10.1152/ajpendo.90506.2008

Ruan, H. B., M. O. Dietrich, Z. W. Liu, M. R. Zimmer, M. D. Li, J. P. Singh, K. Zhang, R. Yin, J. Wu, T. L. Horvath, and X. Yang. 2014. O-GlcNAc transferase enables AgRP neurons to suppress browning of white fat. Cell 159(2):306-317. doi: 10.1016/j.cell.2014.09.010

Ruan, H. B., X. Han, M. D. Li, J. P. Singh, K. Qian, S. Azarhoush, L. Zhao, A. M. Bennett, V. T. Samuel, J. Wu, J. R. Yates, 3rd, and X. Yang. 2012. O-GlcNAc transferase/host cell factor C1 complex regulates gluconeogenesis by modulating PGC-1alpha stability. Cell Metab 16(2):226-237. doi: 10.1016/j.cmet.2012.07.006

Ruan, H. B., J. P. Singh, M. D. Li, J. Wu, and X. Yang. 2013. Cracking the O-GlcNAc code in metabolism. Trends Endocrinol Metab 24(6):301-309. doi: 10.1016/j.tem.2013.02.002

Rubinstein, M. P., M. Kovar, J. F. Purton, J. H. Cho, O. Boyman, C. D. Surh, and J. Sprent. 2006a. Converting IL-15 to a superagonist by binding to soluble IL-15R alpha. Proc Natl Acad Sci U S A 103(24):9166-9171. doi: 10.1073/pnas.0600240103

Rubinstein, M. P., M. Kovar, J. F. Purton, J. H. Cho, O. Boyman, C. D. Surh, and J. Sprent. 2006b. Converting IL-15 to a superagonist by binding to soluble IL-15R{alpha}. Proc Natl Acad Sci U S A 103(24):9166-9171. doi: 10.1073/pnas.0600240103

Shi, H., A. Munk, T. S. Nielsen, M. R. Daughtry, L. Larsson, S. Li, K. F. Hoyer, H. W. Geisler, K. Sulek, R. Kjobsted, T. Fisher, M. M. Andersen, Z. Shen, U. K. Hansen, E. M. England, Z. Cheng, K. Hojlund, J. F. P. Wojtaszewski, X. Yang, M. W. Hulver, R. F. Helm, J. T. Treebak, and D. E. Gerrard. 2018. Skeletal muscle O-GlcNAc transferase is important for muscle energy homeostasis and whole-body insulin sensitivity. Mol Metab 11:160-177. doi: 10.1016/j.molmet.2018.02.010

Shulman, G. I., D. L. Rothman, T. Jue, P. Stein, R. A. DeFronzo, and R. G. Shulman. 1990. Quantitation of muscle glycogen synthesis in normal subjects and subjects with non-insulin-dependent diabetes by 13C nuclear magnetic resonance spectroscopy. N Engl J Med 322(4):223-228. doi: 10.1056/NEJM199001253220403

Slawson, C., R. J. Copeland, and G. W. Hart. 2010. O-GlcNAc signaling: a metabolic link between diabetes and cancer? Trends Biochem Sci 35(10):547-555. doi: 10.1016/j.tibs.2010.04.005

Song, R., W. Peng, Y. Zhang, F. Lv, H. K. Wu, J. Guo, Y. Cao, Y. Pi, X. Zhang, L. Jin, M. Zhang, P. Jiang, F. Liu, S. Meng, X. Zhang, P. Jiang, C. M. Cao, and R. P. Xiao. 2013. Central role of E3 ubiquitin ligase MG53 in insulin resistance and metabolic disorders. Nature 494(7437):375-379. doi: 10.1038/nature11834

Stoklasek, T. A., K. S. Schluns, and L. Lefrancois. 2006. Combined IL-15/IL-15Ralpha immunotherapy maximizes IL-15 activity in vivo. J Immunol 177(9):6072-6080. doi: 10.4049/jimmunol.177.9.6072

Watt, M. J., N. Dzamko, W. G. Thomas, S. Rose-John, M. Ernst, D. Carling, B. E. Kemp, M. A. Febbraio, and G. R. Steinberg. 2006. CNTF reverses obesity-induced insulin resistance by activating skeletal muscle AMPK. Nat Med 12(5):541-548. doi: 10.1038/nm1383

Winder, W. W., B. F. Holmes, D. S. Rubink, E. B. Jensen, M. Chen, and J. O. Holloszy. 2000. Activation of AMP-activated protein kinase increases mitochondrial enzymes in skeletal muscle. J Appl Physiol (1985) 88(6):2219-2226. doi: 10.1152/jappl.2000.88.6.2219

Wu, X., Y. He, H. Hsuchou, A. J. Kastin, J. C. Rood, and W. Pan. 2010a. Essential role of interleukin-15 receptor in normal anxiety behavior. Brain Behav Immun 24(8):1340-1346. doi: 10.1016/j.bbi.2010.06.012

Wu, X., H. Hsuchou, A. J. Kastin, Y. He, R. S. Khan, K. P. Stone, M. S. Cash, and W. Pan. 2011. Interleukin-15 affects serotonin system and exerts antidepressive effects through IL15Ralpha receptor. Psychoneuroendocrinology 36(2):266-278. doi: 10.1016/j.psyneuen.2010.07.017

Wu, X., W. Pan, K. P. Stone, Y. Zhang, H. Hsuchou, and A. J. Kastin. 2010b. Expression and signaling of novel IL15Ralpha splicing variants in cerebral endothelial cells of the blood-brain barrier. J Neurochem 114(1):122-129. doi: 10.1111/j.1471-4159.2010.06729.x

Zachara, N., Y. Akimoto, and G. W. Hart. 2015. The O-GlcNAc Modification. In: rd, A. Varki, R. D. Cummings, J. D. Esko, P. Stanley, G. W. Hart, M. Aebi, A. G. Darvill, T. Kinoshita, N. H. Packer, J. H. Prestegard, R. L. Schnaar and P. H. Seeberger, editors, Essentials of Glycobiology, Cold Spring Harbor (NY). p. 239-251.

Zhao, H., and H. Huang. 2012. Functional capability of IL-15-Akt signaling in the denervated muscle. Cytokine 60(3):608-615. doi: 10.1016/j.cyto.2012.08.026

Chapter 4. O-GlcNAc transferase is required to maintain satellite cell function

Abstract

O-GlcNAcylation is a post-translational modification considered to be a nutrient sensor that reports nutrient scarcity or surplus. Although O-GlcNAcylation exists in a wide range of cells and/or tissues, its functional role in muscle satellite cells (SCs) remains largely unknown. Using a genetic approach, we ablated O-GlcNAc transferase (OGT), and thus O-GlcNAcylation, in SCs. We first evaluated SC function *in vivo* using a muscle injury model and found that OGT deficient SCs had compromised capacity to repair muscle after an acute injury compared to the wild-type SCs. By tracing SC cycling rates *in vivo* using the doxycycline-inducible H2B-GFP mouse model, we found that SCs lacking OGT cycled at lower rates and reduced in abundance with time. Additionally, the self-renewal ability of OGT-deficient SCs after injury was decreased compared to that of the wild-type SCs. Moreover, *in vivo, in vitro,* and *ex vivo* proliferation assays revealed that SCs lacking OGT were incapable of expanding compared to their wild-type counterparts, a phenotype that may be explained, at least in part, by an HCF1-mediated arrest in the cell cycle. Taken together, our findings suggest that O-GlcNAcylation plays a critical role in the maintenance of SC health and function in normal and injured skeletal muscle.

Key words: UDP-O-GlcNAc, nutrient sensing, muscle stem cells, regenerative myogenesis

Introduction

Adult skeletal muscle contains a population of resident stem cells called satellite cells (SCs) that remain dormant for prolonged periods of time between the basal lamina and sarcolemma of muscle fibers (Katz, 1961; Mauro, 1961; Schultz et al., 1978). Upon activation by various insults, SCs undergo a defined path of lineage progression to form new muscle fibers, a process called muscle regeneration (Moss and Leblond, 1971; Schultz, 1976; Snow, 1978; McCormick and Schultz, 1994). Briefly, SCs are activated by stimuli, such as muscle injury, proliferate to expand in number, and differentiate into multinucleated fibers (Schultz et al., 1978; Snow, 1978; Collins et al., 2005). In the course of adult regenerative myogenesis, a small subpopulation of the activated SCs re-enter into the quiescent status after injury and renew SC pools (Kuang et al., 2007; Day et al., 2010; Lepper et al., 2011; Murphy et al., 2011; Sambasivan et al., 2011).

Over the past half century, we have gained extensive insights into SC behaviors in response to nutrient availability at the cellular level. However, at the molecular level, there remains a gap in our understanding of how external signals dictate SC homeostasis and how SCs interpret, and thus adapt their behaviors to, cues from their microenvironment. It has long been observed that SCs are located in close proximity to blood vessels (Mounier et al., 2011), implying that SCs may rely on the nutrients, hormones, and other factors to maintain their quiescent status or to support their activation and proliferation following muscle injury. For example, high circulating levels of glucose and amino acids have been shown to promote SC lineage progression through the mTOR pathway (Kim and Guan, 2011; Dai et al., 2015). Further, it has been shown that insulin can promote SC proliferation through AKT/mTOR pathway (Han et al., 2008) and enhance SC differentiation through PI3K/AKT (Tureckova et al., 2001) and p38-MAPK pathways (Gonzalez et al., 2004). Intrinsically, it has been shown that a lack of nutrients may activate the AMP kinase

(AMPK) cascade by increasing the AMP/ATP ratio, and a loss of AMPK signaling may impair SC activation, proliferation, self-renewal and muscle regeneration after injury (Hardie et al., 2003; Fu et al., 2016). Together, these findings suggest that SC behaviors can be governed by the external stimuli emanated from its niche microenvironment.

UDP-GlcNAc, a product of the hexosamine biosynthetic pathway (HBP), can integrate carbohydrate, lipid, protein, and nucleotide metabolisms and has been established as a nutrient gauge in a wide range of cells (Love and Hanover, 2005; Butkinaree et al., 2010). In this sense, O-GlcNAc cycling on and off the target proteins by O-GlcNAc transferase (OGT) and O-GlcNAcase (OGA) respectively, can serve as a nutrient sensor for cells to make decisions and adjust their behaviors accordingly (Hanover et al., 2012). O-GlcNAcylation is critical to maintain skeletal muscle metabolic homeostasis. For instance, high levels of O-GlcNAcylation has been linked to insulin resistance; whereas genetic ablation of muscle O-GlcNAcylation protects animals against high fat diet-induced obesity and insulin resistance (McClain et al., 2002; Shi et al., 2018). Further, an increase in O-GlcNAcylation by disrupting OGA expression impairs myogenesis in C2C12 myoblasts *in vitro* (Ogawa et al., 2012) and induces muscle atrophy *in vivo* (Huang et al., 2011). Although these findings highlight the importance of O-GlcNAcylation in muscle and whole-body glucose and metabolic homeostasis, the functional role of this pathway in SCs remains largely unknown. Herein we conditionally ablated OGT, and thus O-GlcNAcylation, in SCs and studied the behavioral changes in SCs. Our findings show that O-GlcNAcylation is required to maintain SC quiescence under normal physiological conditions and is indispensable in adult regenerative myogenesis. These findings suggest that O-GlcNAcylation's role as a nutrient sensing pathway is universal, in that it is critical not only in metabolically active cells such as muscle fibers, but also in quiescent cells such as adult muscle stem cells.

Materials and methods

Mouse Model

Mice were generated and maintained at Virginia Polytechnic Institute and State University and all experiments were approved by the Institution for Animal Use and Care Committee. Conditional SC-specific *Ogt* deletion was accomplished by breeding *Pax7*$^{CreER/+}$; *Ogt*$^{loxP/Y}$ males (Jax Mice strain: B6.Cg-Pax7 $^{tm1(cre/ERT2)Gaka}$ /J) with *Ogt*$^{loxP/loxP}$ females (Jax Mice strain: B6. 129-Ogt$^{tm16wh /J}$) to generate *Pax7*$^{+/+}$; *Ogt*$^{loxP/Y}$ (WT) or *Pax7*$^{CreER/+}$; *Ogt*$^{loxP/Y}$ (cKO) males. Conditional SC-specific *Ogt* deletion in GFP expressing mice (H2B-GFP, JaxMice strain: B6;129S4-Gt(ROSA)26Sor$^{tm1(rtTA*M2)Jae}$ Col1a1$^{tm(tet0-HIST1H2BJ/GFP)Jae}$/J) was achieved by breeding *Pax7*$^{CreER/+}$; *Ogt*$^{loxP/Y}$ males with *Ogt*$^{loxP/loxP}$; ROSA$^{GFP/GFP}$ females to generate *Pax7*$^{+/+}$; *Ogt*$^{loxP/Y}$; *ROSA*$^{GFP/+}$ (WT-GFP) or *Pax7*$^{CreER/+}$; *Ogt*$^{loxP/Y}$; *ROSA*$^{GFP/+}$ (cKO-GFP) males. Mice harboring conditional YFP expressing satellite cells lacking *Ogt* were generated by breeding *Pax7*$^{c/+}$; *Ogt*$^{loxP/Y}$ males with *Ogt*$^{+/+}$; *ROSA*$^{YFP/YFP}$ females to generate *Pax7*$^{CreER/+}$; *Ogt*$^{+/Y}$; *ROSA*$^{YFP/+}$ (WT-YFP), or by breeding *Pax7*$^{c/+}$; *Ogt*$^{loxP/Y}$ males with *Ogt*$^{loxP/loxP}$; *ROSA*$^{YFP/YFP}$ females to generate *Pax7*$^{CreER/+}$; *Ogt*$^{loxP/Y}$; *ROSA*$^{YFP/+}$ (cKO-YFP). Gene deletion was induced by intraperitoneal injection of 10mg of tamoxifen over a consecutive 5d period. All mice were given at least 14 d after injection before experiments were conducted unless otherwise stated.

Muscle Damage and Tissue Collection

All mice were injected with tamoxifen intraperitoneally either 14 d before injury or at the time of injury (time of injection specified in each figure). Mice were anesthetized with isoflurane and 50 μL or 200 μL of 0.1 mg/mL cardiotoxin from *Naja Pallida* (EMD Millipore Sigma, Norwood, OH, USA) was injected into the right tibialis anterior (TA), gastrocnemius (GA), and soleus muscles. The left TA or GA was used as an undamaged control. Mice were given a 7, 10,

or 50 d recovery period after injury. Muscles were then isolated, weighed, and frozen in liquid nitrogen cooled isopentane. Muscles were then transferred to a -80°C freezer and stored until analysis.

Hematoxylin & Eosin Staining

Ten micron thick sections were cut using a cryostat microtome and placed on saline-coated slides. Slides were placed in hematoxylin (Sigma-Aldrich, St. Louis, MO) for 6 min followed by 5 min in running deionized water. Slides were immersed in eosin (Sigma-Aldrich, St. Louis, MO) for 2 sec and rinsed briefly in deionized water. Slides were submerged in 50% ethanol and 70% ethanol for 10 sec each followed by 30 sec in 95% ethanol and 60 sec in 100% ethanol. Slides were rinsed in xylene for 7 sec, dried with a kimwipe (Fisher Scientific, Hudson, NH), and mounted. Images were taken using a Nikon Eclipse 80i (Nikon Instruments Inc., Melville, NY).

Immunohistochemical Staining of SCs

Slides were washed with PBS, fixed with ice-cold 4% formaldehyde for 10 min, washed in PBS, and permeabilized in 0.2% Triton-X-100 (Sigma Aldrich, St. Louis, MO) for 15 min at RT. After an additional PBS wash, sections were blocked with 5% goat serum in PBS containing 0.1% Triton-X-100 for 1 hr followed by overnight 4°C incubation with an anti-Pax7 (1:50 DSHB, Iowa City, IA) primary antibody diluted in blocking buffer. The following day, slides were washed with PBS and incubated in Alexa Fluor 555 goat anti-mouse IgG (1:1000) and DAPI (1 μg/mL) for 1 hr at RT. Slides were washed with PBS, dried with a Kimwipe, and mounted. Images were taken using a Nikon ECLIPSE 8oi fluorescent microscope (Nikon Instruments Inc., Melville, NY).

BrdU Incorporation Assay

Twenty-four hrs after GA damage, bromodeoxyuridine (BrdU; 100mg/kg BW) was injected intraperitoneally. Muscle was collected 18 hrs later, paraffin embedded, and 10 micron thick sections were cut. Sections were deparafinized by submerging in xylene for 3 min twice followed by an additional 3 min incubation in a 1:1 xylene: ethanol solution. Sections were rehydrated by submerging in the following for 3 min each: 100% ethanol twice, 95%, 70%, and 50% ethanol. Slides were rinsed and incubated in 10 mM sodium citrate buffer at 95°C for 30 min and allowed to cool for 20 min. Slides were washed with PBS and treated with 1.5M hydrochloric acid and allowed to sit at RT for 30 min. Slides were washed twice with PBS and blocked with 5% goat serum for 1 hr at RT. Slides were incubated overnight at 4 °C with an anti-BrdU antibody (clone G3G4, DSHB, Iowa City, IA) diluted 1:500 in blocking buffer. The following day, slides were washed with PBS and incubated in blocking buffer containing the secondary antibody Alexa Fluor 555 goat anti-mouse IgG (Life Sciences Technologies, Eugene, OR; 1:1000) and DAPI (1 µg/mL) for 1 hr at RT. Slides were washed with PBS, mounted, and imaged for analysis. The number of BrdU positive nuclei were quantified as a percentage of total nuclei as an indicator of cell proliferation rate.

Single Fiber Isolation and Staining

Gastrocnemius muscles were digested in DMEM (Dulbecco's modified Eagle's medium; high glucose, L-glutamine with 110 mg/mL sodium pyruvate) containing 0.2% collagenase type 1 (Worthington Biochemical Corporation, Lakewood, NJ) for 1 hr at 37°C with 5% CO_2. Muscles were transferred to wash medium (high glucose DMEM containing 1% penicillin/streptomycin) with a large bore pipet coated in horse serum and gently flushed. Fibers were individually transferred with a Pasteur pipet and washed to remove debris. Fibers were either immediately fixed with 4% paraformaldehyde for staining or transferred to 10 mm dishes coated in horse serum

containing culture media (DMEM containing 20% FBS, 1% chicken embryo extract, and 1% penicillin/streptomycin) for 3 days of incubation. Fixed fibers were washed in PBS, permeabilized with 0.1% Triton-X-100 in PBS for 10 min and blocked with 5% goat serum in PBS for 1 hr at RT. Fibers were incubated with anti-Pax7 (1:50 DSHB, Iowa City, IA), anti-OGT (1:200, Abcam, Cambridge, UK), or anti-HCF-1 (1:100, Bethyl Laboratories, Montgomery, TX) antibodies overnight at 4°C. The following day, fibers were washed with PBS and incubated in secondary antibodies (1:1000, Alexa Fluor 488 goat anti-rabbit IgG or Alexa Fluor 555 goat anti-mouse IgG) and counterstained with DAPI (1 μg/ml) for 1 hr at RT. Fibers were washed with PBS, mounted and imaged using a Nikon ECLIPSE 8oi fluorescent microscope or using the Virginia Tech Fralin Imaging Facility's Ziess LSM 800 confocal microscope (ZIESS, Oberkochen, Germany).

Satellite Cell Isolation

Immediately after euthanasia, mice were rinsed briefly in 70% ethanol and muscles from the hind limbs, lower back, and diaphragm were isolated and transferred to sterile PBS. Muscles were washed and excess connective tissue, adipose tissue, blood, and hair were removed. Pooled muscles were then minced with sterile scissors and digested in Ham's F10 medium (Fisher Scientific, Hampton, NH) containing 10% horse serum (Invitrogen, Carlsbad, CA) and collagenase II (500 units per mL; Invitrogen) in a 15 mL centrifuge tube for 90 min at 37°C under agitation. Digests were triturated 20 times using a 10 mL serological pipette and centrifuged at 500 X g for 1 min to pellet down the myofibers. Supernatants were discarded, and pellets were suspended in 10 mL washing buffer (Ham's F10 medium containing 10% HS and 1% penicillin-streptomycin) (pen/strep, Sigma-Aldrich, St. Louis, MO). Pellets were triturated 10 times and allowed to incubate for 1 min to allow the clusters of non-digested fibers containing fibroblasts to fall to the bottom of the tube. Supernatants containing single fiber fragments were then transferred into a

new 15 mL tube and centrifuged. After centrifugation, supernatants were discarded, 10 mL of washing buffer was added, and the pellet was triturated again 10 times and centrifuged. This step was repeated for three times. Fragmented myofibers were then digested in 3 mL of Ham's F-10 containing 10% HS, 0.5 U/mL dispase (Invitrogen), and 38 U/mL collagenase type II (US Biological, Salem, MA) for 30 min at 37°C with agitation. After digestion, 10 mL of wash buffer was added to the digest and satellite cells were liberated from the myofibers by trituration 10 times with a 20-gauge syringe and centrifuged. Supernatants were filtered through 40-μm sterile filters. The flow-through was centrifuged at 800 X g for 5 min to pellet satellite cells. Supernatants were discarded, and cells were suspended in 1 mL of Ham's F-10 containing 20% FBS (Genesee Scientific, San Diego, CA), 1% pen/strep, and 5 ng/mL basic fibroblast growth factor (Thermo Fisher Scientific, Gibco, Gaithersburg, MD). Cells were triturated 10 times to disperse and suspensions were quantified using a hemocytometer. Cells were seeded on collagen-coated 12-well plates at 0.1 x 10^6 cells/well for proliferation assays. Plates were incubated at 5% CO_2 at 37°C.

SC Clonal Assay

SCs were isolated from mice expressing SC-specific yellow fluorescent protein under the *Pax7* promoter and were seeded in growth media (Ham's F-10 containing 20% FBS and 5 ng/mL basic fibroblast growth factor) on collagen-coated 12-well plates at 0.1 x 10^6 cells/well. At the time of seeding, cells were transfected with 1μg of plasmid DNA, 20nM of ON-TARGETplus mouse *Hcfc1* siRNA (Dharmacon, Lafayette, CO), Scrambled Negative Control DsiRNA (Integrated DNA Technologies, Coralville, IA), or *Silencer*™ Cy™3-labeled Negative Control No. 1 siRNA (ThermoFisher Scientific, Waltham, MA) using a LipoJet *in vitro* transfection kit (LifeSct LLC, Rockville, MD). The plasmids pCGN-HCF1-C600 and pCGN-HCF1-WT were

generously provided by Dr. Herr (Capotosti et al., 2011). Eighteen hours after transfection, cells were changed to normal growth media and incubated for 7 d. Cells were fixed with 4% paraformaldehyde and stained with an anti-GFP primary antibody (Cell Signaling Technology, Danvers, MA) and an Alexa Fluor 555 goat anti-rabbit secondary antibody following the previously mentioned protocol. Wells were imaged using a Nikon ECLIPSE 8oi fluorescent microscope and number of SCs per clone were counted.

Flow Cytometry

Pooled red or white muscles were minced and digested in collagenase B and dispase II enzymes (Worthington Biochemical Corporation, Lakewood, NJ) for 1 hr at 37C with agitation. Samples were triturated every 15 min. Digestions were neutralized with FBS and pelleted at 350 x g for 5 min. Digests were stained with CD31-APC, CD45-APC, Sca1-APC, and Vcam-1-biotin. After a brief wash, digests were incubated with a streptavidin-PE-Cy7 conjugated secondary antibody. Prior to analysis, propidium iodide (selection for dead cells) and calcein violet (selection for live cells) were added. Samples were analyzed and sorted using FACSAria I (BD Biosciences, San Jose, CA). Data was analyzed using FlowJo software (FlowJo, LLC, Ashland, OR).

Statistical Analysis

Results are presented as means ± SEM. Comparison between two groups was performed using Student's t test with two-tailed distribution. For multiple-group comparisons, one-way and two-way ANOVAs were used to test for no differences among the group means. All statistical analysis was conducted using JMP Pro (SAS Institute, Cary, NC).

Results

Loss of OGT impairs adult regenerative myogenesis

To understand the functional role of O-GlcNAcylation in SCs, we bred male mice expressing Cre recombinase with *Ogt* floxed females to generate conditional OGT knockout (cKO) mice. Adult mice were administered tamoxifen, an estrogen analog, for five consecutive days to induce the deletion of OGT. Ablation of OGT was confirmed by immunocytochemical staining of SCs on isolated single myofibers (Fig. 4-1A). To evaluate the functional consequences of OGT ablation in SCs, we injected the tibialis anterior (TA) and gastrocnemius (GA) muscles of WT and cKO mice with cardiotoxin to induce muscle injury. Satellite cells from conditional knockout mice exhibited impaired ability to repair muscle damage, as evidenced by a lack of uniform myofiber formation and few embryonic myosin heavy chain (eMyHC) positive fibers in cKO muscles 7d post-injury (Fig. 4-1B). Although the majority of eMyHC positive fibers in cKO muscle had a CSA less than 1,500 μm^2, a small percentage of large eMyHC positive fibers were present in cKO muscle (Fig. 4-1C). Additionally, TA muscle weights were reduced in cKO mice 10d post-injury (Fig. 4-1D). These results suggest OGT is required for SC function during adult muscle regeneration. To investigate whether muscle repair was simply delayed rather than compromised in cKO muscle, we assessed muscle recovery 50d post-injury (Fig. 4-2A). Compared to WT, cKO mice showed a 62 and 63% reduction in gastrocnemius (Fig. 4-2B) and tibialis anterior (Fig. 4-2C) muscle mass, respectively. Consistent with reduced cKO muscle mass, damaged GA and soleus fiber size distribution shifted to the left in cKO mice (Fig. 4-2D,E), which indicates WT mice have larger fibers than cKO mice. Additionally, loss of OGT in SCs led to a 42 and 69% reduction in the SC population within the undamaged GA (Fig. 4-2F) and soleus (Fig. 4-2G) muscles, respectively, suggesting that O-GlcNAc signaling is necessary for maintaining SC

viability *in vivo*. Upon muscle injury, SC content was further reduced to 74 and 75% in the GA (Fig. 4-2F) and soleus (Fig. 4-2G) muscles, respectively. Collectively, these data argue that OGT is critical for the maintenance of SC and tissue health.

OGT ablation-induced muscle regeneration defect is time-sensitive

To investigate whether OGT action during SC regenerative myogenesis is restricted to a certain stage of SC lineage progression, we changed the time window of OGT ablation before injury (Fig. 4-3A). When tamoxifen was injected at the same time as muscle injury, GA and TA muscles of the cKO mice recovered to a weight comparable to that of WT mice (Fig. 4-3B,C). In agreement, fiber size distribution was normal in WT and cKO damaged GA and soleus muscles (Fig. 4-3D,E). Interestingly, after 50 days of recovery, the SC pool was reduced in both undamaged and damaged cKO muscles compared to the WT controls (Fig. 4-3F,G). These results suggest that O-GlcNAcylation is critical in the early stages of SC lineage progression as well as SC self-renewal.

OGT ablation perturbs SC homeostasis in vivo

To gain insight into the role of OGT in SCs under normal physiological conditions, we employed an *in vivo* lineage tracing strategy using H2B-GFP mice. These mice harbor a histone 2B-GFP gene allowing for ubiquitous GFP expression in response to doxycycline feeding (Foudi et al., 2009). The engineered H2B-GFP fusion protein can be retained for up to 72 wks in non-dividing cells (Foudi et al., 2009), making it a unique tool for studying long-term cell kinetics in dormant cell types such as quiescent SCs. We fed H2B-GFP mice doxycycline food for 10 wks (pulse period) to induce GFP expression (Fig. 4-4A). After the pulse period, mice were injected with tamoxifen to ablate OGT and were then switched to normal food without doxycycline (chase

period) (Fig. 4-4A). After a 10.5-wk chase period, we isolated SCs and performed flow cytometric analysis. SCs were identified by the surface markers Vcam1^{+} CD45^{-} CD31^{-} Sca1^{-} and further classified by as either GFP label retaining cells (LRCs) or GFP non-retaining cells (non-LRCs) (Collins et al., 2005; Orford and Scadden, 2008; Chakkalakal et al., 2012). Using this approach, the intensity of GFP served as a proxy for SC cycling properties during the chase period. We showed that cKO SCs from both red and white muscles had a respective 30 and 21% increase in LRCs compared to WT (Fig. 4-4B,C) suggesting that SCs from muscle of cKO mice divided less frequently compared to their WT counterparts. Additionally, cKO SC content was reduced by 70 and 50% compared to the WT population from red and white muscle, respectively (Fig. 4-4D). These data suggest loss of OGT slows SC cycling while dwindling the SC pool, further demonstrating the importance of OGT in SC population maintenance.

OGT ablation reduces SC expansion after activation

To investigate the role of OGT in SC expansion after activation, we performed a BrdU incorporation assay *in vivo* and found that cKO cells have a two-fold reduction in proliferation rate compared to controls (Fig. 4-5A). We then examined SC behaviors in single muscle cell explant cultures, a unique *ex vivo* system in which SCs progress through their lineage within a 3d time frame while still attached to muscle fibers. Although WT SCs rapidly expanded in number, as much as 8-fold within 3 days (Fig. 4-5B), this expansion was lost in cKO SCs, with a mere 2-fold increase in numbers over the same time frame (Fig. 4-5B). This deficiency was evident by day 2 of culture, highlighted by a 50% reduction in BrdU positive cells in cKO explants compared to the WT controls (Fig. 4-5C). Additionally, isolated cKO SCs exhibited a reduction in the number of cells per clone after 7d in culture compared to WT SCs (Fig. 4-5D). To determine if cKO SCs are unable to proliferate due to impaired activation, we quantified the percentage of MyoD/Ki67

positive SCs immediately after isolation and after 3d of single fiber explant culture. Interestingly, cKO explants had a profound increase in $Pax7^{+}$; $MyoDKi67^{+}$ cells immediately after isolation and on D3 of culture (Figure 4-5E), which indicates cKO SCs are hyperactivated. As metabolic state plays a role in SC lineage progression (Moyes et al., 1997; Remels et al., 2010), we also assessed mitochondrial content in SCs immediately after isolation. Indeed, cKO SCs have a greater mitochondrial content (Figure 4-5F), which presumably hinders the ability of cKO SCs to remain and/or re-enter a quiescent state (Rocheteau et al., 2012). Together, these findings show that OGT is required for proper SC activation and proliferation *in vivo*, *ex vivo, and in vitro*.

HCF-1 mediates OGT action in SCs

To explore the molecular mechanisms of OGT action, we examined the interaction between OGT and host-cell factor 1 (HCF1) and its significance in SC division. HCF1 undergoes OGT-mediated proteolytic cleavage and the resulting products, HCF1N (Goto et al., 1997; Julien and Herr, 2003; Tyagi and Herr, 2009) and HCF1C (Julien and Herr, 2004), promote cell cycle progression through the G1 and M phases of the cell cycle, respectively. These cleaved peptides are vital for cell cycle progression in cytokine-producing cells, cancer cells and many other highly proliferative cell types (Goto et al., 1997; Julien and Herr, 2003; Capotosti et al., 2011; Daou et al., 2011; Lazarus et al., 2013). Hence, we speculated that SCs lacking OGT may not cleave HCF1, thereby arresting cell cycle progression and thus cell division/expansion. To test this hypothesis, we first examined whether HCF1 was expressed in SCs. We stained SCs on isolated single fibers with antibodies against HCF1 and Pax7 and found that HCF1 was abundantly expressed in SCs (Fig. 4-6A). We then isolated SCs and used siRNA to knock down HCF1 to examine whether lack of HCF1 can mimic the effect of OGT knockout on SCs. Confirmation of successful plasmid and siRNA transfection was assessed using a fluorescent tagged negative control Cy3 siRNA and GFP

plasmid (Fig. 4-6B). Clonal assay revealed that HCF1 knockdown recapitulated the proliferative defect observed in OGT deficient SCs (Fig. 4-6C). To assess whether the cleaved HCF1 could rescue proliferation in cKO SCs, we introduced plasmids containing the full length HCF1 protein or the mature C-terminal HCF1C subunit (pC600) (Capotosti et al., 2011). Plasmid expression was confirmed with a Western blot to detect HCF1 and Myc-tag expression in C2C12 cell lysates transfected with the HCF1 WT plasmid (Fig. 4-6D). Expression of pC600 increased SC number per clone, partially rescuing the proliferative capacity of cKO SCs (Fig. 4-6E). In contrast, the HCF1 WT plasmid ($pWT_{HCF\text{-}1}$) containing the full length, immature HCF1 protein had no effect (Fig. 4-6E), highlighting the importance of HCF1 cleavage and maturation in SC division. Partial rescue of SC proliferation by the C-terminal HCF1 may reflect the fact that SCs need both C- and N-terminal to cycle properly. However, in this case, we could not introduce the HCF1N subunit because it will not be properly O-GlcNAcylated, and thus not functional, in OGT deficient SCs (Capotosti et al., 2011).

In summary, these data suggest that OGT, and thus O-GlcNAcylation, is important for SC function in both quiescent and activated statuses. Loss of OGT disrupts SC viability and function, thereby compromising its ability to repair adult muscle after injury.

Discussion

O-GlcNAcylation is regarded as a nutrient sensing pathway in a wide range of cellular processes in normal physiology as well as diseased circumstances (Butkinaree et al., 2010; Hanover et al., 2012). Using a genetic approach, we show that O-GlcNAcylation plays an essential role in SC maintenance and function. There are several lines of evidence that support our conjecture. First, SCs lacking OGT have compromised ability to regenerate muscles after injury. Second, our *in vivo* lineage tracing studies showed that a lack of OGT reduces SC content and activity (replication) in both red and white muscles. Third, OGT knockout reduces the capacity of SCs to self-renew. Lastly, the proliferative capacity of SCs is greatly reduced *in vivo*, *ex vivo*, and *in vitro* in the absence of OGT.

Adult stem cells are quiescent in nature, with minimal transcriptional and metabolic activities (Schultz et al., 1978). Nonetheless, recent studies show that these cells are metabolically "active" during quiescence (Cheung and Rando, 2013; Takubo et al., 2013), and metabolic state is a key regulator of SC behavior. For example, Rocheteau et al. reported a subpopulation of $Pax7^{hi}$ SCs that have a low mitochondrial content, are less primed for myogenic commitment, and have delayed rates of mitosis compared to the $Pax7^{lo}$ population with greater mitochondrial content. As OGT acts as a cellular nutrient gauge, it is a reasonable assumption that SCs may use OGT as one of the mechanisms to sense environmental nutrient availability and translate these nutritional signals into a metabolic response to dictate SC behavior. As shown in our lineage tracing data, when SCs lack OGT they cycle slower compared to their WT counterparts. This may be a result of greater mitochondrial content in cKO SCs, as an increase in glycolytic flux is necessary to support proliferation (Ryall et al., 2015). For example, many critical glycolytic enzymes in cancer cells including pyruvate kinase (Wang et al., 2017), glucose-6-phosphate dehydrogenase (Rao et

al., 2015), and phosphofructokinase 1 (Yi et al., 2012) are all O-GlcNAcylated. Because adult stem cells adopt a glycolytic paradigm, it is reasonable to believe that OGT-mediated O-GlcNAcylation of key glycolytic enzymes may play an essential role in maintaining stem cell metabolic homeostasis. Interestingly, OGT represses gene transcription through EZH2-mediated histone 3 trimethylation (Chu et al., 2014), a process adopted by cells to "shut down" selectively the expression of a wide range of "unnecessary" genes to maintain certain status. Given the critical role of OGT in glycolysis and epigenetic regulation, it is not surprising to observe that knockout of OGT, and thus O-GlcNAcylation, dramatically perturbs SC quiescence and cycling properties *in vivo*.

In addition to its function in SC quiescence, OGT is also required for SC activation and proliferation during chemical-induced muscle regeneration. It is reasonable to speculate that when SCs sense a lack of nutrients from its microenvironment through OGT-mediated O-GlcNAcylation, they not to divide and/or proliferate, as demonstrated by a lack of BrdU incorporation *in vivo*, reduced clonal size *in vitro*, and decreased SC number in single fiber explants *ex vivo*. It is also possible the reduction in SC number is a result of cKO SCs undergoing apoptosis after an arrest in the cell cycle without OGT-mediated HCF-1 maturation. At the molecular level, OGT has more than 1,000 substrates (Hanover et al., 2012) across a wide range of cell types. Hence, we speculate that SCs may utilize O-GlcNAcylation as a nutrient sensing mechanism to drive DNA replication, protein synthesis, and mitosis. Specifically, we hypothesize that OGT drives SC cell cycle progression through O-GlcNAcylating and cleaving HCF-1, among other mechanisms. As evidence, our results show that lack of HCF-1 can recapitulate the phenotype of OGT deficiency. Furthermore, forced expression of a C-terminal HCF-1 partially rescues the OGT knockout effect. These data suggest that once activated, SCs, like many other

cell types, employ O-GlcNAcylation as a sensing mechanism to adapt to nutrient availability and decide whether or not to proceed through the cell cycle.

Self-renewal is requisite for quiescent adult muscle stem cells but may occur differently under normal physiological conditions than those situations requiring regenerative myogenesis (Conboy and Rando, 2002). Kuang et al. showed that SCs lacking the myogenic regulator Myf5 give rise to both Myf5 negative and positive subpopulations in normal adult muscle. Based on these observations, this group proposed that Myf5 negative SCs represent a progenitor population of muscle stem cells while the Myf5 positive SCs are a more downstream lineage progression phenotype (Kuang et al., 2007). Further, Rocheteau et al. classified SCs normal adult muscle into high- and low-Pax7 expression subpopulations and discovered that the former was not primed for commitment, strongly suggesting a divergent population of SCs in normal adult muscle. Finally, Rando's group proposed that SCs self-renew through asymmetric division where the immortal DNA template is preferentially segregated to renewed, quiescent SCs (Rando, 2006, 2007). In contrast, stem cell self-renewal during adult regenerative myogenesis occurs through an obligatory lineage progression trajectory (Ono et al., 2012). In this case, SCs first become activated, then withdraw from the cell cycle and revert back to an original quiescent status. In our study, we found that cKO SCs were hyperactivated and had a greater mitochondrial content, which may prevent proper self-renewal and contribute to the reduced SC pool in mice lacking OGT under normal physiological conditions. After muscle injury, SCs number was further reduced in OGT deficient mice compared to wild-type, and this deficiency was accompanied by a reduction in muscle mass indicative of a failed muscle regeneration. Further, when we injected cardiotoxin (to induce injury) and tamoxifen (to induce *Ogt* knockout) at the same time, muscle mass of the knockout mice was comparable to that of the wild-type mice even though SC number in fully recovered KO muscle

was still decreased compared to that of wild-type mice. These data provide strong evidence that OGT is indispensable for proper SC self-renewal in regenerative myogenesis.

In conclusion, our studies are the first to reveal the critical role of O-GlcNAcylation, a post-translational modification, in SC function and maintenance. These findings may apply to other adult stem cells since these cells share similar characteristics such as quiescence, having the ability to differentiate, and self-renewal. Further analysis of this pathway in other stem cell type may help find new avenues to improve adult stem cell longevity and its ability to repair the injured tissues.

Acknowledgements

The authors wish to thank Ashley Geiger, Jennifer Cobb, Kelly Ramos, Taylor Fisher, Nicole Paris, Hannah Geisler, Jing Luo, and Zhengzing Shen for their contributions to the study.

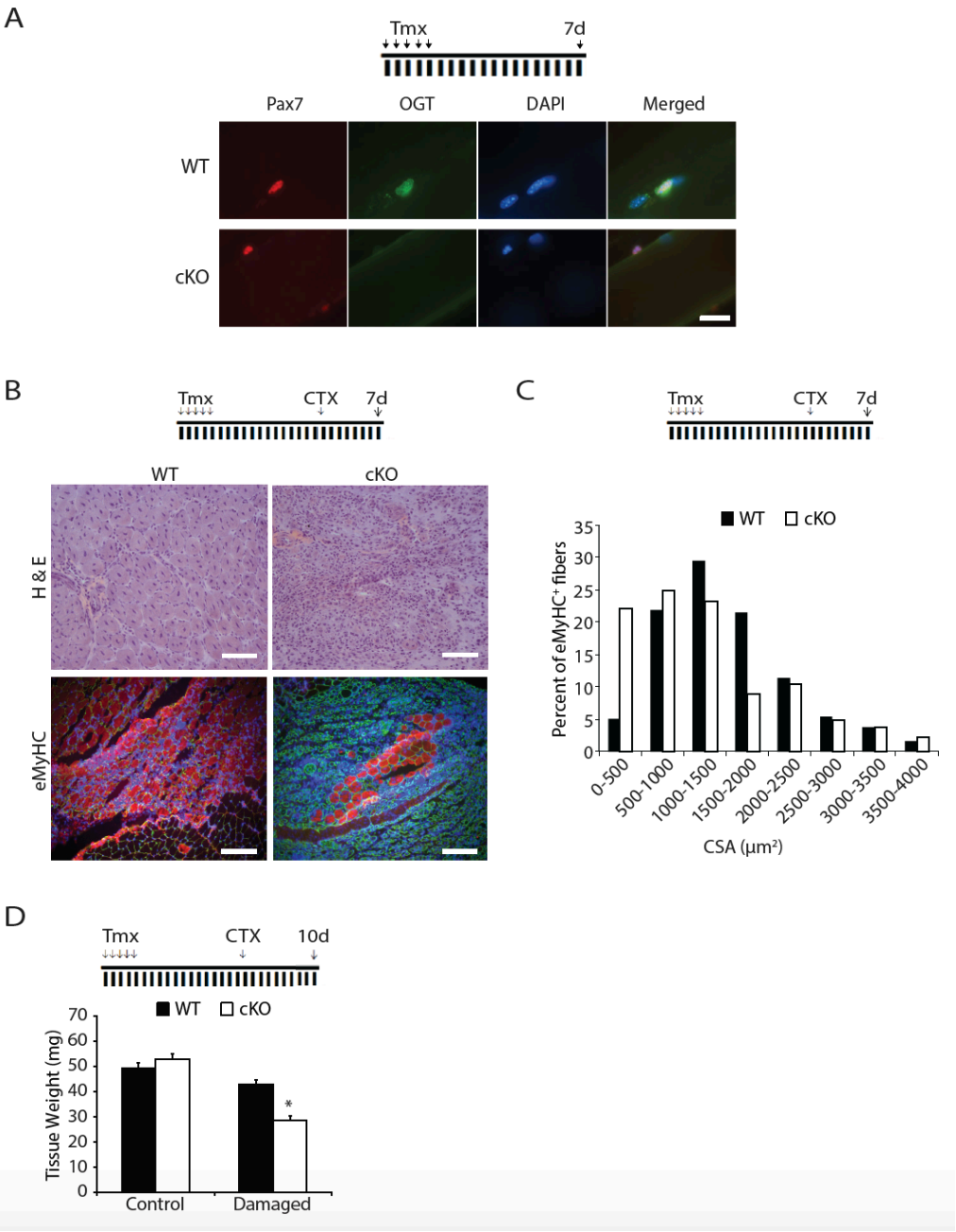

Figure 4-1. Ablation of OGT impairs muscle regeneration. **(A)** Single myofibers stained with Pax7 and OGT specific antibodies, counterstained with DAPI. Scale bar = 20µm. **(B)** Representative H&E stained (top) and eMyHC (red), laminin (green), and DAPI (blue) stained (bottom) GA muscles 7d after CTX injury. Scale bar = 100µm. **(C)** Histogram of GA muscle fiber sizes from eMyHC positive fibers 7d after CTX injury. **(D)** TA muscle weights 10d after CTX injury. Values represent means ± SEM. n=4. * $P < 0.05$ when compared to WT. Abbreviations: TMX = tamoxifen; CTX = cardiotoxin; TA = tibialis anterior GA = gastrocnemius; eMyHC= embryonic myosin heavy chain.

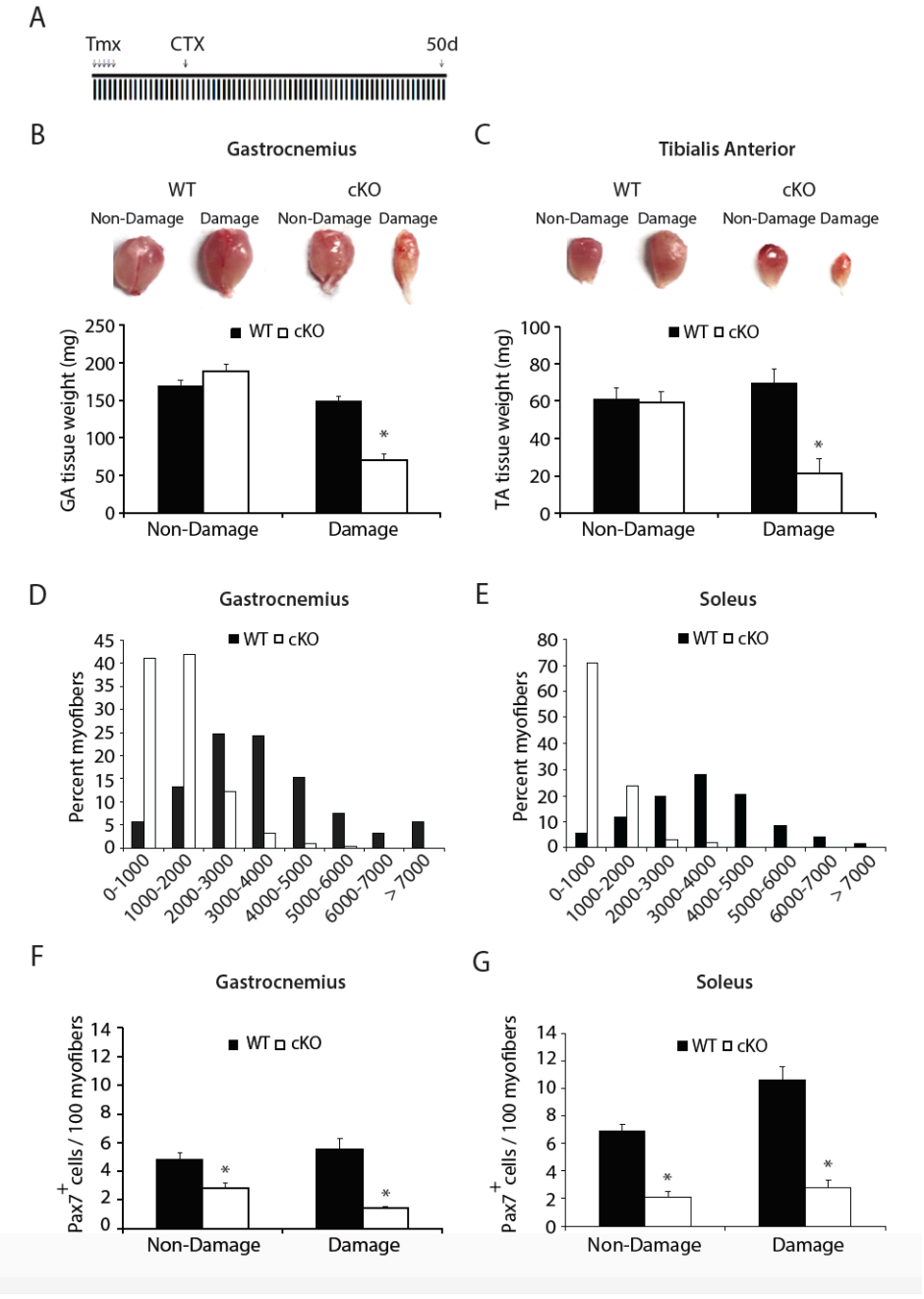

Figure 4-2. OGT is critical for maintenance of muscle mass and SC number in adult regenerative myogenesis. (A) Experimental scheme B-E: muscle was damaged 2-wks after TMX injection followed by a 50d recovery period. Cardiotoxin was injected into the right tibialis anterior, gastrocnemius, and soleus muscles. Non-damaged control muscles were collected from the left leg. **(B-C)** Representative images and tissue weights of non-damaged (control) and damaged gastrocnemius (B) and tibialis anterior (C) muscles. **(D-E)** Histogram of muscle fiber sizes from damaged (D) gastrocnemius and (E) soleus muscles. **(F-G)** Quantification of Pax7 positive cells in non-damaged (control) and damaged gastrocnemius (F) and soleus (G) muscles. Values represent means ± SEM. n=4. * $P < 0.05$ when compared to WT.

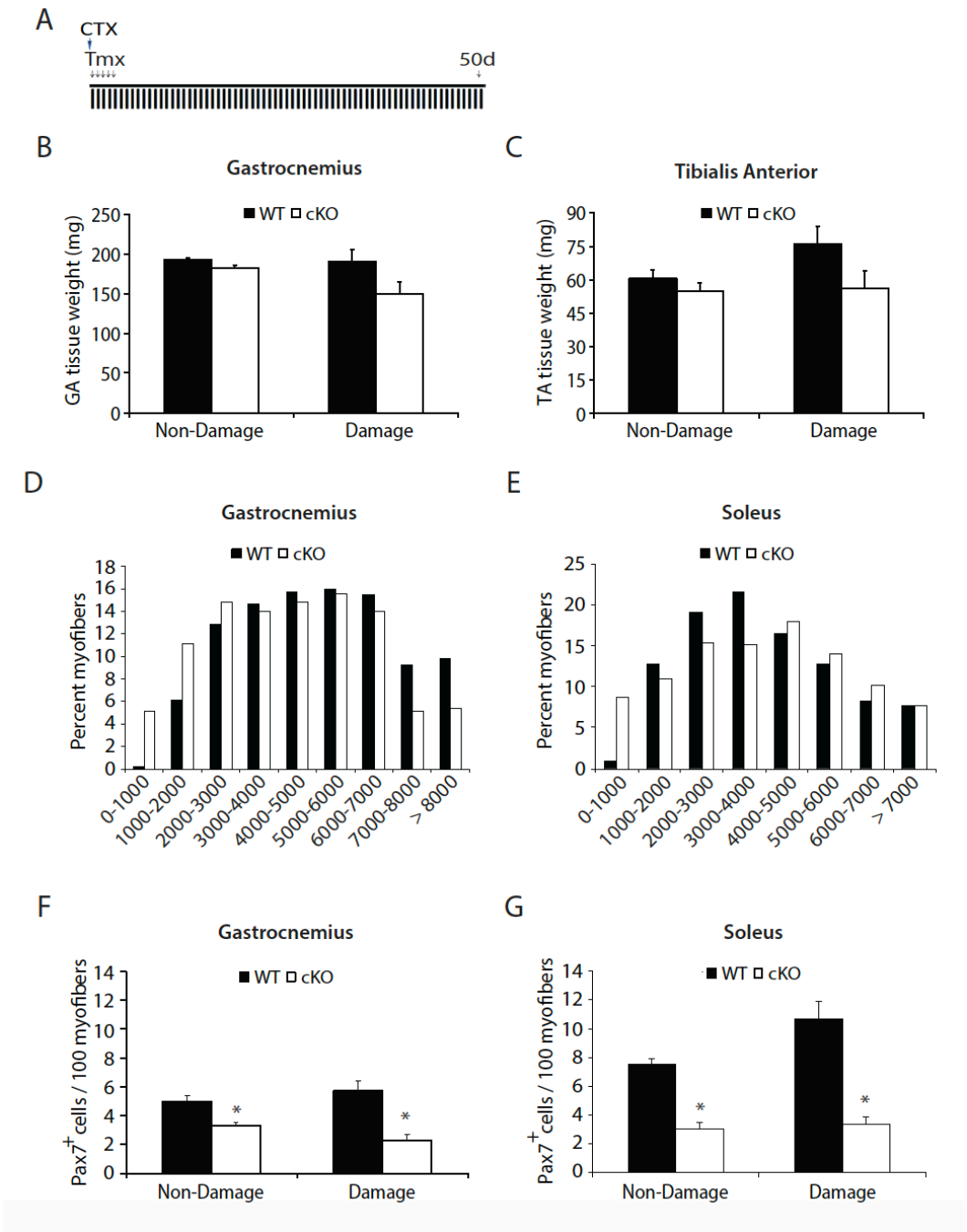

Figure 4-3. Timing is critical for OGT action in muscle regeneration. (A) Experimental scheme B-E: TMX was injected on the same day as muscle injury followed by a 50d recovery period. Cardiotoxin was injected into the right tibialis anterior, gastrocnemius, and soleus muscles. Non-damaged control muscles were collected from the left leg. **(B-C)** Tissue weights of non-damaged (control) and damaged gastrocnemius (B) and tibialis anterior (C) muscles. **(D-E)** Quantification of Pax7 positive cells in non-damaged (control) and damaged gastrocnemius (D) and soleus (E) muscles. **(F-G)** Histogram of muscle fiber sizes from damaged (F) gastrocnemius and (G) soleus muscles. Values represent means ± SEM. n=4. * $P < 0.05$ when compared to WT.

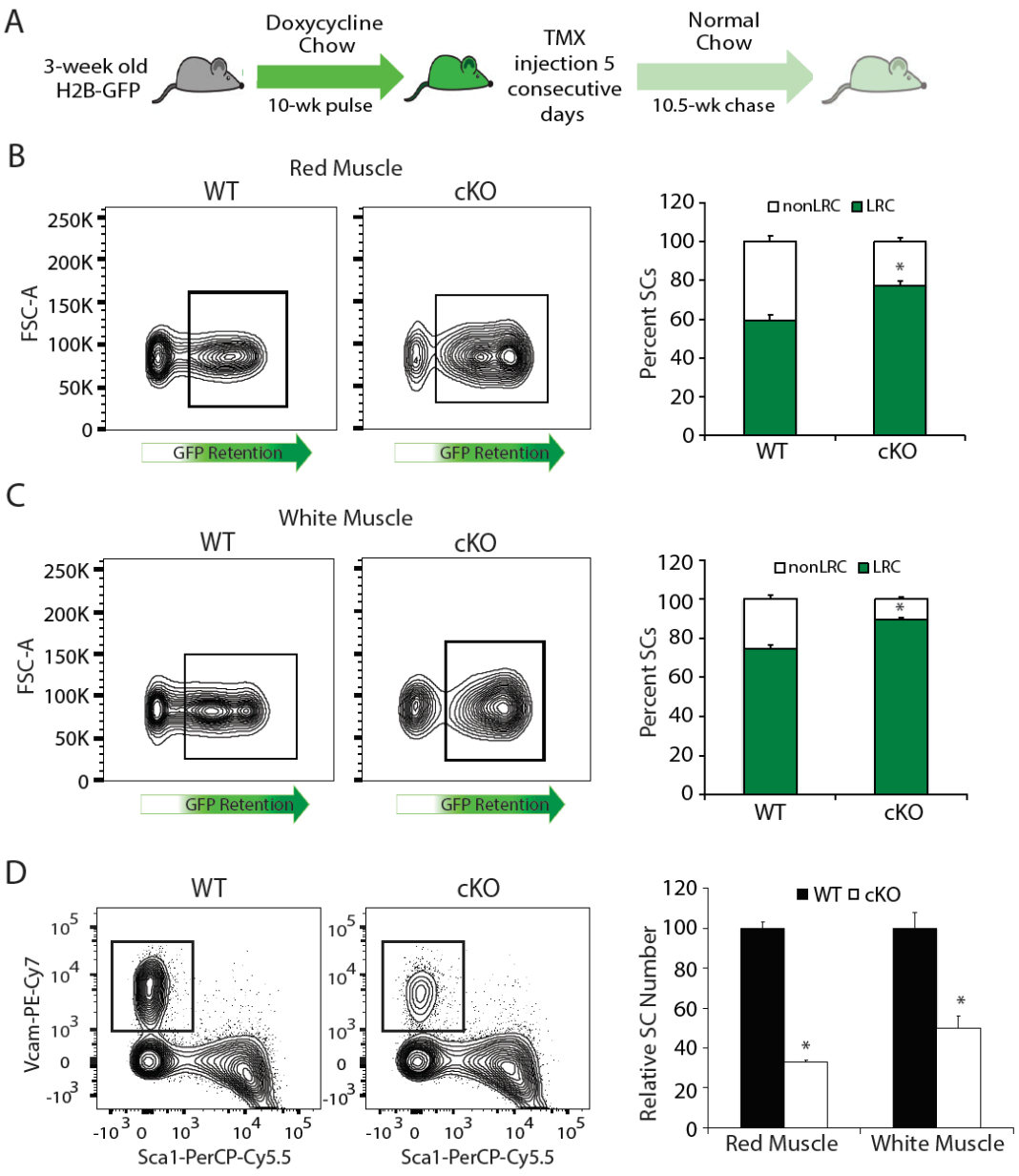

Figure 4-4. O-GlcNAc signaling is necessary for SC cycling and self-renewal. **(A)** Scheme of experimental design B-D: 3-wk old mice were fed doxycycline chow for 10-wks (pulse) followed by 5 days of TMX injections and switched to a normal chow diet (chase). **(B, C)** Representative contour plots and quantification of GFP retention in SCs isolated from red (B) and white (C) muscles after the 10.5-wk chase. **(D)** Representative contour plots of SC populations isolated from red muscle and relative abundance of SCs isolated from red and white muscles after the 10.5-wk chase. SCs were identified by markers Vcam1^{+}; Sca1^{-}; CD45^{-}; CD31^{-}. Values are means ± SEM. n=4. *$P < 0.05$ when compared to WT.

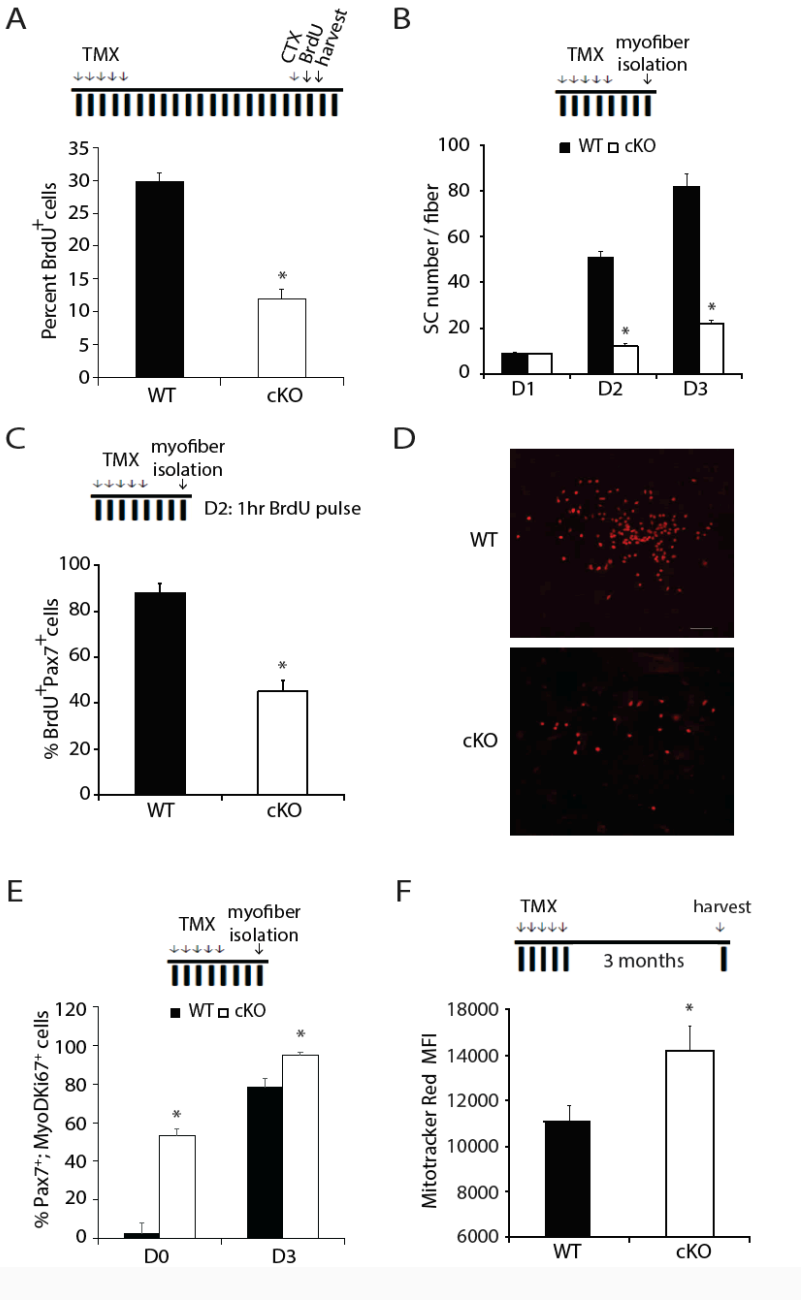

Figure 4-5. OGT is required for proper proliferation. (A) BrdU incorporation *in vivo*. **(B)** SC number per fiber on D1, D2, and D3 of culture. Myofibers were isolated for culture 3d after final TMX injection. **(C)** Quantification of BrdU positive cells on single myofibers after 2d of culture. **(D)** Representative image of SC clones after 7d culture. **(E)** Percentage of $Pax7^{+}$; $MyoDKi67^{+}$ cells immediately after SC isolation and 3d of single fiber explant culture. **(F)** Mean fluorescent intensity of Mitotracker Red immediately after SC isolation. SCs were identified by markers $Vcam1^{+}$; $Sca1^{-}$; $CD45^{-}$; $CD31^{-}$. Values represent means ± SEM. n=4. * $P < 0.05$ when compared to WT.

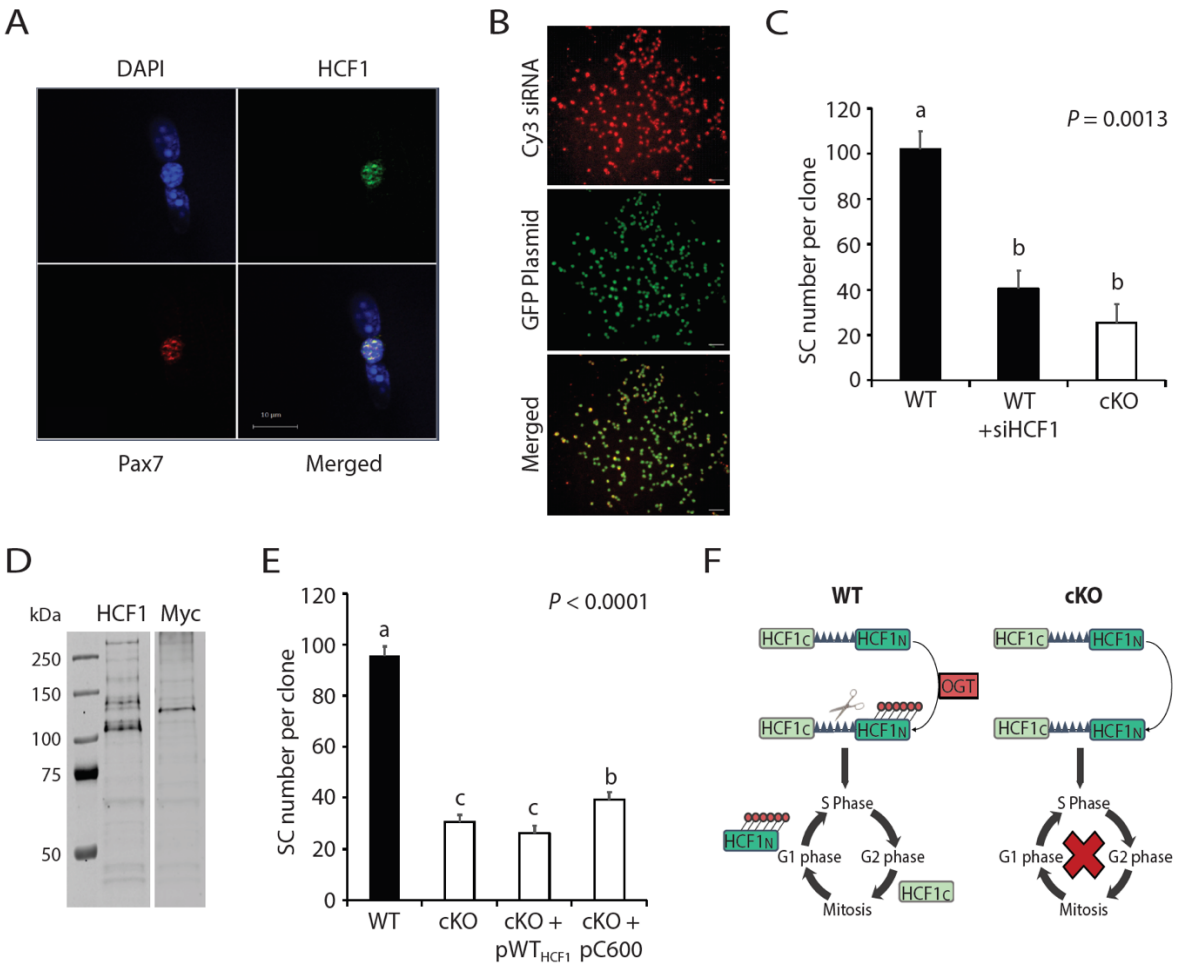

Figure 4-6. HCF-1 presumably mediates OGT action in SCs. (A) Immunocytochemical staining of HCF-1 in SCs on single myofibers. **(B)** Representative images of SCs transfected with Cy3 siRNA and GFP plasmid. **(C)** Clonal analysis of isolated SCs from WT (black bars) with or without HCF-1 knockdown and cKO (white bars) mice. **(D)** Western blot detecting HCF-1 (left) and Myc-tag (right) in C2C12 myoblast overexpressing pWT$_{HCF-1}$. **(E)** Clonal analysis of SCs treated with plasmids to overexpress the full length, immature HCF1 protein or the mature HCF1 C subunit. **(F)** Hypothetical model for OGT action in SCs. Experiments were conducted in technical triplicates using SCs isolated from 4 mice from each genotype. Values represent means ± SEM. $^{a\text{-}c}$Means lacking a common letter differ significantly. Abbreviations = siHCF-1: siRNA targeting HCF-1; pWT$_{HCF-1}$: plasmid to overexpress the full length, immature form of HCF-1; pC600: plasmid to overexpress the cleaved HCF1C subunit.

References

Butkinaree, C., K. Park, and G. W. Hart. 2010. O-linked beta-N-acetylglucosamine (O-GlcNAc): Extensive crosstalk with phosphorylation to regulate signaling and transcription in response to nutrients and stress. Biochim Biophys Acta 1800(2):96-106. doi: 10.1016/j.bbagen.2009.07.018

Capotosti, F., S. Guernier, F. Lammers, P. Waridel, Y. Cai, J. Jin, J. W. Conaway, R. C. Conaway, and W. Herr. 2011. O-GlcNAc transferase catalyzes site-specific proteolysis of HCF-1. Cell 144(3):376-388. doi: 10.1016/j.cell.2010.12.030

Chakkalakal, J. V., K. M. Jones, M. A. Basson, and A. S. Brack. 2012. The aged niche disrupts muscle stem cell quiescence. Nature 490(7420):355-360. doi: 10.1038/nature11438

Cheung, T. H., and T. A. Rando. 2013. Molecular regulation of stem cell quiescence. Nat Rev Mol Cell Biol 14(6):329-340. doi: 10.1038/nrm3591

Chu, C. S., P. W. Lo, Y. H. Yeh, P. H. Hsu, S. H. Peng, Y. C. Teng, M. L. Kang, C. H. Wong, and L. J. Juan. 2014. O-GlcNAcylation regulates EZH2 protein stability and function. Proc Natl Acad Sci U S A 111(4):1355-1360. doi: 10.1073/pnas.1323226111

Collins, C. A., I. Olsen, P. S. Zammit, L. Heslop, A. Petrie, T. A. Partridge, and J. E. Morgan. 2005. Stem cell function, self-renewal, and behavioral heterogeneity of cells from the adult muscle satellite cell niche. Cell 122(2):289-301. doi: 10.1016/j.cell.2005.05.010

Conboy, I. M., and T. A. Rando. 2002. The regulation of Notch signaling controls satellite cell activation and cell fate determination in postnatal myogenesis. Dev Cell 3(3):397-409.

Dai, J. M., M. X. Yu, Z. Y. Shen, C. Y. Guo, S. Q. Zhuang, and X. S. Qiu. 2015. Leucine Promotes Proliferation and Differentiation of Primary Preterm Rat Satellite Cells in Part through mTORC1 Signaling Pathway. Nutrients 7(5):3387-3400. doi: 10.3390/nu7053387

Daou, S., N. Mashtalir, I. Hammond-Martel, H. Pak, H. Yu, G. Sui, J. L. Vogel, T. M. Kristie, and B. Affar el. 2011. Crosstalk between O-GlcNAcylation and proteolytic cleavage regulates the host cell factor-1 maturation pathway. Proc Natl Acad Sci U S A 108(7):2747-2752. doi: 10.1073/pnas.1013822108

Day, K., G. Shefer, A. Shearer, and Z. Yablonka-Reuveni. 2010. The depletion of skeletal muscle satellite cells with age is concomitant with reduced capacity of single progenitors to produce reserve progeny. Dev Biol 340(2):330-343. doi: 10.1016/j.ydbio.2010.01.006

Foudi, A., K. Hochedlinger, D. Van Buren, J. W. Schindler, R. Jaenisch, V. Carey, and H. Hock. 2009. Analysis of histone 2B-GFP retention reveals slowly cycling hematopoietic stem cells. Nat Biotechnol 27(1):84-90. doi: 10.1038/nbt.1517

Fu, X., M. Zhu, S. Zhang, M. Foretz, B. Viollet, and M. Du. 2016. Obesity Impairs Skeletal Muscle Regeneration Through Inhibition of AMPK. Diabetes 65(1):188-200. doi: 10.2337/db15-0647

Gonzalez, I., G. Tripathi, E. J. Carter, L. J. Cobb, D. A. Salih, F. A. Lovett, C. Holding, and J. M. Pell. 2004. Akt2, a novel functional link between p38 mitogen-activated protein kinase and phosphatidylinositol 3-kinase pathways in myogenesis. Mol Cell Biol 24(9):3607-3622.

Goto, H., S. Motomura, A. C. Wilson, R. N. Freiman, Y. Nakabeppu, K. Fukushima, M. Fujishima, W. Herr, and T. Nishimoto. 1997. A single-point mutation in HCF causes temperature-sensitive cell-cycle arrest and disrupts VP16 function. Genes Dev 11(6):726-737.

Han, B., J. Tong, M. J. Zhu, C. Ma, and M. Du. 2008. Insulin-like growth factor-1 (IGF-1) and leucine activate pig myogenic satellite cells through mammalian target of rapamycin (mTOR) pathway. Mol Reprod Dev 75(5):810-817. doi: 10.1002/mrd.20832

Hanover, J. A., M. W. Krause, and D. C. Love. 2012. Bittersweet memories: linking metabolism to epigenetics through O-GlcNAcylation. Nat Rev Mol Cell Biol 13(5):312-321. doi: 10.1038/nrm3334

Hardie, D. G., J. W. Scott, D. A. Pan, and E. R. Hudson. 2003. Management of cellular energy by the AMP-activated protein kinase system. FEBS Lett 546(1):113-120.

Huang, P., S. R. Ho, K. Wang, B. C. Roessler, F. Zhang, Y. Hu, D. B. Bowe, J. E. Kudlow, and A. J. Paterson. 2011. Muscle-specific overexpression of NCOATGK, splice variant of O-GlcNAcase, induces skeletal muscle atrophy. Am J Physiol Cell Physiol 300(3):C456-465. doi: 10.1152/ajpcell.00124.2010

Julien, E., and W. Herr. 2003. Proteolytic processing is necessary to separate and ensure proper cell growth and cytokinesis functions of HCF-1. EMBO J 22(10):2360-2369. doi: 10.1093/emboj/cdg242

Julien, E., and W. Herr. 2004. A switch in mitotic histone H4 lysine 20 methylation status is linked to M phase defects upon loss of HCF-1. Mol Cell 14(6):713-725. doi: 10.1016/j.molcel.2004.06.008

Katz, B. 1961. Terminations of Afferent Nerve Fibre in Muscle Spindle of Frog. Philos T Roy Soc B 243(703):221-240. doi: DOI 10.1098/rstb.1961.0001

Kim, J., and K. L. Guan. 2011. Amino acid signaling in TOR activation. Annu Rev Biochem 80:1001-1032. doi: 10.1146/annurev-biochem-062209-094414

Kuang, S., K. Kuroda, F. Le Grand, and M. A. Rudnicki. 2007. Asymmetric self-renewal and commitment of satellite stem cells in muscle. Cell 129(5):999-1010. doi: 10.1016/j.cell.2007.03.044

Lazarus, M. B., J. Jiang, V. Kapuria, T. Bhuiyan, J. Janetzko, W. F. Zandberg, D. J. Vocadlo, W. Herr, and S. Walker. 2013. HCF-1 is cleaved in the active site of O-GlcNAc transferase. Science 342(6163):1235-1239. doi: 10.1126/science.1243990

Lepper, C., T. A. Partridge, and C. M. Fan. 2011. An absolute requirement for Pax7-positive satellite cells in acute injury-induced skeletal muscle regeneration. Development 138(17):3639-3646. doi: 10.1242/dev.067595

Love, D. C., and J. A. Hanover. 2005. The hexosamine signaling pathway: deciphering the "O-GlcNAc code". Sci STKE 2005(312):re13. doi: 10.1126/stke.3122005re13

Mauro, A. 1961. Satellite cell of skeletal muscle fibers. J Biophys Biochem Cytol 9:493-495.

McClain, D. A., W. A. Lubas, R. C. Cooksey, M. Hazel, G. J. Parker, D. C. Love, and J. A. Hanover. 2002. Altered glycan-dependent signaling induces insulin resistance and hyperleptinemia. Proc Natl Acad Sci U S A 99(16):10695-10699. doi: 10.1073/pnas.152346899

McCormick, K. M., and E. Schultz. 1994. Role of satellite cells in altering myosin expression during avian skeletal muscle hypertrophy. Dev Dyn 199(1):52-63. doi: 10.1002/aja.1001990106

Moss, F. P., and C. P. Leblond. 1971. Satellite cells as the source of nuclei in muscles of growing rats. Anat. Record 170(4):421-435. doi: 10.1002/ar.1091700405

Mounier, R., F. Chretien, and B. Chazaud. 2011. Blood vessels and the satellite cell niche. Curr Top Dev Biol 96:121-138. doi: 10.1016/B978-0-12-385940-2.00005-X

Moyes, C. D., O. A. Mathieu-Costello, N. Tsuchiya, C. Filburn, and R. G. Hansford. 1997. Mitochondrial biogenesis during cellular differentiation. Am J Physiol 272(4 Pt 1):C1345-1351. doi: 10.1152/ajpcell.1997.272.4.C1345

Murphy, M. M., J. A. Lawson, S. J. Mathew, D. A. Hutcheson, and G. Kardon. 2011. Satellite cells, connective tissue fibroblasts and their interactions are crucial for muscle regeneration. Development 138(17):3625-3637. doi: 10.1242/dev.064162

Ogawa, M., H. Mizofuchi, Y. Kobayashi, G. Tsuzuki, M. Yamamoto, S. Wada, and K. Kamemura. 2012. Terminal differentiation program of skeletal myogenesis is negatively regulated by O-GlcNAc glycosylation. Biochim Biophys Acta 1820(1):24-32. doi: 10.1016/j.bbagen.2011.10.011

Ono, Y., S. Masuda, H. S. Nam, R. Benezra, Y. Miyagoe-Suzuki, and S. Takeda. 2012. Slow-dividing satellite cells retain long-term self-renewal ability in adult muscle. J Cell Sci 125(Pt 5):1309-1317. doi: 10.1242/jcs.096198

Orford, K. W., and D. T. Scadden. 2008. Deconstructing stem cell self-renewal: genetic insights into cell-cycle regulation. Nat Rev Genet 9(2):115-128. doi: 10.1038/nrg2269

Rando, T. A. 2006. Stem cells, ageing and the quest for immortality. Nature 441(7097):1080-1086. doi: 10.1038/nature04958

Rando, T. A. 2007. The immortal strand hypothesis: segregation and reconstruction. Cell 129(7):1239-1243. doi: 10.1016/j.cell.2007.06.019

Rao, X., X. Duan, W. Mao, X. Li, Z. Li, Q. Li, Z. Zheng, H. Xu, M. Chen, P. G. Wang, Y. Wang, B. Shen, and W. Yi. 2015. O-GlcNAcylation of G6PD promotes the pentose phosphate pathway and tumor growth. Nat Commun 6:8468. doi: 10.1038/ncomms9468

Remels, A. H., R. C. Langen, P. Schrauwen, G. Schaart, A. M. Schols, and H. R. Gosker. 2010. Regulation of mitochondrial biogenesis during myogenesis. Mol Cell Endocrinol 315(1-2):113-120. doi: 10.1016/j.mce.2009.09.029

Rocheteau, P., B. Gayraud-Morel, I. Siegl-Cachedenier, M. A. Blasco, and S. Tajbakhsh. 2012. A subpopulation of adult skeletal muscle stem cells retains all template DNA strands after cell division. Cell 148(1-2):112-125. doi: 10.1016/j.cell.2011.11.049

Ryall, J. G., S. Dell'Orso, A. Derfoul, A. Juan, H. Zare, X. Feng, D. Clermont, M. Koulnis, G. Gutierrez-Cruz, M. Fulco, and V. Sartorelli. 2015. The NAD(+)-dependent SIRT1 deacetylase translates a metabolic switch into regulatory epigenetics in skeletal muscle stem cells. Cell Stem Cell 16(2):171-183. doi: 10.1016/j.stem.2014.12.004

Sambasivan, R., R. Yao, A. Kissenpfennig, L. Van Wittenberghe, A. Paldi, B. Gayraud-Morel, H. Guenou, B. Malissen, S. Tajbakhsh, and A. Galy. 2011. Pax7-expressing satellite cells are indispensable for adult skeletal muscle regeneration. Development 138(17):3647-3656. doi: 10.1242/dev.067587

Schultz, E. 1976. Fine structure of satellite cells in growing skeletal muscle. Am J Anat 147(1):49-70. doi: 10.1002/aja.1001470105

Schultz, E., M. C. Gibson, and T. Champion. 1978. Satellite cells are mitotically quiescent in mature mouse muscle: an EM and radioautographic study. J Exp Zool 206(3):451-456. doi: 10.1002/jez.1402060314

Shi, H., A. Munk, T. S. Nielsen, M. R. Daughtry, L. Larsson, S. Li, K. F. Hoyer, H. W. Geisler, K. Sulek, R. Kjobsted, T. Fisher, M. M. Andersen, Z. Shen, U. K. Hansen, E. M. England, Z. Cheng, K. Hojlund, J. F. P. Wojtaszewski, X. Yang, M. W. Hulver, R. F. Helm, J. T. Treebak, and D. E. Gerrard. 2018. Skeletal muscle O-GlcNAc transferase is important for muscle energy homeostasis and whole-body insulin sensitivity. Mol Metab 11:160-177. doi: 10.1016/j.molmet.2018.02.010

Snow, M. H. 1978. An autoradiographic study of satellite cell differentiation into regenerating myotubes following transplantation of muscles in young rats. Cell Tissue Res 186(3):535-540.

Takubo, K., G. Nagamatsu, C. I. Kobayashi, A. Nakamura-Ishizu, H. Kobayashi, E. Ikeda, N. Goda, Y. Rahimi, R. S. Johnson, T. Soga, A. Hirao, M. Suematsu, and T. Suda. 2013. Regulation of glycolysis by Pdk functions as a metabolic checkpoint for cell cycle quiescence in hematopoietic stem cells. Cell Stem Cell 12(1):49-61. doi: 10.1016/j.stem.2012.10.011

Tureckova, J., E. M. Wilson, J. L. Cappalonga, and P. Rotwein. 2001. Insulin-like growth factor-mediated muscle differentiation: collaboration between phosphatidylinositol 3-kinase-Akt-signaling pathways and myogenin. J Biol Chem 276(42):39264-39270. doi: 10.1074/jbc.M104991200

Tyagi, S., and W. Herr. 2009. E2F1 mediates DNA damage and apoptosis through HCF-1 and the MLL family of histone methyltransferases. EMBO J 28(20):3185-3195. doi: 10.1038/emboj.2009.258

Wang, Y., J. Liu, X. Jin, D. Zhang, D. Li, F. Hao, Y. Feng, S. Gu, F. Meng, M. Tian, Y. Zheng, L. Xin, X. Zhang, X. Han, L. Aravind, and M. Wei. 2017. O-GlcNAcylation destabilizes the active tetrameric PKM2 to promote the Warburg effect. Proc Natl Acad Sci U S A 114(52):13732-13737. doi: 10.1073/pnas.1704145115

Yi, W., P. M. Clark, D. E. Mason, M. C. Keenan, C. Hill, W. A. Goddard, 3rd, E. C. Peters, E. M. Driggers, and L. C. Hsieh-Wilson. 2012. Phosphofructokinase 1 glycosylation regulates cell growth and metabolism. Science 337(6097):975-980. doi: 10.1126/science.1222278

Chapter 5. Mitochondrial ATP production is dispensable in IGF-1 stimulated myogenesis

Abstract

Insulin-like growth factor 1 (IGF-1) is a potent stimulator of myogenesis. Recent findings suggest mitochondria play an essential role in IGF-1 mediated myogenesis, yet the underlying mechanism remains largely unknown. We hypothesized OxPhos-dependent and -independent functions of mitochondria play different roles in the IGF-1 myogenic program. To this end, we disrupted mitochondrial ATP production (OxPhos) by knocking out *ATP synthase F1 β-subunit* (ATP5β) and abolished the mitochondrial membrane potential (ΔΨm) by ablating *ubiquinol-cytochrome C reductase iron-sulfur subunit* (UQCRFS1) in C2C12 myoblasts. Deletion of Atp5β decreased ADP-stimulated respiration (P = 0.0001), maintained ΔΨm through uncoupled respiration, enhanced glucose uptake (P = 0.014), increased lactate production (P = 0.009), and increased pyruvate entry into the TCA cycle (P < 0.0001). However, UQCRFS1 deletion disrupted ΔΨm and mitochondrial respiration. Ablation of UQCRFS1, but not ATP5β, impaired myoblast proliferation; nonetheless, lack of either gene profoundly compromised myoblast fusion. Interestingly, addition of the potent myogenic stimulator IGF-1 only rescued ATP5β fusion and could not override UQCRFS1 knockout effects on either myoblast proliferation or differentiation. These data suggest an OxPhos-independent pathway is required for IGF-1 stimulated myogenesis. Further examination of ΔΨm related metabolic pathways will shed light on how mitochondria relay IGF-1 signaling in myogenesis.

Key words: ATP synthesis, myogenic program, IGF-1 signaling, mitochondrial bioenergetics

Introduction

Myogenesis is a tightly regulated process orchestrated by defined metabolic shifts. Myoblast proliferation is characterized by an increase in glycolysis, glutaminolysis, and activation of the pentose phosphate pathway (Ryall et al., 2015) to support the macromolecule biosynthesis necessary for proliferation. During differentiation, myoblasts undergo metabolic reprogramming characterized by an increase in mitochondrial content and oxidative capacity (Remels et al., 2010) (Moyes et al., 1997). Disruption of metabolic reprogramming by inhibiting mitochondrial protein synthesis (Korohoda et al., 1993; Rochard et al., 2000), mitochondrial DNA replication (Brunk and Yaffe, 1976; Herzberg et al., 1993), oxidative phosphorylation (Pawlikowska et al., 2006), or pyruvate metabolism (Hori et al., 2019) impairs differentiation. While accumulating evidence supports the notion that mitochondria are essential for myogenic differentiation (Herzberg et al., 1993; Hamai et al., 1997; Rochard et al., 2000; Bloemberg and Quadrilatero, 2016), the underpinning mechanisms remain largely unknown, partially due to the functional complexity of mitochondria in a wide range of cellular processes. For example, in addition to their traditional role as the powerhouse of the cell, mitochondria are an active player in metabolic signaling (Hansford and Zorov, 1998; Bohovych and Khalimonchuk, 2016; Martinez-Reyes and Chandel, 2020), reactive oxygen species production/signaling and scavenging (Skulachev, 1996; Aon et al., 2010; Brand, 2010), cell death (Goldstein et al., 2000), ion and metabolite transport (Palmieri and Pierri, 2010), iron-sulfur protein biogenesis (Nuth et al., 2002; Bulteau et al., 2004; Yoon and Cowan, 2004), and calcium homeostasis (Deluca and Engstrom, 1961; Vasington and Murphy, 1962; Rottenberg and Scarpa, 1974).

Insulin-like growth factor 1 (IGF-1) is a polypeptide hormone that significantly contributes to growth, development, and metabolic regulation of most tissues. In skeletal muscle, IGF-1 is a

potent stimulator of myogenesis by initially stimulating proliferation and then functioning as a strong inducer of differentiation (Rosenthal and Cheng, 1995; Engert et al., 1996). Myoblast proliferation is enhanced by IGF-1 stimulation through activation of the phosphatidylinositol 3'-kinase/Akt (PI 3-kinase/Akt) pathway which facilitates the downregulation of $p27^{KIP1}$, a cell cycle inhibitor (Chakravarthy et al., 2000). On the other hand, IGF-1 can induce differentiation through activation of PI 3-kinase/Akt and the downstream activation of mammalian target of rapamycin (mTOR) and p70S6 kinase to promote protein synthesis and inhibit protein degradation (Rommel et al., 2001; Tureckova et al., 2001). Several reports have shown IGF-1 (Bijur and Jope, 2003; Li et al., 2013; Song et al., 2018; Ohwada et al., 2020) or insulin-mediated activation of the PI3-K/Akt pathway (Yang et al., 2009; Yang et al., 2013) induces phosphorylation and translocation of Akt to mitochondria. Following translocation, mitochondrial Akt phosphorylates glycogen synthase kinase-3β (GSK3β) and the α and β-subunit of ATP synthase (ATP5α and ATP5β) (Bijur and Jope, 2003; Li et al., 2013). These modifications presumably modulate mitochondria metabolism, as GSK3β phosphorylation (inactivation) removed its inhibition on pyruvate dehydrogenase (Hoshi et al., 1996) and phosphorylation of ATP5α and ATP5β increased complex V activity in hepatocytes (Li et al., 2013). In insulin-stimulated C2C12 myoblasts, pharmacological inhibition of PI 3-kinase reduced Akt phosphorylation and severely blunted fusion, which was recapitulated with inhibitors of the ETC or inhibitors of mitochondrial protein synthesis (Pawlikowska et al., 2006). These studies suggest mitochondria play an important metabolic role in IGF-1 mediated myogenesis, yet how mitochondria mediate IGF-1 action in myogenesis remains largely unknown.

To determine the metabolic role of mitochondria in IGF-1 mediated myogenesis, we divided mitochondrial functions into OxPhos-dependent and -independent roles by knocking out

ATP synthase F1 subunit beta (ATP5β) and *Ubiquinol-cytochrome C reductase iron-sulfur subunit* (UQCRFS1), respectively. *Atp5b* encodes the β-subunit of the ATP synthase catalytic core (F1) that harbors the catalytic nucleotide binding sites for ATP synthesis. Deletion of ATP5β disrupted energy production but preserved (membrane potential) ΔΨm through uncoupled mitochondrial respiration, generating myoblasts that lack the capacity for mitochondrial ATP production (OxPhos). *Uqcrfs1* encodes a catalytic core subunit of complex III that contains an iron-sulfur cluster responsible for receiving and transferring electrons from ubiquinol to cytochrome c1, respectively. As a result, UQCRFS1 is essential for CIII enzymatic activity (Diaz et al., 2012), and its deletion obstructed ΔΨm, mitochondrial respiration, and energy production. Using this strategy, we showed that OxPhos is not necessary for IGF-1 mediated myogenesis but an OxPhos-independent function of mitochondria is imperative.

Materials and Methods

Cell Culture and Treatments

Skeletal muscle C2C12 mouse myoblasts (ATCC CRL-1772) were maintained in growth media (GM; DMEM containing 10% fetal bovine serum, 1% penicillin/streptomycin, 0.1 mg/ml normocin) in 5% CO_2 at 37ºC. Treatments include 10 ng/mL LONG R^3 IGF-1 human (Sigma-Aldrich, St. Louis, MO), 0.5 mM nicotinamide mononucleotide (Sigma Aldrich, St. Louis, MO), and/or 25 μM DS16570511 (Cayman Chemical Company, ANN Arbor, MI). All myoblast experiments including a treatment were incubated for 18hrs and collected for analysis.

For differentiation studies, when cells reached confluence, media was changed to differentiation media (DM; DMEM containing 2% horse serum, 1% penicillin/streptomycin, 0.1 mg/ml normocin). Treatments were added on D1 on incubation for 18 hrs followed by the addition

of fresh DM. Cells that received nicotinamide mononucleotide (NMN) as a treatment were supplied with 0.5 mM NMN for the remainder of differentiation.

Design and Preparation of sgRNA

Guide RNA with minimum off-targets and a high-quality score were designed using the CRISPR design tool (http://crispr.mit.edu). Targeting sgRNA 1, sgRNA 2, and sgRNA 3 were designed for exons 1 and 2 of *Atp5β* and *Uqcrfs1* genes. Oligonucleotides ordered from IDT (Integrated DNA Technologies, Coralville, IA) for each sgRNA were paired, annealed, and cloned into the pSpCas9(BB)-2A-Puro V2.0 plasmid (Addgene #62988) according to Ran et al. (2013). Proper insertion of the 20-nt guide sequence was confirmed using Sanger sequencing.

Plasmid Transfection

C2C12 myoblasts were grown to 60-70% confluency in 150 mm dishes and transfected with PeneFect™ Transfection Reagent (LifeSct LLC, Rockville, MD). Briefly, 13 μg of each plasmid containing sgRNAs 1-3, totaling 39 μg of plasmid DNA targeting *Atp5β* or *Uqcrfs1* or a vector control, was combined with 80 μL PeneFect™ and added dropwise to each 150 mm culture plate. Media was replaced with fresh GM after 18 hrs and cells were incubated for an additional 30 hrs. Puromycin was added to a final concentration of 4 μg/mL and incubated 48 hrs. Selected C2C12 myoblasts were then replated for experiments and a subset collected for Western blotting to ensure an absence of ATP5β or UQCRFS1 protein.

Western Blotting

Cellular proteins were lysed on ice with sample buffer containing 50 mM Tris-Cl pH 6.8, 2% SDS, 10% glycerol, 1% β-mercaptoethanol. Protein concentration was determined using

Pierce™ BCA Protein Assay Kit (ThermoFisher, Waltham, MA). Cell lysates were separated using SDS-PAGE, transferred to nitrocellulose membranes, and immunoblotted with primary antibodies specific for ATP5β (ThermoFisher, Waltham, MA) or UQCRSF1 (Abcam, Cambridge, UK). Bands were visualized with IRDye fluorescent secondary antibodies (LI-COR Biosciences, Lincoln, NE) and quantified using LI-COR Biosciences Odyssey imaging system and LI-COR Image Studio software.

Flow Cytometry

Myoblasts were seeded in 6-well plates at a density of $5x10^5$ cells/ well. The following day, 2 μM JC-1 (Abcam, Cambridge, UK) and 100 nM MitoTracker DeepRed (ThermoFisher, Waltham, MA) were added to each well and incubated at 37ºC with 5% CO_2 for 30 min. Myoblasts were removed using 1:4 diluted trypsin-EDTA (ThermoFisher, Waltham, MA), centrifuged, and resuspended in PBS containing 3 g/L glucose and 2% fetal bovine serum. Samples were analyzed and sorted using FACSAria I (BD Biosciences, San Jose, CA). Data was analyzed using FlowJo software (FlowJo LLC, Ashland, OR).

Mitochondrial Respiration

Myoblasts were seeded in a Seahorse XF Cell Culture 96-well Microplate (Agilent Technologies, Santa Clara, CA) at a density of 15 $x10^3$ cell/well and cultured overnight at 37ºC with 5% CO_2 in GM. The following day, GM was replaced with XF Media containing 10.5 mM sodium pyruvate, 10 mM glucose, and 1% GlutaMax. Mitochondrial respiration was measured using an XF96 extracellular flux analyzer (Agilent Technologies, Santa Clara, CA). Oxygen consumption rate (OCR) was measured at basal conditions followed by a series of injections

including 1 μg/mL oligomycin, 2μM FCCP, and 2μM antimycin A. All experiments were conducted at 37ºC. OCR values were normalized to μg of protein per well.

Metabolite Analysis

Myoblasts were seeded in a 6-well plate at a density of $5x10^5$ cells/well and allowed to grow for two days. After 48hrs, 1mL of media was collected from each well, combined with 100μL of 0.5M perchloric acid, incubated on ice for 15 min, and neutralized with 20 μL of 2M KOH. Samples were then frozen until analysis.

To determine media glucose concentration, 1.8 mL of glucose buffer containing 6.25% triethanolamine, 25 mM EDTA pH 7.4, 35 mM $MgCl_2$, and 1.28 mM NADP was added to each 5 mL borosilicate glass tube. Next, 300 μL of 1:6 diluted sample was added to its corresponding tube, and OD1 was measured spectrophotometrically at 340 nm in triplicate using 96-well plate. Following OD1, 35 μL of 1:10 glucose-6-dehydrogenase dehydrogenase (Sigma-Aldrich, St. Louis, MO) was added to each tube, incubated at RT for 15 min, and OD2 was measured. Following OD2, 40 μL of 11 mg/mL Na-ATP (Sigma-Aldrich, St. Louis, MO) and 21 μL of 1:10 hexokinase (Sigma-Aldrich, St. Louis,MO) was added to each tube, incubated at RT for 20 min, and OD3 was measured. Media glucose concentration was determined by subtracting OD3 from OD1 and calculated using a standard curve. Media glucose concentration was subtracted from the starting media glucose concentration to determine glucose uptake over 48 hrs.

To determine media lactate concentration, 1.5 mL of lactate buffer was added to each 5 mL borosilicate glass tube. A 100 μL aliquot of 1:2 diluted sample was added to its corresponding tube, and OD1 was measured spectrophotometrically at 340 nm in triplicate using 96-well plate. Following OD1, 35 μL of L-lactic dehydrogenase from bovine heart (Sigma-Aldrich, St. Louis,

MO) was added to each tube, incubated at RT for 2 hrs, and OD2 was measured. Media lactate concentration was determined by subtracting OD2 from OD1 and calculated using a standard curve.

ATP and ADP was separated with an HP Agilent 1100 (Agilent Technologies, Santa Clara, CA) using an Accucore C18 2.6 μm 50 mm x 4.6 mm column (Thermo Scientific, Pittsburg, PA), detected at 254 nm with gradient separation (Bernocchi et al., 1994; Williams et al., 2008), and quantified using commercially available ATP and ADP as a standard (Sigma-Aldrich, St. Louis, MO).

NAD:NADH ratio

Ratio of NAD+ to NADH was determined using NAD/NADH Cell-Based Assay Kit (Item No. 600480; Cayman Chemical Company, ANN Arbor, MI) according to manufacture's instructions.

[U-$^{13}C_6$]glucose Tracing and GCMS Analysis

Myoblasts were seeded on 150 mm dishes and grown until reaching approximately 70% confluency. GM was then changed to DMEM without glucose or sodium pyruvate, 10 mM [U-$^{13}C_6$]glucose (Cambridge Isotope Lab, Tewksburg, MA), 10% FBS, 1% penicillin/streptomycin, and 0.1 mg/ml normocin. Myoblasts were incubated in the labelled glucose media for 18 hrs.

Cells were then washed and 200 μL of 0.5 M perchloric acid was added to each dish, scrapped, collected into a centrifuge tube, set on ice for 15 min, and centrifuged at 13,000 X g for 5 min at 4ºC. Supernatants were transferred to a new centrifuge tube containing 40 μL of 2 M KOH and vortexed. Next, 300 μL of 5 M hydroxylamine hydrochloride was added followed by

350 μL of 4 M KOH and sonicated for 60 min at 65ºC. After the incubation, samples were acidified with 150 μL of 6 M HCl, saturated with NaCl, and extracted with ethyl acetate. For the first extraction, 0.8 mL ethyl acetate was added and incubated on a shaker for 15 min followed by centrifugation. The organic phase was separated with a Pasteur pipette, transferred to drum vials, and evaporated under N_2 at 40ºC. For the second extraction, 0.6 mL ethyl acetate was added and incubated on a shaker for 15 min. Supernatants were combined and evaporated to dryness under N_2 at 40ºC. Equal amounts of MTBSTFA (UCT Special Ties LLC, Bristol, PA) and ethyl acetate were mixed (1:1), and 20 μL of the mixture was added to samples and incubated at 65ºC for 1 hr. After the incubation, samples were transferred to GC vials and analyzed using an Agilent 7890 Series GC System with a 5975 mass selective detector (Agilent Technologies, Wilmington, DE) and a 30 m x 0.25 mm x 0.25 μm HP-5MS fused silica capillary column (Agilent Technologies, Wilmington, DE).

BrdU Analysis

Myoblasts were seeded on 24-well plates at a density of $5x10^4$ cells/well. The following day, BrdU labelling reagent (Invitrogen, Carlsbad, CA) was added at a 1:100 dilution and cultures were incubated at 37ºC for 1 hr. Cells were then washed with ice-cold PBS, fixed with ice-cold 70% ethanol for 5 min at RT, washed with PBS, and incubated in 1.5 M hydrochloric acid for 30 min at RT. Plates were then washed three times with PBS, blocked with PBS containing 5% goat serum for 1 hr at RT, and incubated overnight at 4ºC with a BrdU primary antibody (clone G3G4, DSHB, Iowa City, IA) diluted 1:100 in blocking buffer. The following day, plates were washed three times and incubated with Alexa Flour 555 goat anti-mouse IgG (Life Technologies, Eugene, OR) diluted 1:1000 in blocking buffer for 2 hrs at RT. Nuclei were counterstained with 4',6-Diamidino-2-Phenylindole (DAPI) diluted 1:500 in blocking buffer. Plates were washed three

times and images were collected using a Nikon ECLIPSE Ti-E fluorescent microscope (Nikon Instruments Inc., Melville, NY). Number of nuclei positive for BrdU was quantified as a percent of total nuclei as an indicator of cell proliferation rate.

Fusion Index

Myoblasts were seeded on 24-well plates at a density of 2 x 10^5 cell/well in GM. The following day, media were changed to DM and cells were allowed to differentiate for 4 days. On D4, plates were washed with ice-cold PBS once and fixed with ice-cold 100% methanol for 10 min at RT. Plates were then washed, blocked with PBS containing 5% goat serum, and incubated overnight at 4ºC with a myosin primary antibody (MF20; DSHB, Iowa City, IA) diluted 1:100 in blocking buffer. The following day, plates were washed three times and incubated with Alexa Fluor 555 goat anti-mouse IgG (Life Technologies, Eugene, OR) diluted 1:1000 in blocking buffer for 2 hrs at RT. Again, nuclei were stained with DAPI. Plates were washed three times and images were collected using a Nikon ECLIPSE Ti-E fluorescent microscope (Nikon Instruments Inc., Melville, NY). Fusion index was calculated by dividing the number of nuclei within multinucleated fibers by the total number of nuclei within a field.

Statistical Analysis

Results are presented as means ± SEM. Comparison between two groups was performed using Student's t-test with two-tailed distribution. For multiple-group comparisons, one-way and two-way ANOVAs were used to test for no differences among the group means. In the cases of significant interactions, Tukey' multiple comparisons test was performed post hoc. P-values less than or equal to 0.05 were considered statistically significant, while those less than 0.08 were considered trending.

Results

Generation of CRISPR/Cas-9-mediated ATP5β and UQCRFS1 knockout C2C12 myoblasts

To investigate the roles of OxPhos-dependent and -independent mitochondrial functions in myogenesis, we used CRISPR-Cas9 to knockout ATP5β and UQCRFS1 in C2C12 myoblasts. Guide RNAs were used to target multiple regions of exon 1 and 2 of *Atp5b* and *Uqcrsf1* (Fig. 5-1A,C), and gene deletion was confirmed by Western blotting (Fig. 5-1B,D). To evaluate the functional consequences of ATP5β and UQCRFS1 deletion, we assessed mitochondrial membrane potential (ΔΨm) and mitochondrial respiration. Deletion of ATP5β reduced basal respiration but permitted uncoupled respiration ($P < 0.0001$; Fig. 5-2A) to sustain ΔΨm (Fig. 5-2C). In contrast, UQCRFS1 deletion reduced ΔΨm ($P < 0.0001$; Fig. 5-2B), reduced basal respiration ($P < 0.0001$Fig. 5-2C), and inhibited uncoupled mitochondrial respiration (Fig. 5-2C). Together, ATP5β deletion preserved ΔΨm but disrupted mitochondrial energy production, whereas UQCRFS1 deletion disrupted ΔΨm and subsequently mitochondrial function.

Deletion of ATP5β and UQCRFS1 evoke unique metabolic responses

To determine how disruption of mitochondrial bioenergetics impacts metabolism, we assessed various metabolic characteristics. Mitochondrial content was reduced in ATP5β KO and UQCRFS1 KO myoblasts compared to WT ($P < 0.0001$; Fig. 5-3A,B). To determine if glycolytic flux increased to accommodate cellular energy demands, we measured glucose uptake and lactate excretion by analyzing the culture media after 18 hrs of incubation. Glucose uptake and lactate excretion were increased in ATP5β KO ($P = 0.014$, $P = 0.009$, respectively; Fig. 5-3C,D) myoblasts compared to WT, indicating an increase in glycolytic flux; however, there was no difference between UQCRFS1 KO and WT myoblasts (Fig. 5-3C,D). Further, the ratio of ATP to

ADP was measured as an indicator of glycolytic or oxidative metabolism, as a decrease in ATP:ADP has been associated with the Warburg effect (Maldonado and Lemasters, 2014). Indeed, the ratio of ATP to ADP in ATP5β KO myoblasts decreased corresponding to an increase in glycolytic flux (P = 0.079; Fig. 5-3E). We also measured the cellular NAD^+/NADH ratio to determine if the cellular redox state was altered. The ratio of NAD^+/NADH decreased in UQCRFS1 KO myoblast ($P < 0.0001$; Fig. 5-3F), which feasibly decreased the availability of NAD^+ for tricarboxylic acid cycle (TCA) redox reactions.

To determine if carbons derived from glucose enter the TCA cycle in KO myoblasts, we implemented a universally labelled glucose tracing strategy. Myoblasts were incubated with growth media containing [U-$^{13}C_6$]glucose for 18 hrs and collected for analysis to quantify the contribution of glucose to fluxes through key entry points of the TCA cycle. Fully labelled lactate and pyruvate increased in ATP5β KO myoblasts compared to WT and UQCRFS1 KO myoblasts ($P < 0.0001$; Fig. 5-4A,B). The majority of ATP5β KO pyruvate entry into the TCA cycle proceeded through pyruvate dehydrogenase, indicated by the predominate form of citrate containing two ^{13}C carbons (derived from fully labelled acetyl Co-A; Fig. 5-4C). However, ATP5β KO myotubes also had isotopic forms of oxaloacetate and malate containing two or three ^{13}C carbons (Fig. 5-4E,F), which correspond with the increase in citrate containing four or five ^{13}C carbons (Fig. 5-4C). This labelling pattern (oxaloacetate with two or three ^{13}C carbons combining with the fully labelled 2-carbon acetyl moiety to produce citrate containing either four or five ^{13}C carbons) indicates some level of pyruvate entry into the TCA cycle through pyruvate carboxylase. This pattern also explains the presence of α-ketoglutarate containing four ^{13}C carbons in ATP5β KO myoblasts (Fig. 5-4D). Collectively, ATP5β KO myoblasts exhibited a predominate utilization of glucose, not only for fueling glycolysis but for the anaplerosis of TCA intermediates. In contrast,

UQCRFS1 KO myoblasts did not increase glycolytic flux or glucose oxidation, which may be attributed to reduced levels of NADH exhibiting an inhibitory effect on glycolytic enzyme activity (Pena et al., 2015).

Deletion of ATP5β and UQCRFS1 restricts myoblasts to a single cell state

To determine if the altered metabolism of ATP5β KO and UQCRFS1 KO myoblasts impacts cell behavior, we evaluated their proliferation and differentiation. To assess proliferation, we pulsed myoblasts with BrdU and analyzed its incorporation rate. There was no difference between WT and ATP5β KO myoblasts, although BrdU incorporation in UQCRFS1 KO myoblast was reduced ($P = 0.001$; Fig. 5-5A). To assess differentiation, we allowed the cells to differentiate for 4d and analyzed the fusion index. Both ATP5β KO and UQCRFS1 KO had a reduced fusion index compared to WT; however, UQCRFS1 KO fusion was significantly lower than ATP5β KO ($P < 0.001$; Fig. 5-5B,C). Together, these data show inhibition of mitochondrial energy production restricted myoblast to a proliferative, single-cell state, whereas the loss of membrane potential not only impaired differentiation but also reduced proliferative capacity.

IGF-1 mediated myogenesis does not require mitochondrial energy production

To understand the metabolic role of mitochondria in IGF-1 mediated myogenesis, we stimulated WT, ATP5β KO, and UQCRFS1 KO myoblasts with IGF-1 and assessed myoblast proliferation and differentiation. IGF-1 stimulation increased BrdU incorporation in WT and ATP5β KO myoblasts ($P < 0.0001$), while BrdU incorporation in UQCRFS1 KO myoblast remained unchanged (Fig. 5-6A). Similarly, WT and ATP5β KO fusion index increased after IGF-1 stimulation ($P < 0.0001$), but UQCRFS1 KO fusion remained unchanged (Fig. 5-6B). These data show mitochondrial ATP production is not necessary for IGF-1 stimulated myogenesis.

We also assessed several metabolic characteristics of WT, ATP5β KO, and UQCRFS1 KO myoblasts stimulated with IGF-1. Glycolytic flux nearly doubled in IGF-1 stimulated UQCRFS1 KO myoblasts compared to non-stimulated UQCRFS1 KO myoblasts, a rate equivalent to ATP5β KO myoblasts ($P = 0.0002$; Fig. 5-6C,D). However, increased glycolytic energy production was not adequate to rescue UQCRFS1 KO proliferation or differentiation, suggesting adequate energy supply is not a limiting factor of IGF-1 mediated myogenesis. Nonetheless, NAD^+ concentrations remain low in IGF-1 treated UQCRFS1 KO myoblasts ($P < 0.0001$; Fig. 5-6E), presumably inhibiting TCA enzyme activity. To alleviate low NAD^+ concentrations in UQCRFS1 KO myoblasts, we supplemented the IGF-1 treatment with the NAD^+ precursor nicotinamide mononucleotide (NMN). To assess the contribution of glucose to fluxes through key entry points of the TCA cycle after IGF-1 stimulation with or without NMN supplementation, we implemented a [U-$^{13}C_6$]glucose tracing strategy in WT, ATP5β KO, and UQCRFS1 KO myoblasts. The main effect of treatment was not significant for the intermediates analyzed (Fig. 5-7 A-F) nor were there any significant interactions between genotype and treatment, indicating the addition of IGF-1 with or without NMN supplementation did not alter glucose utilization in WT, ATP5β KO, or UQCRFS1 KO myoblast. Further, IGF-1 stimulated UQCRFS1 KO fusion supplemented with NMN remained impaired compared to ATP5β KO and WT myotubes (Fig. 5-7G). Collectively, these data show IGF-1 stimulated myogenesis is not supported greater glucose oxidation or mitochondrial ATP production.

Mitochondrial calcium uptake is a putative stimulator of IGF-1 mediated myogenesis

To further explore OxPhos-independent roles of mitochondria in IGF-1 stimulated myogenesis, we investigated mitochondrial Ca^{2+} uptake. Mitochondria Ca^{2+} signaling is pivotal in skeletal muscle glucose oxidation (Gherardi et al., 2019), substrate utilization (Kwong et al., 2018),

and activation of several TCA enzymes (McCormack and Denton, 1979; McCormack et al., 1990; McCormack and Denton, 1993). The mitochondrial calcium uniporter (MCU) is the major site of entry for Ca^{2+} into the matrix (Pan et al., 2013), and its regulatory subunit M1CU1 is a target of mitochondrial Akt phosphorylation to increase basal mitochondrial Ca^{2+} levels (Marchi et al., 2019). Therefore, we blocked the MCU, using the cell permeable MCU inhibitor DS16570511 (Kon et al., 2017), in IGF-1 stimulated cells during differentiation. MCU inhibition crippled the fusion index of WT and ATP5β KO cells ($P < 0.0001$), recapitulating the phenotype of UQCRFS1 KO fusion (Fig. 5-8A,B). These findings imply mitochondrial calcium uptake may be one of the key regulators of IGF-1 mediated myogenesis.

Discussion

In skeletal muscle, IGF-1 signaling and activation of its downstream targets is critical for efficient myogenesis (Coleman et al., 1995; Musaro et al., 2001; Fiorotto et al., 2003; Lai et al., 2004; Blaauw et al., 2009). Although mitochondria have been suggested to play an important role in IGF-1 mediated myogenesis (Bijur and Jope, 2003; Pawlikowska et al., 2006; Rotwein and Wilson, 2009; Santi and Lee, 2010; Chae et al., 2016), their metabolic role in the process remains poorly defined. To fill this gap, we first examined the role of mitochondria alone in myogenesis by separating its functions into OxPhos- dependent and -independent roles. To disrupt OxPhos-dependent functions of mitochondria, we knocked out ATP5β in C2C12 myotubes. ATP5β KO myoblasts preserved ΔΨm through uncoupled respiration and compensated for the loss of mitochondrial energy production through an increase in glycolytic flux, which presumably restricted cells to a single cell state because ATP5β ablation did not impair proliferative capacity but inhibited fusion. To impede OxPhos-independent roles, we knocked out UQCRFS1 which resulted in disrupted ΔΨm and minimal mitochondrial respiration. UQCRFS1 KO myoblast

proliferation and differentiation were severely impaired. As the maintenance of ΔΨm is vital to mitochondrial integrity and function (Zorova et al., 2018), it is reasonable to assume UQCRFS1 KO myoblast lack nearly all mitochondrial function. Together, these data support the necessity of mitochondrial function for efficient myogenic progression. However, ATP5β KO fusion can be rescued with the potent myogenic stimulator IGF-1, which demonstrates mitochondrial ATP production is not the "metabolic switch" that governs myogenic programs but rather an OxPhos-independent role of mitochondria.

Next, we investigated OxPhos-independent functions in IGF-1 stimulated myogenesis. Activation of the PI3-K/Akt pathway through IGF-1 or insulin stimulation induces activation and translocation of Akt to mitochondria, which can alter glucose oxidation and mitochondrial respiration (Hoshi et al., 1996; Bijur and Jope, 2003; Li et al., 2013). As deletion of Akt in myoblasts inhibits myogenesis (Tureckova et al., 2001; Wilson and Rotwein, 2007; Rotwein and Wilson, 2009; Moriya and Miyazaki, 2018), we hypothesized mitochondria play a regulatory role in IGF-1 stimulated myogenesis. To better understand OxPhos-independent mitochondrial functions necessary for IGF-1 mediated myogenesis, we first investigated pyruvate entry into the TCA cycle because IGF-1 induced translocation of Akt to mitochondria permits removal of GSK3β inhibition on pyruvate dehydrogenase (Hoshi et al., 1996). Although it is important to note ATP5β KO myoblast had a drastic increase in pyruvate entry into the TCA cycle compared to WT, IGF-1 stimulation did not alter the abundance of TCA intermediates derived from glucose in any genotype. This suggests improved glucose oxidation is not a requirement for IGF-1 stimulated myogenesis, albeit sufficient pyruvate entry into the TCA cycle is essential (Fulco et al., 2008; Hori et al., 2019). Although we did not investigate amino acid metabolism, it is important to acknowledge that perturbations in amino acid flux through the TCA cycle also disturb myogenic

progression (Girven et al., 2016; Zhang et al., 2020). Moreover, UQCRFS1 KO myoblast stimulated with IGF-1 had a profound increase in glycolytic flux, which may be attributed to the ability of IGF-1 to increase lactate dehydrogenase (LDH) activity (Semsarian et al., 1999) and replenish NAD^+ pools for greater glycolytic flux. Although a significant increase in NAD^+ to NADH ratio was not observed in UQCRFS1 KO myoblast treated with IGF-1, their increased lactate secretion supports this construct. However, they remain unable to efficiently proliferate or fuse. These data show myoblast lacking mitochondrial function are not simply hindered by a lack of energy currency but rather the loss of OxPhos-independent mitochondrial function.

Next, we investigated the role of mitochondrial calcium (Ca^{2+}) uptake in IGF-1 mediated myogenesis. The ability of mitochondria to sequester Ca^{2+} makes them a key contributor to the regulation of cytosolic free calcium concentrations and Ca^{2+}mediated signaling (Nicholls, 1978; Nicholls and Scott, 1980). The mitochondrial calcium uniporter (MCU) catalyzes the passive uptake of Ca^{2+}, driven by the membrane potential (Bernardi, 1999; Biswas et al., 1999), and is the predominant route of Ca^{2+} influx into the matrix. In skeletal muscle, an increase in mitochondrial Ca^{2+} uptake by MCU overexpression induced hypertrophy through retrograde activation of IGF1-Akt/PKB hypertrophic pathways (Mammucari et al., 2015). Anterograde activation of this pathway has recently been established in tumor cells, in which mitochondrial Akt phosphorylates the regulatory subunit of MCU, M1CU1, and increases basal mitochondrial Ca^{2+} levels (Marchi et al., 2019). To determine if mitochondrial Ca^{2+} uptake plays a role in the IGF-1-$\Delta\Psi$m axis, we used DS16570511 to inhibit MCU-mediated Ca^{2+} uptake, which recapitulated the UQCRFS1 KO phenotype in WT and ATP5β KO myoblast. These data indicate mitochondrial Ca^{2+} uptake is necessary for IGF-1 mediated myogenesis. Although we were not able to provide direct evidence of Akt-mediated mitochondrial Ca^{2+} uptake in the IGF-1-$\Delta\Psi$m axis, we demonstrated the necessity

of a ΔΨm-driven mitochondrial function that is independent of mitochondrial ATP production and seemingly requires mitochondrial Ca^{2+} uptake. As Ca^{2+} is an extremely versatile signaling molecule and electron transport chain inhibitors increase cytosolic Ca^{2+} levels in C2C12 myoblasts (Biswas et al., 1999), we cannot exclude other retrograde Ca^{2+} signaling pathways that may modulate myogenesis. Nonetheless, further investigation into the role of mitochondrial Ca^{2+} sequestration in the IGF-1- ΔΨm axis is warranted.

In summary, we are the first to report mitochondrial ATP production is not required for IGF-1 mediated myogenesis. Rather, an OxPhos-independent function of mitochondria is indispensable. Further investigation into specific mitochondrial membrane potential-driven pathways in myogenesis will undoubtedly broaden our understanding of mitochondria not just as a power plant, but also as a coordinator that mediates a hierarchy of signaling cascades to modulate myogenic progression.

Acknowledgements

The authors wish to thank Dr. Kiho Lee, Dr. Samer El-Kadi, Con-Ning Yen, Joseph Yonke, and Kelsey O'Brien for their contributions to this study.

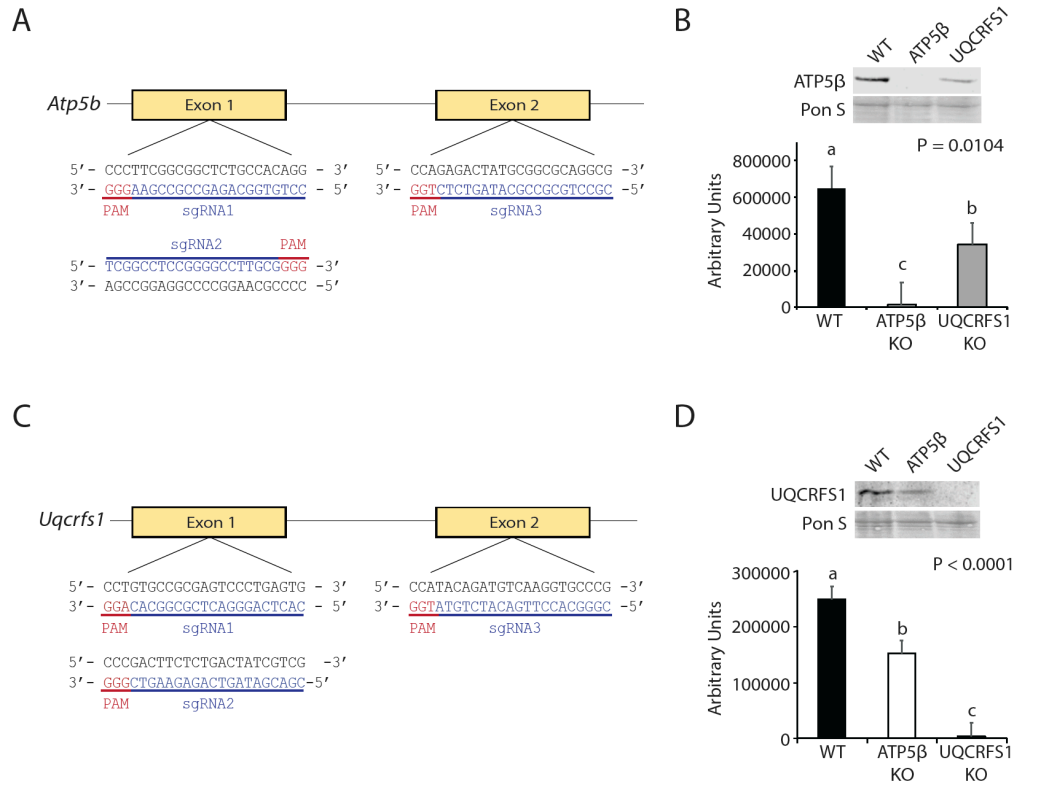

Figure 5-1. Generation of ATP5β and UQCRFS1 knockout C2C12 myoblasts. **(A, C)** Schematic diagram of guide sequences targeting (A) *Atp5β* and (C) *Uqcrfs1* genes. **(B-D)** Representative Western blot (top) and relative band intensity (bottom) of (B) ATP5β and (D) UQCRSF1 in WT, ATP5β KO, and UQCRFS1 KO myoblasts. Values represent means ± SEM of 5 independent cultures.

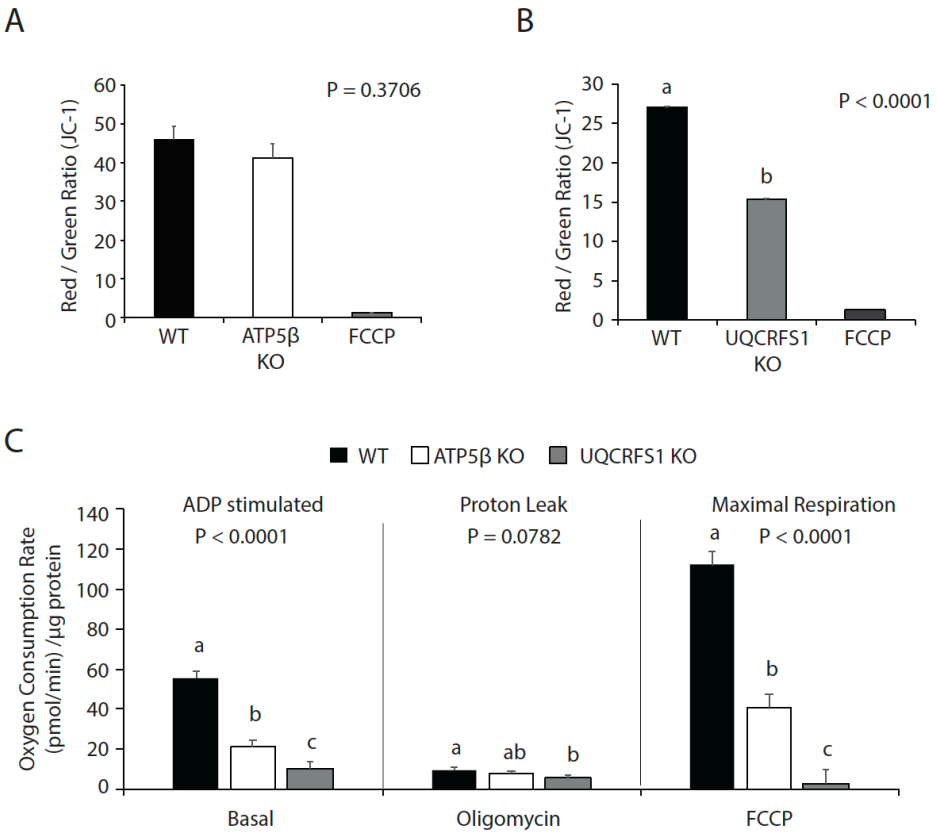

Figure 5-2. Assessment of mitochondrial membrane potential (ΔΨm) and respiration. (A-B) JC-1 fluorescence ratio of (A) ATP5β KO, (B) UQCRFS1 KO, and WT myoblasts. **(C)** Oxygen consumption rate was measured under basal conditions with ADP followed by the addition of oligomycin and FCCP. Values normalized to µg of total cell protein. Values represent means ± SEM. n = 5-8.

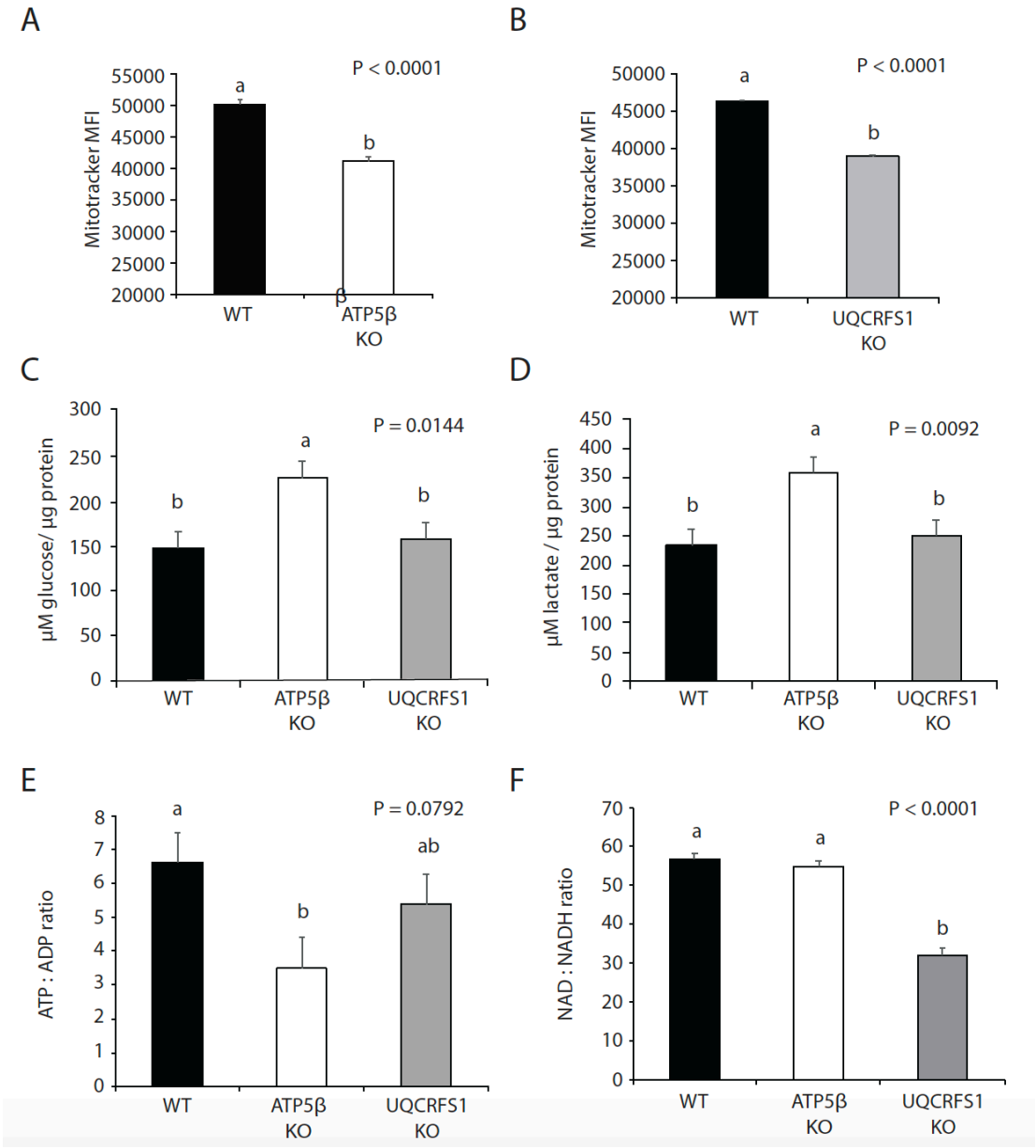

Figure 5-3. Disruption of OxPhos and ΔΨm alters myoblast metabolism. (A-B) MitoTracker Deep Red mean fluorescent intensity of ATP5β KO (A), UQCRFS1 KO (B), and WT myoblasts. **(C-D)** Quantification of (C) glucose uptake and (D) lactate secretion from 24 hrs of culture. Values normalized to µg of total cell protein. n=8. **(E)** Ratio of ATP to ADP and **(F)** ratio of NAD^+ to NADH in ATP5β KO, UQCRFS1 KO, and WT myoblasts. Values represent means ± SEM. n = 5-8.

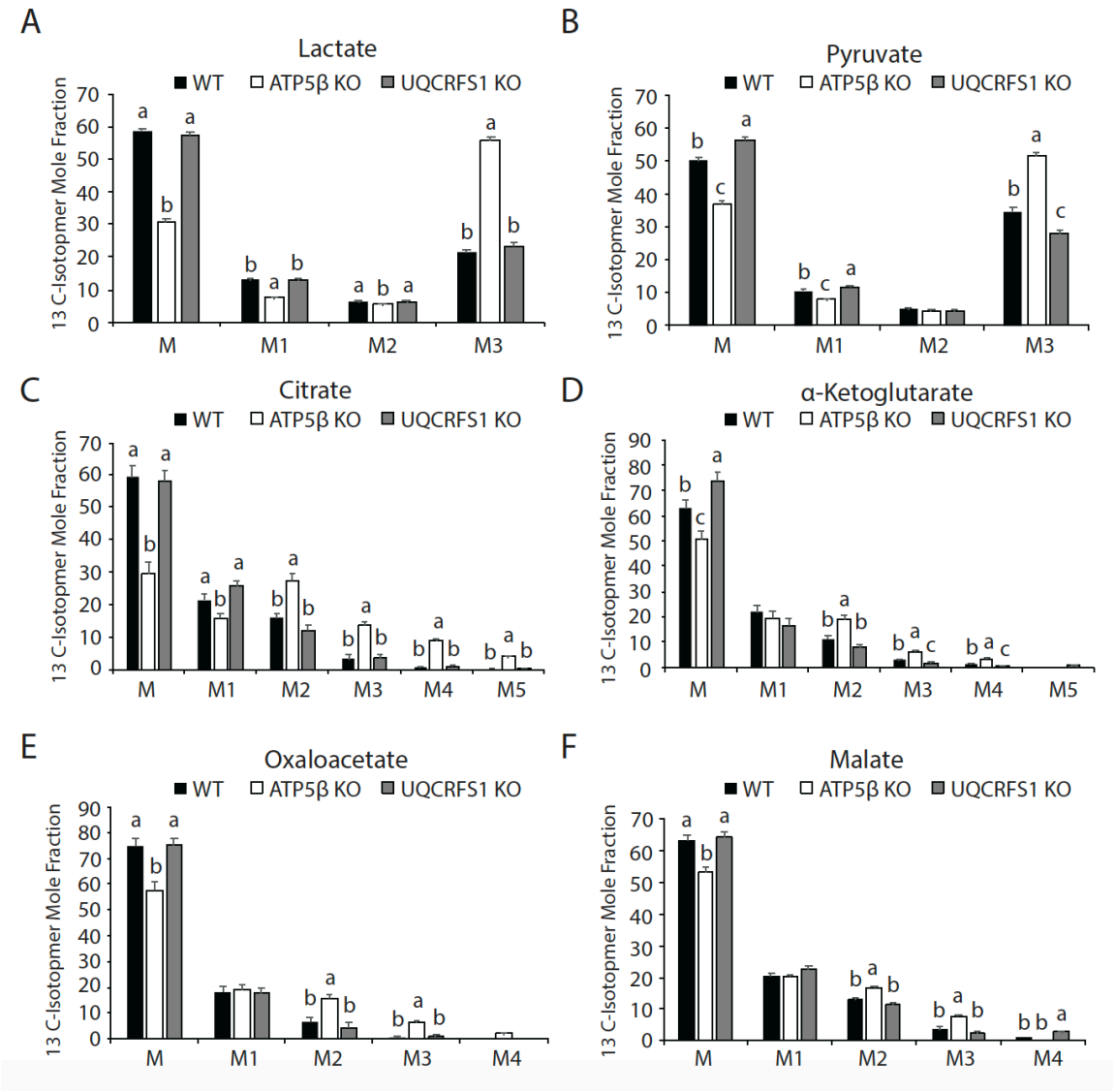

Figure 5-4. Loss of ATP5β, but not UQCRFS1, improves glucose utilization. (A-H) (A) Lactate, (B) pyruvate, (C) oxaloacetate, (D) citrate, (E) α-ketoglutarate, (F) succinate, (G) fumarate, and (H) malate isotopomer mole fraction resulting from 24hrs of culture with [U-$^{13}C_6$]glucose. Values represent means ± SEM. n = 18.

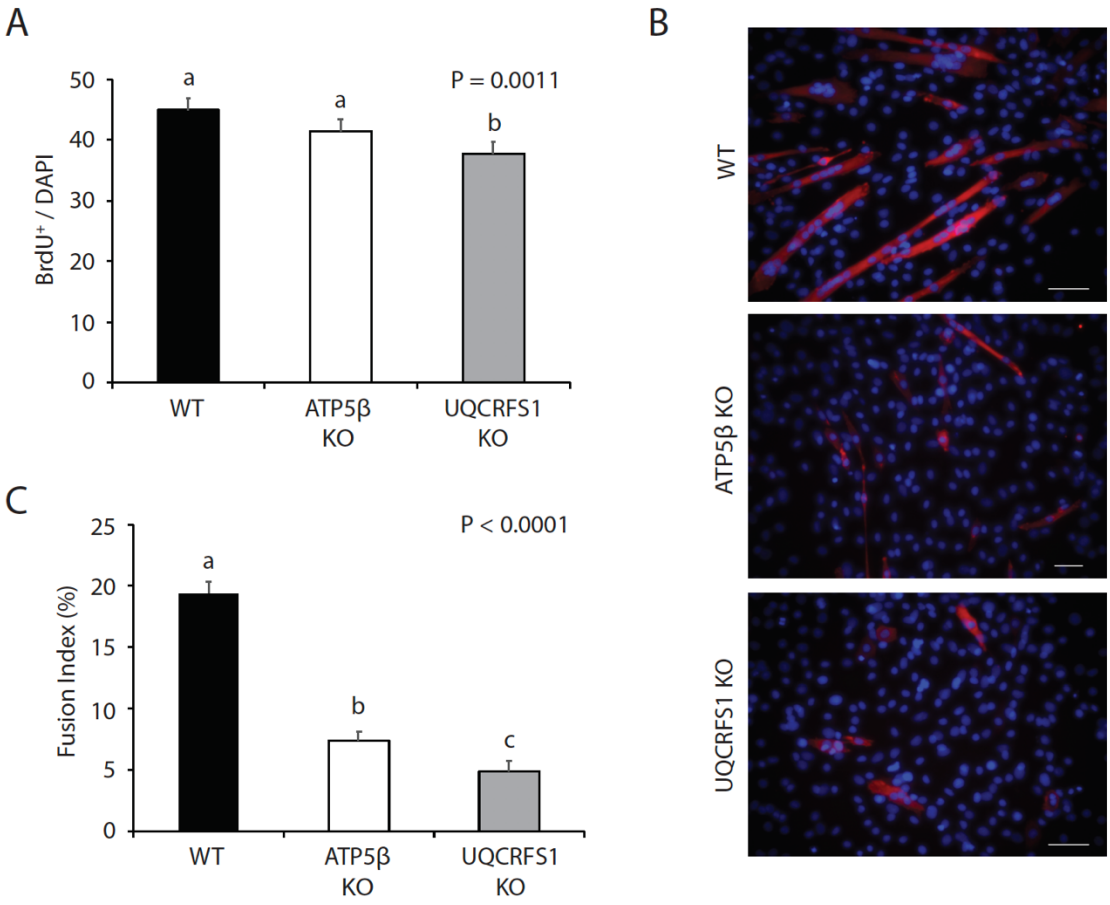

Figure 5-5. Disruption of mitochondrial bioenergetics restricts myoblasts to a single cell state. (A) Quantification of BrdU incorporation. **(B)** Representative images of myotubes stained with MF20 and counterstained with DAPI. Scale bar = 50μm. **(C)** Fusion index of ATP5β KO, UQCRFS1 KO, and WT myotubes after 4d of differentiation. Values represent means ± SEM. n = 8.

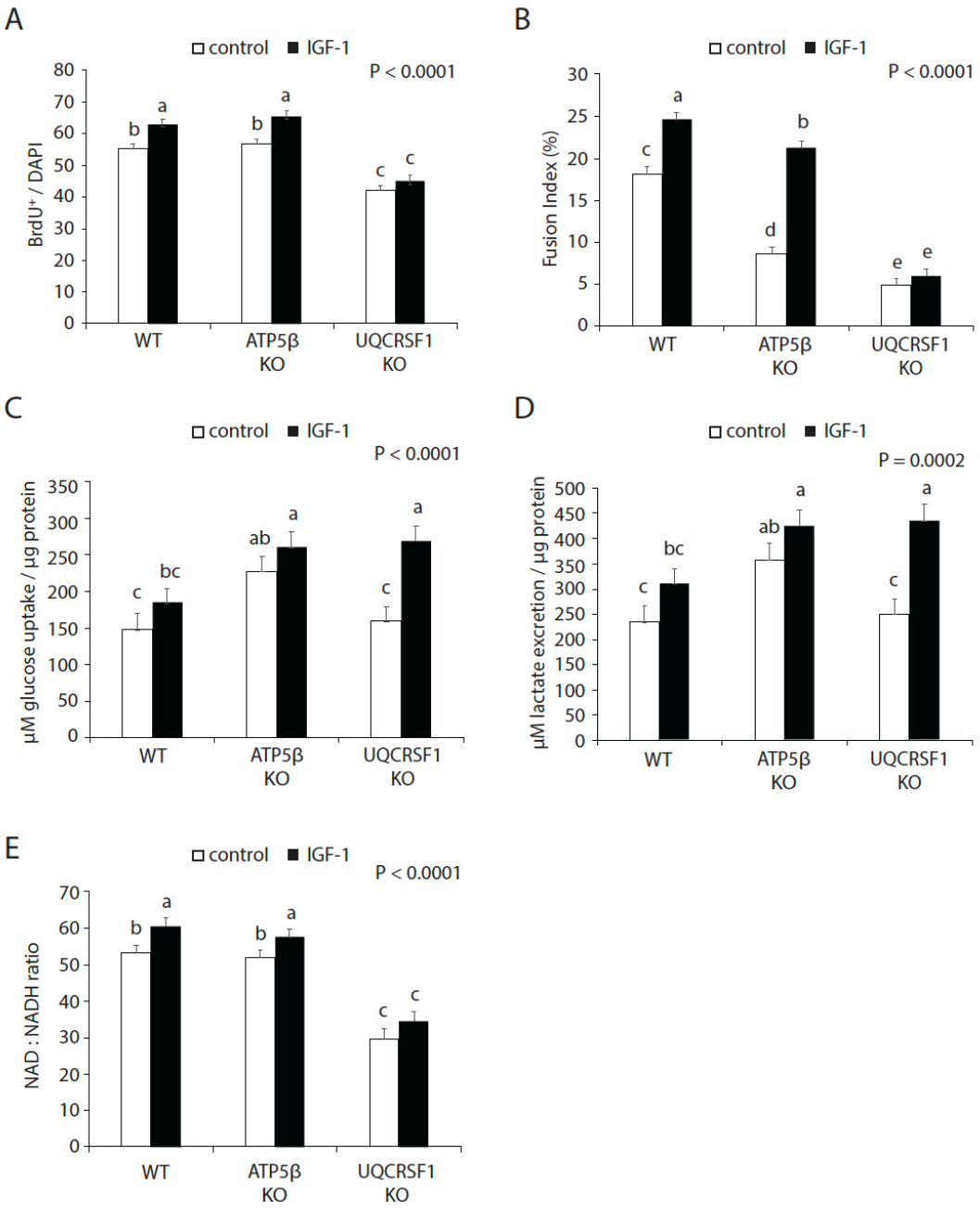

Figure 5-6. OxPhos is not required for IGF-1 stimulated myogenesis but rather an OxPhos-independent function. (A) Quantification of BrdU incorporation after 18hrs of IGF-1 treatment. **(B)** IGF-1 was added for 18hrs after 1d of differentiation. Fusion index was quantified after 4d. **(C-D)** Quantification of (C) lactate secretion and (D) glucose uptake from 24 hrs of culture. Values normalized to µg of total cell protein. **(E)** Ratio of NAD^+ to NADH in ATP5β KO, UQCRFS1 KO, and WT myoblasts with or without 18hr IGF-1 treatment. Values represent means ± SEM. n = 8.

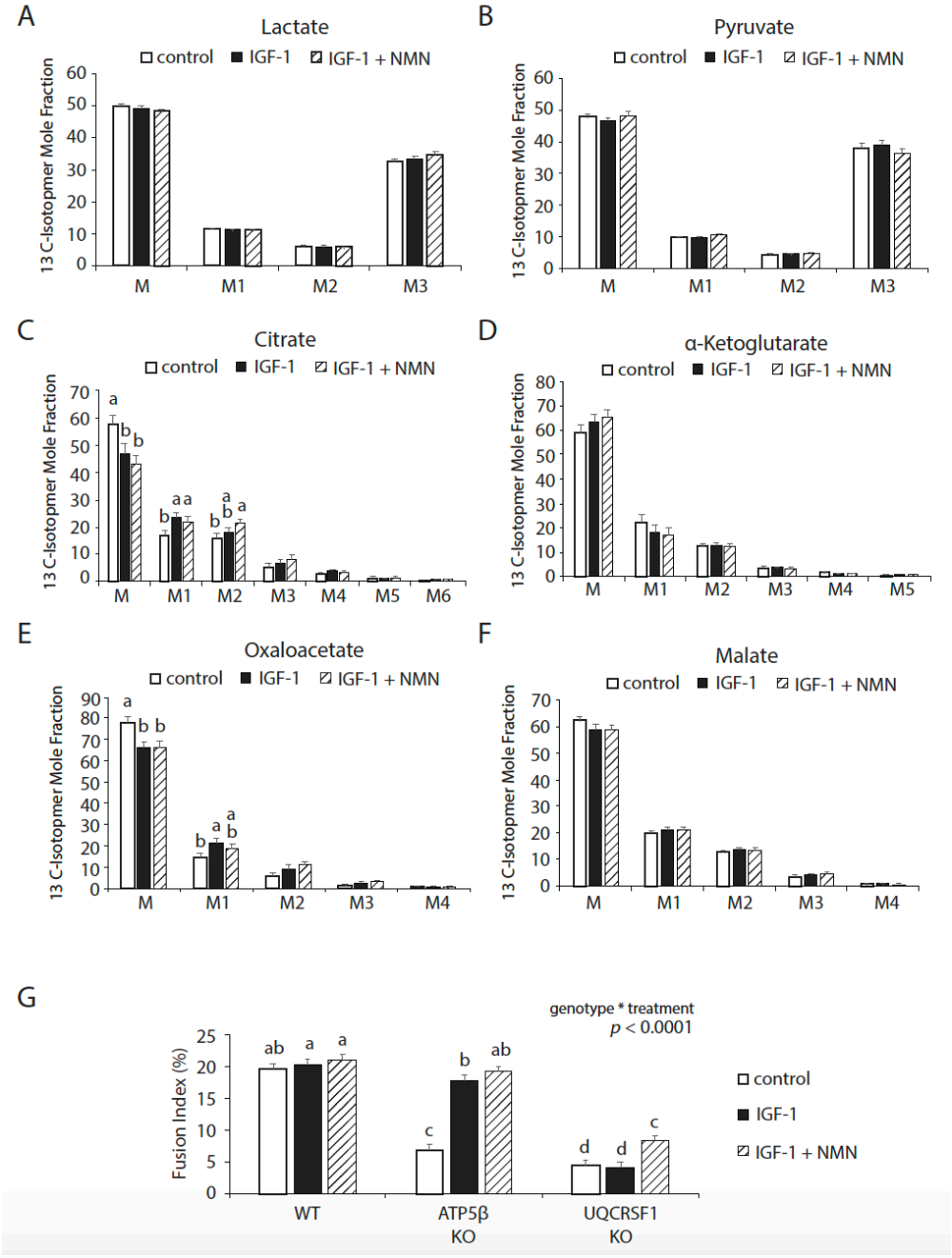

Figure 5-7. IGF-1 stimulation does not alter glucose utilization. (A-F) (A) Lactate, (B) pyruvate, (C) citrate, (D) α-ketoglutarate, (E) oxaloacetate, and (I) malate isotopomer mole fraction resulting from 24hrs of culture containing [U-$^{13}C_6$]glucose with IGF-1 stimulation with or without NMN supplementation. **(G)** Fusion index of myotubes stimulated with IGF-1 and supplemented with 0.5mM nicotinamide mononucleotide (NMN). NMN wells were supplemented with NMN for the duration of differentiation. Fusion index was quantified after 4d of differentiation. Values represent means ± SEM. n = 8-18.

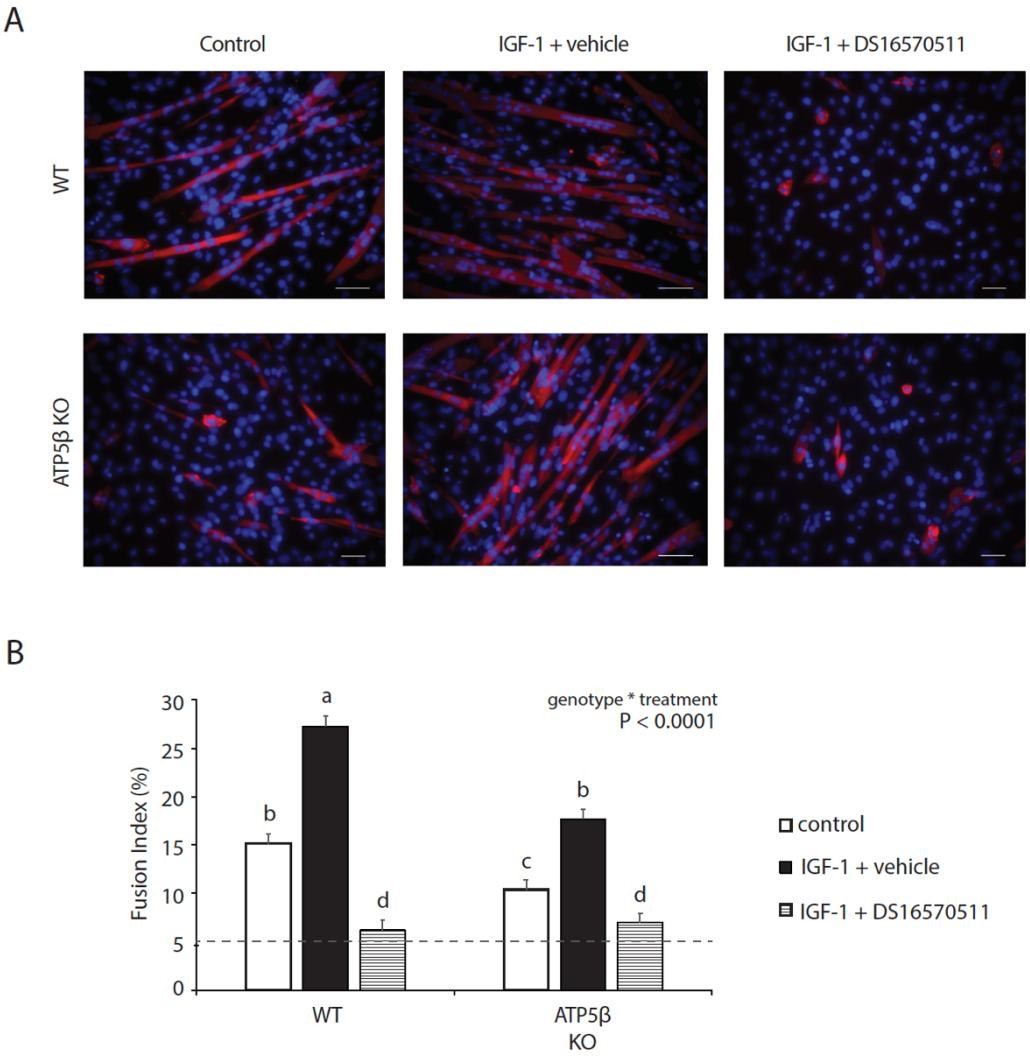

Figure 5-8. MCU-mediated mitochondrial Ca^{2+} uptake is necessary for myoblast fusion. (A) Representative images of myotubes stained with MF20 and counterstained with DAPI. Scale bar = 50μm. **(B)** Fusion index of IGF-1 stimulated myotubes with or without MCU inhibition by DS16570511. Fusion index was quantified after 4d of differentiation. Values represent means ± SEM. Dashed line represents UQCRFS1 fusion index average for reference. n = 8.

References

Aon, M. A., S. Cortassa, and B. O'Rourke. 2010. Redox-optimized ROS balance: a unifying hypothesis. Biochim Biophys Acta 1797(6-7):865-877. doi: 10.1016/j.bbabio.2010.02.016

Bernardi, P. 1999. Mitochondrial transport of cations: channels, exchangers, and permeability transition. Physiol Rev 79(4):1127-1155. doi: 10.1152/physrev.1999.79.4.1127

Bernocchi, P., C. Ceconi, A. Cargnoni, P. Pedersini, S. Curello, and R. Ferrari. 1994. Extraction and assay of creatine phosphate, purine, and pyridine nucleotides in cardiac tissue by reversed-phase high-performance liquid chromatography. Anal Biochem 222(2):374-379. doi: 10.1006/abio.1994.1505

Bijur, G. N., and R. S. Jope. 2003. Rapid accumulation of Akt in mitochondria following phosphatidylinositol 3-kinase activation. J Neurochem 87(6):1427-1435. doi: 10.1046/j.1471-4159.2003.02113.x

Biswas, G., O. A. Adebanjo, B. D. Freedman, H. K. Anandatheerthavarada, C. Vijayasarathy, M. Zaidi, M. Kotlikoff, and N. G. Avadhani. 1999. Retrograde Ca2+ signaling in C2C12 skeletal myocytes in response to mitochondrial genetic and metabolic stress: a novel mode of inter-organelle crosstalk. EMBO J 18(3):522-533. doi: 10.1093/emboj/18.3.522

Blaauw, B., M. Canato, L. Agatea, L. Toniolo, C. Mammucari, E. Masiero, R. Abraham, M. Sandri, S. Schiaffino, and C. Reggiani. 2009. Inducible activation of Akt increases skeletal muscle mass and force without satellite cell activation. FASEB J 23(11):3896-3905. doi: 10.1096/fj.09-131870

Bloemberg, D., and J. Quadrilatero. 2016. Effect of mitochondrial fission inhibition on C2C12 differentiation. Data Brief 7:634-640. doi: 10.1016/j.dib.2016.02.070

Bohovych, I., and O. Khalimonchuk. 2016. Sending Out an SOS: Mitochondria as a Signaling Hub. Front Cell Dev Biol 4:109. doi: 10.3389/fcell.2016.00109

Brand, M. D. 2010. The sites and topology of mitochondrial superoxide production. Exp Gerontol 45(7-8):466-472. doi: 10.1016/j.exger.2010.01.003

Brunk, C. F., and D. Yaffe. 1976. The reversible inhibition of myoblast fusion by ethidium bromide (EB). Exp Cell Res 99(2):310-318. doi: 10.1016/0014-4827(76)90588-7

Bulteau, A. L., H. A. O'Neill, M. C. Kennedy, M. Ikeda-Saito, G. Isaya, and L. I. Szweda. 2004. Frataxin acts as an iron chaperone protein to modulate mitochondrial aconitase activity. Science 305(5681):242-245. doi: 10.1126/science.1098991

Chae, Y. C., V. Vaira, M. C. Caino, H. Y. Tang, J. H. Seo, A. V. Kossenkov, L. Ottobrini, C. Martelli, G. Lucignani, I. Bertolini, M. Locatelli, K. G. Bryant, J. C. Ghosh, S. Lisanti, B. Ku, S. Bosari, L. R. Languino, D. W. Speicher, and D. C. Altieri. 2016. Mitochondrial Akt Regulation of Hypoxic Tumor Reprogramming. Cancer Cell 30(2):257-272. doi: 10.1016/j.ccell.2016.07.004

Chakravarthy, M. V., T. W. Abraha, R. J. Schwartz, M. L. Fiorotto, and F. W. Booth. 2000. Insulin-like growth factor-I extends in vitro replicative life span of skeletal muscle satellite cells by enhancing G1/S cell cycle progression via the activation of phosphatidylinositol 3'-kinase/Akt signaling pathway. J Biol Chem 275(46):35942-35952. doi: 10.1074/jbc.M005832200

Coleman, M. E., F. DeMayo, K. C. Yin, H. M. Lee, R. Geske, C. Montgomery, and R. J. Schwartz. 1995. Myogenic vector expression of insulin-like growth factor I stimulates muscle cell differentiation and myofiber hypertrophy in transgenic mice. J Biol Chem 270(20):12109-12116. doi: 10.1074/jbc.270.20.12109

Deluca, H. F., and G. W. Engstrom. 1961. Calcium uptake by rat kidney mitochondria. Proc Natl Acad Sci U S A 47:1744-1750. doi: 10.1073/pnas.47.11.1744

Diaz, F., J. A. Enriquez, and C. T. Moraes. 2012. Cells lacking Rieske iron-sulfur protein have a reactive oxygen species-associated decrease in respiratory complexes I and IV. Mol Cell Biol 32(2):415-429. doi: 10.1128/MCB.06051-11

Engert, J. C., E. B. Berglund, and N. Rosenthal. 1996. Proliferation precedes differentiation in IGF-I-stimulated myogenesis. J Cell Biol 135(2):431-440. doi: 10.1083/jcb.135.2.431

Fiorotto, M. L., R. J. Schwartz, and M. C. Delaughter. 2003. Persistent IGF-I overexpression in skeletal muscle transiently enhances DNA accretion and growth. FASEB J 17(1):59-60. doi: 10.1096/fj.02-0289fje

Fulco, M., Y. Cen, P. Zhao, E. P. Hoffman, M. W. McBurney, A. A. Sauve, and V. Sartorelli. 2008. Glucose restriction inhibits skeletal myoblast differentiation by activating SIRT1 through AMPK-mediated regulation of Nampt. Dev Cell 14(5):661-673. doi: 10.1016/j.devcel.2008.02.004

Gherardi, G., L. Nogara, S. Ciciliot, G. P. Fadini, B. Blaauw, P. Braghetta, P. Bonaldo, D. De Stefani, R. Rizzuto, and C. Mammucari. 2019. Loss of mitochondrial calcium uniporter rewires skeletal muscle metabolism and substrate preference. Cell Death Differ 26(2):362-381. doi: 10.1038/s41418-018-0191-7

Girven, M., H. F. Dugdale, D. J. Owens, D. C. Hughes, C. E. Stewart, and A. P. Sharples. 2016. l-glutamine Improves Skeletal Muscle Cell Differentiation and Prevents Myotube Atrophy After Cytokine (TNF-alpha) Stress Via Reduced p38 MAPK Signal Transduction. J Cell Physiol 231(12):2720-2732. doi: 10.1002/jcp.25380

Goldstein, J. C., N. J. Waterhouse, P. Juin, G. I. Evan, and D. R. Green. 2000. The coordinate release of cytochrome c during apoptosis is rapid, complete and kinetically invariant. Nat Cell Biol 2(3):156-162. doi: 10.1038/35004029

Hamai, N., M. Nakamura, and A. Asano. 1997. Inhibition of mitochondrial protein synthesis impaired C2C12 myoblast differentiation. Cell Struct Funct 22(4):421-431. doi: 10.1247/csf.22.421

Hansford, R. G., and D. Zorov. 1998. Role of mitochondrial calcium transport in the control of substrate oxidation. Mol Cell Biochem 184(1-2):359-369.

Herzberg, N. H., R. Zwart, R. A. Wolterman, J. P. Ruiter, R. J. Wanders, P. A. Bolhuis, and C. van den Bogert. 1993. Differentiation and proliferation of respiration-deficient human myoblasts. Biochim Biophys Acta 1181(1):63-67. doi: 10.1016/0925-4439(93)90091-e

Hori, S., Y. Hiramuki, D. Nishimura, F. Sato, and A. Sehara-Fujisawa. 2019. PDH-mediated metabolic flow is critical for skeletal muscle stem cell differentiation and myotube formation during regeneration in mice. FASEB J 33(7):8094-8109. doi: 10.1096/fj.201802479R

Hoshi, M., A. Takashima, K. Noguchi, M. Murayama, M. Sato, S. Kondo, Y. Saitoh, K. Ishiguro, T. Hoshino, and K. Imahori. 1996. Regulation of mitochondrial pyruvate dehydrogenase activity by tau protein kinase I/glycogen synthase kinase 3beta in brain. Proc Natl Acad Sci U S A 93(7):2719-2723. doi: 10.1073/pnas.93.7.2719

Kon, N., M. Murakoshi, A. Isobe, K. Kagechika, N. Miyoshi, and T. Nagayama. 2017. DS16570511 is a small-molecule inhibitor of the mitochondrial calcium uniporter. Cell Death Discov 3:17045. doi: 10.1038/cddiscovery.2017.45

Korohoda, W., Z. Pietrzkowski, and K. Reiss. 1993. Chloramphenicol, an inhibitor of mitochondrial protein synthesis, inhibits myoblast fusion and myotube differentiation. Folia Histochem Cytobiol 31(1):9-13.

Kwong, J. Q., J. Huo, M. J. Bround, J. G. Boyer, J. A. Schwanekamp, N. Ghazal, J. T. Maxwell, Y. C. Jang, Z. Khuchua, K. Shi, D. M. Bers, J. Davis, and J. D. Molkentin. 2018. The mitochondrial calcium uniporter underlies metabolic fuel preference in skeletal muscle. JCI Insight 3(22)doi: 10.1172/jci.insight.121689

Lai, K. M., M. Gonzalez, W. T. Poueymirou, W. O. Kline, E. Na, E. Zlotchenko, T. N. Stitt, A. N. Economides, G. D. Yancopoulos, and D. J. Glass. 2004. Conditional activation of akt in adult skeletal muscle induces rapid hypertrophy. Mol Cell Biol 24(21):9295-9304. doi: 10.1128/MCB.24.21.9295-9304.2004

Li, C., Y. Li, L. He, A. R. Agarwal, N. Zeng, E. Cadenas, and B. L. Stiles. 2013. PI3K/AKT signaling regulates bioenergetics in immortalized hepatocytes. Free Radic Biol Med 60:29-40. doi: 10.1016/j.freeradbiomed.2013.01.013

Maldonado, E. N., and J. J. Lemasters. 2014. ATP/ADP ratio, the missed connection between mitochondria and the Warburg effect. Mitochondrion 19 Pt A:78-84. doi: 10.1016/j.mito.2014.09.002

Mammucari, C., G. Gherardi, I. Zamparo, A. Raffaello, S. Boncompagni, F. Chemello, S. Cagnin, A. Braga, S. Zanin, G. Pallafacchina, L. Zentilin, M. Sandri, D. De Stefani, F. Protasi, G. Lanfranchi, and R. Rizzuto. 2015. The mitochondrial calcium uniporter controls skeletal muscle trophism in vivo. Cell Rep 10(8):1269-1279. doi: 10.1016/j.celrep.2015.01.056

Marchi, S., M. Corricelli, A. Branchini, V. A. M. Vitto, S. Missiroli, G. Morciano, M. Perrone, M. Ferrarese, C. Giorgi, M. Pinotti, L. Galluzzi, G. Kroemer, and P. Pinton. 2019. Akt-mediated phosphorylation of MICU1 regulates mitochondrial Ca(2+) levels and tumor growth. EMBO J 38(2)doi: 10.15252/embj.201899435

Martinez-Reyes, I., and N. S. Chandel. 2020. Mitochondrial TCA cycle metabolites control physiology and disease. Nat Commun 11(1):102. doi: 10.1038/s41467-019-13668-3

McCormack, J. G., and R. M. Denton. 1979. The effects of calcium ions and adenine nucleotides on the activity of pig heart 2-oxoglutarate dehydrogenase complex. Biochem J 180(3):533-544. doi: 10.1042/bj1800533

McCormack, J. G., and R. M. Denton. 1993. Mitochondrial Ca2+ transport and the role of intramitochondrial Ca2+ in the regulation of energy metabolism. Dev Neurosci 15(3-5):165-173. doi: 10.1159/000111332

McCormack, J. G., A. P. Halestrap, and R. M. Denton. 1990. Role of calcium ions in regulation of mammalian intramitochondrial metabolism. Physiol Rev 70(2):391-425. doi: 10.1152/physrev.1990.70.2.391

Moriya, N., and M. Miyazaki. 2018. Akt1 deficiency diminishes skeletal muscle hypertrophy by reducing satellite cell proliferation. Am J Physiol Regul Integr Comp Physiol 314(5):R741-R751. doi: 10.1152/ajpregu.00336.2017

Moyes, C. D., O. A. Mathieu-Costello, N. Tsuchiya, C. Filburn, and R. G. Hansford. 1997. Mitochondrial biogenesis during cellular differentiation. Am J Physiol 272(4 Pt 1):C1345-1351. doi: 10.1152/ajpcell.1997.272.4.C1345

Musaro, A., K. McCullagh, A. Paul, L. Houghton, G. Dobrowolny, M. Molinaro, E. R. Barton, H. L. Sweeney, and N. Rosenthal. 2001. Localized Igf-1 transgene expression sustains hypertrophy and regeneration in senescent skeletal muscle. Nat Genet 27(2):195-200. doi: 10.1038/84839

Nicholls, D. G. 1978. The regulation of extramitochondrial free calcium ion concentration by rat liver mitochondria. Biochem J 176(2):463-474. doi: 10.1042/bj1760463

Nicholls, D. G., and I. D. Scott. 1980. The regulation of brain mitochondrial calcium-ion transport. The role of ATP in the discrimination between kinetic and membrane-potential-dependent calcium-ion efflux mechanisms. Biochem J 186(3):833-839. doi: 10.1042/bj1860833

Nuth, M., T. Yoon, and J. A. Cowan. 2002. Iron-sulfur cluster biosynthesis: characterization of iron nucleation sites for assembly of the [2Fe-2S]2+ cluster core in IscU proteins. J Am Chem Soc 124(30):8774-8775. doi: 10.1021/ja0264596

Ohwada, W., M. Tanno, T. Yano, S. B. Ong, K. Abe, T. Sato, A. Kuno, T. Miki, H. Sugawara, Y. Igaki, and T. Miura. 2020. Distinct intra-mitochondrial localizations of pro-survival kinases and regulation of their functions by DUSP5 and PHLPP-1. Biochim Biophys Acta Mol Basis Dis 1866(10):165851. doi: 10.1016/j.bbadis.2020.165851

Palmieri, F., and C. L. Pierri. 2010. Mitochondrial metabolite transport. Essays Biochem 47:37-52. doi: 10.1042/bse0470037

Pan, X., J. Liu, T. Nguyen, C. Liu, J. Sun, Y. Teng, M. M. Fergusson, Rovira, II, M. Allen, D. A. Springer, A. M. Aponte, M. Gucek, R. S. Balaban, E. Murphy, and T. Finkel. 2013. The physiological role of mitochondrial calcium revealed by mice lacking the mitochondrial calcium uniporter. Nat Cell Biol 15(12):1464-1472. doi: 10.1038/ncb2868

Pawlikowska, P., B. Gajkowska, J. F. Hocquette, and A. Orzechowski. 2006. Not only insulin stimulates mitochondriogenesis in muscle cells, but mitochondria are also essential for insulin-mediated myogenesis. Cell Prolif 39(2):127-145. doi: 10.1111/j.1365-2184.2006.00376.x

Pena, A., N. S. Sanchez, O. Gonzalez-Lopez, and M. Calahorra. 2015. Mechanisms involved in the inhibition of glycolysis by cyanide and antimycin A in Candida albicans and its reversal by hydrogen peroxide. A common feature in Candida species. FEMS Yeast Res 15(8)doi: 10.1093/femsyr/fov083

Ran, F. A., P. D. Hsu, J. Wright, V. Agarwala, D. A. Scott, and F. Zhang. 2013. Genome engineering using the CRISPR-Cas9 system. Nat Protoc 8(11):2281-2308. doi: 10.1038/nprot.2013.143

Remels, A. H., R. C. Langen, P. Schrauwen, G. Schaart, A. M. Schols, and H. R. Gosker. 2010. Regulation of mitochondrial biogenesis during myogenesis. Mol Cell Endocrinol 315(1-2):113-120. doi: 10.1016/j.mce.2009.09.029

Rochard, P., A. Rodier, F. Casas, I. Cassar-Malek, S. Marchal-Victorion, L. Daury, C. Wrutniak, and G. Cabello. 2000. Mitochondrial activity is involved in the regulation of myoblast differentiation through myogenin expression and activity of myogenic factors. J Biol Chem 275(4):2733-2744. doi: 10.1074/jbc.275.4.2733

Rommel, C., S. C. Bodine, B. A. Clarke, R. Rossman, L. Nunez, T. N. Stitt, G. D. Yancopoulos, and D. J. Glass. 2001. Mediation of IGF-1-induced skeletal myotube hypertrophy by PI(3)K/Akt/mTOR and PI(3)K/Akt/GSK3 pathways. Nat Cell Biol 3(11):1009-1013. doi: 10.1038/ncb1101-1009

Rosenthal, S. M., and Z. Q. Cheng. 1995. Opposing early and late effects of insulin-like growth factor I on differentiation and the cell cycle regulatory retinoblastoma protein in skeletal myoblasts. Proc Natl Acad Sci U S A 92(22):10307-10311. doi: 10.1073/pnas.92.22.10307

Rottenberg, H., and A. Scarpa. 1974. Calcium uptake and membrane potential in mitochondria. Biochemistry 13(23):4811-4817. doi: 10.1021/bi00720a020

Rotwein, P., and E. M. Wilson. 2009. Distinct actions of Akt1 and Akt2 in skeletal muscle differentiation. J Cell Physiol 219(2):503-511. doi: 10.1002/jcp.21692

Ryall, J. G., S. Dell'Orso, A. Derfoul, A. Juan, H. Zare, X. Feng, D. Clermont, M. Koulnis, G. Gutierrez-Cruz, M. Fulco, and V. Sartorelli. 2015. The NAD(+)-dependent SIRT1 deacetylase translates a metabolic switch into regulatory epigenetics in skeletal muscle stem cells. Cell Stem Cell 16(2):171-183. doi: 10.1016/j.stem.2014.12.004

Santi, S. A., and H. Lee. 2010. The Akt isoforms are present at distinct subcellular locations. 298(3):C580-591. doi: 10.1152/ajpcell.00375.2009

Semsarian, C., P. Sutrave, D. R. Richmond, and R. M. Graham. 1999. Insulin-like growth factor (IGF-I) induces myotube hypertrophy associated with an increase in anaerobic glycolysis in a clonal skeletal-muscle cell model. Biochem J 339 (Pt 2):443-451.

Skulachev, V. P. 1996. Role of uncoupled and non-coupled oxidations in maintenance of safely low levels of oxygen and its one-electron reductants. Q Rev Biophys 29(2):169-202. doi: 10.1017/s0033583500005795

Song, H. P., Z. G. Chu, D. X. Zhang, Y. M. Dang, and Q. Zhang. 2018. PI3K-AKT Pathway Protects Cardiomyocytes Against Hypoxia-Induced Apoptosis by MitoKATP-Mediated Mitochondrial Translocation of pAKT. Cell Physiol Biochem 49(2):717-727. doi: 10.1159/000493037

Tureckova, J., E. M. Wilson, J. L. Cappalonga, and P. Rotwein. 2001. Insulin-like growth factor-mediated muscle differentiation: collaboration between phosphatidylinositol 3-kinase-Akt-signaling pathways and myogenin. J Biol Chem 276(42):39264-39270. doi: 10.1074/jbc.M104991200

Vasington, F. D., and J. V. Murphy. 1962. Ca ion uptake by rat kidney mitochondria and its dependence on respiration and phosphorylation. J Biol Chem 237:2670-2677.

Williams, J. H., S. E. Vidt, and J. Rinehart. 2008. Measurement of sarcoplasmic reticulum Ca2+ ATPase activity using high-performance liquid chromatography. Anal Biochem 372(2):135-139. doi: 10.1016/j.ab.2007.09.020

Wilson, E. M., and P. Rotwein. 2007. Selective control of skeletal muscle differentiation by Akt1. J Biol Chem 282(8):5106-5110. doi: 10.1074/jbc.C600315200

Yang, J. Y., W. Deng, Y. Chen, W. Fan, K. M. Baldwin, R. S. Jope, D. C. Wallace, and P. H. Wang. 2013. Impaired translocation and activation of mitochondrial Akt1 mitigated mitochondrial oxidative phosphorylation Complex V activity in diabetic myocardium. J Mol Cell Cardiol 59:167-175. doi: 10.1016/j.yjmcc.2013.02.016

Yang, J. Y., H. Y. Yeh, K. Lin, and P. H. Wang. 2009. Insulin stimulates Akt translocation to mitochondria: implications on dysregulation of mitochondrial oxidative phosphorylation in diabetic myocardium. J Mol Cell Cardiol 46(6):919-926. doi: 10.1016/j.yjmcc.2009.02.015

Yoon, T., and J. A. Cowan. 2004. Frataxin-mediated iron delivery to ferrochelatase in the final step of heme biosynthesis. J Biol Chem 279(25):25943-25946. doi: 10.1074/jbc.C400107200

Zhang, L., Y. Duan, Q. Guo, W. Wang, and F. Li. 2020. A selectively suppressing amino acid transporter: Sodium-coupled neutral amino acid transporter 2 inhibits cell growth and mammalian target of rapamycin complex 1 pathway in skeletal muscle cells. Animal Nutrition doi: 10.1016/j.aninu.2020.03.010

Zorova, L. D., V. A. Popkov, E. J. Plotnikov, D. N. Silachev, I. B. Pevzner, S. S. Jankauskas, D. B. Zorov, V. A. Babenko, and S. D. Zorov. 2018. Functional Significance of the

Mitochondrial Membrane Potential. Biochemistry (Moscow) Supplement Series A: Membrane and Cell Biology 12(1):20-26. doi: 10.1134/S1990747818010129

Chapter 6. Summary

Skeletal muscle is a highly plastic tissue that can respond to a wide variety of external and internal stimuli. The scope of this work is aimed at generating a deeper understanding of how skeletal muscle can sense and respond to different nutrient conditions at a cellular level and the subsequent impact on animal growth efficiency. Therefore, we first investigated the nutrient sensitive post-translational modification O-GlcNAcylation in skeletal muscle and satellite cells (SCs), the resident stem cell population of skeletal muscle. Next, we explored the intrinsic metabolic regulation of myoblasts by investigating the role of mitochondria in IGF-1 mediated myogenesis. Briefly, we showed O-GlcNAcylation is necessary for the maintenance of skeletal muscle metabolism, and ablation of O-GlcNAc transferase (OGT) in skeletal muscle has profound implications on global metabolism. In particular, mice lacking skeletal muscle OGT (mKO) had greater lipolysis, energy expenditure, and protection against high-fat diet (HFD) induced obesity. We proposed the lean mKO phenotype was a result of increased interleukin-15 (IL-15) expression in muscle and circulation. Indeed, concurrent ablation of interleukin-15 receptor alpha (IL-15rα) and OGT in skeletal muscle (mDKO) largely negated the lean phenotype after HFD feeding. In conclusion, we showed O-GlcNAcylation is required for proper muscle metabolism and its dysregulation in skeletal muscle can elicit responses in other tissues to mobilize substrates to support its needs. These findings have implications on human health, as a target to ameliorate metabolic diseases, and in animal agriculture, as an indicator of metabolic status of growing tissues or as a target to augment animal growth.

In SCs, we showed O-GlcNAcylation is critical for proper SC function and metabolic homeostasis. Specifically, proper O-GlcNAcylation is essential for SC population maintenance and adult regenerative myogenesis. Although we failed to elucidate the mechanism of OGT action on myogenic progression, our data suggests the OGT-HCF1 axis plays an important role in SC expansion and OGT-mediated perturbation of SC metabolic state has negative implications on quiescence and/or cell cycle entry. Defining the role of O-GlcNAcylation in myogenic progression will provide insight into how SCs adapt their biological processes to correspond to extrinsic nutrient conditions. For example, SCs can “sense” conditions of

nutrient excess and contribute additional DNA to support an increase in protein accretion. As such, a deeper understanding of this process will provide valuable information to improve the efficiency of lean growth.

Intrinsically, insulin-like growth factor-1 (IGF-1) and its downstream signaling is required for proper muscle development. Recent findings suggest mitochondria play a significant role in IGF-1 mediated myogenesis, yet this mechanism remains undefined. To this end, we deleted *ATP synthase F1 beta subunit* (ATP5β KO), to impair mitochondrial energy production, and *ubiquinol-cytochrome c reductase iron-sulfur subunit* (UQCRFS1 KO), to disrupt the mitochondrial membrane potential. We showed mitochondrial ATP production is not essential for IGF-1 mediated myogenesis; however, an energy-independent function of mitochondria is required. Further investigation revealed IGF-1 stimulation in ATP5β KO and UCRFS1 KO myoblast increased glycolytic flux but not glucose oxidation in either genotype. These findings suggest myoblast with disrupted mitochondrial bioenergetics are not restricted by a lack of energy currency but rather an energy independent function of mitochondria. We also investigated the role of mitochondria calcium uptake in IGF-1 mediated myogenic progression and found inhibition of the mitochondrial calcium uniporter, the predominate site of calcium entry into the matrix, negated IGF-1 stimulated fusion to recapitulate UQCFS1 KO fusion. These data suggest the energy independent mitochondrial function essential to IGF-1 mediated myogenesis may be mitochondrial calcium sequestration. However, we failed to establish a causal relationship between IGF-1 signaling and mitochondrial calcium uptake. Regardless, these findings call for further exploration into the role of mitochondria calcium sequestration in myogenesis. Although we did not fully define the IGF1-mitochondria axis, this work undoubtably shows an energy independent function of mitochondria plays an indispensable role in IGF-1 mediated myogenesis.

In summary, skeletal muscle and SCs use highly integrated signaling pathways to relay extrinsic nutritional cues and intrinsic metabolic changes to adapt its cellular biological processes accordingly. Our findings show skeletal muscle uses O-GlcNAcylation, presumably to sense changing nutrient conditions, to maintain metabolic homeostasis. As perturbations to skeletal metabolism have profound implications on

global metabolism, a deeper understanding of skeletal muscle O-GlcNAcylation will empower scientists to ameliorate metabolic diseases. Additionally, these findings can be translated to livestock production to improve the efficiency of animal growth or as a tool to monitor the metabolic status of growing tissues, as different feeding strategies evoke unique O-GlcNAcylation patterns in bovine skeletal muscle (Apaoblaza et al., 2020).

In SCs, we showed O-GlcNAcylation is required for proper SC function. As additional DNA incorporation through SC mediated events supports hypertrophy, further investigation into how SCs use O-GlcNAcylation to respond to different nutrient and substrate availability would provide valuable information to animal scientists to develop innovative strategies for improving animal growth. Intrinsically, we showed an energy independent function of mitochondria is required for IGF-1 mediated myogenesis. Although further investigation into the IGF1-mitochondria axis is needed, elucidation of this signaling mechanism will shed light on mitochondria as a mediator of signaling cascades that modulate myogenesis. In conclusion, these findings call for greater exploration into the signaling pathways that regulate skeletal muscle metabolism and growth as defining these novel pathways will empower scientists to improve quality of life in humans and improve the efficiency of animal growth.

References

Apaoblaza, A., S. D. Gerrard, S. K. Matarneh, J. C. Wicks, L. Kirkpatrick, E. M. England, T. L. Scheffler, S. K. Duckett, H. Shi, S. L. Silva, A. L. Grant, and D. E. Gerrard. 2020. Muscle from grass- and grain-fed cattle differs energetically. Meat Sci 161:107996. doi: 10.1016/j.meatsci.2019.107996